1 **Desorption Lifetimes and Activation Energies Influencing Gas-Surface Interactions and**

2 **Multiphase Chemical Kinetics**

4 *Daniel A. Knopf[1,2,*], Markus Ammann[3], Thomas Berkemeier[4], Ulrich Pöschl[4], Manabu Shiraiwa[5,*]*

5 1.   School of Marine and Atmospheric Sciences, Stony Brook University, Stony Brook, New York,

6 USA.

7 2.   Department of Chemistry, Stony Brook University, Stony Brook, New York, USA.

8 3.   Laboratory of Environmental Chemistry, Paul Scherrer Institute, Villigen, Switzerland

9 4.   Multiphase Chemistry Department, Max Planck Institute for Chemistry, Mainz, Germany

10 5.   Department of Chemistry, University of California Irvine, California, USA

11 *Correspondence to*: [*]daniel.knopf@stonybrook.edu; m.shiraiwa@uci.edu

Abstract

Adsorption and desorption of gases on liquid or solid substrates are involved in multiphase processes and heterogeneous chemical reactions. The desorption energy (E_{des}^0), which depends on the intermolecular forces between adsorbate and substrate, determines the residence time of chemical species at interfaces. We show how E_{des}^0 and temperature influence the net uptake or release of gas species, the rates of surface-bulk exchange and surface or bulk reactions, and the equilibration timescales of gas-particle partitioning. Using literature data, we derive a parameterization to estimate E_{des}^0 for a wide range of chemical species based on the molecular mass, polarizability, and oxygen to carbon ratio of the desorbing species independent of substrate-specific properties, which is possible because of the dominant role of the desorbing species' properties. Correlations between E_{des}^0 and the enthalpies of vaporization and solvation are rooted in molecular interactions. The relation between E_{des}^0 and desorption kinetics reflects the key role of interfacial exchange in multiphase processes. For small molecules and semi-volatile organics (VOC, IVOC, SVOC), E_{des}^0 values around 10 - 100 kJ mol^{-1} correspond to desorption lifetimes around nanoseconds to days at room temperature. Even higher values up to years are obtained at low temperatures and for low volatile organic compounds (LVOC, ELVOC/ULVOC) relevant for secondary organic aerosols (SOA). Implications are discussed for SOA formation, gas-particle partitioning, organic phase changes, and indoor surface chemistry. We expect these insights to advance the mechanistic and kinetic understanding of multiphase processes in atmospheric and environmental physical chemistry, aerosol science, materials science, and chemical engineering.

1. Introduction

The interaction of gases with condensed phase matter via heterogeneous or multiphase reactions is of importance for a variety of disciplines such as chemical engineering, catalysis, materials science, and environmental and atmospheric chemistry (Cussler, 2009; Chorkendorff and Niemantsverdriet, 2007; Finlayson-Pitts and Pitts, 2000; Ravishankara, 1997; Solomon, 1999; Hoffmann et al., 1995; Beller et al., 2012; Hanefeld and Lefferts, 2018). In the atmosphere, gas-particle interactions and multiphase chemical processes involve gaseous and condensed-phase species manifesting in condensation, gas-particle partitioning, and alteration in the physicochemical properties of aerosol particles and cloud droplets (Pöschl et al., 2007; Kolb et al., 2010; Rudich et al., 2007; George and Abbatt, 2010; Pöschl and Shiraiwa, 2015; Moise et al., 2015; Ammann et al., 2013; Crowley et al., 2013; Kroll et al., 2011; Donahue et al., 2011; Jimenez et al., 2009; Abbatt and Ravishankara, 2023; Ravishankara, 1997; Penkett et al., 1979; Hoffmann and Edwards, 1975; Davidovits et al., 2006). The dramatic effects of multiphase reactions in the atmosphere are most impressively demonstrated by the large-scale stratospheric ozone depletion (ozone hole) over the south pole during Antarctic winter and spring, where inactive gaseous chlorine species are converted to active gas species on cloud particles (Solomon, 1999; Rowland, 1991; Peter, 1997; Koop et al., 1997; Muller et al., 1997; Carslaw et al., 1997).

Atmospheric aerosol particles and environmental interfaces are often chemically complex systems comprising multiple components in multiple phases. The large compositional variety of airborne particulate matter and gas species including reactive radicals, oxidants, and volatile inorganic and volatile organic compounds (VOCs), in addition to the wide temperature and humidity range present in the atmosphere, poses challenges to resolve multiphase chemical kinetics on a molecular level. The underlying molecular processes are important for the scientific

understanding and reliable description of gas uptake and chemical transformation of aerosols (Shiraiwa et al., 2011a; Berkemeier et al., 2013; Zhou et al., 2013; Abbatt et al., 2012; Kolb et al., 2010; Schwartz, 1986; Hanson and Lovejoy, 1995; Hanson et al., 1996; Shen et al., 2022; Willis and Wilson, 2022), the chemical evolution of secondary organic aerosol (SOA) including the partitioning of semivolatile species (Shiraiwa and Seinfeld, 2012; Shiraiwa et al., 2013b; Perraud et al., 2012; Donahue et al., 2011; Ingram et al., 2021), and the impact of multiphase reactions on the particles' activation as cloud condensation nuclei (CCN) or ice-nucleating particles (INPs) (Slade et al., 2015; Slade et al., 2017; Petters et al., 2006; Wang et al., 2012; Wang and Knopf, 2011; Knopf et al., 2018; Knopf and Alpert, 2023).

Atmospheric multiphase reactions usually involve an adsorbed state of gas species at the surface of a liquid or solid material (Langmuir, 1918, 1916, 1915; Iupac, 1997), which can be regarded as physisorption or chemisorption depending on the nature and intensity of the surface interaction. Physisorption is caused by weak intermolecular interactions (van der Waals, hydrogen bond, ionic and hydrophobic interactions, Table 1) with energies up to ~50 kJ mol^{-1}, whereas chemisorption involves changes of chemical bonds with higher interaction energies (Desjonqueres and Spanjaard, 1996; Masel, 1996; Pöschl et al., 2007). The phenomenon of reversible adsorption is easiest to depict on solid surfaces but applies also to liquid surfaces, where it is coupled to the exchange with the bulk liquid (Langmuir, 1918, 1916, 1915; Nathanson, 2004; Ringeisen et al., 2002a, b; Behr et al., 2001; Morris et al., 2000; Masel, 1996; Nathanson et al., 1996; Rettner et al., 1996; Donaldson and Anderson, 1999; Donaldson et al., 1995; Donaldson, 1999; Pöschl et al., 2007).

According to the Frenkel equation, the desorption lifetime (τ_{des}) of a surface-adsorbed chemical species (adsorbate) follows an Arrhenius-type behavior (Arrhenius, 1889b; Arrhenius, 1889a; Laidler, 1949; Frenkel, 1924; Laidler et al., 1940):

80 $$\tau_{\text{des}} = \frac{1}{k_{\text{des}}} = \frac{1}{A_{\text{des}}} e^{\left(E^0_{\text{des}}/(RT)\right)} ,$$ (1)

81 where k_{des} is a first-order desorption rate coefficient, A_{des} is a pre-exponential factor, in more

82 detail discussed below, R is the gas constant, and T is the temperature. E^0_{des} is the desorption

83 energy with the energy reference of the gas molecule at rest at $T = 0$ K. E^0_{des} is referred to as the

84 activation energy of desorption. In terms of the theory of the kinetics of desorption, desorption is

85 always considered an activated process, independent of whether E^0_{des} corresponds to just the

86 energy difference between gas and adsorbed state or also include an energy barrier on top of that

87 (Knopf and Ammann, 2021). In case of physisorption, E^0_{des} is equal to the negative value of the

88 enthalpy of adsorption with a correction for the change in degree of freedom between gas and

89 adsorbed phase (see below and Knopf and Ammann, 2021; Kolasinski, 2012). In turn, in the other

90 direction, for the kinetics of the process from the gas phase to the adsorbed state, the adsorption

91 rate normalized to the gas kinetic collision rate is often expressed as the surface accommodation

92 coefficient as discussed below.

93 Atmospheric trace gases and water vapor adopt reversibly adsorbed states on aerosol, cloud, and

94 ground surfaces over a wide range of temperatures from below 200 to above 300 K. The rate of

95 interfacial processes, which may involve reversible, reactive and catalytic steps, generally depends

96 on the concentration of surface-adsorbed reactants and hence on τ_{des}. Especially at low

97 temperatures, high values of τ_{des} can (over)compensate for the low rates of thermally activated

98 chemical reactions and diffusion and thereby enhance the overall gas uptake (Ammann et al., 2013;

99 Crowley et al., 2013; Kolb et al., 2010; Pöschl et al., 2007).

100 Factors influencing gas uptake are competitive co-adsorption of other species (Pöschl et al.,

101 2001; Pöschl et al., 2007; Slade and Knopf, 2014; Kaiser et al., 2011; Springmann et al., 2009;

Shiraiwa et al., 2009), solvent dynamics and polarization effects (Ringeisen et al., 2002b; Morris et al., 2000; Klassen et al., 1997; Nathanson et al., 1996; Jungwirth et al., 2006), thermodynamics and kinetics of surface – bulk exchange and bulk diffusivity in viscous liquids (Lakey et al., 2016; Berkemeier et al., 2016; Steimer et al., 2015; Shiraiwa et al., 2014; Shiraiwa et al., 2013a; Houle et al., 2018; Wiegel et al., 2017; Davies and Wilson, 2015; Marshall et al., 2016; Marshall et al., 2018), and phase separations or heterogeneous structures in the condensed phase (You and Bertram, 2015; You et al., 2014; You et al., 2012; Bertram et al., 2011; Huang et al., 2021).

Apart from adsorption and desorption, further processes influencing gas-particle interactions and multiphase chemical kinetics include mass transport to the condensed phase by gas-phase diffusion and accommodation at the interface; chemical reactions at the surface following Langmuir-Hinshelwood or Eley-Rideal type mechanisms; dissolution, diffusion, and chemical reactions in the bulk. Together with desorption, these processes may proceed sequentially or in parallel for multiple chemical species, which can be described by appropriate differential equations and numerical models (Shiraiwa et al., 2010; Shiraiwa et al., 2009; Ammann and Pöschl, 2007; Pöschl et al., 2007; Shiraiwa et al., 2012; Wilson et al., 2022).

Traditionally, the uptake of trace gases by solid and liquid particles or substrates has often been analyzed by the so-called resistor model, treating each of the above processes in analogy to parallel or serial resistors in an electrical circuit (Schwartz, 1986; Worsnop et al., 2002; Hanson and Lovejoy, 1995; Hanson et al., 1994; Ammann et al., 2013; Crowley et al., 2010). Despite constraints and limitations such as the required approximations regarding steady state and mixing, and a limited capability to describe multicomponent systems, the resistor model has proven to be useful for the investigation and characterization of various processes and substrates, including mineral dust, ice, sulfuric acid, and organic and inorganic particles (Pöschl et al., 2007; Hanson,

125   1997; Davidovits et al., 2006; Crowley et al., 2010; Kolb et al., 2010; Hanson et al., 1994; Ammann

126   et al., 2013; Ammann et al., 2003; Knopf et al., 2005; Li and Knopf, 2021; Schwartz, 1986). In the

127   resistor model approach, the uptake of a gas species with reaction at the surface and in the bulk is

128   described by the following or equivalent equations (Pöschl et al., 2007):

129    $$\frac{1}{\gamma} = \frac{1}{\alpha_s} + \frac{1}{\Gamma_s + \frac{1}{\frac{1}{\Gamma_{sb}} + \frac{1}{\Gamma_b}}} \ . \tag{2}$$

130   Here, γ is the uptake coefficient, defined as the overall loss rate from the gas phase normalized to

131   the gas kinetic collision rate, and α_s is the surface accommodation coefficient, which represents

132   the probability for a gas molecule colliding with the surface to be accommodated at the surface for

133   period longer than the duration of an elastic scattering process (Pöschl et al., 2007). This parameter

134   thus represents the adsorption rate normalized to the gas kinetic collision rate. The term Γ_s

135   represents the normalized loss rate due to surface reaction, Γ_{sb} is the normalized rate of surface to

136   bulk transfer, and Γ_b is the normalized loss rate in the bulk-phase induced by solubility, diffusion

137   and reaction (Hanson et al., 1994; Ammann et al., 2013; Crowley et al., 2013; Kolb et al., 2010;

138   Ammann and Pöschl, 2007; Pöschl et al., 2007; Wilson et al., 2022; Shiraiwa and Pöschl, 2021).

139   By virtue of the coupled nature of the involved elementary processes, the desorption rate

140   coefficient can influence the rates of all other surface and bulk processes involving this species,

141   i.e., k_{des} can influence Γ_s, Γ_{sb}, and Γ_b (Pöschl et al., 2007). For example, the terms Γ_s , Γ_{sb} and Γ_b

142   governed by the competition between desorption and surface reaction, between desorption and

143   surface to bulk transfer, or between desorption and surface to bulk transfer coupled to reaction and

144   diffusion, respectively, are inversely proportional to k_{des} and can be expressed as follows:

145    $$\Gamma_s = \alpha_S \frac{k_s}{k_{des}} \ , \tag{3}$$

146    $$\Gamma_{sb} = \alpha_s \frac{k_{sb}}{k_{des}}, \tag{4}$$

147 $$\Gamma_b = \alpha_S \frac{k_{sb}}{k_{des}} \frac{\sqrt{k_b D_b}}{k_{bs}} .$$ (5)

148 Here, k_s is a first-order rate coefficient of chemical reaction at the surface; k_{sb} is a first-order rate

149 coefficient for the transfer of molecules from the surface into the bulk (solvation); k_b is a first-

150 order rate coefficient of chemical reaction in the bulk; D_b is the diffusion coefficient of the trace

151 gas in the bulk; k_{bs} is a first-order rate coefficient for the transfer of molecules from the bulk to

152 the surface. Even though the rate coefficients for these elementary processes are independent of

153 k_{des}, the overall normalized rates of Γ_s, Γ_{sb}, and Γ_b are. Similarly, the overall rate of transfer of a

154 gas molecule into the bulk of a liquid or (semi)solid particle (independent of whether diffusion and

155 reaction therein contributes to loss) also depends on k_{des} and can be expressed by the bulk

156 accommodation coefficient, α_b (Pöschl et al., 2007; Edwards et al., 2022):

157 $$\alpha_b = \alpha_s \frac{k_{sb}}{k_{sb} + k_s + k_{des}} .$$ (6)

158 Hence, the desorption rate coefficient is a critical parameter influencing all ~~processes~~ overall

159 rates involved in the uptake of a gas species by condensed matter (Li and Knopf, 2021).

160 The role of reversible adsorption and desorption has been addressed in many studies of gas

161 uptake and heterogeneous chemistry in particular for the decoupling of mass transport and

162 chemical reaction (Kolb et al., 1995; Hanson and Ravishankara, 1991; Kolb et al., 2010; Ammann

163 et al., 2013; Crowley et al., 2013; Pöschl and Shiraiwa, 2015; Tabazadeh et al., 1994; Peter, 1997;

164 Carslaw et al., 1997; Hanson et al., 1994; Hanson and Lovejoy, 1995). More recently, kinetic

165 multilayer model analyses of measured uptake coefficients for OH radicals on levoglucosan

166 substrates (Arangio et al., 2015) and the heterogeneous reaction of ozone with shikimic acid

167 (Berkemeier et al., 2016; Steimer et al., 2015) and oleic acid aerosol (Berkemeier et al., 2021)

168 demonstrated the complex dependency of the reactive uptake coefficient on the elementary steps,

169 such as surface accommodation, desorption, surface reaction and bulk diffusion by virtue of Eq.

170 (3-5). The range of experimental conditions was not sufficient to constrain the associated

171 coefficients unambiguously. To determine a best estimate for the surface reaction rate coefficient,

172 it was thus necessary to assume a realistic value for α_s and τ_{des} derived from molecular dynamics

173 simulations (Vieceli et al., 2005; Von Domaros et al., 2020). *Li and Knopf* (2021) made use of the

174 temperature-dependent measurement of OH uptake to decouple τ_{des} from surface reactivity. The

175 intimate coupling of adsorption and desorption with other multiphase processes has also been

176 discussed in the context of many other reaction systems. Ground-breaking work driving much of

177 the developments of the kinetic concepts introduced above was directed at halogen activation on

178 stratospheric aerosol and polar stratospheric clouds (Tabazadeh et al., 1994; Peter, 1997; Carslaw

179 et al., 1997; Hanson et al., 1994; Hanson and Lovejoy, 1995). ~~These~~ Others include the uptake of

180 SO$_2$ into sulfuric acid (Jayne et al., 1990; Ammann and Pöschl, 2007), adsorption of acetone on

181 ice and HNO$_3$ on mineral dust (Bartels-Rausch et al., 2005; Vlasenko et al., 2009; Cwiertny et al.,

182 2008; Usher et al., 2003), ozonolysis in liquid, viscous, and solid particles (Knopf et al., 2005;

183 Berkemeier et al., 2016; Steimer et al., 2015; Shiraiwa et al., 2011a; Hearn and Smith, 2007; Pöschl

184 et al., 2001; Shiraiwa et al., 2009; Zhou et al., 2013; Kahan et al., 2006; Kwamena et al., 2004;

185 Mu et al., 2018; Knopf et al., 2011; Willis and Wilson, 2022), and gas-particle partitioning of SOA

186 (Shiraiwa et al., 2013a; Ingram et al., 2021; Schervish and Shiraiwa, 2023). Accordingly, the

187 design and interpretation of heterogeneous and multiphase reaction rate measurements should

188 include a careful assessment whether reversible adsorption is an important or even rate-limiting

189 step, whereby the applicable kinetic regime, may vary with reaction time and conditions

190 (Berkemeier et al., 2013; Berkemeier et al., 2016; Shiraiwa et al., 2014; Ingram et al., 2021; Willis

191 and Wilson, 2022). Hence, desorption lifetimes and related activation energies are important for

192 describing the interaction of gas phase and condensed phase species.

193   To address and elucidate these issues, the remainder of this article is structured as follows: In

194   Section 2, we discuss the molecular interactions underlying adsorption and desorption, and we

195   outline the relevant thermodynamic and kinetic equations and parameters. In Section 3, we compile

196   and present a comprehensive set of desorption energies and thermodynamic parameters for

197   environmentally and atmospherically relevant gas species and substrates. In Section 4, we evaluate

198   the role of the desorption energy in reactive and non-reactive gas uptake by solid and liquid

199   substrates considering characteristic tropospheric temperatures by exploratory kinetic flux model

200   simulations. In Section 5, we develop and present a simplified parameterization for estimating E_{des}^0

201   based on the gas species' polarizability and oxygen to carbon (*O:C*) ratio. Section 6 outlines the

202   role of E_{des}^0 in selected atmospheric implications including the formation and properties of viscous

203   secondary organic aerosol (SOA). We conclude the document with a summary and open questions.

204

205   **2. Thermodynamic Relations**

206   A detailed discussion of the microscopic and thermodynamic treatments of adsorption and

207   desorption and implications for uncertainties in E_{des}^0 is given in *Knopf and Ammann* (2021). Here

208   we provide the key relationships and concepts needed to follow our assumptions when applying

209   literature obtained E_{des}^0 values for derivation of a parameterization.

210   Typically, the adsorption rate is a measure of the amount of gas molecules that adsorb on the

211   surface as a consequence of gas kinetic collisions. As mentioned above, in the atmospheric

212   sciences this is often expressed with the surface accommodation coefficient α_s (Kolb et al., 2010),

213   operationally defined as the probability that a gas kinetic collision leads to adsorption. The

214   adsorbed molecules may be considered an ideal 2D gas, meaning that the molecules have

215   equilibrated with the surface in terms of the degrees of freedom perpendicular to the surface but

216   may still retain some kinetic energy parallel to the surface. Alternatively, the adsorbed molecules

217   may be considered an ideal 2D lattice gas, where the degrees of freedom in the horizontal plane

218   are restricted to vibrations. Also, other models describing intermediate situations have been

219   suggested (Savara et al., 2009; Campbell et al., 2016; Kisliuk, 1957). Here, we use α_s to describe

220   the rate of adsorption into either adsorbed state. The term thermal accommodation coefficient, α_t,

221   is commonly used for the case where the adsorbed molecule is fully thermally equilibrated with

222   the substrate, thus close to the case of the ideal 2D lattice gas. Adsorption can be considered a non-

223   activated process, though in presence of an energy barrier, adsorption has to be treated as an

224   activated process (Knopf and Ammann, 2021). The corresponding energy barrier directly impacts

225   α_s (Knopf and Ammann, 2021). In contrast, desorption is always treated as an activated process,

226   even in the absence of an energy barrier. The explicit treatment of an additional energy barrier

227   when deriving adsorption and desorption rates is given in *Knopf and Ammann* (2021). Here we

228   solely consider E_{des}^0 as reported in the literature, independent of whether an additional activation

229   barrier was included in the analysis. As discussed below, the choice of adsorbate model and

230   standard state will impact the value and uncertainties in E_{des}^0 (Knopf and Ammann, 2021; Savara,

231   2013; Campbell et al., 2016).

232   Adsorption proceeds spontaneously and this implies an exergonic process with the

233   thermodynamic condition (Bolis, 2013):

234    $$\Delta G_{ads}^0 = \Delta H_{ads}^0 - T\Delta S_{ads}^0 < 0 \,, \tag{6}$$

235   where ΔG_{ads}^0 represents the standard Gibbs free energy change of adsorption, ΔH_{ads}^0 is the

236   standard enthalpy change of adsorption (in this case negatively defined), ΔS_{ads}^0 is the standard

237   entropy change of adsorption, and T is temperature. Adsorption of a gas on a substrate results in

238   an increase of order, thus, $\Delta S_{ads}^0 < 0$. This is because the degrees of freedom of the adsorbed

239   molecules are more constrained than in the gas phase. Often, the adsorbed molecule may be

240   considered a 2D ideal gas, a 2D ideal lattice gas, or an ideal hindered translator on the surface,

241   with the motion perpendicular to the surface strongly constrained but with varying freedom parallel

242   to the surface (Hill, 1986; Campbell et al., 2016; Savara et al., 2009; Sprowl et al., 2016). Since

243   $\Delta S^0_{ads} < 0$, the change in enthalpy ΔH^0_{ads} has to be negative. The adsorption enthalpy is determined

244   by the binding energy of a gas on the surface, thus on the molecular interactions between gas

245   species and substrates, including hydrogen bonds and van der Waals forces (Poe et al., 1988;

246   Valsaraj and Thibodeaux, 1988; Valsaraj, 1988a, b; Goss and Eisenreich, 1995b; Goss, 1993,

247   1994b; Valsaraj, 1994; Valsaraj et al., 1993). The van der Waals forces comprise London

248   dispersion forces between instantaneously induced dipoles, Debye forces between permanent and

249   induced dipoles, and Keesom forces between permanent dipoles (Iupac, 1997). For organic

250   molecules, the strength of both van der Waals and hydrogen bonds depends on the polarity of

251   functional groups and commonly follows the order (Jeffrey, 1997; Jeffrey and Saenger, 1991;

252   Vinogradov and Linnell, 1971):

253   Amide > Acid > Alcohol > Ketone ≈ Aldehyde > Amine > Ester > Ether > Alkane .

254   Table 1 gives an overview of intermolecular forces active among functional groups present in

255   typical gas- and condensed-phase atmospheric species. While all molecules exhibit van der Waals

256   forces, their thermodynamic properties are largely determined by the number and type of hydrogen

257   bonds they can form. The presence of charged groups, e.g., due to a dipole moment, can

258   significantly increase binding energy. The hydrogen bond strength in liquid water is around 10-19

259   kJ mol^{-1} (Hakem et al., 2007), and with a few exceptions, usually involving fluorine, the energies

260   associated with hydrogen bonding are typically less than 20-25 kJ mol^{-1} per hydrogen bond

261   (Steiner, 2002; Jeffrey, 1997; Jeffrey and Saenger, 1991; Brini et al., 2017; Iupac, 1997).

262   The complexity of the interaction between adsorbate and substrate can go beyond the 2D ideal

263   gas, 2D ideal lattice gas, and hindered translator model depending on how physisorption and

264   chemisorption are considered. For example, the Kisliuk precursor mechanism allows for more

265   complex configurations of the adsorbate that could include adsorbate-adsorbate interactions

266   (Kisliuk, 1957; Tully, 1994; Campbell et al., 2016; Kisliuk, 1958). Hence, the overall adsorbate-

267   substrate binding energy may involve contributions from adsorbate-surface as well as adsorbate-

268   adsorbate interactions (see e.g. Meyer et al., 2001). Moroever, the binding energy may vary

269   between different types of adsorption sites co-existing on real surfaces, depending on the

270   morphology and chemical heterogeneities of the substrate (Kolasinski, 2012). In view of the

271   complex mixture of substances present in the atmosphere, such effects and variations are not

272   explicitly resolved in this study. Instead, we assume that the energetics of reversible adsorption on

273   atmospheric surfaces can be approximated by effective average values characterizing the binding

274   energy to the substrate. The assumption of reversible adsorption has been crucial in studies of gas

275   uptake and heterogeneous or multiphase chemical reactions when decoupling mass transport and

276   chemical reaction (Kolb et al., 2010; Hanson and Ravishankara, 1991; Ammann et al., 2013;

277   Crowley et al., 2013; Pöschl and Shiraiwa, 2015; Li and Knopf, 2021). The assumption of

278   reversible adsorption directly leads to $\Delta H_{ads}^0 = -\Delta H_{des}^0$ and $\Delta S_{ads}^0 = -\Delta S_{des}^0$, where ΔH_{des}^0 and

279   ΔS_{des}^0 represent the changes in the desorption enthalpy and entropy, respectively.

280   The free energy change is the driving force for desorption from the thermodynamic point of

281   view. The Frenkel equation, given by Eq. (1), is usually applied to describe the kinetics of

282   desorption. By itself it does not differentiate between physisorption and chemisorption. For the

283   description and understanding of atmospheric heterogeneous and multiphase kinetics, it is useful

284   to treat chemisorption as a chemical reaction following physisorption (Pöschl et al., 2007; Hanson

et al., 1994; George and Abbatt, 2010), as expressed in Eqs. (2) to (5). We note that the energy

range of 50 kJ mol^{-1} mentioned above to distinguish between physisorption and chemisorption is

not necessarily appropriate, if chemisorption is reflecting the fact that chemical bonds are formed

or disrupted. Large molecules may undergo a multitude of van der Waals and hydrogen bonds

adding up to large interaction energies, which would still be considered physisorption. As outlined

above, for these cases we regard the adsorption process to be reversible.

Knopf and Ammann (2021) have provided the thermodynamic and microscopic equations, the

latter based on conventional transition state (TS) theory, that are implicitly included in the Frenkel

equation, while accounting for the choice of standard states. For example, for the case of a 2D

ideal gas as adsorbate model, the desorption rate expressed in thermodynamic quantities is

$$k_{\text{des}} = \kappa \left(\frac{k_{\text{B}}T}{h} \right) \frac{(N_{\text{TS}}/\mathcal{A})^0}{(N_{\text{ads}}/\mathcal{A})^0} e^{-\Delta G_{\text{des}}^0/RT} = \kappa \left(\frac{k_{\text{B}}T}{h} \right) e^{-\Delta G_{\text{des}}^0/RT}, \tag{7}$$

where κ is a transmission coefficient giving the probability with which an activated complex

proceeds to desorption (Kolasinski, 2012), k_{B} is the Boltzmann constant, and h is the Planck

constant. Furthermore, we assume the standard concentration of molecules in the TS, $(N_{\text{TS}}/\mathcal{A})^0$,

is equal to the standard concentration of adsorbed molecules, $(N_{\text{ads}}/\mathcal{A})^0$, i.e., $\frac{(N_{\text{TS}}/\mathcal{A})^0}{(N_{\text{ads}}/\mathcal{A})^0} = 1$.

In microscopic quantities, k_{des} is derived as

$$k_{\text{des}} = \kappa \left(\frac{k_{\text{B}}T}{h} \right) \left(\frac{q_{\text{TS}}^{0\prime}}{q_{\text{ads}}^0} \right) \frac{(N_{\text{TS}}/\mathcal{A})^0}{(N_{\text{ads}}/\mathcal{A})^0} e^{-\frac{\left(E_{\text{des}}^0 \right)}{RT}}, \tag{8}$$

where $q_{\text{TS}}^{0\prime}$ and q_{ads}^0 are the standard partition functions for the TS and adsorbate, respectively,

evaluated using standard molar volume and area. Equations (7) and (8) clearly demonstrate the

importance of the choice of standard state when comparing measured k_{des} and evaluated E_{des}^0.

Looking at the equations for k_{des} allows to derive the pre-exponential factor of the Frenkel

equation as (Knopf and Ammann, 2021)

307 $$A_{\text{des}} = \kappa \left(\frac{k_B T}{h}\right)\left(\frac{q'_{\text{TS}}}{q_{\text{ads}}}\right) = \kappa \left(\frac{k_B T}{h}\right)\frac{(N_{\text{TS}}/\mathcal{A})^0}{(N_{\text{ads}}/\mathcal{A})^0} e^{\Delta S^0_{\text{des}}/R} ,$$ (9)

308   where q'_{TS} and $q_{\text{ads,2D}}$ are the partition functions for the TS and adsorbate, respectively. The

309   microscopic interpretation of A_{des} shows that A_{des} depends on temperature and the choice of

310   adsorbate model, expressed as partition functions. The thermodynamic interpretation of A_{des}

311   demonstrates its dependency on standard concentrations and the change in entropy when desorbing

312   from the substrate surface into the activated TS.

313   We can now interpret A_{des} for the case of a 2D ideal gas adsorbate model. If we assume $\kappa \approx 1$,

314   and adsorbate and TS are 2D ideal gases with similar degrees of freedom (neglecting vibrations),

315   i.e., $\frac{q'_{\text{TS}}}{q_{\text{ads}}} = 1$, then we obtain $A_{\text{des}} \approx \frac{k_B T}{h} = 6 \times 10^{12} \approx 10^{13}$ s^{-1} at room temperature (298 K).

316   This is the commonly applied value for the pre-exponential factor. In this case, Eq. (9)

317   demonstrates that the change in ΔS^0_{des} must be negligible. However, significant deviations from

318   this benchmark factor can occur. For example, if going from the adsorbate state to the activated

319   TS coincides with $\Delta S^0_{\text{des}} > 0$, and thus $\frac{q'_{\text{TS}}}{q_{\text{ads}}} > 1$, implying more degrees of freedom in the TS, then

320    $A_{\text{des}} > 10^{13}$ s^{-1}. In contrast, if the TS is more constrained, e.g., only a limited number of molecular

321   orientations are allowed, then $\Delta S^0_{\text{des}} < 0$, and thus $\frac{q'_{\text{TS}}}{q_{\text{ads}}} < 1$, then $A_{\text{des}} < 10^{13}$ s^{-1}. A similar analysis

322   has been provided for the 2D ideal lattice gas adsorbate model (Knopf and Ammann, 2021). A_{des}

323   varies between 180 and 300 K for a 2D ideal gas and 2D ideal lattice gas adsorbate model by about

324   a factor of 2 and 3, respectively, indicating minor temperature effects (Knopf and Ammann, 2021).

325   However, A_{des} can differ by about 3 orders of magnitude between the 2D ideal gas and 2D ideal

326   lattice gas adsorbate models.

327   Experimental studies usually yield pre-exponential factors in the range between 1×10^{11} to

328   1×10^{12} s^{-1} for smaller molecules such as methane and 1×10^{13} s^{-1} for larger alkanes (Fichthorn and

329   Miron, 2002). For large adsorbates, A_{des} can be several orders of magnitude larger (Fichthorn and

330   Miron, 2002). For example, adsorption of benzene and toluene by graphite surfaces exhibit A_{des}

331   of about 10^{15} and 10^{19} s^{-1}, respectively (Ulbricht et al., 2006). In general, the larger the adsorbate

332   molecule, the larger A_{des} (Ulbricht et al., 2006).

333   Nevertheless, for this study and the compilation of literature data of E_{des}^0, we have assumed a

334   constant pre-exponential factor $A_{des} = 1 \times 10^{13}$ s^{-1}, being aware of the underlying assumptions

335   discussed above. We justify this approach by noting that our aim is to derive E_{des}^0 estimates for

336   complex substrate systems, including multicomponent and multiphase aerosol particles, which will

337   impose additional uncertainties in E_{des}^0. Due to the involvement of entropic contributions to the

338   pre-exponential factor, experimentally derived A_{des} values often contain not well-documented

339   implicit standard state assumptions (related to experimental surface to volume ratios) (Donaldson

340   et al., 2012a; Campbell et al., 2016; Savara, 2013) and thus carry more uncertainty than the E_{des}^0

341   obtained from the slope of temperature dependent data.

342   Figure 1 displays the dependency of τ_{des} on E_{des}^0 and temperature using the Eq. (1). As

343   illustrated in Fig. 1a, the temperature dependency of τ_{des} increases with increasing E_{des}^0.

344   Calculations have been performed with $A_{des} = 10^{13}$ s^{-1}, while the shading represents the

345   application of A_{des} being one order of magnitude greater or smaller, thereby covering the typical

346   temperature dependency of A_{des}. Clearly, temperature can significantly increase the residence time

347   of a molecule on the substrate surface, by several orders of magnitude, thereby, potentially,

348   allowing different reaction pathways. It is also evident that uncertainties in A_{des} directly translate

349   into corresponding uncertainties in τ_{des}. Hence, assuming $A_{des} = 10^{13}$ s^{-1} in the analysis of

350   literature data will yield uncertainties in E_{des}^0 values. For example, one order of magnitude

351   uncertainty in A_{des}, changes E_{des}^0 by ~4-6 kJ mol^{-1} over a temperature range of 210 to 300 K.

352 Conversely, an uncertainty of E_{des}^0 by 5 kJ mol^{-1} imposes an uncertainty in τ_{des} of about a factor

353 of ~7-17 for a similar temperature range. These interdependencies are further outlined in Fig. 1b

354 showing typical τ_{des} for given temperatures and E_{des}^0, again derived assuming $A_{des} = 10^{13}$ s^{-1}.

355 This discussion implies an uncertainty in our E_{des}^0 values of about ±5 kJ mol^{-1}. However, as

356 outlined in detail in *Knopf and Ammann* (2021), additional uncertainties in E_{des}^0 can arise when

357 the appropriate adsorbate model is not known and if the surface coverage of the adsorbate is

358 uncertain. For example, for a given τ_{des}, E_{des}^0 can differ by 10-15 kJ mol^{-1} when assuming either

359 a 2D ideal gas or 2D ideal lattice gas adsorbate model. If a surface is assumed to be pristine but

360 actual coverage is about 20%, E_{des}^0 may be uncertain by 10-20 kJ mol^{-1}. In summary, literature

361 E_{des}^0 values applied in this analysis, assuming a conservative estimate, may be uncertain by up to

362 ~±15 kJ mol^{-1}.

363   In the formulation of the kinetic and thermodynamic concepts and expressions, we have not

364 made an explicit assumption about the physical state of the condensed phase - solid, liquid,

365 crystalline or amorphous. Lattice gas statistics can be applied generally in different dimensions

366 and has been used for liquids, sorption of ions to proteins or polymer wires (Hill, 1986). In spite

367 of the simplifying assumptions, we use the equations summarized above and derived in more detail

368 in (Knopf and Ammann, 2021) for all substrates, including liquids. This is straightforward for

369 poorly soluble gases. For soluble gases, however, the full thermochemical cycle also involves the

370 dissolved state (Donaldson, 1999). We also note that the system free energy change upon

371 adsorption of a gas on a liquid manifests in a surface tension change, with the Gibbs adsorption

372 isotherm relating the surface tension change to surface excess (Kolasinski, 2012; Donaldson,

373 1999). The manifestation of the change in surface tension convolutes the complex response of

374 structure and dynamics at a liquid interface to an adsorbing molecule (Brini et al., 2017).

375 Depending on the polarity of the adsorbate, the structural features of the interface may then also

376 deviate significantly from that of an adsorbate on a solid surface, as exemplified in recent theory

377 work by Cruzeiro et al. (2022) and Galib and Limmer (2021) for the interaction of N_2O_5 with

378 water.

379 **3. Compilation of Desorption Energies for Solid and Liquid Substrates**

380 To derive a parameterization of E_{des}^0 applicable to typical gas-aerosol particle systems,

381 literature values of E_{des}^0 reflecting typical atmospheric constituents or serving as aerosol surrogates

382 have been compiled. If available, E_{des}^0 reflects values derived from lowest surface coverage,

383 preferentially below one monolayer. Tables A1-A7, A8, and A9-A15 provide thermodynamic and

384 physicochemical literature values for gas-to-solid, gas-to-ice, and gas-to-liquid substrate

385 interactions, respectively. For derivation of E_{des}^0 and τ_{des} values, we use Eq. (1) and assume

386 $A_{des} = 10^{13}$ s^{-1}, if not otherwise noted. We assume the temperature effect on A_{des} (proportional

387 to T, see Eq. (9)) and changes in the desorption entropy to be negligible compared to the Arrhenius

388 factor (Eq. (8)). The tables include the parameters E_{des}^0, τ_{des}, and for the gas species the molar

389 mass (M), enthalpy of vaporization (ΔH_{vap}), polarizability (α), dipole moment (μ), *O:C*, and

390 enthalpy of solvation (ΔH_{sol}). Lastly, the dielectric constant or relative permittivity of the substrate

391 (ε_r) is given. E_{des}^0 values are obtained from different experimental techniques and theoretical

392 studies described briefly below.

393

394 **3.1 Experimental and theoretical techniques yielding desorption energies**

395 Temperature programmed desorption (TPD), sometimes also termed thermal desorption

396 spectroscopy (TDS), is an experimental technique where the flux of desorbing molecules is

397 observed as the surface temperature is increased. TDS can yield coverages, activation energies,

398 and pre-exponential factors for desorption (Ulbricht et al., 2006). Thermal gravimetry with

399 differential scanning calorimetry (TG-DSC) determines the amount and rate (velocity) of change

400 in the mass of a sample as a function of temperature or time in a controlled atmosphere in addition

401 to thermophysical and thermoplastic properties derived by DSC (Giraudet et al., 2006). In general,

402 if heats of adsorption are measured experimentally by, e.g., calorimetric methods, the accurate

403 thermodynamic definitions have to be applied since heat is not a state function (Bolis, 2013). In

404 Knudsen cells and diffusion tubes coupled to mass spectrometric detection (KN) the rate of

405 molecules desorbing from a substrate can be selectively measured (Caloz et al., 1997; Koch and

406 Rossi, 1998b; Tolbert et al., 1987; Alcala-Jornod et al., 2000). Scattering experiments of molecular

407 beams (MB) are applied to directly measure desorption from and adsorption of gas species to solid

408 or liquid substrates (Thomson et al., 2011; Morris et al., 2000; Nathanson et al., 1996). While

409 straightforward in use and interpretation for solid surfaces in high vacuum, the developments

410 around using MB techniques for atmospherically relevant volatile liquids is experimentally

411 challenging and also data interpretation with respect to desorption is less straightforward

412 (Nathanson, 2004; Ringeisen et al., 2002b; Morris et al., 2000; Klassen et al., 1997; Nathanson et

413 al., 1996; Gao and Nathanson, 2022), as discussed below. Inverse gas chromatography (IGC)

414 applies the solid of interest as the chromatographic sorbent (stationary phase) and yields sorption

415 coefficients of gas species (Mader et al., 1997). Vacuum microbalance (VM) determines the

416 change in weight due to adsorbed gases (Rouquerol and Davy, 1978; Thomas and Williams, 1965).

417 The desorption rate can be determined by measuring the time evolution of the adsorbed phase by

418 using diffuse reflectance infrared Fourier transform spectroscopy (DRIFT), while the gas phase is

419 monitored by selected-ion flow-tube mass spectrometry (SIFT−MS) and long path transmission

420 Fourier transform infrared spectroscopy (FTIR) (Romanias et al., 2016). Since measurement of the

desorption rate requires pressures in the molecular flow regime, this is only straightforward for low vapor pressure materials, such as mineral dust or dry salts. For high vapor pressure materials (aqueous or organic liquids and ice) or materials featuring complex microstructure (mineral dust, soot), complications arise from the convolutions of pore space (Woodill et al., 2013; Keyser et al., 1991), bulk liquid diffusion (Koop et al., 2011b; Pöschl et al., 2007), gas phase diffusion (Knopf et al., 2015; Fuchs and Sutugin, 1971; Fuchs, 1964; Seinfeld and Pandis, 1998; Pöschl et al., 2007) and other coupled processes, making the determination of desorption life time an indirect and often difficult task. Kinetic uptake (KU) experiments operated in the molecular flow regime can yield estimates of species' surface residence times (Alcala-Jornod et al., 2000; Koch and Rossi, 1998a; Koch et al., 1997). KU experiments using laminar flow tube reactors can also yield estimates of the residence time of adsorbed species via determination of the Langmuir equilibrium constant (Pöschl et al., 2001; Von Hessberg et al., 2008; Slade and Knopf, 2013). Vibrational spectroscopy (VS) is used to study the interaction of molecules with, e.g., ice surfaces, by examining the shifted dangling hydrogen bond of ice in presence of an adsorbed molecule (Silva and Devlin, 1994). Surface tension (ST) measurements of adsorbing gases on liquid substrates can yield directly the thermodynamic parameters describing adsorption (Hauxwell and Ottewill, 1968; Donaldson, 1999), and the molecular level relationship between surface excess and surface coverage can be assessed by direct spectroscopy (Lee et al., 2016).

IGC derives sorption coefficients which can yield estimates of E_{des}^0 via the van't Hoff equation (Goss and Eisenreich, 1996). For experimental TPD and TDS desorption data analysis usually the Redhead equation (Redhead, 1962) is applied that considers the heating rate and gas species surface coverage. k_{des} derived from DRIFT studies yields τ_{des} which allows derivation of E_{des}^0 according to Eq. (1), with similar constraints with respect to effusion times from packed powder

444   samples (Woodill et al., 2013; Keyser et al., 1991). MB methods allow to uniquely differentiate

445   thermal desorption of molecules from those undergoing elastic or inelastic scattering, or from those

446   undergoing exchange with the bulk and/or reaction. For solid surfaces the interpretation is

447   straightforward, and corresponding desorption lifetimes can directly be observed. For liquid

448   surfaces, this is less straightforward, since the trajectory of a desorbing molecule may involve

449   diffusion into and out of the near-surface bulk layers (Faust et al., 2013), so that the 'surface

450   residence time' is not strictly a true desorption lifetime. Equilibrium measurements of surface

451   tension as a function of partial pressure of the trace gas allows to determine ΔG_{ads}^0 and ΔH_{ads}^0, if

452   the latter is assumed to be independent of temperature (Donaldson, 1999).

453   The choice of standard states can impact data interpretation. Standard free energies of formation

454   are typically referenced to 1 bar or 1 mol L^{-1} (at 298 K) (Donaldson et al., 2012a). Commonly it

455   can be assumed that standard enthalpy values are not strongly dependent on the choice of standard

456   state, because the dependence of enthalpy on pressure is weak (Donaldson et al., 2012a). However,

457   the standard entropies of phase transfer will depend on the choice of the standard-state (Donaldson

458   et al., 2012a; Knopf and Ammann, 2021; Campbell et al., 2016; Savara, 2013). Further

459   complications arise when choosing standard states for different adsorbate-surface interactions

460   (Campbell et al., 2016). This can impact standard state surface concentrations, equilibrium

461   constants and rate constants, and renders the adsorbate chemical potential dependent on surface

462   coverage (Campbell et al., 2016; Savara, 2013).

463   Molecular dynamics (MD) simulations can provide estimates of the residence time of gas

464   species at a surface or interface (Vieceli et al., 2005; Von Domaros et al., 2020). MD simulations

465   can yield residence times at the interface or substrate surface and as such an estimate of τ_{des}. Then,

466   for given A_{des} and temperature, E_{des}^0 can be estimated using Eq. (1). Density functional theory

467 (DFT) represents a computational quantum mechanical modelling method to compute the

468 electronic structure of matter (Meng et al., 2004). Monte Carlo (MC) methods based on

469 computational algorithms rely on repeated random sampling to obtain numerical results (Remorov

470 and Bardwell, 2005). Grand canonical Monte Carlo (GCMC) simulations account for density

471 fluctuations at fixed volume and temperature and represents the preferred choice for the

472 investigation of interfacial phenomena (Croteau et al., 2009; Collignon et al., 2005). A theoretical

473 approach to the description of the electronic structure of molecules adsorbed on solid surfaces and

474 surface reactions is the embedded cluster theory (ECT) (Whitten, 1993). This allows ab initio

475 calculations of molecular properties of the lattice-absorbate system. The dipped adcluster model

476 (DAM) is applied to study chemisorption and surface reactions in which an adcluster (admolecule

477 + cluster) is dipped onto the electron bath of a solid metal (Nakatsuji, 1987). This treatment allows

478 to derive adsorption energies (Hu and Nakatsuji, 1999).

479

480 **3.2 Atmospherically Relevant Gas-Substrate Systems**

481 **Gas Adsorption by Solid Substrates.** Gas adsorption and desorption is important when

482 describing the reactivity between trace gases and solid interfaces in terms of removal rates and

483 gas-particle partitioning (Kolb et al., 2010; Pöschl et al., 2007). It also constitutes a significant

484 removal process of gaseous organic compounds by partitioning between gas and solid phases

485 (Goss and Eisenreich, 1996, 1995a; Goss, 1993). Mineral dust particles are the most abundant

486 aerosol particles globally by mass, providing ample solid surface area for adsorption of gasous

487 species (Usher et al., 2003; Tang et al., 2016). Atmospheric soot particles also represent a solid

488 surface which allows for multiphase chemistry involving adsorption and reaction of atmospheric

489 oxidants (Pöschl et al., 2001; Shiraiwa et al., 2009; Kaiser et al., 2011; Springmann et al., 2009),

490   though soot can be complex consisting of solid graphite structures coated by organic carbon, the

491   latter being amorphous or soft in nature (Bond et al., 2013; China et al., 2013; Cappa et al., 2012).

492   Also, amorphous solid organic particles (Virtanen et al., 2010; Koop et al., 2011b; Shiraiwa et al.,

493   2017a) provide solid substrates that serve as adsorption and reactive sites for trace gas species

494   (Knopf et al., 2018; Slade et al., 2017; Slade and Knopf, 2014, 2013; Houle et al., 2018; Hearn

495   and Smith, 2007; Lakey et al., 2016; Berkemeier et al., 2016; Steimer et al., 2015; Shiraiwa et al.,

496   2011a; Li and Knopf, 2021; Li et al., 2020).

497   In the atmosphere, adsorbing trace gases including oxidants, radicals, and VOCs compete with

498   adsorbing water for substrate surface sites. A mineral dust surface is usually hydroxylated and

499   covered by a monolayer of water at about 20-30% relative humidity (Usher et al., 2003; Tang et

500   al., 2016; Goss, 1994a). Adsorption of water by mineral dust is also crucial for our understanding

501   of the ability of dust particles to serve as CCN (Tang et al., 2016) and INPs (Kanji et al., 2017;

502   Knopf et al., 2018; Knopf and Koop, 2006; Hoose and Möhler, 2012; Knopf and Alpert, 2023).

503   Since water vapor is abundant in our environment, adsorption of a reactive or non-reactive gas

504   species will likely always proceed in competition with co-adsorbing water molecules (Kaiser et

505   al., 2011; Springmann et al., 2009). Reactive uptake of O_3 and OH radicals by insoluble organic

506   aerosol surfaces has been shown to decrease as humidity increases, following a Langmuir-

507   Hinshelwood mechanism, where water vapor co-adsorbs and competes for surface sites (Pöschl et

508   al., 2001; Slade and Knopf, 2014). Condensation of water may lead to dissolution of soluble gas

509   species and coating material on top of solid substrates, e.g., present as an aqueous organic coating

510   on soot (Charnawskas et al., 2017). Those cases should then be considered as a solid substrate

511   covered by a liquid layer and adsorption or uptake processes should be treated as proceeding on a

512   liquid substrate. Tables A1-A7 present a compilation of E_{des}^0 and other molecular parameters for

513   a selection of atmospherically relevant reactive and non-reactive trace gases interacting with

514   various solid substrates serving as surrogates of aerosol particles.

515

516   **Gas Adsorption by Ice.** Ice is among the most abundant solid materials on the Earth's surface.

517   Roughly 50% of the northern hemisphere landmass is covered by ice and snow in winter (Bartels-

518   Rausch, 2013). Adsorption and desorption of trace gases on ice impact gas-phase chemistry in the

519   stratosphere and upper troposphere (Solomon, 1999; Borrmann et al., 1996; Voigt et al., 2006;

520   Huthwelker et al., 2006), snow chemistry and boundary layer gas-phase chemistry over perennial

521   and permanent snowpacks and gas-phase chemistry above sea-ice (Bartels-Rausch et al., 2014;

522   Artiglia et al., 2017; Raso et al., 2017; George et al., 2015; Mcneill et al., 2012; Abbatt et al., 2012;

523   Jeong et al., 2022; Mcnamara et al., 2021). Partitioning of gases to ice in polar and high-alpine

524   snow also result in signals in ice cores used to reconstruct past climates and environmental

525   conditions (Vega et al., 2015). In comparison to other solid materials, ice is a high-temperature

526   material existing in the environment at temperatures relatively close to its melting point. As in

527   other molecular solids this leads to surface premelting and thus a disordered interface, also referred

528   to as quasi-liquid layer, the properties of which are a matter of ongoing debate (Bartels-Rausch et

529   al., 2014; Asakawa et al., 2016; Cho et al., 2002; Slater and Michaelides, 2019). Since this layer

530   is the interface with which adsorbing gases interact, the mutual interplay between the properties

531   of the disordered interface and the nature of the interaction of gases have spurred speculations

532   about whether it should be treated as a thin aqueous solution layer or a purely solid surface. Recent

533   spectroscopic evidence indicates that soluble gases form solvation shells similar as in liquid water

534   without, however, modifying the remaining ice structure significantly (Bartels-Rausch et al.,

535   2017). Thus under typical atmospherically relevant conditions with low coverages of volatile

536   gases, the surface remains dominated by the properties of ice. A template for this may be the case

537   of HCl adsorption on ice (Huthwelker et al., 2006), for which singly hydrogen bonded HCl is

538   adsorbed at the outermost surface (Kong et al., 2017), while upon hydration and dissociation,

539   chloride enters deeper into the interface (Zimmermann et al., 2016; Mcneill et al., 2007; Mcneill

540   et al., 2006). This is in accord with a low desorption energy and thus low coverage with molecular

541   HCl (Table A8). This behavior can mask the weak temperature dependence of the total coverage

542   by HCl (molecular and dissociated). Similar conclusions come from MB experiments, e.g., with

543   NO_y compounds, where the desorption kinetics are characterized directly (Lejonthun et al., 2014).

544   An exception may be the case of H_2O itself, where the MB experiments may not have been able

545   to resolve singly hydrogen bonded H_2O desorbing, but only completely hydrated ones desorbing

546   more slowly (Kong et al., 2014b; Kong et al., 2014a). Therefore, adsorption on ice may well be

547   considered as adsorption within the simplified scheme adopted in this work even for very soluble

548   and more straightforwardly for less soluble molecules. Table A8 summarizes the thermodynamic

549   literature data on gas species adsorption by ice substrates applied in this study.

550

551   **Gas Adsorption by Water and Aqueous Solutions**. Liquid water and aqueous solutions are a

552   dominant form of condensed matter in the environment including aerosol particles, clouds, or

553   ocean surfaces. In aerosol particles, aqueous solutions may range from dilute solutions at very high

554   humidity and at or close to the point of activation into a cloud droplet to very concentrated

555   supersaturated solutions at low relative humidity. High solute strength solutions may yield highly

556   viscous, semi-solid and glassy particle phase states occuring throughout the atmosphere (Shiraiwa

557   et al., 2017a; Koop et al., 2011b; Mikhailov et al., 2009; Zobrist et al., 2008; Klassen et al., 1998).

558   Decreasing bulk diffusivity in these viscous phases increases the relative importance of the

559   desorption lifetime as exchange with the bulk is retarded (Behr et al., 2009; Knox and Phillips,

560   1998; Li and Knopf, 2021) (see Eq. (4)).

561   The notion that adsorbed molecules on liquid surfaces represent a distinct feature comes from

562   both spectroscopic and kinetic evidence. MB experiments of HCl on deuterated sulfuric acid

563   clearly identified collision-, adsorption-, and desorption trajectories (Behr et al., 2001; Morris et

564   al., 2000; Gao and Nathanson, 2022), as a direct and unique manifestation of Langmuir's view of

565   adsorption (Langmuir, 1918). The time the HCl molecule spends on the surface is directly related

566   to E_{des}^0 and A_{des}. In other cases studied by the MB technique, the picosecond scale hydrogen bond

567   exchange dynamics and fast diffusion (nanoseconds – microseconds for diffusion into and out of

568   depths of several nanometers) prevented unambiguous separation of pure desorption from

569   trajectories including entry into the liquid (Ringeisen et al., 2002a, b; Brastad et al., 2009; Faust

570   and Nathanson, 2016; Faust et al., 2016; Faust et al., 2013). A comparable situation as for HCl has

571   been documented through the MB technique for N_2O_5 (Shaloski et al., 2017). Later high-level

572   theory work established the interaction of this important trace gas with the hydrogen bonding

573   network of water that then subsequently controls hydrolysis (Cruzeiro et al., 2022; Galib and

574   Limmer, 2021). Similar conclusions about adsorption – desorption trajectories in the case of

575    $H_2O(g)$ on liquid water may be drawn from different isotope exchange kinetics for HDO with H_2O

576   and $H_2^{18}O$ with H_2O that require different degrees of hydration on the water surface (Davidovits

577   et al., 2011, 2006). The suggestion that a distinct population of H_2O molecules exists that is singly

578   hydrogen bonded at the liquid water surface comes from detailed interpretation of IR spectra in

579   line with theory (Devlin et al., 2000). The high vapor pressure of environmentally relevant liquids

580   and other difficulties (including those related to fast exchange with the bulk liquid) prevent direct

581   determination of desorption kinetics for many relevant trace gas – substrate pairs. In spite of this

582   situation, we suggest to apply the same concept of converting desorption energies (derived from

583   partitioning or chromatographic methods) into desorption lifetimes as for solid surfaces.

584   The fact that molecules at the aqueous solution or liquid water – air interface experience a

585   different environment than in the bulk liquid is straightforward. The density drops over molecular

586   length scales and the hydrogen bond dynamics and orientation in water and aqueous solutions on

587   average lead to a strongly asymmetric environment at the interface (Brini et al., 2017; Ahmed et

588   al., 2021; Hao et al., 2022). The extension of the interface depends on the type of solutes and

589   adsorbates present, as molecules with larger hydrophobic moieties or when charges are present at

590   the adsorbate interacting with solute ions, which may establish a larger interfacial thickness (Brini

591   et al., 2017; Zhao et al., 2020). The asymmetric environment at the interface leads to specific

592   molecular interaction options (as described above) and in turn to specific binding energies as result

593   of these. Changes to the equilibrium surface tension of aqueous solutions in response to adsorption

594   of gases is the consequence of the changes in the surface free energy. Its temperature dependence

595   is reflecting the energy gain as a result of the sum of these interactions. Tables A9 to A15 are a

596   compilation of E_{des}^0 for a range of inorganic and organic trace gases on pure water or on aqueous

597   solutions. The simplest case $H_2O(g)$ on $H_2O(l)$, exhibits a single hydrogen bond and a

598   corresponding low E_{des}^0 value. Among the given families of species, interaction energies scale with

599   molar mass or the degree of substitution with functional groups that alter the amount of weak or

600   strong molecular interactions. The degree of substitution may be represented by the dipole moment

601   (μ) and *O:C* for organic molecules as outlined in the discussion of paramaterized E_{des}^0. The

602   presence of hydrophilic functional groups with strong hydrogen bonding interaction options leads

603   to correspondingly larger E_{des}^0. Since these groups also interact with the hydrogen bonding

604   network of water, these interactions are sensitive to the presence of other solutes or, especially,

605   ions (Demou and Donaldson, 2002; Lee et al., 2019; Ohrwall et al., 2015; Ekholm et al., 2018).

606

607   **4. Impact of Desorption Lifetime on Gas Uptake**

608   To assess the impact of τ_{des} on multiphase chemical kinetics, the kinetic multi-layer models of

609   aerosol surface and bulk chemistry (K2-SURF, KM-SUB) are applied (Shiraiwa et al., 2010;

610   Shiraiwa et al., 2009). These models are based on the PRA framework (Ammann and Pöschl, 2007;

611   Pöschl et al., 2007) and describe the gas-particle interface by implementation of several model

612   compartments and molecular layers in which species can undergo mass transport and chemical

613   reactions. Here, the compartments included are: gas phase, near-surface gas phase, sorption layer,

614   quasi-static surface layer, and a number of bulk layers.

615   Gas-phase diffusion of a species X from the gas phase to the near-surface gas-phase surrounding

616   the particle is treated by the net flux of gas-phase diffusion:

617      $$J_{g,X} = 2\pi(d_p + 2\lambda D_g([X]_g - [X]_{gs}) , \qquad (10)$$

618   where d_p is the particle diameter, λ is the mean free path, D_g is the gas diffusivity and $[X]_g$ and

619      $[X]_{gs}$ are concentrations of X in the gas and near-surface gas phases, respectively (Pöschl et al.,

620   2007; Knopf et al., 2015; Li et al., 2018). The mass balance and rate equation for X in the near-

621   surface gas phase can be described as:

622      $$\frac{d[X]_{gs}}{dt} = \frac{J_{g,X} - (J_{ads,X} - J_{des,X})A_s}{V_{gs}} , \qquad (11)$$

623   where A_s is the particle surface area and V_{gs} is the volume of the near-surface gas phase. $J_{des,X}$ is

624   the desorption flux defined as $J_{des,X} = k_{des,X}[X]_s = \tau_{des,X}^{-1}[X]_s$. $J_{ads,X}$ is the adsorption flux defined

625   as $J_{\text{ads,X}} = \alpha_{\text{s,X}} J_{\text{coll,X}}$, where $\alpha_{\text{s,X}}$ repesents the surface accommodation coefficient, and the

626   collision flux is defined as $J_{\text{coll,X}} = \frac{1}{4} \omega_{\text{X}} [X]_{\text{gs}}$ with ω_{X} being the mean thermal velocity of X.

627   The surface-layer reaction (SLR), involving only the adsorbed species, X(s), or components of

628   the quasi-static layer, Y(ss), such as X(s) + Y(ss) → products, is described by the second-order

629   rate coefficient k_{SLR}. The surface reaction rate is described as $L_{\text{s}} = k_{\text{SLR}}[X]_{\text{s}}[Y]_{\text{ss}}$. The mass

630   balance and rate equations for X in the near-surface gas phase and at the surface can be described

631   as below:

632      $\frac{d[X]_{\text{s}}}{dt} = J_{\text{ads,X}} - J_{\text{des,X}} - L_{\text{s}} - J_{\text{s,b,X}} + J_{\text{b,s,X}}$,   (12)

633   where $J_{\text{s,b,X}}$ and $J_{\text{b,s,X}}$ are the fluxes from the surface to the near-surface bulk and from the near-

634   surface bulk to the surface of X, respectively ($J_{\text{s,b,X}} = J_{\text{bsb,X}} = 0$ in the absence of bulk diffusion),

635   and treated as a function of the bulk diffusion coefficient. The reactive uptake coefficient, γ, is

636   usually the experimentally accessible parameter and the one used in atmospheric modeling studies.

637   γ of a gas species X is defined as

638      $\gamma_{\text{X}} = \frac{J_{\text{ads,X}} - J_{\text{des,X}}}{J_{\text{coll,X}}}$.   (13)

639

640   **Simulation of reactive gas uptake by solid substrates.** We apply the kinetic double-layer model

641   of aerosol surface chemistry (K2-SURF; (Shiraiwa et al., 2009)) to investigate the sensitivity of γ

642   to the desorption lifetime for a solid substrate. The surface reaction of an adsorbed species X with

643   condensed species Y is considered, while surface-bulk exchange and bulk diffusion and reaction

644   are not considered for simplicity. The α_{s} on an adsorbate-free substrate is assumed to be one for

645   all simulations. Figure 2 shows the dependence of γ on τ_{des} and k_{SLR} at constant temperature. γ

646   values represent steady-state values. Higher k_{SLR} leads to higher γ at fixed τ_{des} due to faster

647   surface reaction rates. At fixed k_{SLR}, longer τ_{des} leads to higher surface concentrations of X, and

648   consequently to higher surface reaction rates and γ. In turn, with sufficiently long residence times

649   of the adsorbed gas species, low k_{SLR} can still lead to high values of γ. It is evident that different

650   pairs of τ_{des} and k_{SLR} can yield the same γ value. Furthermore, when k_{SLR} is known, uncertainties

651   in τ_{des} can result in large differences in γ. This exercise demonstrates that experimentally derived

652   γ values do not sufficiently constrain the heterogeneous reaction process to yield unambiguous

653   τ_{des} and k_{SLR} values, unless a significant parameter space is covered by the experiment to constrain

654   them individually. For instance, at large enough gas phase partial pressure the surface gets

655   saturated (fully covered by the adsorbate), which leads to decoupling of τ_{des} and k_{SLR} (Knopf et

656   al., 2011; Artiglia et al., 2017; Berkemeier et al., 2016; Steimer et al., 2015). However, this is often

657   not possible due to technical constraints. Therefore, constraining τ_{des} by application of E^0_{des}, or

658   best estimates of E^0_{des}, can significantly improve our molecular understanding of the underlying

659   processes in multiphase chemical kinetics and support the development of parameterizations for

660   modelling purposes.

661   Figure 3 displays the temperature dependence of γ with E^0_{des} of 30 – 50 kJ mol^{-1}. The pre-

662   exponential frequency factor A_{des} was set to 10^{13} s^{-1} and k_{SLR} was set to (a) 10^{-12} and (b) 10^{-9} cm^2

663   s^{-1}. Temperature dependence of k_{SLR} was not considered in these simulations to evaluate only the

664   effects of temperature-dependent τ_{des} on γ. The modeling results suggest that γ depends strongly

665   on temperature, where lower temperatures yield higher γ values. This is because lower

666   temperatures lead to longer τ_{des} and hence higher surface concentrations of X and reaction rates.

667   Generally, γ is more temperature-dependent at higher values of E^0_{des}. However, if E^0_{des} is close to

668   values typical for chemisorption (~50 kJ mol^{-1}), γ is close to 1 in this calculation. Further away

669   from this special case and natural cap of $\gamma = 1$, γ increases by about two orders of magnitude over

670   a temperature range of 80 K. These modeling results indicate that extrapolating multiphase

671   chemical kinetics acquired at room temperature to lower temperatures, can result in significantly

672   different reactive uptake coefficients. Clearly, a detailed understanding of the molecular processes

673   is necessary when applying multiphase reaction kinetics to environmental and atmospheric

674   conditions.

675   Even though the above simulations clearly suggest potentially large effects of the temperature

676   dependence of τ_{des} on γ, surface reaction rate coefficients are also temperature dependent which

677   in turn affect γ as well (Li and Knopf, 2021; Li et al., 2020). To further investigate the role of

678   temperature on heterogeneous reaction kinetics, we apply the K2-SURF model to heterogeneous

679   reactions between O_3 and polycyclic aromatic hydrocarbons (PAHs) adsorbed on soot. This

680   reaction proceeds with a multi-step Langmuir-Hinshelwood mechanism that includes I) O_3

681   physisorption, II) decomposition of O_3 into long-lived reactive oxygen intermediates (ROIs, O

682   atoms), and III) reactions of O atoms with PAHs (Shiraiwa et al., 2011b):

683   I. $O_3(g) \leftrightarrow O_3(s)$ $E_{\text{des}}^0 = 10, 20, 30, 40, 50$ kJ mol^{-1}

684   II. $O_3(s) \rightarrow O + O_2$ $E_{\text{a,pc}} = 40$ kJ mol^{-1}

685   III. $O + Y \rightarrow$ products $E_{\text{ox}} = 80$ kJ mol^{-1}

686   The activation energy for physisorbed O_3 to dissociated into chemisorbed O ($E_{\text{a,pc}}$) is ~40 kJ mol$^-$

687   ^{1} and the activation energy for O reacting to oxidation products (E_{ox}) is ~80 kJ mol^{-1} (Berkemeier

688   et al., 2016; Shiraiwa et al., 2011b). Temperature dependence of the reaction rate coefficients of

689   reactions II and III are considered using an Arrhenius equation. We examine the response of this

690   reaction system to changes in initial E_{des}^0 of O_3 (reaction I) and temperature.

691   Figure 4 shows the results of such simulations. Higher E_{des}^0 yields higher surface concentrations

692   of physisorbed O_3, and hence higher concentrations of O and reaction rates, yielding higher γ

693   values. γ decreases as temperature decreases, which is in contrast to above sensitivity studies

694   shown in Fig. 3. This is because the overall temperature dependency of the gas uptake is mostly

695   determined by the temperature dependency of the rate-limiting reaction III and also influenced by

696   thermally-activated chemical reaction II. Although physisorbed O_3 molecules can reside

697   significantly longer on the PAH surface at lower temperatures, the decrease in the formation rate

698   of ROIs and subsequent oxidation reaction rate govern γ, suggesting lower γ values at lower

699   temperatures.

700   Clearly, E^0_{des} and activation energies for chemical reactions are crucial parameters to predict

701   multiphase chemical kinetic processes under tropospheric conditions. Conducting temperature-

702   dependent reactive uptake experiments of known reaction systems can be used to determine

703   coupled desorption lifetimes and reaction rates (e.g., Kerbrat et al., 2010; Li and Knopf, 2021).

704   For example, *Li and Knopf* (2021) measured the reactive uptake of OH radicals by triacontane for

705   temperatures between 213 and 293 K. By having a temperature-dependent multiphase kinetics data

706   set, E^0_{des} and k_{SLR} could be decoupled and individually assessed.

707

708   **Non-reactive gas uptake into liquids.** To demonstrate the effect of τ_{des} on the equilibration

709   timescale of non-reactive gas uptake by a liquid substrate, the kinetic multi-layer model for aerosol

710   surface and bulk chemistry (KM-SUB) (Shiraiwa et al., 2010) was applied (Fig. 5). We simulate

711   non-reactive uptake of species X with a constant gas-phase concentration of 1 ppb into a particle

712   with 100 nm diameter that initially contains no amount of X. The Henry's law constant of X was

713   set to be 1×10^{-5} mol cm^{-3} atm^{-1} at 298 K and its temperature dependence was considered using the

714   van't Hoff equation with a solvation enthalpy of 20 kJ mol^{-1}; these values are chosen to be

715   comparable with ozone solvation into water (Sander, 2015, 2023). The temperature dependence of

716   the Henry's law constant is shown in Fig. S1. The particle is assumed to be liquid with a

717   temperature-dependent bulk diffusion coefficient following the parameterization of Zobrist *et al.*

718   (2011) for pure water, which varies from $2\times10^{-5} - 2\times10^{-6}$ cm^2 s^{-1} in this temperature range. E^0_{des}

719   values in the range of $10 - 80$ kJ mol^{-1} were used, and the temperature dependence of τ_{des} was

720   considered using the Frenkel equation (see Eq. (1) and Fig. 1). Here, X can be regarded as a small

721   molecule with moderate water solubility such as ozone for the simulations at low E^0_{des}, or a

722   carboxylic acid with similar water solubility (e.g., nonanoic acid) for the simulations at high E^0_{des}.

723   The equilibration time is defined as the time after which the surface and particle bulk

724   concentrations deviate by less than a factor of 1/e from their equilibrium or steady-state value.

725   The simulations show that equilibration times can vary over many orders of magnitude in the

726   investigated range of E^0_{des} (Fig. 5). For $E^0_{des} < 30$ kJ mol^{-1}, the timescales of surface equilibration

727   (black solid lines) are shorter than the timescale of bulk equilibration (blue dashed lines). The

728   convergence of the blue lines at low E^0_{des} (< 30 kJ mol^{-1}) reflects the kinetic limitation of gas-

729   particle equilibration by diffusion inside the particle bulk (2×10^{-7} s^{-1}; (Shiraiwa et al., 2011a)). At

730   higher E^0_{des}, the increase of desorption lifetime leads to the increase of the equilibration times, as

731   a larger amount of X is needed to saturate the surface; in fact, at $E^0_{des} \geq 15$ kJ mol^{-1}, the majority

732   of molecules reside on the surface and the partitioning is governed by the surface processes in this

733   simulation.

734   In the range of E^0_{des} around 40 to 60 kJ mol^{-1}, surface and bulk equilibration times coincide, as

735   the simulated 100 nm particles are well-mixed and non-reactive uptake is limited by interfacial

736   transport from the gas phase. The flattening and convergence of the black lines at $E^0_{des} > 60$ kJ

737   mol^{-1} reflects the kinetic limitation of gas-particle equilibration by interfacial transport (surface

738   adsorption and surface-bulk exchange) if the surface gets fully covered by the adsorbate. The bulk

739 equilibration (blue lines) and thus also the overall gas-particle equilibration time still increase for

740 $E_{des}^0 > 60\,kJ\,mol^{-1}$ with decreasing temperature, because interfacial transport is slowed by the high

741 surface propensity of X and its full surface coverage. Note that the slowing of bulk equilibration

742 time as a consequence of sorption layer coverage is a direct consequence of using a Langmuir

743 adsorption model. In case of multilayer adsorption and bulk condensation, especially at high E_{des}^0,

744 results may differ, which will be explored in follow-up studies (see also Sect. "Gas-particle

745 Partitioning of Secondary Organic Aerosol"). Also note that the increased surface propensity of X

746 with increasing E_{des}^0 is not a general rule, but a consequence of the fixed Henry's law solubility

747 coefficient in this sensitivity study.

748 The calculations for Fig. 5 represent an open system in which the gas-phase concentration of X

749 is held constant. *Wilson et al.* (2021) investigated equilibration timescales for gas uptake of PAHs

750 on soot surfaces in the closed system, i.e., where a fixed amount of X is distributed between the

751 gas and particulate phases. In that study, equilibration timescales were either controlled by the

752 adsorption or by the desorption process, depending on whether the particle surface was under- or

753 oversaturated with X at the start of the model simulations, respectively. Temperature strongly

754 influenced equilibration timescales in the desorption-controlled regime, whereas particle number

755 concentrations influenced adsorption-controlled systems. Note that in the presence of chemical

756 reactions in the gas phase or on the surface, the partitioning equilibrium can be perturbed and adopt

757 a quasi-stationary state that differs from thermodynamic equilibrium.

758 For reactions occurring in liquids, the same features apply as for the case of surface reactions on

759 solids, i.e., the temperature dependence of an activated reaction may counteract the temperature

760 dependencies of desorption and solubility, e.g., for the reactions on sulfuric acid aerosol of HCl

761 with HONO (Longfellow et al., 1998; Ammann et al., 2013) or with $ClONO_2$ (Shi et al., 2001).

762   These cold and viscous sulfuric acid aerosols, but also viscous aqueous organic aerosols are also

763   at the same time high solute strength systems. The situation then is very complex since viscosity

764   is modulated by temperature and humidity, thereby impacting diffusion and salting out effects, and

765   thus, ultimately, solubility and kinetics (Edebeli et al., 2019; Li and Knopf, 2021; Li and Shiraiwa,

766   2019).

767

768   **5. Derivation of a Parameterization of the Desorption Energy**

769   Thermodynamic and chemical parameters given in Tables A1-A15 provide the basis to derive

770   E_{des}^0 estimates for application in multiphase chemical kinetics involving atmospheric gas species

771   and aerosol particles. This analysis includes over 500 gas species-substrate systems. As discussed

772   above, we note the underlying caveats in this analysis. The pre-exponential factor is set to 10^{13} s$^-$

773   ^{1}. The dependence of E_{des}^0 on absorbate model and surface coverage is neglected. Thus, a highly

774   accurate prediction of E_{des}^0 is not possible. However, the goal here is to provide a best estimate of

775   E_{des}^0 in agreement with this training data set (Tables A1-A15) to enable improved analyses of

776   environmental multiphase chemical kinetics under the wide range of thermodynamic conditions

777   encountered in the Earth's environment. Furthermore, it would be desirable to predict E_{des}^0 from

778   commonly measured and accessible parameters, e.g., derived by mass spectroscopy, such as molar

779   mass, molecular structure, and oxidation state.

780   Following our previous discussion on the intermolecular bonding between adsorbate and

781   substrate, gas species polarizability, α, should serve as predictor of E_{des}^0. Larger α should, in

782   general, coincide with an increase in E_{des}^0. The oxidation state of an organic gas species,

783   represented in a simplified way by the ratio $O:C$, reflects the number of oxygenated functional

784   groups, typically monitored by mass spectrometry (Isaacman-Vanwertz et al., 2018). An increase

785   in the gas species' oxidation state should also yield an increase in E_{des}^0. Figure 6 displays a

786   multilinear regression analysis using all available data including solid, ice, and liquid substrates

787   (Tables A1-A15) to derive a relationship between E_{des}^0, α, and $O:C$. Figure S2 depicts the same

788   data in more detail as two separate plots. Figure 6 indicates that E_{des}^0 increases with increasing α

789   and $O:C$, as one would expect from considerations of intermolecular bonding discussed above.

790   This is also corroborated by a principal component analysis given in Fig. S3, showing significant

791   correlation between E_{des}^0 and α. The regression analysis yields the following model (with an $R^2 =$

792   0.559 and a root mean squared error (RMSE) = 25.4):

793        $$E_{des}^0(\alpha, O:C) = 25.895 + 2.330\alpha + 12.367(O:C) \,, \qquad\qquad (14)$$

794   where E_{des}^0 is in units kJ mol^{-1}and α is in units 10^{-24} cm^3.

795   Figure 7 shows α as a function of molar mass and $O:C \leq 1$. Note that the few data for the three

796   gas species with $O:C \geq 1$, namely CO_2 (Tabe A3), formic acid (Table A7), and, peroxyacetyl

797   nitrate, PAN (Table A8) are colored as $O:C = 1$ for better visibility of the overall training set.

798   Figure 6 shows the few data points for $O:C > 1$. The data show a strong linear correlation between

799   α and M, where $O:C$ appears to play a less significant role. This can be understood by realizing

800   that a carbon atom in a molecule contributes three times more to α than an oxygen atom (Bosque

801   and Sales, 2002), discussed in more detail below. Hence, the number of methylene groups can

802   dominate α for larger molecules. Thus, the polarizability can be described, applying regression

803   analysis, as a linear function of molar mass ($R^2 = 0.952$ and RMSE = 2.765):

804        $$\alpha(M) = -0.837 + 0.128M \,, \qquad\qquad (15)$$

805   where M is in units g mol^{-1}. The linear regression is shown as a red line in Fig. 7.

806   We can now combine Eqs. (14) and (15) to obtain a parameterization to calculate E_{des}^0 from

807   knowledge of the gas species' molar mass and $O:C$:

808 $$E_{\mathrm{des}}^0(M, O{:}C) = 25.895 + 2.330(-0.837 + 0.128M) + 12.367(O{:}C) . \qquad (16)$$

809   Figure 8 shows E_{des}^0 values derived from Eq. (16) using M and $O{:}C$ values given by the training

810 datasets as input. Similarly to Fig. 7, we have color-coded $O{:}C$ for values up to one for better data

811 visibility. Figure S4 shows E_{des}^0 values derived from the training data set separated by different

812 substrate types corroborating the correlation displayed in Fig. 8. Figure S5 shows E_{des}^0 values

813 derived from Eq. (16) using arbitrary M and $O{:}C$ values. For application of inorganic gas species

814 with $C = 0$, $O{:}C$ should be set to zero. E_{des}^0 shows a linear relationship with M where deviation

815 from linearity is only found at $M < 250$ g mol^{-1}. Figure 8B demonstrates that gas species with

816 larger $O{:}C$ show larger E_{des}^0. To understand this trend in the data, we have to address the role of

817 the gas species' dipole moment and substrate in the derivation of the E_{des}^0 values. Equation (16)

818 provides estimates of E_{des}^0 without specifically addressing substrate properties. As discussed, its

819 dependency solely on M and $O{:}C$ is advantageous for application to complex gas species-particle

820 composition data. Considering the underlying uncertainties due to unknown applied standard

821 states, absorbate model, and assumed pre-factor, this parameterization is accurate within those

822 limits. However, one would expect that gas species' μ and the substrate's ε_{r} impact E_{des}^0.

823   We recommend application of this parameterization (Eq. (16)) for gas species with $O{:}C \lesssim 1$.

824 Due to the few data points at $O{:}C \gtrsim 1$, E_{des}^0 could be significantly under- or overestimated in this

825 range. For example, for CO_2 (Table A3), tabulated $E_{\mathrm{des}}^0 = 16.4$ kJ mol^{-1}, while the parameterization

826 yields 61.8 kJ mol^{-1}. In the case of formic acid (Table A7), the tabulated $E_{\mathrm{des}}^0 = 94.6$ kJ mol^{-1},

827 while the parameterization yields 62.4 kJ mol^{-1}. Hence, when applying Eq. (16) to gas species with

828 $O{:}C \gtrsim 1$, considering additional information or constraints is recommended.

829   For our data set, the principal component analysis in Fig. S3 indicates no strong correlation

830 between ε_{r} and E_{des}^0. Fig. 9 corroborates the negligible dependence of E_{des}^0 on ε_{r}. However, one

831   would expect that greater μ, α, and ε_r result in larger E_{des}^0 due to enhanced molecular interactions.

832   The derivation of our parameterization exploited the strong dependency of E_{des}^0 on α. We suggest

833   that the underlying reason for this dependency is the competing effects of μ and α on E_{des}^0 as

834   outlined below.

835   Small molecules with polar groups can exert significant dipole moments while the polarizability

836   is still small. As depicted in Fig. S6, smaller molecules exert greater μ while $O:C$ values are high

837   and α is low (see also Fig. 7). Note that alkanes and PAHs in the data set, following common

838   convention, have zero dipole moments. Gas species with greater μ may interact more strongly with

839   polarizable substrates expressed by ε_r, yielding larger E_{des}^0. However, as the gas molecules become

840   larger, their α increases, e.g., by the addition of methylene groups (Bosque and Sales, 2002),

841   thereby dominating over the impact of μ on E_{des}^0. Figure S2 supports this trend where molecules

842   with largest α have low $O:C$ and small μ. Hence, this data set yields a negative correlation between

843   μ and α. As a consequence, for larger molecules the role of the molecule's μ interacting with the

844   substrate becomes less important. Thus, in a way, the range of available desorption data could be

845   responsible for the negligible correlation between E_{des}^0 and substrate ε_r (Fig. 9). In other words,

846   polarizability α, which is strongest for molecules with small μ and low $O:C$, compensates and

847   dominates the impact of the dipole moment on E_{des}^0 and, in turn, renders the substrate of less

848   importance for parameterizing E_{des}^0. This is also evident in Fig. 10, where the scatter of

849   parameterization-derived E_{des}^0 values is largest for molecules with lower M and lower α. We can

850   attribute the scatter in E_{des}^0 at lower M to the competing contributions of the gas species' μ, here

851   accounted by $O:C$ and α. These may be the reasons why E_{des}^0 can be reasonably parameterized

852   from our data set without accounting for the substrate's ε_r and gas species' μ. Though, we would

853   expect with more available data, the role of gas species' μ and substrate's ε_r to likely be resolved

854   in a parameterization.

855   Considering the significant number of data and omission of substrate specific properties in the

856   parameterization, the scatter in E_{des}^0 is not very large. This suggests that this parameterization can

857   serve as a reasonable first estimate of E_{des}^0 for a complex environmental substrate such as an

858   aerosol particle. We would expect that with increasing number of desorption data that include

859   larger molecules with larger $O{:}C$ or μ and applied known standard states and absorbate models,

860   the scatter in E_{des}^0 at lower molar masses can be resolved.

861

862   **Relationship Between Desorption Energy and Enthalpy of Vaporization.** To examine the

863   relationship between E_{des}^0 and ΔH_{vap}, we have plotted the data given in supplemental tables (not

864   the parameterized values) separated for the different substrate types in Fig. 11. Our data supports

865   a positive correlation between E_{des}^0 and ΔH_{vap}, where E_{des}^0 for most instances is larger than ΔH_{vap}.

866   The role of $O{:}C$ in the relationship between E_{des}^0 and ΔH_{vap} is not clearly identifiable for the cases

867   that include all, solid, and ice substrates data. However, for liquid substrates, the data suggest that

868   for given ΔH_{vap}, larger $O{:}C$ yields larger E_{des}^0. Figure S7 provides a linear regression model for

869   the case of liquid substrates. As shown above, larger $O{:}C$ correlates with a larger μ, which may

870   exert a greater impact on E_{des}^0 in the case of a liquid substrate. In fact, the interaction strength at

871   the surface often exceeds the enthalpy of condensation between gas and its condensed liquid for

872   the same species family, e.g., in the case of methyl-substituted benzenes (Raja et al., 2002; Bruant

873   and Conklin, 2002), but also for other species like alcohols, acids, amines and ketones (Mmereki

874   et al., 2000) and alkanes (Goss, 2009) and halogenated alkanes (Bruant and Conklin, 2001). This

875   indicates that the aqueous solution – air interface allows for a two-dimensional environment in

876   which the intermolecular interactions are as important as in the bulk condensed phase of the

877   adsorbate alone (Valsaraj, 1988a, 2009).

878

879   **Relationship Between Desorption Energy and Enthalpy of Solvation for Aqueous**

880   **Substrates.** To examine the relationship between E_{des}^0 and ΔH_{solv}, we have plotted the data for

881   liquid substrates, consisting mostly of water and few aqueous solutions (Tables A9 to A15) in Fig.

882   12. Despite the scatter in the data, a positive correlation between E_{des}^0 and ΔH_{solv} can be identified.

883   The data falls symmetrically around the 1:1 line, indicating no strong bias. In the case of liquid

884   substrates, the correlation between E_{des}^0 and ΔH_{solv} is comparable to that observed between E_{des}^0

885   and ΔH_{vap} (Fig. 11c). Figure S8 provides a linear regression model for the data shown in Fig. 12.

886   The relationship between E_{des}^0 and ΔH_{solv} shown in Fig. 12 can be understood in the following

887   way. For large non-polar molecules, the free energy cost of entering the aqueous solution is mostly

888   driven by enthalpic changes, because hydrogen bonds need to be disrupted to form a cavity around

889   the molecule (Kronberg, 2016; Valsaraj, 1988a; Brini et al., 2017). The surface energy in that

890   cavity is then driven by the surface energy of pure water and the hydrophobic interactions with the

891   solute (Chandler, 2005). This is then somewhat similar to the situation when the same molecule is

892   adsorbed at the aqueous solution – air interface. Thus, for the larger non-polar molecules, the

893   contribution of the enthalpy of cavity formation can be identified as a dominating factor of the

894   solvation process, which in turn depends on the intermolecular strength between adsorbing

895   molecule and liquid. This, hence, can explain the correlation between E_{des}^0 and ΔH_{solv} for the case

896   of the non-polar molecules.

897   For small non-polar molecules, the transfer to the aqueous phase is mostly entropy-driven,

898   because the hydrogen bonds do not need to be disrupted but need to reorganize around the solute

899   (Kronberg, 2016; Shinoda, 1992, 1977; Hvidt, 1983; Brini et al., 2017). Polar molecules would be

900   comparable to ions, but also in this case, the size and charge distribution determine the cost of

901   solvation through the number and strength of hydrogen bonds to water, which lead to a correlation

902   of and ΔH_{solv} with the number of hydrophilic groups. The latter also determine E_{des}^0 (i.e., $O:C$

903   correlates with μ). Among the small organic molecules contained in Fig. 12, with the increasing

904   presence of hydrophilic functional groups, the larger $O:C$ ratios lead to larger E_{des}^0. For these

905   reasons, the relationship between E_{des}^0 and ΔH_{solv} shown in Fig. 12 supports the specific and

906   physical interaction model at the aqueous solution – air interface mentioned above: E_{des}^0 scales

907   with the magnitude of hydrophobic interactions for non-polar molecules and with the presence of

908   hydrophilic functional groups (i.e., $O:C$ correlates with μ) for polar molecules, and thus the

909   correlation with ΔH_{solv} is a logical consequence.

910   Note that since both E_{des}^0 and ΔH_{solv} are correlated, and are mostly independent of temperature

911   (Hildebrand and Scott, 1964) within the idealized concept presented here, the temperature

912   dependence of τ_{des} may apparently dominate the temperature dependence of solvation when

913    $E_{des}^0 > \Delta H_{solv}$. This idea of parallel behavior of desorption and solvation is also supported by a

914   very recent experimental study that provides in situ measurements of the uptake of gas-phase water

915   into ionic liquids at the gas-liquid interface using ambient pressure X-ray photoelectron

916   spectroscopy (Broderick et al., 2019). These measurements indicate that, dependent on water mole

917   fraction and temperature, solvation is governed by similar thermodynamics as relevant for crossing

918   the gas-liquid interface during the mass-transfer process (Broderick et al., 2019). The positive

919   correlation between the E_{des}^0 and ΔH_{solv} values displayed in Fig. 12 supports this notion, ascribing

920   the molecular interactions controlling τ_{des} and solvation an important role in the molecular

921   understanding of gas-substrate interactions.

922

6. Atmospheric Implications

923   **6. Atmospheric Implications**

924   The discussion in the above sections demonstrated the importance of accurate knowledge of E_{des}^0

925   for the representation of multiphase chemical reactions across various environmental interfaces

926   and phase states including aerosol particles. Analyses of experimentally conducted multiphase

927   chemical kinetics studies as well modeling the detailed processes that lead to the physicochemical

928   transformation of particles and define their atmospheric fate will greatly benefit from improved

929   estimates of E_{des}^0 (Su et al., 2020; Zheng et al., 2020; Shiraiwa et al., 2017a; Shiraiwa et al., 2017b;

930   Shrivastava et al., 2017b; Shrivastava et al., 2017a; Li and Knopf, 2021; Kaiser et al., 2011;

931   Springmann et al., 2009; Mu et al., 2018; Hems et al., 2021; Laskin et al., 2015). Below we discuss

932   further relevant atmospheric chemistry processes that connect to and/or make use of E_{des}^0 including

933   gas-particle partitioning, secondary organic aerosol (SOA) formation, indoor air chemistry, and

934   glass transition of OA particles.

935   **Gas-Particle Partitioning of Secondary Organic Aerosol.** Organic aerosol is ubiquitous,

936   consists of numerous chemical species, and represents a large mass fraction (20–90%) of the total

937   submicron particles in the troposphere (Nizkorodov et al., 2011; Jimenez et al., 2009; Hallquist et

938   al., 2009; Kanakidou et al., 2005). The formation of SOA proceeds by complex pathways including

939   reaction and mass transport in the gas and condensed phases. The equilibration timescale for gas-

940   particle partitioning for SOA particles and particle-particle mixing of varying viscosity has been

941   evaluated (Shiraiwa and Seinfeld, 2012; Berkemeier et al., 2020; Schervish and Shiraiwa, 2023;

942   Li and Shiraiwa, 2019; Schervish et al., 2023). In some of those modeling studies a fixed τ_{des} =

943   10^{-9} s, which corresponds to about E_{des}^0 = 22 kJ mol^{-1} at 293 K, was applied. The simulation results

944   shown in Fig. 5, however, demonstrated that we can expect significant changes in condensed phase

945   equilibration times for gas-particle partitioning when E_{des}^0 and temperature change. Our tabulated

946   data suggests that oxygenated VOCs will exert larger E_{des}^0 and, as such, longer τ_{des}.

947   It has been shown that SOA oxidation products with a variety of functional groups fall into

948   molecular corridors characterized by a tight inverse correlation between volatility (or saturation

949   mass concentration, C_0) and molar mass as depicted in Fig. 13 (Li et al., 2016; Shiraiwa et al.,

950   2014). They are constrained by two boundary lines corresponding to the volatility of n-alkanes

951   C_nH_{2n+2} and sugar alcohols $C_nH_{2n+2}O_n$, which we now identify as "van der Waals" and "hydrogen-

952   bonding" dominated boundaries. This interpretation can be understood by the governing

953   intermolecular forces. For example, using the EVAPORATION model (Compernolle et al., 2011),

954   the vapor pressures for alkane, ketone, alcohol, and acid with a molecular weight of about 142 g

955   mol^{-1} at 298 K yield: $p^0(C_{10}H_{22})$ = 1.73 hPa, $p^0(H_7C_3C(O)C_5H_{11})$ = 0.084 hPa, $p^0(C_9H_{19}OH)$ =

956   0.023 hPa, and $p^0(C_7H_{15}COOH)$ = 1.62×10^{-3} hPa, respectively. The decrease of about three orders

957   of magnitude in the vapor pressure between the alkane and the carboxylic acid is mainly due to

958   two carboxylic acid molecules forming hydrogen bonds, resulting in a dimer. A highly-oxidized

959   amide having ketone and alcohol groups such as N=CC(O)C(O)C(O)CO and M =149.146 g mol^{-1}

960   has p^0 = 8.93×10^{-7} hPa. This is due to the fact that this molecule not only establishes the van der

961   Waals forces such as London dispersion and Keesom forces but also hydrogen bonding with three

962   hydrogen bond donors and multiple hydrogen bond acceptors. As can be seen in Fig. 13, the change

963   in C_0 derived from decane to C_0 of the highly-oxidized amide spans the identified molecular

964   corridor around M = 145 g mol^{-1}, indicating that the van der Waals forces and the number of

965   hydrogen bonds that can be established by a particular molecule may fundamentally describe the

966   volatility range of the organic species.

967   Keeping this approach in mind, we can ask: what are the extreme limits of the saturation mass

968   concentration? The smallest organic molecule is methane, only prone to London dispersion forces.

969     $p^0(CH_4)$ = 46000 hPa with $\log_{10}(C_0)$ = 10.5, which corresponds to the upper bound of the

970   molecular corridor. Ammonia (NH_3) has a similar molar mass as CH_4 but has lower vapor pressure,

971   because NH_3 can establish two hydrogen bonds. N_2O_5 does not form hydrogen bonds and locates

972   above the alkane line. The lower bound of the molecular corridor is mainly defined by the

973   molecule's permanent dipole moments and number of hydrogen bonds it can entertain. Clearly,

974   these attributes are likely to be found in larger and highly-oxidized compounds. Water constitutes

975   a peculiarity when looking at its position in the $C_0 - M$ framework depicted in Fig. 13. There is no

976   other molecule with this small size that can form four hydrogen bonds. Sulfuric acid (H_2SO_4) can

977   also form four hydrogen bonds and locates close to the lower bound of the molecular corridor. As

978   molecules become larger, there are steric hindrances that likely inhibit stronger intermolecular

979   bonding, whereas water with its small size is ideal. This reason may ultimately limit the lower

980   bound of the molecular corridor and thus the lowest volatilities experienced by OA species.

981   As we have discussed above, E_{des}^0 and ΔH_{vap} are positively correlated and E_{des}^0 in most cases

982   is larger than ΔH_{vap} (Fig. 11). Also, we found that gas species with higher $O:C$, and thus larger μ,

983   exhibit larger E_{des}^0 values. This indicates that intermolecular interactions at the interface are as

984   important as in the condensed phase of the adsorbate alone (Valsaraj, 2009, 1988a). We expect

985   this also to hold for the case of SOA formation. It is generally observed that the composition of

986   the organic matrix, barring any mass-transport limitations, has little influence on the gas-particle

987   partitioning equilibrium (Donahue et al., 2012; Donahue et al., 2011). Oxygenated VOCs have

988   higher $O:C$ and larger μ. Saturation vapor pressure or volatility provides guidance in this regard

989   (Epstein et al., 2010), however, our study suggests that considering desorption, i.e., E_{des}^0 values,

990   can impact equilibrium times of gas-particle partitioning as outlined in the gas uptake multilayer

991   model simulations discussed in section 4.

992   Figure 13A shows that the compiled data sets fall within the $C_0 - M$ framework. In comparison,

993   Fig. 13B shows the distribution of SOA oxidation products (916 different species) in the $C_0 - M$

994   space evaluated previously by *Shiraiwa et al.* (2014). Since the gas species discussed in this work

995   cover a similar C_0 and M range as the SOA oxidation products, we can apply the parameterization

996   of E_{des}^0 to provide estimates of E_{des}^0 for gas species typically involved in SOA gas-particle

997   partitioning. This will allow a more detailed understanding and prediction of SOA formation, in

998   particular for temperatures typically encountered in the troposphere during transport.

999   We derive E_{des}^0 of SOA oxidation products by application of Eq. (14). Since we know the

1000   molecular structure of the SOA oxidation products, we can calculate polarizability using the

1001   equation provided by Bosque and Sales (2002), instead of using Eq. (15):

1002 $$\alpha = 1.51\#C + 0.17\#H + 0.57\#O + 1.05\#N + 2.99\#S + 2.48\#P + 0.22\#F +$$

1003 $$2.16\#Cl + 3.29\#Br + 5.45\#I + 0.32 , \tag{20}$$

1004   where #C, #H, #O, #N, #S, #P, #F, #Cl, #Br, and #I represent the respective numbers of atoms in

1005   the molecule.

1006   Figure 14 displays E_{des}^0 values for the molecular corridor data of SOA precursors gases and

1007   oxidation products from Fig. 13 as a function of molar mass and its dependence on $O:C$ and

1008   polarizability, following the molecular corridor approach using molar mass as the primary

1009   parameter characterizing a the physicochemical properties of a molecule (Shiraiwa et al., 2014).

1010   Figures S9 provides the same analysis using parameterization Eq. (16). For the majority of data

1011   points the predicted E_{des}^0 values are within ±10 % of the values shown in Fig. 14 and within the

1012   expected general uncertainty of E_{des}^0 as discussed above. Figure 14A demonstrates the impact of

1013 $O{:}C$ on E_{des}^0, where alkanes, constituting the upper bound in the molecular corridor, have the

1014   lowest E_{des}^0 for a given molar mass. With increasing molecule $O{:}C$, E_{des}^0 increases as expected

1015   from our previous analyses and discussions. The largest impact of molecule $O{:}C$ is at smallest

1016   molar masses. Figure 14B corroborates the strong correlation between molar mass and

1017   polarizability. Figure S9 depicts a tighter correlation of E_{des}^0 with molar mass and polarizability

1018   due to the linear representation of polarizability (Eq. (15)). Estimates of E_{des}^0 for these SOA

1019   oxidation products will allow refinement of gas-particle partitioning timescales, specifically when

1020   temperature changes are considered as outlined in our example shown in Fig. 5.

1021   Figure 15 relates saturation vapor pressures (p^0) at 298 K, estimated using the

1022   EVAPORATION model (Compernolle et al., 2011), to estimated E_{des}^0, derived using Eq. 14, for

1023   selected compounds relevant for atmospheric chemistry and SOA molecular corridor data from

1024   Figs. 13 (Shiraiwa et al., 2014). The top axis of Fig. 15 shows the corresponding desorption

1025   lifetimes τ_{des} at 298 K using the Frenkel equation (Eq. 1) with a pre-exponential factor A_{des} of

1026 10^{13} s^{-1}. The linear behavior in semi-logarithmic space (black solid line) reflects an exponential

1027   relation between p^0 and E_{des}^0 and a linear relation between p^0 and τ_{des}. Similar relationships are

1028   known for p^0 and ΔH_{vap} (Epstein et al., 2010), which underscores the correlation of these two

1029   quantities as observed in Fig. 11. We find, however, a steeper slope of p^0 with E_{des}^0 than previously

1030   found for p^0 and ΔH_{vap}, which suggests $E_{\text{des}}^0 < \Delta H_{\text{vap}}$ for large, oxygenated molecules with low

1031   vapor pressures. Note, however, that those gas species are lacking in our datasets. The relation of

1032 E_{des}^0 and ΔH_{vap} and its consequences for gas-particle partitioning of SOA will be further

1033   investigated in follow-up studies.

1034   Table 2 summarizes characteristic values of p^0, E_{des}^0, and τ_{des} for the categories of a volatility

1035   basis set (VBS) widely used for the description of SOA: intermediate volatility organic compounds

1036 (IVOC), semi-volatile organic compounds (SVOC), low volatility compounds (LVOC), extremely

1037 low volatility compounds (ELVOC), and ultra-low volatility compounds (ULVOC) (Schervish

1038 and Donahue, 2020; Donahue et al., 2009). We obtain characteristic desorption lifetimes of

1039 nanoseconds to milliseconds for VOC, milliseconds to hours for IVOC, and seconds to months for

1040 SVOC, respectively. For LVOC, ELVOC, and ULVOC we obtain τ_{des} values in the range of

1041 minutes to years and millennia. The latter, however, have to be considered as rough estimates,

1042 because the amounts of data available for parameterizing p^0 and E_{des}^0 at low volatility are very

1043 sparse. Note that these VBS categories were originally defined in terms of saturation mass

1044 concentration C^0. To express the categories in terms of p^0, we applied a constant conversion factor

1045 of 10^{-10} atm m^3 µg^{-1}, i.e., assuming a molar mass of 244 g mol^{-1}, for general orientation. For

1046 applications in which keeping the exact definition is required, a more nuanced conversion to vapor

1047 pressures could be achieved by parameterizing typical values of molar mass as a function of vapor

1048 pressure along the SOA molecular corridor. We provide an analogous figure displaying saturation

1049 mass concentrations in the Supplement (Fig. S10).

1050 Gas–particle partitioning plays an important role in chemical transport models, which describe

1051 the long-distance transport and chemical degradation of atmospheric constituents. In these models,

1052 gas–particle partitioning is often treated with instantaneous-equilibration approaches. Desorption

1053 lifetimes crucially determine the position of partitioning steady states and thus affect chemical

1054 degradation rates. Moreover, they have a significant influence on the validity of the instantaneous-

1055 equilibration assumption (Wilson et al., 2021; Stolzenburg et al., 2018).

1056 Adsorption and desorption processes of semi-volatile species are important in indoor

1057 environments, as large surface area-to-volume ratios indoors favor heterogeneous interactions. The

1058 deposition of semi-volatile organic compounds on impermeable indoor surfaces can lead to the

1059 formation of thin organic films (Weschler and Nazaroff, 2017). The desorption lifetime is a critical

1060 parameter for the initial film formation via multi-layer adsorption and the subsequent film growth

1061 (Lakey et al., 2021). These surface films act as reservoirs of semivolatile compounds and also

1062 serve as reaction media, affecting indoor air composition (Wang et al., 2020; Lakey et al., 2023).

1063

1064 **Summary and Conclusions**

1065 We have compiled computationally and experimentally derived desorption energy data to

1066 provide estimates of E_{des}^0 for a variety of gas species and solid, liquid, and ice substrates, thereby

1067 covering a range of relevant aerosol particle systems. The desorption energies have been placed in

1068 context with intermolecular forces. We were able to express E_{des}^0 as a function of molecular weight

1069 and $O{:}C$ ratio only, facilitating the application of the proposed parameterization. The important

1070 role of gas species' polarizability and dipole moment governing E_{des}^0 have been recognized. We

1071 demonstrated the importance of correct E_{des}^0 values for interpretation of multiphase chemical

1072 reactions and gas-particle partitioning, especially when extrapolating laboratory findings to

1073 atmospherically relevant temperature ranges. For example, assessment of chemical aging of

1074 aerosol particles during transport relies on E_{des}^0 values for various atmospheric oxidants.

1075 The compiled literature data allowed us to correlate E_{des}^0 with the enthalpy of vaporization and

1076 solvation, thereby evaluating the role of desorption in these interfacial processes. We identified a

1077 positive correlation between E_{des}^0 and ΔH_{vap}, where E_{des}^0 values are often larger than ΔH_{vap}. For

1078 liquid substrates, we observe a correlation with molecule oxidation state as well, indicating the

1079 importance of intermolecular interactions when looking at interfacial processes.

1080   A positive correlation has been observed between E_{des}^0 and ΔH_{solv} in liquid substrates. This

1081   trend could be related to the gas species' dipole moment and the interfacial interactions among the

1082   adsorbed gas species and molecules in the liquid phase.

1083   We demonstrated the relevance of E_{des}^0 in gas-particle partitioning and its relationship to the

1084   concept of molecular corridors. E_{des}^0 values for many SOA components were derived allowing for

1085   in detail simulation of SOA formation and growth processes. Accurate representation of particle

1086   growth and SOA formation processes requires E_{des}^0 for typically oxygenated VOCs. The relevance

1087   of E_{des}^0 for application in indoor air chemistry has been highlighted. Furthermore, in the Appendix

1088   A1 we outline the correlation of glass transition points with E_{des}^0 which adds another layer of

1089   complexity when modeling multiphase chemical reactions (through the potential of viscous phase

1090   states). Our findings identify the following areas of further research needs:

1091   -   More adsorption and desorption data for environmentally-relevant interfaces, including

1092   multicomponent aerosol particle surfaces, are needed. Experimental and computational

1093   approaches can yield necessary E_{des}^0 values.

1094   -   Reporting and application of adsorption and/or desorption data should consider applied

1095   standard states and adsorption models to better constrain E_{des}^0 (Donaldson et al., 2012b;

1096   Savara, 2013; Campbell et al., 2016; Knopf and Ammann, 2021).

1097   -   Desorption kinetic measurements involving liquids with high vapor pressure are needed.

1098   Furthermore, the role of solutes in aqueous solutions on the hydrogen bonding network and

1099   in turn on the desorption process is not well understood. For example, adsorbates with

1100   hydrophilic functional groups exert greater E_{des}^0. Systematic examination of desorption

1101   kinetics as a function of varying solute concentration and gas species $O{:}C$ and dipole

1102   moment are needed to improve our understanding of adsorption and desorption processes

1103   on liquid surfaces.

1104   - Experimental and theoretical multiphase chemical kinetics studies should aim to represent

1105   the typical atmospheric temperature range. This can add to further complications with

1106   regard to the underlying thermodynamics and kinetics in addition to possibly phase state

1107   changes of the substrate (Li and Knopf, 2021; Li et al., 2020; Slade et al., 2017; Knopf et

1108   al., 2005; Davies and Wilson, 2015; Chan et al., 2014; Hearn and Smith, 2007).

1109   - Advancing our understanding of the interfacial processes that govern mass

1110   accommodation, solvation, and vaporization is needed. Adsorption and desorption can play

1111   a role in these processes. However, the degree of how much impact E_{des}^0 has on gas species'

1112   solvation or vaporization depends on its relationship with ΔH_{vap} and ΔH_{solv}. Considering

1113   that aerosol particles are chemically complex and exhibit multiple phases and phase states,

1114   these advances will improve representation of gas-particle partitioning.

1115

Appendix

This appendix provides a discussion of observed correlation between E_{des}^0 and T_g, nomenclature used in this study, and lists the applied data sets to develop the E_{des}^0 parameterization and to produce correlation plots. The parameters given in Tables are also available electronically (Knopf et al., 2023).

A1. Glass Transition

Molecular corridors yield also significant insight into particle phase state and viscosity. The glass transition temperature (T_g) characterizes the non-equilibrium phase change from a glassy solid state to a more pliable semi-solid state upon an increase of temperature or humidity (Koop et al., 2011b). T_g depends primarily on the molar mass and secondarily on the $O{:}C$ (Koop et al., 2011a; Shiraiwa et al., 2017a). Organic compounds with greater molar mass and lower volatility have higher T_g, indicating that these compounds adopt an amorphous (semi-) solid phase with higher viscosity. For weakly functionalized compounds, viscosity and T_g are sensitive to addition of carboxylic acid (COOH) and hydroxyl (OH) groups compared to carbonyl (CO) and methylene (CH_2) (Rothfuss and Petters, 2017; Galeazzo and Shiraiwa, 2022). It has been demonstrated that on average the addition of one OH group increases the viscosity by a factor of approximately 22 to 45 (Grayson et al., 2017). These studies imply that hydrogen bonding may play an important role in determining viscosity, which is consistent with its role in influencing glass transition temperatures (Nakanishi and Nozaki, 2011; Van Der Sman, 2013).

Recent studies have shown that a glassy surface can be much more dynamic with lower viscosity than anticipated based on T_g and bulk viscosity (Tian et al., 2022; Zhang and Fakhraai, 2017; Sikorski et al., 2010). The enhanced surface mobility, however, is mostly shown by two

1139 typical amorphous polymers of polystyrene and poly(methyl methacrylate) (Tian et al., 2022).

1140 Though it is likely that also enhanced mobility on the surface compared to the bulk is relevant for

1141 atmospheric organic matter, further studies are necessary to assess if this is applicable to

1142 atmospheric glassy SOA particles, which are highly complex multicomponent mixtures that are

1143 very different from polymers.

1144 Application of our parameterization of E_{des}^0, we can now construct a relationship between E_{des}^0

1145 and T_g of the SOA oxidation products shown in Fig. 1. T_g was derived applying the

1146 parameterization presented in (Shiraiwa et al., 2017a) using molar mass and $O{:}C$ as input

1147 variables. E_{des}^0 was derived applying Eqs. (14) and (20). Since both of our parameterizations of

1148 E_{des}^0 and T_g depend on molar mass and $O{:}C$ ratio, it is reasonable to expect we can now construct

1149 a positive relationship between E_{des}^0 and T_g of the SOA oxidation products. Figure A1 shows that

1150 gas species with lower E_{des}^0 have lower T_g and vice versa. Figure A1A demonstrates that for gas

1151 species with same E_{des}^0, an increase in $O{:}C$ results in a significant increase of T_g pointing to

1152 enhanced molecular interactions. Hence, alkanes represent species with lowest T_g at given E_{des}^0.

1153 Figure A1B further corroborates this fact. T_g has a strong dependency on molar mass. However,

1154 for the same molar mass, T_g can vary by 100 K (which coincides with only small changes in E_{des}^0),

1155 which can now be attributed to the impact of $O{:}C$. In other words, increased molecular interactions

1156 can significantly increase T_g, when other parameters remain the same. Similar trends hold for E_{des}^0,

1157 thereby allowing to recognize that comparable molecular interactions control the properties of the

1158 amorphous phase state of a system and its E_{des}^0. In absence of knowing the molecular structure,

1159 Fig. S11 provides the same analysis of the relationship between E_{des}^0 and T_g of the SOA oxidation

1160 products using parameterization Eq. (16) for comparison. We see that without knowing the

1161 molecular structure, a tighter correlation between E_{des}^0 and T_g is observed due to the linearization

1162 of the gas species' polarizability. Similarly to Figs. 14 and S6, the predicted E_{des}^0 values in Fig.

1163 S11 are within ±10 % of the values shown in Fig. A1 and within the expected general uncertainty

1164 of E_{des}^0.

1165 The correlation between E_{des}^0 and T_g serves as empirical and observational evidence. The

1166 theoretical and physical basis are yet to be established. It does not account for the potentially

1167 enhanced mobility on the surface of glassy matter (Tian et al., 2022; Zhang and Fakhraai, 2017;

1168 Sikorski et al., 2010). One would expect that surface mobility would similarly scale with the

1169 strength of intermolecular interactions. Molecules with high E_{des}^0 interact strongly with molecules

1170 of the same kind at the surface and in the bulk, are expected to also exhibit reduced dynamics in

1171 their own condensed phase (or in a mixture of similar molecules) and thus high viscosity. The

1172 presented correlation observed is meaningful for advancing our understanding of interfacial

1173 processes and supports further investigations.
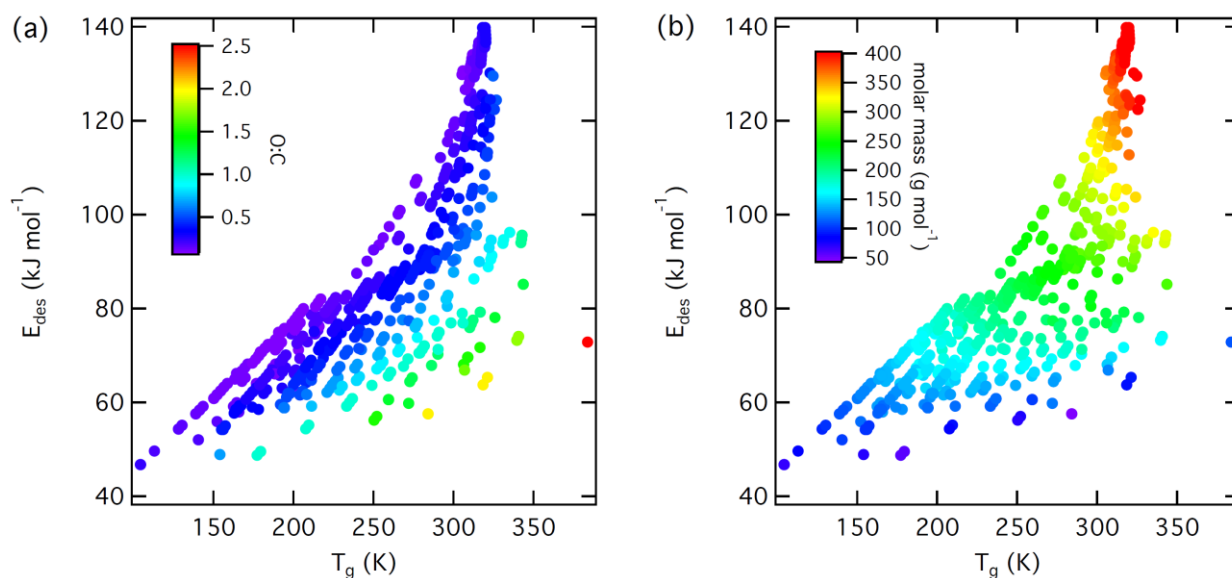
1174

1175 **Figure A1.** Relationship between calculated desorption energies (E_{des}^0) of SOA precursor gases
1176 from *Shiraiwa et al.* (2014) and species' glass transition temperature (T_g) and its dependence on
1177 $O:C$ (a) and molar mass (b). This analysis applies parameterizations given in Eqs. (14) and (20).

1178

 A2. Nomenclature

τ_{des}	desorption lifetime
k_{des}	first-order desorption rate coefficient
A_{des}	pre-exponential factor
E_{des}^0	desorption energy with the energy reference of the gas molecule at rest at $T = 0$ K
γ	uptake coefficient
α_s	surface accommodation coefficient
Γ_b	normalized loss rate in the bulk-phase induced by solubility, diffusion and reaction
Γ_{sb}	normalized rate of surface to bulk transfer
Γ_s	normalized loss rate due to surface reaction
k_s	first-order rate coefficient of chemical reaction at the surface
k_{sb}	first-order rate coefficient for the transfer of molecules from the surface into the bulk (solvation)
k_{bs}	first-order rate coefficient for the transfer of molecules from the bulk to the surface
α_b	bulk accommodation coefficient
ΔG_{ads}^0	Gibbs free energy change of adsorption
ΔH_{ads}^0	standard enthalpy change of adsorption
ΔS_{ads}^0	standard entropy change of adsorption
κ	transmission coefficient
$(N_{TS}/\mathcal{A})^0$	standard concentration of molecules in the TS
$(N_{ads}/\mathcal{A})^0$	standard concentration of adsorbed molecules
$q_{TS}^{0\prime}$	standard partition functions for the TS
q_{ads}^0	standard partition functions for the adsorbate
$q_{TS}^{\prime}$	partition functions for the TS
q_{ads}	partition functions for the adsorbate

M	molar mass
ΔH_{vap}	enthalpy of vaporization
α	polarizability
μ	dipole moment
$O{:}C$	oxygen to carbon ratio
ΔH_{sol}	enthalpy of solvation
ε_{r}	relative permittivity of the substrate
TPD	temperature programmed desorption
TDS	thermal desorption spectroscopy
TG-DSC	thermal gravimetry with differential scanning calorimetry
KN	Knudsen cell
MB	molecular beams
IGC	inverse gas chromatography
VM	vacuum microbalance
DRIFT	diffuse reflectance infrared fourier transform spectroscopy
FTIR	Fourier transform infrared spectroscopy
KU	kinetic uptake
VS	vibrational spectroscopy
ST	surface tension
MD	molecular dynamics
DFT	density functional theory
MC	Monte Carlo
GCMC	grand canonical Monte Carlo
ECT	embedded cluster theory
DAM	dipped adcluster model

1180

1181

Table A1. Compiled absorbate-substrate data for water vapor and heavy water vapor adsorbed on various mineral and clay substrates, inorganics, organics, and carbonaceous substrayes. Gas species, gas species' molar mass, substrate, experimental or theoretical method, desorption energy (E_{des}^0), and desorption lifetimes (τ_{des}) evaluated at 293 K using $A_{des} = 10^{13}$ s^{-1}, enthalpy of vaporization (ΔH_{vap}), gas species' polarizability (α), gas species' dipole moment (μ), substrate's relative permittivity (ε_r), and gas species' oxygen to carbon ration ($O:C$) are given.

Gas Species	Molar Mass / g mol^{-1}	Substrate	Method	E_{des}^0 / kJ mol^{-1}	$\tau_{des}^{293\,K}$ / s	ΔH_{vap} (T) / kJ mol^{-1}	α / 10^{-24} cm^3	μ / D	ε_r	O:C
H$_2$O	18.02	clay: orthic luvisol	VM	9.7 (Sokolowska et al., 1993)	5.4×10^{-12}	44 (Chickos and Acree, 2003)	1.45 (Lide, 2008)	1.85 (Lide, 2008)	2 (Daniels, 2004)	0
H$_2$O	18.02	clay: mollic gleysol	VM	11.2 (Sokolowska et al., 1993)	1.0×10^{-11}	44 (Chickos and Acree, 2003)	1.45 (Lide, 2008)	1.85 (Lide, 2008)	2 (Daniels, 2004)	0
H$_2$O	18.02	clay: eutric cambisol	VM	13.2 (Sokolowska et al., 1993)	2.3×10^{-11}	44 (Chickos and Acree, 2003)	1.45 (Lide, 2008)	1.85 (Lide, 2008)	2 (Daniels, 2004)	0
H$_2$O	18.02	clay: stagn. phaeozem	VM	12.8 (Sokolowska et al., 1993)	1.9×10^{-11}	44 (Chickos and Acree, 2003)	1.45 (Lide, 2008)	1.85 (Lide, 2008)	2 (Daniels, 2004)	0
H$_2$O	18.02	clay: eutric cambisol	VM	12.6 (Sokolowska et al., 1993)	1.7×10^{-11}	44 (Chickos and Acree, 2003)	1.45 (Lide, 2008)	1.85 (Lide, 2008)	2 (Daniels, 2004)	0
H$_2$O	18.02	kaolinite, si, spc/e	GCMC	21.6 (Croteau et al., 2009)	7.1×10^{-10}	44 (Chickos and Acree, 2003)	1.45 (Lide, 2008)	1.85 (Lide, 2008)	5.10 (Leluk et al., 2010)	0
H$_2$O	18.02	kaolinite, al, spc/e	GCMC	46.4 (Croteau et al., 2009)	1.9×10^{-5}	44 (Chickos and Acree, 2003)	1.45 (Lide, 2008)	1.85 (Lide, 2008)	5.10 (Leluk et al., 2010)	0
H$_2$O	18.02	kaolinite, unprotonated edge, spc/e	GCMC	73.5 (Croteau et al., 2009)	1.3	44 (Chickos and Acree, 2003)	1.45 (Lide, 2008)	1.85 (Lide, 2008)	5.10 (Leluk et al., 2010)	0
H$_2$O	18.02	kaolinite, protonated edge, spc/e	GCMC	94.1 (Croteau et al., 2009)	6.0×10^3	44 (Chickos and Acree, 2003)	1.45 (Lide, 2008)	1.85 (Lide, 2008)	5.10 (Leluk et al., 2010)	0
H$_2$O	18.02	kaolinite (Al)	DRIFTS	56.0 (Budi et al., 2018)	9.6×10^{-4}	44 (Chickos and Acree, 2003)	1.45 (Lide, 2008)	1.85 (Lide, 2008)	5.10 (Leluk et al., 2010)	0
H$_2$O	18.02	kaolinite (Si)	DRIFTS	21.2 (Budi et al., 2018)	6.0×10^{-10}	44 (Chickos and Acree, 2003)	1.45 (Lide, 2008)	1.85 (Lide, 2008)	5.10 (Leluk et al., 2010)	0
H$_2$O	18.02	Arizona test dust (0-3 µm)	DRIFTS	53.6	3.6×10^{-4}	44 (Chickos and Acree, 2003)	1.45 (Lide, 2008)	1.85 (Lide, 2008)	5.00 (Sharif, 1995)	0
H$_2$O	18.02	Arizona test dust particles (5-10 µm)	DRIFTS	50.5 (Ibrahim et al., 2018)	1.0×10^{-4}	44 (Chickos and Acree, 2003)	1.45 (Lide, 2008)	1.85 (Lide, 2008)	5.00 (Sharif, 1995)	0
H$_2$O	18.02	Arizona test dust particles (10-20 µm)	DRIFTS	49.5 (Ibrahim et al., 2018)	6.7×10^{-5}	44 (Chickos and Acree, 2003)	1.45 (Lide, 2008)	1.85 (Lide, 2008)	5.00 (Sharif, 1995)	0
H$_2$O	18.02	Arizona test dust particles (20-40 µm)	DRIFTS	48.9 (Ibrahim et al., 2018)	5.2×10^{-5}	44 (Chickos and Acree, 2003)	1.45 (Lide, 2008)	1.85 (Lide, 2008)	5.00 (Sharif, 1995)	0

H$_2$O	18.02	Arizona test dust particles (40-80 μm)	DRIFTS	48.3 (Ibrahim et al., 2018)	4.1×10^{-5}	44 (Chickos and Acree, 2003)	1.45 (Lide, 2008)	1.85 (Lide, 2008)	5.00 (Sharif, 1995)	0
H$_2$O	18.02	NaCl (100)	DFT	40.6 (Meyer et al., 2001)	1.7×10^{-6}	44 (Chickos and Acree, 2003)	1.45 (Lide, 2008)	1.85 (Lide, 2008)	5.9 (Lide, 2008)	0
H$_2$O	18.02	KCl (100)	DFT	32.3 (Meyer et al., 2001)	5.7×10^{-8}	44 (Chickos and Acree, 2003)	1.45 (Lide, 2008)	1.85 (Lide, 2008)	4.86 (Lide, 2008)	0
H$_2$O	18.02	NaCl(001)	FTIR	48.0 (Foster and Ewing, 2000)	3.6×10^{-5}	44 (Chickos and Acree, 2003)	1.45 (Lide, 2008)	1.85 (Lide, 2008)	5.9 (Lide, 2008)	0
H$_2$O	18.02	Al(111)	DFT	56 (Hai et al., 2023)	9.6×10^{-4}	44 (Chickos and Acree, 2003)	1.45 (Lide, 2008)	1.85 (Lide, 2008)		0
H$_2$O	18.02	α-Al$_2$O$_3$(0001, hydroxylated)	TPD	134 (Nelson et al., 1998)	7.7×10^{10}	44 (Chickos and Acree, 2003)	1.45 (Lide, 2008)	1.85 (Lide, 2008)	9.34 (Lide, 2008)	0
H$_2$O	18.02	α-Al$_2$O$_3$	FTIR	52.0 (Goodman et al., 2001)	1.9×10^{-4}	44 (Chickos and Acree, 2003)	1.45 (Lide, 2008)	1.85 (Lide, 2008)	9.34 (Lide, 2008)	0
H$_2$O	18.02	SiO$_2$	FTIR	50.3(Goodman et al., 2001)	9.3×10^{-5}	44 (Chickos and Acree, 2003)	1.45 (Lide, 2008)	1.85 (Lide, 2008)	4.42 (Lide, 2008)	0
H$_2$O	18.02	TiO$_2$	FTIR	54.6(Goodman et al., 2001)	5.4×10^{-4}	44 (Chickos and Acree, 2003)	1.45 (Lide, 2008)	1.85 (Lide, 2008)	86 (Lide, 2008)	0
H$_2$O	18.02	γ-Fe$_2$O$_3$	FTIR	53.7(Goodman et al., 2001)	3.7×10^{-4}	44 (Chickos and Acree, 2003)	1.45 (Lide, 2008)	1.85 (Lide, 2008)	4.5 (Lide, 2008)	0
H$_2$O	18.02	CaO	FTIR	49.2(Goodman et al., 2001)	5.9×10^{-5}	44 (Chickos and Acree, 2003)	1.45 (Lide, 2008)	1.85 (Lide, 2008)	11.8 (Lide, 2008)	0
H$_2$O	18.02	MgO	FTIR	50.2(Goodman et al., 2001)	8.9×10^{-5}	44 (Chickos and Acree, 2003)	1.45 (Lide, 2008)	1.85 (Lide, 2008)	9.65 (Lide, 2008)	0
H$_2$O	18.02	NaCl powder	DRIFTS	51.7 (Woodill et al., 2013)	1.6×10^{-4}	44 (Chickos and Acree, 2003)	1.45 (Lide, 2008)	1.85 (Lide, 2008)	5.9 (Lide, 2008)	0
H$_2$O	18.02	catechol coated NaCl	DRIFTS	49.0 (Woodill et al., 2013)	5.4×10^{-5}	44 (Chickos and Acree, 2003)	1.45 (Lide, 2008)	1.85 (Lide, 2008)	~3.52(Kronberger and Weiss, 1944)	0
H$_2$O	18.02	catechol coated NaCl + O$_3$	DRIFTS	50.1 (Woodill et al., 2013)	8.4×10^{-5}	44 (Chickos and Acree, 2003)	1.45 (Lide, 2008)	1.85 (Lide, 2008)	~3.52(Kronberger and Weiss, 1944)	0
H$_2$O	18.02	Al$_2$O$_3$ powder	DRIFTS	55.1 (Woodill et al., 2013)	6.6×10^{-4}	44 (Chickos and Acree, 2003)	1.45 (Lide, 2008)	1.85 (Lide, 2008)	9.34 (Lide, 2008)	0
H$_2$O	18.02	catechol coated Al$_2$O$_3$	DRIFTS	49.8 (Woodill et al., 2013)	7.5×10^{-5}	44 (Chickos and Acree, 2003)	1.45 (Lide, 2008)	1.85 (Lide, 2008)	~3.52(Kronberger and Weiss, 1944)	0
H$_2$O	18.02	Catechol coated Al$_2$O$_3$ + O$_3$	DRIFTS	49.8 (Woodill et al., 2013)	7.5×10^{-5}	44 (Chickos and Acree, 2003)	1.45 (Lide, 2008)	1.85 (Lide, 2008)	~3.52(Kronberger and	0

									Weiss, 1944)	
H$_2$O	18.02	CaCO$_3$	DFT	80.0 (Budi et al., 2018)	18	44 (Chickos and Acree, 2003)	1.45 (Lide, 2008)	1.85 (Lide, 2008)	8.67 (Lide, 2008)	0
H$_2$O	18.02	CaCO$_3$	TPD	79.1 (Dickbreder et al., 2023)	13	44 (Chickos and Acree, 2003)	1.45 (Lide, 2008)	1.85 (Lide, 2008)	8.67 (Lide, 2008)	0
H$_2$O	18.02	CaCO$_3$	TPD	106.1 (Dickbreder et al., 2023)	8.2×10^5	44 (Chickos and Acree, 2003)	1.45 (Lide, 2008)	1.85 (Lide, 2008)	8.67 (Lide, 2008)	0
H$_2$O	18.02	SiO$_2$	DFT	53.1 (Budi et al., 2018)	2.9×10^{-4}	44 (Chickos and Acree, 2003)	1.45 (Lide, 2008)	1.85 (Lide, 2008)	4.42 (Lide, 2008)	0
H$_2$O	18.02	Au(111)	DFT	10.1 (Meng et al., 2004)	6.3×10^{-12}	44 (Chickos and Acree, 2003)	1.45 (Lide, 2008)	1.85 (Lide, 2008)	6.9 (Shklyarevskii and Pakhomov, 1973)	0
H$_2$O	18.02	Pt(111)	DFT	28.1 (Meng et al., 2004)	1.0×10^{-8}	44 (Chickos and Acree, 2003)	1.45 (Lide, 2008)	1.85 (Lide, 2008)		0
H$_2$O	18.02	Pd(111)	DFT	29.3 (Meng et al., 2004)	1.7×10^{-8}	44 (Chickos and Acree, 2003)	1.45 (Lide, 2008)	1.85 (Lide, 2008)		0
H$_2$O	18.02	Ru(0001)	DFT	39.5 (Meng et al., 2004)	1.1×10^{-6}	44 (Chickos and Acree, 2003)	1.45 (Lide, 2008)	1.85 (Lide, 2008)		0
H$_2$O	18.02	Rh(111)	DFT	39.4 (Meng et al., 2004)	1.1×10^{-6}	44 (Chickos and Acree, 2003)	1.45 (Lide, 2008)	1.85 (Lide, 2008)		0
H$_2$O	18.02	steel	KU	60.4 (Koch et al., 1997)	5.9×10^{-3}	44 (Chickos and Acree, 2003)	1.45 (Lide, 2008)	1.85 (Lide, 2008)		0
H$_2$O	18.02	pyrex Glass	KU	56.1 (Koch et al., 1997)	1.0×10^{-3}	44 (Chickos and Acree, 2003)	1.45 (Lide, 2008)	1.85 (Lide, 2008)	5.0 (Lide, 2008)	0
H$_2$O	18.02	SAM-acid	TPD	45.2 (Dubois et al., 1990)	1.1×10^{-5}	44 (Chickos and Acree, 2003)	1.45 (Lide, 2008)	1.85 (Lide, 2008)	4.1 (Millany and Jonscher, 1980)	0
H$_2$O	18.02	SAM-methyl	TPD	35.1 (Dubois et al., 1990)	1.8×10^{-7}	44 (Chickos and Acree, 2003)	1.45 (Lide, 2008)	1.85 (Lide, 2008)	2.1 (Akkerman et al., 2007; Rampi et al., 1998)	0
H$_2$O	18.02	SAM-alcohol	TPD	39.3 (Dubois et al., 1990)	1.0×10^{-6}	44 (Chickos and Acree, 2003)	1.45 (Lide, 2008)	1.85 (Lide, 2008)		0
H$_2$O	18.02	SAM-amide	TPD	38.5 (Dubois et al., 1990)	7.3×10^{-7}	44 (Chickos and Acree, 2003)	1.45 (Lide, 2008)	1.85 (Lide, 2008)	2 (Romaner et al., 2008)	0
H$_2$O	18.02	SAM-ester	TPD	37.2 (Dubois et al., 1990)	4.3×10^{-7}	44 (Chickos and Acree, 2003)	1.45 (Lide, 2008)	1.85 (Lide, 2008)		0
H$_2$O	18.02	HOPG	TDS	37.2 (Ulbricht et al., 2006)	4.3×10^{-7}	44 (Chickos and Acree, 2003)	1.45 (Lide, 2008)	1.85 (Lide, 2008)	13 (Dovbesh	0

									ko et al., 2015)	
H₂O	18.02	graphene	CCSD(T)	13.0 (Voloshina et al., 2011)	1.6×10⁻⁵	44 (Chickos and Acree, 2003)	1.45 (Lide, 2008)	1.85 (Lide, 2008)	13 (Dovbeshko et al., 2015)	0
H₂O	18.02	graphene	DFT	12.5 (Liang et al., 2021)	1.7×10⁻¹¹	44 (Chickos and Acree, 2003)	1.45 (Lide, 2008)	1.85 (Lide, 2008)	13 (Dovbeshko et al., 2015)	0
H₂O	18.02	graphene, Stone-Wales	DFT	13.5 (Liang et al., 2021)	2.6×10⁻¹¹	44 (Chickos and Acree, 2003)	1.45 (Lide, 2008)	1.85 (Lide, 2008)	13 (Dovbeshko et al., 2015)	0
H₂O	18.02	graphene, single vacancy defect	DFT	51.1 (Liang et al., 2021)	1.3×10⁻⁴	44 (Chickos and Acree, 2003)	1.45 (Lide, 2008)	1.85 (Lide, 2008)	13 (Dovbeshko et al., 2015)	0
H₂O	18.02	graphene, double vacancy defect	DFT	15.4 (Liang et al., 2021)	5.6×10⁻¹¹	44 (Chickos and Acree, 2003)	1.45 (Lide, 2008)	1.85 (Lide, 2008)	13 (Dovbeshko et al., 2015)	0
H₂O	18.02	grey Soot	KU	29.3 (Alcala-Jornod et al., 2002)	1.7×10⁻⁸	44 (Chickos and Acree, 2003)	1.45 (Lide, 2008)	1.85 (Lide, 2008)	13 (Dovbeshko et al., 2015)	0
H₂O	18.02	black Soot	KU	37.7 (Alcala-Jornod et al., 2002)	5.3×10⁻⁷	44 (Chickos and Acree, 2003)	1.45 (Lide, 2008)	1.85 (Lide, 2008)	13 (Dovbeshko et al., 2015)	0
H₂O	18.02	soot-OH	DFT	18.0 (Collignon et al., 2005)	1.6×10⁻¹⁰	44 (Chickos and Acree, 2003)	1.45 (Lide, 2008)	1.85 (Lide, 2008)	~13 (Dovbeshko et al., 2015)	0
H₂O	18.02	soot-COOH	DFT	38.4 (Collignon et al., 2005)	7.0×10⁻⁷	44 (Chickos and Acree, 2003)	1.45 (Lide, 2008)	1.85 (Lide, 2008)	~13 (Dovbeshko et al., 2015)	0
H₂O	18.02	benzo[a]pyrene/soot	KU	50.0 (Pöschl et al., 2001)	8.2×10⁻⁵	44 (Chickos and Acree, 2003)	1.45 (Lide, 2008)	1.87 (Townes and Schawlow, 1975)	3.52(Kronberger and Weiss, 1944)	0
D₂O	20.03	SAM-methyl	TPD	34.0 (Grimm et al., 2008)	1.2×10⁻⁷	45.14 (Crabtree and Siman-Tov, 1993)	1.26 (Lide, 2008)	1.87 (Townes and Schawlow, 1975)	2.1 (Akkerman et al., 2007; Rampi et al., 1998)	0
D₂O	20.03	SAM-COOH	TPD	50.0 (Grimm et al., 2008)	8.2×10⁻⁵	45.14 (Crabtree and Siman-Tov, 1993)	1.26 (Lide, 2008)	1.87 (Townes and Schawlow, 1975)	4.1 (Millany and Jonscher, 1980)	0
D₂O	20.03	uncoated glass	TPD	50.0 (Moussa et al., 2009)	8.2×10⁻⁵	45.14 (Crabtree and Siman-Tov, 1993)	1.26 (Lide, 2008)	1.87 (Townes and Schawl	4.42 (Lide, 2008)	

								ow, 1975)		
D₂O	20.03	C18-SAM	TPD	36.0 (Moussa et al., 2009)	2.6×10⁻⁷	45.14 (Crabtree and Siman-Tov, 1993)	1.26 (Lide, 2008)	1.87 (Townes and Schawlow, 1975)	2.1 (Akkerman et al., 2007; Rampi et al., 1998)	0
D₂O	20.03	C8=SAM	TPD	40.0 (Moussa et al., 2009)	1.4×10⁻⁶	45.14 (Crabtree and Siman-Tov, 1993)	1.26 (Lide, 2008)	1.87 (Townes and Schawlow, 1975)	2.03 (Crossley, 1973)	0
D₂O	20.03	KMnO₄, O₃ oxidized SAM	TPD	44.0 (Moussa et al., 2009)	7.0×10⁻⁶	45.14 (Crabtree and Siman-Tov, 1993)	1.26 (Lide, 2008)	1.87 (Townes and Schawlow, 1975)	~4.1 (Millany and Jonscher, 1980)	0
D₂O	20.03	methanol on HOPG	MB	45.3 (Thomson et al., 2011)	1.2×10⁻⁵	45.14 (Crabtree and Siman-Tov, 1993)	1.26 (Lide, 2008)	1.87 (Townes and Schawlow, 1975)		0
D₂O	20.03	solid butanol	MB	27.0 (Johansson et al., 2019)	6.5×10⁻⁹	45.14 (Crabtree and Siman-Tov, 1993)	1.26 (Lide, 2008)	1.87 (Townes and Schawlow, 1975)	17.84* (Lide, 2008)	0
D₂O	20.03	solid acetic acid	DFT	19.0 (Allouche and Bahr, 2006)	2.4×10⁻¹⁰	45.14 (Crabtree and Siman-Tov, 1993)	1.26 (Lide, 2008)	1.87 (Townes and Schawlow, 1975)	6.2* (Lide, 2008)	0
D₂O	20.03	solid nopinone	MB	26.0 (Johansson et al., 2020)	4.3×10⁻⁹	45.14 (Crabtree and Siman-Tov, 1993)	1.26 (Lide, 2008)	1.87 (Townes and Schawlow, 1975)		0
D₂O	20.03	nitric acid monolayer	MB	49.2 (Thomson et al., 2015)	5.9×10⁻⁵	45.14 (Crabtree and Siman-Tov, 1993)	1.26 (Lide, 2008)	1.87 (Townes and Schawlow, 1975)		0

*Applied the value for liquid phase of substrate species.

Table A2. Compiled absorbate-substrate interaction energies for reactive gases on solid substrates. Gas species, gas species' molar mass, substrate, experimental or theoretical method, desorption energy (E_{des}^0), and desorption lifetimes (τ_{des}) evaluated at 293 K using $A_{des} = 10^{13}$ s⁻¹, enthalpy of vaporization (ΔH_{vap}), gas species' polarizability (α), gas species' dipole moment (μ), substrate's relative permittivity (ε_r), and gas species' oxygen to carbon ration ($O:C$) are given.

Gas Species	Molar Mass / g mol^{-1}	Substrate	Method	E^0_{des} / kJ mol^{-1}	$\tau^{293\,K}_{des}$ / s	ΔH_{vap} (T) / kJ mol^{-1}	α / 10^{-24} cm^3	μ / D	ε_r	O:C
OH	17.01	A$_{l2}$O$_3$	MC	47.5 (Remorov and Bardwell, 2005)	2.9×10^{-5}		7.11 (Zen et al., 2014)	1.65 (Lide, 2008)	9.34 (Lide, 2008)	0
OH	17.01	NaCl	MC	42.7 (Remorov and Bardwell, 2005)	4.1×10^{-6}		7.11 (Zen et al., 2014)	1.65 (Lide, 2008)	5.90 (Lide, 2008)	0
OH	17.01	NH$_4$NO$_3$	MC	42.7 (Remorov and Bardwell, 2005)	4.1×10^{-6}		7.11 (Zen et al., 2014)	1.65 (Lide, 2008)	10.70 (Lide, 2008)	0
OH	17.01	NH$_4$HSO$_4$	MC	41 (Remorov and Bardwell, 2005)	2.0×10^{-6}		7.11 (Zen et al., 2014)	1.65 (Lide, 2008)	165 (Lide, 2008)	0
OH	17.01	(NH$_4$)$_2$SO$_4$	MC	43.1 (Remorov and Bardwell, 2005)	4.8×10^{-6}		7.11 (Zen et al., 2014)	1.65 (Lide, 2008)	10 (Lide, 2008)	0
OH	17.01	Ni(100)	ECT	292.9$^\$$ (Yang and Whitten, 1997)	1.6×10^{39}		7.11 (Zen et al., 2014)	1.65 (Lide, 2008)		0
OH	17.01	Ni(111)	ECT	309.6$^\$$ (Yang and Whitten, 1997)	1.6×10^{42}		7.11 (Zen et al., 2014)	1.65 (Lide, 2008)		0
OH	17.01	Fe(110)	ECT	284.5$^\$$ (Yang and Whitten, 1997)	5.3×10^{37}		7.11 (Zen et al., 2014)	1.65 (Lide, 2008)		0
OH	17.01	Ag(110)	DAM	415.9$^\$$ (Hu and Nakatsuji, 1999)	1.4×10^{61}		7.11 (Zen et al., 2014)	1.65 (Lide, 2008)		0
OH	17.01	Triacontane (solid)	KU	12.7 (Li and Knopf, 2021)	1.8×10^{-11}		7.11 (Zen et al., 2014)	1.65 (Lide, 2008)	1.91* (Lide, 2008)	0
NO$_3$	62.00	oleic acid (monolayer)	K2-SURF	27.8 (Sebastiani et al., 2018)	9.0×10^{-9}		5.15 (Alkorta et al., 2022)		2.34 (Lide, 2008)	0
NO$_3$	62.00	palmitoleic acid (monolayer)	K2-SURF	29.5 (Sebastiani et al., 2018)	1.8×10^{-8}		5.15 (Alkorta et al., 2022)		2.34 (Lide, 2008)	0
NO$_3$	62.00	methyl oleate (monolayer)	K2-SURF	27.8 (Sebastia	9.0×10^{-9}		5.15 (Alkorta et al., 2022)		3.21 (Lide, 2008)	0

Gas Species	Molar Mass	Substrate	Method	E_{des}^0	τ_{des}	ΔH_{vap}	α	μ	ε_r	O:C
				ni et al., 2018)						
NO$_3$	62.00	stearic acid (monolayer)	K2-SURF	29.8 (Sebastiani et al., 2018)	2.1×10^{-8}		5.15 (Alkorta et al., 2022)		2.31 (Lide, 2008)	0
O$_3$	48.00	BaP/soot	KU	85 (Pöschl et al., 2001)	1.4×10^{2}	12.2 (Stull, 1947)	3.21 (Lide, 2008)	0.53 (Mack and Muenter, 1977)	3.52 (Kronberger and Weiss, 1944)	0
O$_3$	48.00	graphene, physisorption	DFT	24.1 (Lee et al., 2009)	2.0×10^{-9}	12.2 (Stull, 1947)	3.21 (Lide, 2008)	0.53 (Mack and Muenter, 1977)	13 (Dovbeshko et al., 2015)	0
O$_3$	48.00	graphene, chemisorption	DFT	31.8 (Lee et al., 2009)	4.7×10^{-8}	12.2 (Stull, 1947)	3.21 (Lide, 2008)	0.53 (Mack and Muenter, 1977)	13 (Dovbeshko et al., 2015)	0
O, ROI	16.00	BaP/soot	K2-SURF	40 (Shiraiwa et al., 2011b)	1.4×10^{-6}		0.79 (Van Duijnen and Swart, 1998; Cambi et al., 1991)		3.52 (Kronberger and Weiss, 1944)	0
O$_2$	32.00	Ir(100)	DFT	187[$] (Cao et al., 2022)	2.2×10^{20}					0

[$]Not applied in analysis.

[*]Applied value for the liquid phase of substrate species.

Table A3. Compiled absorbate-substrate interaction energies for reactive and non-reactive gases on soot of light duty vehicle (LDV) and heavy-duty vehicle (HDV), pyrex glass, steel, salt, mineral, clay, and highly oriented pyrolyzed graphite (HOPG). Gas species, gas species' molar mass, substrate, experimental or theoretical method, desorption energy (E_{des}^0), and desorption lifetimes (τ_{des}) evaluated at 293 K using $A_{des} = 10^{13}$ s^{-1}, enthalpy of vaporization (ΔH_{vap}), gas species' polarizability (α), gas species' dipole moment (μ), substrate's relative permittivity (ε_r), and gas species' oxygen to carbon ration ($O{:}C$) are given.

Gas Species	Molar Mass / g mol^{-1}	Substrate	Method	E_{des}^0 / kJ mol^{-1}	$\tau_{des}^{293\,K}$ / s	ΔH_{vap} (T) / kJ mol^{-1}	α / 10^{-24} cm^3	μ / D	ε_r	O:C
NO$_2$	46.01	soot LDV	KU	54.7 (Messerer et al., 2006)	5.6×10^{-4}	18.89	3.02 (Lide, 2008)	0.316 (Lide, 2008)	~13.00 (Dovbeshko et al., 2015)	0
NO$_2$	46.01	soot HDV	KU	37.6 (Messere	5.0×10^{-7}	18.89	3.02 (Lide, 2008)	0.316 (Lide, 2008)	~13.00 (Dovbesh	0

Species	MW	Surface	Method							
				r et al., 2007)					ko et al., 2015)	
NO_2	46.01	NH_4Cl	KU	34 (Takenaka and Rossi, 2005)	1.2×10^{-7}	18.89	3.02 (Lide, 2008)	0.316 (Lide, 2008)	6.90 (Lide, 2008)	0
NO_2	46.01	HOPG	TDS	37 (Ulbricht et al., 2006)	3.9×10^{-7}	18.89	3.02 (Lide, 2008)	0.316 (Lide, 2008)	13.00 (Dovbeshko et al., 2015)	0
NO_2	46.01	HOPG	TDS	33 (Ulbricht et al., 2006)	7.6×10^{-8}	18.89	3.02 (Lide, 2008)	0.316 (Lide, 2008)	13.00 (Dovbeshko et al., 2015)	0
NO_2	46.01	Model coal surface	DFT	12.04 (Wang et al., 2021)	1.4×10^{-11}	18.89	3.02 (Lide, 2008)	0.316 (Lide, 2008)	13.00 (Dovbeshko et al., 2015)	0
HCl	36.46	pyrex glass	KU	56.7 (Koch et al., 1997)	1.3×10^{-3}	16.15 (Lide, 2008)	2.7 (Lide, 2008)	1.11 (Lide, 2008)	5.00 (Lide, 2008)	0
HCl	36.46	steel	KU	57.4 (Koch et al., 1997)	1.7×10^{-3}	16.15 (Lide, 2008)	2.7 (Lide, 2008)	1.11 (Lide, 2008)		0
HCl	36.46	α-Al_2O_3(0001)	TPD	105 (Nelson et al., 2001)	5.2×10^5	16.15 (Lide, 2008)	2.63 (Lide, 2008)	1.11 (Lide, 2008)	9.34 (Lide, 2008)	0
CO_2	44.01	graphene	TPD	26.1 (Smith and Kay, 2019)	4.5×10^{-9}	16.4 (Chickos and Acree, 2003)	2.91 (Lide, 2008)	0.0001 (Kolomiit sova et al., 2000)	13.00 (Dovbeshko et al., 2015)	2
CO_2	44.01	HOPG	TDS	24 (Ulbricht et al., 2006)	1.9×10^{-9}	16.4 (Chickos and Acree, 2003)	2.91 (Lide, 2008)	0.0001 (Kolomiit sova et al., 2000)	13.00 (Dovbeshko et al., 2015)	2
CO_2	44.01	HOPG	TDS	23 (Ulbricht et al., 2006)	1.3×10^{-9}	16.4 (Chickos and Acree, 2003)	2.91 (Lide, 2008)	0.0001 (Kolomiit sova et al., 2000)	13.00 (Dovbeshko et al., 2015)	2
CO_2	44.01	Calcite	DFT	29.9 (Budi et al., 2018)	2.1×10^{-8}	16.4 (Chickos and Acree, 2003)	2.91 (Lide, 2008)	0.0001 (Kolomiit sova et al., 2000)	8.67 (Lide, 2008)	2
CO_2	44.01	Quartz	DFT	6.8 (Budi et al., 2018)	1.6×10^{-12}	16.4 (Chickos and Acree, 2003)	2.91 (Lide, 2008)	0.0001 (Kolomiit sova et al., 2000)	4.42 (Lide, 2008)	2
CO_2	44.01	kaolinte (Al)	DFT	28.9 (Budi et al., 2018)	1.4×10^{-8}	16.4 (Chickos and Acree, 2003)	2.91 (Lide, 2008)	0.0001 (Kolomiit sova et al., 2000)	5.00 (Robinso n et al., 2002)	2
CO_2	44.01	kaolinite (si)	DFT	9.6 (Budi et al., 2018)	5.1×10^{-12}	16.4 (Chickos and Acree, 2003)	2.91 (Lide, 2008)	0.0001 (Kolomiit sova et al., 2000)	5.00 (Robinso n et al., 2002)	2
CO	28.01	HOPG	TDS	13 (Ulbricht et al., 2006)	2.1×10^{-11}	6.0 (Chickos and Acree, 2003)	1.95 (Lide, 2008)	0.122 (Lide, 2008)	13.00 (Dovbesh ko et al., 2015)	1

Gas Species	Molar Mass / g mol⁻¹	Substrate	Method	E^0_{des} / kJ mol⁻¹	τ_{des} / s	ΔH_{vap} (T) / kJ mol⁻¹	α / 10^{-24} cm³	μ / D	ε_r	O:C
CO	28.01	Au(111)	MB	11.7 (Borodin et al., 2020)	1.2×10⁻¹¹	6.0 (Chickos and Acree, 2003)	1.95 (Lide, 2008)	0.122 (Lide, 2008)		1
N₂	28.01	HOPG	TDS	13 (Ulbricht et al., 2006)	2.1×10⁻¹¹	5.57 (Lide, 2008)	1.74 (Lide, 2008)	0.001 (Gustafsson and Andersson, 2006)	13.00 (Dovbeshko et al., 2015)	0
SF₆	146.06	HOPG	TDS	31 (Ulbricht et al., 2006)	3.4×10⁻⁸	8.99 (Lide, 2008)	6.54 (Lide, 2008)	0.08 (Bruska and Piechota, 2008)	13.00 (Dovbeshko et al., 2015)	0
SF₆	146.06	HOPG	TDS	25 (Ulbricht et al., 2006)	2.9×10⁻⁹	8.99 (Lide, 2008)	6.54 (Lide, 2008)	0.08 (Bruska and Piechota, 2008)	13.00 (Dovbeshko et al., 2015)	0
O₂	32.00	HOPG	TDS	12 (Ulbricht et al., 2006)	1.4×10⁻¹¹	6.82 (Lide, 2008)	1.57 (Lide, 2008)	0.002 (on metal) (Gustafsson and Andersson, 2006)	13.00 (Dovbeshko et al., 2015)	0
O₂	32.00	HOPG	TDS	9 (Ulbricht et al., 2006)	4.0×10⁻¹²	6.82 (Lide, 2008)	1.57 (Lide, 2008)	0.002 (on metal) (Gustafsson and Andersson, 2006)	13.00 (Dovbeshko et al., 2015)	0
Xenon	131.29	HOPG	TD	24 (Ulbricht et al., 2006)	1.9×10⁻⁹	12.57 (Lide, 2008)	4.04 (Cambi et al., 1991)	0	13.00 (Dovbeshko et al., 2015)	0
Xenon	131.29	HOPG	TD	18 (Ulbricht et al., 2006)	1.6×10⁻¹⁰	12.57 (Lide, 2008)	4.04 (Cambi et al., 1991)	0	13.00 (Dovbeshko et al., 2015)	0

1206

Table A4. Compiled absorbate-substrate interaction energies for organic gases on self-assembled monolayers, salt, fly ash, and urban aerosol. Gas species, gas species' molar mass, substrate, experimental or theoretical method, desorption energy (E^0_{des}), and desorption lifetimes (τ_{des}) evaluated at 293 K using $A_{des} = 10^{13}$ s⁻¹, enthalpy of vaporization (ΔH_{vap}), gas species' polarizability (α), gas species' dipole moment (μ), substrate's relative permittivity (ε_r), and gas species' oxygen to carbon ration ($O{:}C$) are given.

Gas Species	Molar Mass / g mol⁻¹	Substrate	Method	E^0_{des} / kJ mol⁻¹	$\tau^{293\,K}_{des}$ / s	ΔH_{vap} (T) / kJ mol⁻¹	α / 10^{-24} cm³	μ / D	ε_r	O:C
methanol	32.04	thin nopinone	MB	17.4 (Kong et al., 2021)	1.3×10⁻¹⁰	37.8 (Chickos and Acree, 2003)	3.28 (Lide, 2008)	1.7 (Lide, 2008)		1
methanol	32.04	multilayer nopinone	MB	17.4 (Kong et al., 2021)	1.3×10⁻¹⁰	37.8 (Chickos and Acree, 2003)	3.28 (Lide, 2008)	1.7 (Lide, 2008)		1

methanol	32.04	SAM-methyl	TPD	47.7 (Dubois et al., 1990)	3.2×10^{-5}	37.8 (Chickos and Acree, 2003)	3.28 (Lide, 2008)	1.7 (Lide, 2008)	4.1 (Millany and Jonscher, 1980)	1
methanol	32.04	SAM-acid	TPD	35.1 (Dubois et al., 1990)	1.8×10^{-7}	37.8 (Chickos and Acree, 2003)	3.28 (Lide, 2008)	1.7 (Lide, 2008)	2.1 (Akkerman et al., 2007)	1
methanol	32.04	SAM-amide	TPD	41.0 (Dubois et al., 1990)	2.0×10^{-6}	37.8 (Chickos and Acree, 2003)	3.28 (Lide, 2008)	1.7 (Lide, 2008)		1
n-hexane	86.18	SAM-methyl	TPD	38.5 (Dubois et al., 1990)	7.3×10^{-7}	31.5 (Chickos and Acree, 2003)	11.9 (Lide, 2008)	0 (Yaws, 2014)	4.1 (Millany and Jonscher, 1980)	0
n-hexane	86.18	SAM-acid	TPD	33.9 (Dubois et al., 1990)	1.1×10^{-7}	31.5 (Chickos and Acree, 2003)	11.9 (Lide, 2008)	0 (Yaws, 2014)	2.1 (Akkerman et al., 2007)	0
anthracene	178.23	NaCl	TD	18 (Chu et al., 2010)	1.6×10^{-10}	79.6 (Chickos and Acree, 2003)	25.665 (Lide, 2008)	0 (Yaws, 2014)	5.9 (Lide, 2008)	0
pyrene	202.26	NaCl	TD	19.6 (Chu et al., 2010)	3.1×10^{-10}	78.6 (Chickos and Acree, 2003)	28.22 (Lide, 2008)	0 (Yaws, 2014)	5.9 (Lide, 2008)	0
benzo(a)pyrene	252.32	NaCl	TD	22.8 (Chu et al., 2010)	1.2×10^{-9}	91 (Chickos and Acree, 2003)	35.8 (Mceachran et al., 2018)	0 (Yaws, 2014)	5.9 (Lide, 2008)	0
perylene		NaCl	TD	123.5 (Steiner and Burtscher, 1994)	1.0×10^{9}	78.6 (Chickos and Acree, 2003)	35.8 (Mceachran et al., 2018)	0 (Yaws, 2014)	5.9 (Lide, 2008)	0
phenanthrene	178.23	fly ash	GC	24.3 (Lee and Chen, 1995)	2.2×10^{-9}	78.7 (Chickos and Acree, 2003)	30.75 (Lide, 2008)	0 (Yaws, 2014)	~5 (Sharif, 1995)	0
pyrene	202.26	fly ash	GC	26.6 (Lee and Chen, 1995)	5.5×10^{-9}	78.6 (Chickos and Acree, 2003)	28.22 (Lide, 2008)	0 (Yaws, 2014)	~5 (Sharif, 1995)	0
benzo(a)pyrene	252.33	fly ash	TD	31.2 (Chu et al., 2010)	3.7×10^{-8}	91 (Chickos and Acree, 2003)	35.8 (Mceachran et al., 2018)	0 (Yaws, 2014)	~5 (Sharif, 1995)	0
phenanthrene/ anthracene		urban aerosol	TD	18.9 (Yamasaki et al., 1982; Pankow, 1991)	2.3×10^{-10}			0 (Yaws, 2014)		0

Gas Species	Molar Mass	Substrate	Method	E_{des}^0	τ_{des}	ΔH_{vap}	α	μ	ε_r	O:C
pyrene	202.26	urban aerosol	TD	20.4 (Yamasaki et al., 1982; Pankow, 1991)	4.3×10⁻¹⁰	78.6 (Chickos and Acree, 2003)	28.22 (Lide, 2008)	0 (Yaws, 2014)		0
benzo(a)pyrene/benzo(e)pyrene		urban aerosol	TD	22.3 (Yamasaki et al., 1982; Pankow, 1991)	9.5×10⁻¹⁰			0 (Yaws, 2014)		0
perylene	252.32	carbon	TD	136.5 (Steiner and Burtscher, 1994)	2.2×10¹¹	123.1 (Chickos and Acree, 2003)	35.8 (Mceachran et al., 2018)	0 (Yaws, 2014)	13 (Dovbeshko et al., 2015)	0
perylene	252.32	diesel soot	TD	139 (Steiner and Burtscher, 1994)	6.0×10¹¹	123.1 (Chickos and Acree, 2003)	35.8 (Mceachran et al., 2018)	0 (Yaws, 2014)	13 (Dovbeshko et al., 2015)	0
perylene	252.32	oil burner soot	TD	140 (Steiner and Burtscher, 1994)	9.1×10¹¹	123.1 (Chickos and Acree, 2003)	35.8 (Mceachran et al., 2018)	0 (Yaws, 2014)	13 (Dovbeshko et al., 2015)	0

1213

Table A5. Compiled absorbate-substrate interaction energies of volatile organic compounds (VOCs) on graphite (C(0001)), highly oriented pyrolytic graphite (HOPG), granular activated carbon (GAC), and soot from combustion of kerosene. Gas species, gas species' molar mass, substrate, experimental or theoretical method, desorption energy (E_{des}^0), and desorption lifetimes (τ_{des}) evaluated at 293 K using $A_{des} = 10^{13}$ s⁻¹, enthalpy of vaporization (ΔH_{vap}), gas species' polarizability (α), gas species' dipole moment (μ), substrate's relative permittivity (ε_r), and gas species' oxygen to carbon ration ($O:C$) are given.

Gas Species	Molar Mass / g mol⁻¹	Substrate	Method	E_{des}^0 / kJ mol⁻¹	$\tau_{des}^{293\,K}$ / s	ΔH_{vap} (T) / kJ mol⁻¹	α / 10⁻²⁴ cm³	μ / D	ε_r	O:C
methane	16.04	graphite	TPD	14.1 (Tait et al., 2006)	3.3×10⁻¹¹	8.5 (Chickos and Acree, 2003)	2.59 (Lide, 2008)	0 (Yaws, 2014)	13.0 (Dovbeshko et al., 2015)	0
ethane	30.07	graphite	TPD	24.6 (Tait et al., 2006)	2.4×10⁻⁹	15.3 (Chickos and Acree, 2003)	4.45 (Lide, 2008)	0 (Yaws, 2014)	13.0 (Dovbeshko et al., 2015)	0
propane	44.10	graphite	TPD	32.1 (Tait et al., 2006)	5.3×10⁻⁸	18.8 (Chickos and Acree, 2003)	6.33 (Lide, 2008)	0 (Yaws, 2014)	13.0 (Dovbeshko et al., 2015)	0
butane	58.12	graphite	TPD	40.8 (Tait et al., 2006)	1.9×10⁻⁶	22.4 (Chickos and Acree, 2003)	8.2 (Lide, 2008)	0 (Yaws, 2014)	13.0 (Dovbeshko et al., 2015)	0
pentane	72.15	graphite	TPD	65 (Paserba and	3.9×10⁻²	25 (Chickos and Acree, 2003)	9.99 (Lide, 2008)	0 (Yaws, 2014)	13.0 (Dovbeshk	0

									o et al., 2015)	
hexane	86.18	graphite	TPD	63 (Tait et al., 2006)	1.7×10^{-2}	31.5 (Chickos and Acree, 2003)	11.9 (Lide, 2008)	0 (Yaws, 2014)	13.0 (Dovbeshko et al., 2015)	0
hexane	86.18	graphite	TPD	73.6 (Paserba and Gellman, 2001)	1.3	31.5 (Chickos and Acree, 2003)	11.9 (Lide, 2008)	0 (Yaws, 2014)	13.0 (Dovbeshko et al., 2015)	0
heptane	100.21	graphite	TPD	81.5 (Paserba and Gellman, 2001)	3.4×10^{1}	36.6 (Chickos and Acree, 2003)	13.61 (Lide, 2008)	0 (Yaws, 2014)	13.0 (Dovbeshko et al., 2015)	0
octane	114.23	graphite	TPD	72.6 (Tait et al., 2006)	8.8×10^{-1}	41.6 (Chickos and Acree, 2003)	15.9 (Lide, 2008)	0 (Yaws, 2014)	13.0 (Dovbeshko et al., 2015)	0
octane	114.23	graphite	TPD	88.2 (Paserba and Gellman, 2001)	5.3×10^{2}	41.6 (Chickos and Acree, 2003)	15.9 (Lide, 2008)	0 (Yaws, 2014)	13.0 (Dovbeshko et al., 2015)	0
decane	142.29	graphite	TPD	91.4 (Tait et al., 2006)	2.0×10^{3}	51.4 (Chickos and Acree, 2003)	19.1 (Lide, 2008)	0 (Yaws, 2014)	13.0 (Dovbeshko et al., 2015)	0
decane	142.29	graphite	TPD	101 (Paserba and Gellman, 2001)	1.0×10^{5}	51.4 (Chickos and Acree, 2003)	19.1 (Lide, 2008)	0 (Yaws, 2014)	13.0 (Dovbeshko et al., 2015)	0
dodecane	170.33	graphite	TPD	114.8 (Paserba and Gellman, 2001)	2.9×10^{7}	62.1 (Chickos and Acree, 2003)	22.75 (Lide, 2008)	0 (Yaws, 2014)	13.0 (Dovbeshko et al., 2015)	0
tetradecane	198.39	graphite	TPD	124.7 (Paserba and Gellman, 2001)	1.7×10^{9}	72.1 (Chickos and Acree, 2003)	26.22 (Laib and Mittleman, 2010)	0 (Yaws, 2014)	13.0 (Dovbeshko et al., 2015)	0
hexadecane	226.41	graphite	TPD	134.3 (Paserba and Gellman, 2001)	8.7×10^{10}	81.4 (Chickos and Acree, 2003)	29.84 (Laib and Mittleman, 2010)	0 (Yaws, 2014)	13.0 (Dovbeshko et al., 2015)	0
octadecane	254.50	graphite	TPD	146.7 (Paserba and Gellman, 2001)	1.4×10^{13}	91.8 (Chickos and Acree, 2003)	33.46 (Laib and Mittleman, 2010)	0 (Yaws, 2014)	13.0 (Dovbeshko et al., 2015)	0
icosane	282.55	graphite	TPD	156.2 (Paserba and Gellman, 2001)	7.0×10^{14}	100 (Chickos and Acree, 2003)	37.08 (Laib and Mittleman, 2010)	0 (Yaws, 2014)	13.0 (Dovbeshko et al., 2015)	0

docosane	310.61	graphite	TPD	166.2 (Paserba and Gellman, 2001)	4.3×10^{16}	115.6 (Chickos and Acree, 2003)	40.7 (Laib and Mittleman, 2010)	0 (Yaws, 2014)	13.0 (Dovbeshko et al., 2015)	0
tetracosane	338.65	graphite	TPD	174.2 (Paserba and Gellman, 2001)	1.1×10^{18}	126.8 (Chickos and Acree, 2003)	44.32 (Laib and Mittleman, 2010)	0 (Yaws, 2014)	13.0 (Dovbeshko et al., 2015)	0
hexacosane	366.71	graphite	TPD	182.3 (Paserba and Gellman, 2001)	3.2×10^{19}	106.1 (Chickos and Acree, 2003)	47.94 (Laib and Mittleman, 2010)	0 (Yaws, 2014)	13.0 (Dovbeshko et al., 2015)	0
octacosane	396.79	graphite	TPD	190.7 (Paserba and Gellman, 2001)	9.9×10^{20}	150.8 (Chickos and Acree, 2003)	51.56 (Laib and Mittleman, 2010)	0 (Yaws, 2014)	13.0 (Dovbeshko et al., 2015)	0
dotriacontane	452.88	graphite	TPD	205.5 (Paserba and Gellman, 2001)	4.3×10^{23}	130.5 (Chickos and Acree, 2003)	58.8 (Laib and Mittleman, 2010)	0 (Yaws, 2014)	13.0 (Dovbeshko et al., 2015)	0
hexatriacontane	506.97	graphite	TPD	219.6 (Paserba and Gellman, 2001)	1.4×10^{26}	157 (Chickos and Acree, 2003)	66.04 (Laib and Mittleman, 2010)	0 (Yaws, 2014)	13.0 (Dovbeshko et al., 2015)	0
tetracontane	563.08	graphite	TPD	232.9 (Paserba and Gellman, 2001)	3.3×10^{28}	132.2 (Chickos and Acree, 2003)	73.28 (Laib and Mittleman, 2010)	0 (Yaws, 2014)	13.0 (Dovbeshko et al., 2015)	0
tetratetracontane	619.19	graphite	TPD	246.2 (Paserba and Gellman, 2001)	7.8×10^{30}	140.1 (Chickos and Acree, 2003)	80.52 (Laib and Mittleman, 2010)	0 (Yaws, 2014)	13.0 (Dovbeshko et al., 2015)	0
octatetracontane	677.31	graphite	TPD	256.7 (Paserba and Gellman, 2001)	5.8×10^{32}	145.9 (Chickos and Acree, 2003)	87.76 (Laib and Mittleman, 2010)	0 (Yaws, 2014)	13.0 (Dovbeshko et al., 2015)	0
hexapentacontane	787.50	graphite	TPD	280.5 (Paserba and Gellman, 2001)	1.0×10^{37}	157.8 (Chickos and Acree, 2003)	102.24 (Laib and Mittleman, 2010)	0 (Yaws, 2014)	13.0 (Dovbeshko et al., 2015)	0
hexacontane	843.61	graphite	TPD	289 (Paserba and Gellman, 2001)	3.3×10^{38}	163 (Chickos and Acree, 2003)	109.48 (Laib and Mittleman, 2010)	0 (Yaws, 2014)	13.0 (Dovbeshko et al., 2015)	0
methanol (monomer)	32.04	graphite	MB	17.4 (Kong et al., 2021)	1.3×10^{-10}	37.8 (Chickos and Acree, 2003)	3.28 (Laib and Mittleman, 2010)	1.7 (Lide, 2008)	13.0 (Dovbeshko et al., 2015)	1

methanol (clusters)	32.04	graphite	MB	34.7 (Kong et al., 2019)	1.5×10^{-7}	37.8 (Chickos and Acree, 2003)	3.28 (Laib and Mittleman, 2010)	1.7 (Lide, 2008)	13.0 (Dovbeshko et al., 2015)	1
methanol (monomer)	32.04	graphene	DFT	20.6 (Schroder, 2013)	4.7×10^{-10}	37.8 (Chickos and Acree, 2003)	3.28 (Laib and Mittleman, 2010)	1.7 (Lide, 2008)	13.0 (Dovbeshko et al., 2015)	1
methanol (3 cluster)	32.04	graphene	DFT	30.4 (Schroder, 2013)	2.6×10^{-8}	37.8 (Chickos and Acree, 2003)	3.28 (Laib and Mittleman, 2010)	1.7 (Lide, 2008)	13.0 (Dovbeshko et al., 2015)	1
methanol (5 cluster)	32.04	graphene	DFT	34.9 (Schroder, 2013)	1.7×10^{-7}	37.8 (Chickos and Acree, 2003)	3.28 (Laib and Mittleman, 2010)	1.7 (Lide, 2008)	13.0 (Dovbeshko et al., 2015)	1
methane	16.04	HOPG	TDS	17 (Ulbricht et al., 2006)	1.1×10^{-10}	8.5 (Chickos and Acree, 2003)	2.59 (Laib and Mittleman, 2010)	0 (Yaws, 2014)	13.0 (Dovbeshko et al., 2015)	0
methanol	32.04	HOPG	TDS	48 (Ulbricht et al., 2006)	3.6×10^{-5}	37.8 (Chickos and Acree, 2003)	3.28 (Laib and Mittleman, 2010)	1.7 (Lide, 2008)	13.0 (Dovbeshko et al., 2015)	1
ethanol	46.07	HOPG	TDS	50 (Ulbricht et al., 2006)	8.2×10^{-5}	42.4 (Chickos and Acree, 2003)	5.26 (Laib and Mittleman, 2010)	1.69 (Lide, 2008)	13.0 (Dovbeshko et al., 2015)	0.5
1,1-dichloroethane	98.96	HOPG	TDS	51 (Ulbricht et al., 2006)	1.2×10^{-4}	33.5 (Chickos and Acree, 2003)	8.64 (Laib and Mittleman, 2010)	2.06 (Lide, 2008)	13.0 (Dovbeshko et al., 2015)	0
trichloromethane	119.38	HOPG	TDS	54 (Ulbricht et al., 2006)	4.2×10^{-4}	31.1 (Chickos and Acree, 2003)	8.87 (Laib and Mittleman, 2010)	1.04 (Lide, 2008)	13.0 (Dovbeshko et al., 2015)	0
benzene	78.11	HOPG	TDS	48 (Ulbricht et al., 2006)	3.6×10^{-5}	42.3 (Chickos and Acree, 2003)	10.53 (Laib and Mittleman, 2010)	0 (Yaws, 2014)	13.0 (Dovbeshko et al., 2015)	0
n,n-dimethylformamide	73.09	HOPG	TDS	53 (Ulbricht et al., 2006)	2.8×10^{-4}	46.9 (Chickos and Acree, 2003)	7.93 (Bosque and Sales, 2002)	3.82 (Lide, 2008)	13.0 (Dovbeshko et al., 2015)	0
ethylbenzene	106.17	HOPG	TDS	79 (Ulbricht et al., 2006)	1.2×10^{1}	42.3 (Chickos and Acree, 2003)	14.2 (Laib and Mittleman, 2010)	0.59 (Lide, 2008)	13.0 (Dovbeshko et al., 2015)	0
toluene	92.14	HOPG	TDS	68 (Ulbricht et al., 2006)	1.3×10^{-1}	38.9 (Chickos and Acree, 2003)	12.12 (Laib and Mittleman, 2010)	0.375 (Lide, 2008)	13.0 (Dovbeshko et al., 2015)	0
sigma-dichlorobenzene	147.01	HOPG	TDS	69 (Ulbricht et al., 2006)	2.0×10^{-1}	50.9 (Chickos and Acree, 2003)	14.3 (Mceachran et al., 2018)	2.5 (Lide, 2008)	13.0 (Dovbeshko et al., 2015)	0
naphthalene	128.17	HOPG	TDS	77 (Ulbricht et al., 2006)	5.3	53.4 (Chickos and Acree, 2003)	17 (Laib and Mittleman, 2010)	0 (Yaws, 2014)	13.0 (Dovbeshko et al., 2015)	0

coronene	300.35	HOPG	TDS	127 (Ulbricht et al., 2006)	4.4×10⁹	148 (Chickos and Acree, 2003)	42.5 (Laib and Mittleman, 2010)	0 (Yaws, 2014)	13.0 (Dovbeshko et al., 2015)	0
fullerene	720.66	HOPG	TDS	163 (Ulbricht et al., 2006)	1.1×10¹⁶	42.4 (Chickos and Acree, 2003)	76.5	0 (Yaws, 2014)	13.0 (Dovbeshko et al., 2015)	0
ovalene	398.45	HOPG	TDS	230 (Ulbricht et al., 2006)	1.0×10²⁸	31.6 (Chickos and Acree, 2003)	45.8	0 (Yaws, 2014)	13.0 (Dovbeshko et al., 2015)	0
ethanol	46.07	GAC	TG-DSC	56.8 (Giraudet et al., 2006)	1.3×10⁻³	31.3 (Chickos and Acree, 2003)	5.26 (Lide, 2008)	1.69 (Lide, 2008)	13.0 (Dovbeshko et al., 2015)	0.5
acrylnitrile	53.06	GAC	TG-DSC	49 (Giraudet et al., 2006)	5.4×10⁻⁵	28.8 (Chickos and Acree, 2003)	8.05 (Lide, 2008)	3.87 (Lide, 2008)	13.0 (Dovbeshko et al., 2015)	0
acetone	58.08	GAC	TG-DSC	51.1 (Giraudet et al., 2006)	1.3×10⁻⁴	47.45 (Chickos and Acree, 2003)	6.37 (Lide, 2008)	2.88 (Lide, 2008)	13.0 (Dovbeshko et al., 2015)	0.33
dichloromethane	84.93	GAC	TG-DSC	45.6 (Giraudet et al., 2006)	1.3×10⁻⁵	31.6 (Chickos and Acree, 2003)	7.21 (Lide, 2008)	1.6 (Lide, 2008)	13.0 (Dovbeshko et al., 2015)	0
propanol	60.09	GAC	TG-DSC	52.6 (Giraudet et al., 2006)	2.4×10⁻⁴	33.1 (Chickos and Acree, 2003)	6.74 (Lide, 2008)	2.52 (Lide, 2008)	13.0 (Dovbeshko et al., 2015)	0.33
ethyl formate	74.08	GAC	TG-DSC	52 (Giraudet et al., 2006)	1.9×10⁻⁴	42.3 (Chickos and Acree, 2003)	6.88 (Lide, 2008)	1.9 (Lide, 2008)	13.0 (Dovbeshko et al., 2015)	0.67
cyclohexane	84.16	GAC	TG-DSC	55.7 (Giraudet et al., 2006)	8.5×10⁻⁴	34.5 (Chickos and Acree, 2003)	10.87 (Lide, 2008)	0.61 (Yaws, 2014)	13.0 (Dovbeshko et al., 2015)	0
benzene	78.11	GAC	TG-DSC	56.7 (Giraudet et al., 2006)	1.3×10⁻³	34.7 (Chickos and Acree, 2003)	10.53 (Lide, 2008)	0 (Yaws, 2014)	13.0 (Dovbeshko et al., 2015)	0
fluorobenzene	96.10	GAC	TG-DSC	57.4 (Giraudet et al., 2006)	1.7×10⁻³	36.9 (Chickos and Acree, 2003)	10.3 (Lide, 2008)	1.6 (Lide, 2008)	13.0 (Dovbeshko et al., 2015)	0
methylethylketone	72.11	GAC	TG-DSC	58 (Giraudet et al., 2006)	2.2×10⁻³	30.6 (Chickos and Acree, 2003)	8.19 (Nist, 2018)	2.78 (Lide, 2008)	13.0 (Dovbeshko et al., 2015)	0.25
3-methylbutane-2-one	86.13	GAC	TG-DSC	60.7 (Giraudet et al., 2006)	6.6×10⁻³	31.5 (Chickos and Acree, 2003)	10.02 (Bosque and Sales, 2002)	2.77 (Lide, 2008)	13.0 (Dovbeshko et al., 2015)	0.2
hex-1-ene	84.16	GAC	TG-DSC	62.9 (Giraudet et al., 2006)	1.6×10⁻²	32.1 (Chickos and Acree, 2003)	11.65 (Lide, 2008)	0.4	13.0 (Dovbeshko et al., 2015)	0

hexane	86.18	GAC	TG-DSC	63.4 (Giraudet et al., 2006)	2.0×10^{-2}	34.9 (Chickos and Acree, 2003)	11.9 (Lide, 2008)	0 (Yaws, 2014)	13.0 (Dovbeshko et al., 2015)	0
isopropylether	102.18	GAC	TG-DSC	65.9 (Giraudet et al., 2006)	5.6×10^{-2}	42.4 (Chickos and Acree, 2003)	12.65 (Bosque and Sales, 2002)	1.13 (Lide, 2008)	13.0 (Dovbeshko et al., 2015)	0.17
triethylamine	101.19	GAC	TG-DSC	74.1 (Giraudet et al., 2006)	1.6	31.6 (Chickos and Acree, 2003)	7.97 (Lide, 2008)	0.66 (Lide, 2008)	13.0 (Dovbeshko et al., 2015)	0
phenanthrene	178.23	kerosene soot	KU	85.6 (Guilloteau et al., 2010)	1.8×10^{2}	78.7 (Chickos and Acree, 2003)	30.75 (Lide, 2008)	0 (Yaws, 2014)	13.0 (Dovbeshko et al., 2015)	0
anthracene	178.23	kerosene soot	KU	88.1 (Guilloteau et al., 2010)	5.1×10^{2}	79.6 (Chickos and Acree, 2003)	25.67 (Lide, 2008)	0 (Yaws, 2014)	13.0 (Dovbeshko et al., 2015)	0
fluoranthene	202.26	kerosene soot	KU	93.9 (Guilloteau et al., 2008)	5.5×10^{3}	79.3 (Chickos and Acree, 2003)	23.23	0.23 (Yaws, 2014)	13.0 (Dovbeshko et al., 2015)	0
pyrene	202.26	kerosene soot	KU	95.2 (Guilloteau et al., 2008)	9.4×10^{3}	78.6 (Chickos and Acree, 2003)	28.22 (Lide, 2008)	0 (Yaws, 2014)	13.0 (Dovbeshko et al., 2015)	0
benzo(ghi)fluoranthene	226.28	kerosene soot	KU	112.1 (Guilloteau et al., 2010)	9.6×10^{6}	88.5 (Chickos and Acree, 2003)	32.9 (Mceachran et al., 2018)	0 (Yaws, 2014)	13.0 (Dovbeshko et al., 2015)	0
acepyrene	226.27	kerosene soot	KU	107.1 (Guilloteau et al., 2010)	1.2×10^{6}		31.6 (Mceachran et al., 2018)	0 (Yaws, 2014)	13.0 (Dovbeshko et al., 2015)	0
benzo(a)anthracene	228.29	kerosene soot	KU	113.9 (Guilloteau et al., 2010)	2.0×10^{7}	91 (Chickos and Acree, 2003)	32.86 (Lide, 2008)	0 (Yaws, 2014)	13.0 (Dovbeshko et al., 2015)	0
chrysene	228.29	kerosene soot	KU	114.9 (Guilloteau et al., 2010)	3.0×10^{7}	89.6 (Chickos and Acree, 2003)	33.06 (Lide, 2008)	0 (Yaws, 2014)	13.0 (Dovbeshko et al., 2015)	0
benzo(e)pyrene	252.32	kerosene soot	KU	119.9 (Guilloteau et al., 2010)	2.4×10^{8}	92 (Chickos and Acree, 2003)	35.8 (Mceachran et al., 2018)	0 (Yaws, 2014)	13.0 (Dovbeshko et al., 2015)	0
benzo(b)fluoranthene	252.31	kerosene soot	KU	118.7 (Guilloteau et al., 2010)	1.4×10^{8}	89.7 (Chickos and Acree, 2003)	35.8 (Mceachran et al., 2018)	0 (Yaws, 2014)	13.0 (Dovbeshko et al., 2015)	0
benzo(k)fluoranthene	252.32	kerosene soot	KU	120.8 (Guilloteau et al., 2010)	3.4×10^{8}	88.5 (Chickos and Acree, 2003)	35.8 (Mceachran et al., 2018)	0 (Yaws, 2014)	13.0 (Dovbeshko et al., 2015)	0
benzo(a)pyrene	252.32	kerosene soot	KU	121.8 (Guilloteau et al., 2010)	5.2×10^{8}	91 (Chickos and Acree, 2003)	35.8 (Mceachran et al., 2018)	0 (Yaws, 2014)	13.0 (Dovbeshko et al., 2015)	0

1221

Table A6. Compiled absorbate-substrate interaction energies of volatile organic compounds (VOCs) on MgO(100), Pt(111), Ni(111), and Pd(111). Gas species, gas species' molar mass, substrate, experimental or theoretical method, desorption energy (E_{des}^0), and desorption lifetimes (τ_{des}) evaluated at 293 K using $A_{des} = 10^{13}$ s^{-1}, enthalpy of vaporization (ΔH_{vap}), gas species' polarizability (α), gas species' dipole moment (μ), substrate's relative permittivity (ε_r), and gas species' oxygen to carbon ration ($O{:}C$) are given.

Gas Species	Molar Mass / g mol^{-1}	Substrate	Method	E_{des}^0 / kJ mol^{-1}	$\tau_{des}^{293\,K}$ / s	ΔH_{vap} (T) / kJ mol^{-1}	α / 10^{-24} cm^3	μ / D	ε_r	O:C
methane	16.04	MgO(100)	TPD	12.1 (Tait et al., 2006)	1.4×10^{-11}	8.5 (Chickos and Acree, 2003)	2.59 (Lide, 2008)	0 (Yaws, 2014)	9.65 (Lide, 2008)	0
ethane	30.07	MgO(100)	TPD	22.2 (Tait et al., 2006)	9.1×10^{-10}	15.3 (Chickos and Acree, 2003)	4.45 (Lide, 2008)	0 (Yaws, 2014)	9.65 (Lide, 2008)	0
propane	44.10	MgO(100)	TPD	29 (Tait et al., 2006)	1.5×10^{-8}	18.8 (Chickos and Acree, 2003)	6.33 (Lide, 2008)	0 (Yaws, 2014)	9.65 (Lide, 2008)	0
butane	58.12	MgO(100)	TPD	34.9 (Tait et al., 2006)	1.7×10^{-7}	22.4 (Chickos and Acree, 2003)	8.2 (Lide, 2008)	0 (Yaws, 2014)	9.65 (Lide, 2008)	0
hexane	86.18	MgO(100)	TPD	46.4 (Tait et al., 2006)	1.9×10^{-5}	31.5 (Chickos and Acree, 2003)	11.9 (Lide, 2008)	0 (Yaws, 2014)	9.65 (Lide, 2008)	0
octane	114.23	MgO(100)	TPD	62.9 (Tait et al., 2006)	1.6×10^{-2}	41.6 (Chickos and Acree, 2003)	15.9 (Lide, 2008)	0 (Yaws, 2014)	9.65 (Lide, 2008)	0
decane	142.29	MgO(100)	TPD	77.9 (Tait et al., 2006)	7.7	51.4 (Chickos and Acree, 2003)	19.1 (Lide, 2008)	0 (Yaws, 2014)	9.65 (Lide, 2008)	0
methane	16.04	Pt(111)	TPD	15.2 (Tait et al., 2006)	5.1×10^{-11}	8.5 (Chickos and Acree, 2003)	2.59 (Lide, 2008)	0 (Yaws, 2014)		0
methane	16.04	Pt(111)	TPD	16.1 (Weaver et al., 2003)	7.4×10^{-11}	8.5 (Chickos and Acree, 2003)	2.59 (Lide, 2008)	0 (Yaws, 2014)		0
ethane	30.07	Pt(111)	TPD	28.9 (Tait et al., 2006)	1.4×10^{-8}	15.3 (Chickos and Acree, 2003)	4.45 (Lide, 2008)	0 (Yaws, 2014)		0
ethane	30.07	Pt(111)	TPD	36.8 (Weaver et al., 2003)	3.6×10^{-7}	15.3 (Chickos and Acree, 2003)	4.45 (Lide, 2008)	0 (Yaws, 2014)		0
propane	44.10	Pt(111)	TPD	41.5 (Tait et al., 2006)	2.5×10^{-6}	18.8 (Chickos and Acree, 2003)	6.33 (Lide, 2008)	0 (Yaws, 2014)		0

propane	44.10		Pt(111)	TPD	41.2 (Weaver et al., 2003)	2.2×10^{-6}	18.8 (Chickos and Acree, 2003)	6.33 (Lide, 2008)	0 (Yaws, 2014)	0
butane	58.12		Pt(111)	TPD	50.9 (Tait et al., 2006)	1.2×10^{-4}	22.4 (Chickos and Acree, 2003)	8.2 (Lide, 2008)	0 (Yaws, 2014)	0
butane	58.12		Pt(111)	TPD	60.2 (Weaver et al., 2003)	5.4×10^{-3}	22.4 (Chickos and Acree, 2003)	8.2 (Lide, 2008)	0 (Yaws, 2014)	0
butane	58.12		Pt(111)	TPD	34.3 (Salmeron and Somorjai, 1981)	1.3×10^{-7}	22.4 (Chickos and Acree, 2003)	8.2 (Lide, 2008)	0 (Yaws, 2014)	0
pentane	72.15		Pt(111)	TPD	42.7 (Salmeron and Somorjai, 1981)	4.1×10^{-6}	25 (Chickos and Acree, 2003)	9.99 (Lide, 2008)	0 (Yaws, 2014)	0
hexane	86.18		Pt(111)	TPD	79.8 (Tait et al., 2006)	1.7×10^{1}	31.5 (Chickos and Acree, 2003)	11.9 (Lide, 2008)	0 (Yaws, 2014)	0
hexane	86.18		Pt(111)	TPD	61.9 (Bishop et al., 2000)	1.1×10^{-2}	31.5 (Chickos and Acree, 2003)	11.9 (Lide, 2008)	0 (Yaws, 2014)	0
heptane	100.21		Pt(111)	TPD	66.4 (Bishop et al., 2000)	6.9×10^{-2}	36.6 (Chickos and Acree, 2003)	13.61 (Lide, 2008)	0 (Yaws, 2014)	0
octane	114.23		Pt(111)	TPD	72 (Bishop et al., 2000)	6.8×10^{-1}	41.6 (Chickos and Acree, 2003)	15.9 (Lide, 2008)	0 (Yaws, 2014)	0
nonane	128.20		Pt(111)	TPD	74.2 (Bishop et al., 2000)	1.7	46.55 (Chickos and Acree, 2003)	17.36 (Lide, 2008)	0 (Yaws, 2014)	0
decane	142.29		Pt(111)	TPD	76.1 (Bishop et al., 2000)	3.7	51.4 (Chickos and Acree, 2003)	19.1 (Lide, 2008)	0 (Yaws, 2014)	0
propane	44.10		Ni(111)	DFT	57.9 (Mendes et al., 2019)	1.4×10^{8}	18.8 (Chickos and Acree, 2003)	6.33 (Lide, 2008)	0 (Yaws, 2014)	0
1-propanol	60.09		Ni(111)	DFT	92.6 (Mendes et al., 2019)	3.3×10^{3}	47.45 (Chickos and Acree, 2003)	6.74 (Lide, 2008)	1.58 (Lide, 2008)	0.33
2-propanol	60.09		Ni(111)	DFT	89.7 (Mendes et al., 2019)	9.9×10^{2}	47.45 (Chickos and Acree, 2003)	6.74 (Lide, 2008)	1.58 (Lide, 2008)	0.33
1,2-propanediol	76.09		Ni(111)	DFT	111.0 (Mendes et al., 2019)	6.0×10^{6}	60.0 (Chickos	7.55 (Bosque	2.25 (Lide, 2008)	0.66

						and Acree, 2003)	and Sales, 2002)			
1,3-propanediol	76.09	Ni(111)	DFT	111.0 (Mendes et al., 2019)	6.0×10^6	72.4 (Chickos and Acree, 2003)	7.55 (Bosque and Sales, 2002)	2.55 (Lide, 2008)		0.66
glycerol	92.09	Ni(111)	DFT	118.7 (Mendes et al., 2019)	1.4×10^8	91.7 (Chickos and Acree, 2003)	8.14 (Bosque and Sales, 2002)	2.56 (Lide, 2008)		1
propane	44.10	Pd(111)	DFT	57.9 (Mendes et al., 2019)	2.1×10^{-3}	18.8 (Chickos and Acree, 2003)	6.33 (Lide, 2008)	0 (Yaws, 2014)		0
1-propanol	60.09	Pd(111)	DFT	84.9 (Mendes et al., 2019)	1.4×10^2	47.45 (Chickos and Acree, 2003)	6.74 (Lide, 2008)	1.58 (Lide, 2008)		0.33
2-propanol	60.09	Pd(111)	DFT	85.9 (Mendes et al., 2019)	2.0×10^2	47.45 (Chickos and Acree, 2003)	6.74 (Lide, 2008)	1.58 (Lide, 2008)		0.33
1,2-propanediol	76.09	Pd(111)	DFT	101.3 (Mendes et al., 2019)	1.1×10^5	60.0 (Chickos and Acree, 2003)	7.55 (Bosque and Sales, 2002)	2.25 (Lide, 2008)		0.66
1,3-propanediol	76.09	Pd(111)	DFT	102.3 (Mendes et al., 2019)	1.7×10^5	72.4 (Chickos and Acree, 2003)	7.55 (Bosque and Sales, 2002)	2.55 (Lide, 2008)		0.66
glycerol	92.09	Pd(111)	DFT	116.7 (Mendes et al., 2019)	6.5×10^7	91.7 (Chickos and Acree, 2003)	8.14 (Bosque and Sales, 2002)	2.56 (Lide, 2008)		1
propane	44.10	Pt(111)	DFT	65.6 (Mendes et al., 2019)	5.0×10^{-2}	18.8 (Chickos and Acree, 2003)	6.33 (Lide, 2008)	0 (Yaws, 2014)		0
1-propanol	60.09	Pt(111)	DFT	100.3 (Mendes et al., 2019)	7.7×10^4	47.45 (Chickos and Acree, 2003)	6.74 (Lide, 2008)	1.58 (Lide, 2008)		0.33
2-propanol	60.09	Pt(111)	DFT	99.4 (Mendes et al., 2019)	5.2×10^4	47.45 (Chickos and Acree, 2003)	6.74 (Lide, 2008)	1.58 (Lide, 2008)		0.33
1,2-propanediol	76.09	Pt(111)	DFT	114.8 (Mendes et al., 2019)	2.9×10^7	60.0 (Chickos and Acree, 2003)	7.55 (Bosque and Sales, 2002)	2.25 (Lide, 2008)		0.66
1,3-propanediol	76.09	Pt(111)	DFT	119.6 (Mendes et al., 2019)	2.1×10^8	72.4 (Chickos and Acree, 2003)	7.55 (Bosque and Sales, 2002)	2.55 (Lide, 2008)		0.66
glycerol	92.09	Pt(111)	DFT	133.1 (Mendes et al., 2019)	5.5×10^{10}	91.7 (Chickos and Acree, 2003)	8.14 (Bosque and Sales, 2002)	2.56 (Lide, 2008)		1

1228

1229

1230 **Table A7.** Compiled absorbate-substrate interaction energies of volatile organic compounds
1231 (VOCs) on mineral surrogates and minerals and clays. Gas species, gas species' molar mass,
1232 substrate, experimental or theoretical method, desorption energy (E^0_{des}), and desorption lifetimes
1233 (τ_{des}) evaluated at 293 K using $A_{des} = 10^{13}$ s^{-1}, enthalpy of vaporization (ΔH_{vap}), gas species'
1234 polarizability (α), gas species' dipole moment (μ), substrate's relative permittivity (ε_r), and gas
1235 species' oxygen to carbon ration ($O:C$) are given.

Gas Species	Molar Mass / g mol^{-1}	Substrate	Method	E^0_{des} / kJ mol^{-1}	$\tau^{293\,K}_{des}$ / s	ΔH_{vap} (T) / kJ mol^{-1}	α / 10^{-24} cm^3	μ / D	ε_r	O:C
n-decane	142.29	α-Al$_2$O$_3$	IGC	28.5 (Goss and Eisenreich, 1996)	1.2×10^{-8}	51.4 (Chickos and Acree, 2003)	19.1 (Lide, 2008)	0 (Yaws, 2014)	9.34 (Lide, 2008)	0
o-xylene	106.17	α-Al$_2$O$_3$	IGC	26.6 (Goss and Eisenreich, 1996)	5.5×10^{-9}	42.9 (Chickos and Acree, 2003)	14.25 (Bosque and Sales, 2002)	0.64 (Lide, 2008)	9.34 (Lide, 2008)	0
propylbenzene	120.19	α-Al$_2$O$_3$	IGC	30.3 (Goss and Eisenreich, 1996)	2.5×10^{-8}	46.2 (Chickos and Acree, 2003)	16 (Mceachran et al., 2018)	0.369 (Yaws, 2014)	9.34 (Lide, 2008)	0
1,2-dichlorobenzene	147.01	α-Al$_2$O$_3$	IGC	28.0 (Goss and Eisenreich, 1996)	9.7×10^{-9}	49.9 (Chickos and Acree, 2003)	14.3 (Bosque and Sales, 2002)	2.5 (Lide, 2008)	9.34 (Lide, 2008)	0
1,4-dichlorobenzene	147.01	α-Al$_2$O$_3$	IGC	26.6 (Goss and Eisenreich, 1996)	5.5×10^{-9}	54.8 (Chickos and Acree, 2003)	14.3 (Mceachran et al., 2018)	1.72 (Lide, 2008)	9.34 (Lide, 2008)	0
1,2,3,4-tetrachlorobenzene	215.89	α-Al$_2$O$_3$	IGC	42.7 (Goss and Eisenreich, 1996)	4.0×10^{-6}	60.1 (Chickos and Acree, 2003)	18.2 (Mceachran et al., 2018)	2.42 (Lide, 2008)	9.34 (Lide, 2008)	0
naphthalene	128.17	α-Al$_2$O$_3$	IGC	38.0 (Goss and Eisenreich, 1996)	5.9×10^{-7}	53.4 (Chickos and Acree, 2003)	17 (Lide, 2008)	0 (Yaws, 2014)	9.34 (Lide, 2008)	0
anisole	108.14	α-Al$_2$O$_3$	IGC	37.7 (Goss and Eisenreich, 1996)	5.2×10^{-7}	45.3 (Chickos and Acree, 2003)	13.1 (Lide, 2008)	1.38 (Lide, 2008)	9.34 (Lide, 2008)	0.14
pyridine	79.10	α-Al$_2$O$_3$	IGC	47.0 (Goss and Eisenreich, 1996)	2.4×10^{-5}	40.2 (Chickos and Acree, 2003)	9.34 (Lide, 2008)	2.215 (Lide, 2008)	9.34 (Lide, 2008)	0
ethanol	46.07	α-Al$_2$O$_3$	IGC	48.4 (Goss and Eisenreich, 1996)	4.2×10^{-5}	42.4 (Chickos and Acree, 2003)	5.41 (Lide, 2008)	1.69 (Lide, 2008)	9.34 (Lide, 2008)	0.5
ethyl acetate	88.11	α-Al$_2$O$_3$	IGC	40.2 (Goss and Eisenreich, 1996)	1.5×10^{-6}	35 (Chickos and Acree, 2003)	8.62 (Lide, 2008)	1.78 (Lide, 2008)	9.34 (Lide, 2008)	0.5
acetone	58.08	α-Al$_2$O$_3$	IGC	38.0 (Goss and Eisenreich, 1996)	5.9×10^{-7}	31.3 (Chickos and Acree, 2003)	6.37 (Lide, 2008)	2.88 (Lide, 2008)	9.34 (Lide, 2008)	0.33

n-nonane	128.26	CaCO$_3$	IGC	30.4 (Goss and Eisenreich, 1996)	2.7×10^{-8}	46.55 (Chickos and Acree, 2003)	17.36 (Lide, 2008)	0 (Yaws, 2014)	8.67 (Lide, 2008)	0
p-xylene	106.17	CaCO$_3$	IGC	35.5 (Goss and Eisenreich, 1996)	2.2×10^{-7}	42.3 (Chickos and Acree, 2003)	14.35 (Bosque and Sales, 2002)	0 (Yaws, 2014)	8.67 (Lide, 2008)	0
ethylbenzene	106.17	CaCO$_3$	IGC	34.1 (Goss and Eisenreich, 1996)	1.2×10^{-7}	42.3 (Chickos and Acree, 2003)	14.2 (Lide, 2008)	0.59 (Lide, 2008)	8.67 (Lide, 2008)	0
chlorobenzene	112.56	CaCO$_3$	IGC	28.1 (Goss and Eisenreich, 1996)	1.0×10^{-8}	40.3 (Chickos and Acree, 2003)	13.2 (Lide, 2008)	1.69 (Lide, 2008)	8.67 (Lide, 2008)	0
1,2-dichlorobenzene	147.01	CaCO$_3$	IGC	36.8 (Goss and Eisenreich, 1996)	3.7×10^{-7}	49.9 (Chickos and Acree, 2003)	14.3 (Bosque and Sales, 2002)	2.5 (Lide, 2008)	8.67 (Lide, 2008)	0
anisole	108.14	CaCO$_3$	IGC	38.8 (Goss and Eisenreich, 1996)	8.4×10^{-7}	45.3 (Chickos and Acree, 2003)	13.1 (Lide, 2008)	1.38 (Lide, 2008)	8.67 (Lide, 2008)	0.14
diethyl ether	74.12	CaCO$_3$	IGC	39.3 (Goss and Eisenreich, 1996)	1.0×10^{-6}	27.1 (Chickos and Acree, 2003)	9.47 (Lide, 2008)	1.098 (Lide, 2008)	8.67 (Lide, 2008)	0.25
methanol	32.04	CaCO$_3$	DFT	77.2 (Budi et al., 2018)	5.8	37.8 (Chickos and Acree, 2003)	3.28 (Lide, 2008)	1.7 (Lide, 2008)	8.67 (Lide, 2008)	1
ethanol	46.07	CaCO$_3$	DFT	80.1 (Budi et al., 2018)	19	42.4 (Chickos and Acree, 2003)	5.41 (Lide, 2008)	1.69 (Lide, 2008)	8.67 (Lide, 2008)	0.5
ethanol	46.07	CaCO$_3$	TPD	83.9 (Dickbreder et al., 2023)	91	42.4 (Chickos and Acree, 2003)	5.41 (Lide, 2008)	1.69 (Lide, 2008)	8.67 (Lide, 2008)	0.5
ethanol	46.07	CaCO$_3$	TPD	100.3 (Dickbreder et al., 2023)	7.6×10^4	42.4 (Chickos and Acree, 2003)	5.41 (Lide, 2008)	1.69 (Lide, 2008)	8.67 (Lide, 2008)	0.5
formic acid	46.03	CaCO$_3$	DFT	94.6 (Budi et al., 2018)	7.3×10^3	36 (Chickos and Acree, 2003)	3.4 (Lide, 2008)	1.425 (Lide, 2008)	8.67 (Lide, 2008)	2
acetic acid	60.05	CaCO$_3$	DFT	95.5 (Budi et al., 2018)	1.1×10^4	41.6 (Chickos and Acree, 2003)	5.1 (Lide, 2008)	1.7 (Lide, 2008)	8.67 (Lide, 2008)	1
methane	16.04	CaCO$_3$	DFT	12.5 (Budi et al., 2018)	1.7×10^{-11}	8.5 (Chickos and Acree, 2003)	2.59 (Lide, 2008)	0 (Yaws, 2014)	8.67 (Lide, 2008)	0
ethane	30.07	CaCO$_3$	DFT	17.4 (Budi et al., 2018)	1.3×10^{-10}	15.3 (Chickos and Acree, 2003)	4.45 (Lide, 2008)	0 (Yaws, 2014)	8.67 (Lide, 2008)	0

benzene	78.11	$CaCO_3$	DFT	30.9 (Budi et al., 2018)	3.2×10^{-8}	42.3 (Chickos and Acree, 2003)	10 (Lide, 2008)	0 (Yaws, 2014)	8.67 (Lide, 2008)	0
n-octane	114.23	α-Fe_2O_3	IGC	25.0 (Goss and Eisenreich, 1996)	2.9×10^{-9}	41.6 (Chickos and Acree, 2003)	15.9 (Lide, 2008)	0 (Yaws, 2014)	12.00 (Lide, 2008)	0
n-nonane	128.26	α-Fe_2O_3	IGC	31.3 (Goss and Eisenreich, 1996)	3.9×10^{-8}	46.55 (Chickos and Acree, 2003)	17.36 (Lide, 2008)	0 (Yaws, 2014)	12.00 (Lide, 2008)	0
toluene	92.14	α-Fe_2O_3	IGC	27.5 (Goss and Eisenreich, 1996)	8.1×10^{-9}	38.9 (Chickos and Acree, 2003)	11.8 (Lide, 2008)	0.375 (Lide, 2008)	12.00 (Lide, 2008)	0
p-xylene	106.17	α-Fe_2O_3	IGC	32.7 (Goss and Eisenreich, 1996)	6.9×10^{-8}	42.3 (Chickos and Acree, 2003)	14.35 (Bosque and Sales, 2002)	0 (Yaws, 2014)	12.00 (Lide, 2008)	0
o-xylene	106.17	α-Fe_2O_3	IGC	33.6 (Goss and Eisenreich, 1996)	1.0×10^{-7}	42.9 (Chickos and Acree, 2003)	14.25 (Bosque and Sales, 2002)	0.64 (Lide, 2008)	12.00 (Lide, 2008)	0
ethylbenzene	106.17	α-Fe_2O_3	IGC	32.4 (Goss and Eisenreich, 1996)	6.1×10^{-8}	42.3 (Chickos and Acree, 2003)	14.2 (Lide, 2008)	0.59 (Lide, 2008)	12.00 (Lide, 2008)	0
chlorobenzene	112.56	α-Fe_2O_3	IGC	26.4 (Goss and Eisenreich, 1996)	5.2×10^{-9}	40.3 (Chickos and Acree, 2003)	13.2 (Lide, 2008)	1.69 (Lide, 2008)	12.00 (Lide, 2008)	0
1,2-dichlorobenzene	147.01	α-Fe_2O_3	IGC	35.5 (Goss and Eisenreich, 1996)	2.2×10^{-7}	49.9 (Chickos and Acree, 2003)	14.3 (Bosque and Sales, 2002)	2.5 (Lide, 2008)	12.00 (Lide, 2008)	0
1,4-dichlorobenzene	147.01	α-Fe_2O_3	IGC	32.5 (Goss and Eisenreich, 1996)	6.3×10^{-8}	54.8 (Chickos and Acree, 2003)	14.3 (Mceachran et al., 2018)	1.72 (Lide, 2008)	12.00 (Lide, 2008)	0
anisole	108.14	α-Fe_2O_3	IGC	41.0 (Goss and Eisenreich, 1996)	2.1×10^{-6}	45.3 (Chickos and Acree, 2003)	13.1 (Lide, 2008)	1.38 (Lide, 2008)	12.00 (Lide, 2008)	0.143
acetone	58.08	α-Fe_2O_3	IGC	39.3 (Goss and Eisenreich, 1996)	1.0×10^{-6}	31.3 (Chickos and Acree, 2003)	6.37 (Lide, 2008)	2.88 (Lide, 2008)	12.00 (Lide, 2008)	0.33
diethyl ether	74.12	α-Fe_2O_3	IGC	38.2 (Goss and Eisenreich, 1996)	6.6×10^{-7}	27.1 (Chickos and Acree, 2003)	9.47 (Lide, 2008)	1.098 (Lide, 2008)	12.00 (Lide, 2008)	0.25
n-octane	114.23	quartz/kaolinite	IGC	27.9 (Goss and Eisenreich, 1996)	9.5×10^{-9}	41.6 (Chickos and Acree, 2003)	15.9 (Lide, 2008)	0 (Yaws, 2014)	~4.0 (Leluk et al., 2010)	0
n-nonane	128.26	quartz/kaolinite	IGC	31.6 (Goss and Eisenreich, 1996)	4.3×10^{-8}	46.55 (Chickos and Acree, 2003)	17.36 (Lide, 2008)	0 (Yaws, 2014)	~4.0 (Leluk et al., 2010)	0

n-decane	142.29	quartz/kaolinite	IGC	35.6 (Goss and Eisenreich, 1996)	2.2×10⁻⁷	51.4 (Chickos and Acree, 2003)	19.1 (Lide, 2008)	0 (Yaws, 2014)	~4.0 (Leluk et al., 2010)	0
toluene	92.14	quartz/kaolinite	IGC	31.3 (Goss and Eisenreich, 1996)	3.8×10⁻⁸	38.9 (Chickos and Acree, 2003)	11.8 (Lide, 2008)	0.375 (Lide, 2008)	~4.0 (Leluk et al., 2010)	0
p-xylene	106.17	quartz/kaolinite	IGC	35.6 (Goss and Eisenreich, 1996)	2.2×10⁻⁷	42.3 (Chickos and Acree, 2003)	14.35 (Bosque and Sales, 2002)	0 (Yaws, 2014)	~4.0 (Leluk et al., 2010)	0
o-xylene	106.17	quartz/kaolinite	IGC	36.5 (Goss and Eisenreich, 1996)	3.2×10⁻⁷	42.9 (Chickos and Acree, 2003)	14.25 (Bosque and Sales, 2002)	0.64 (Lide, 2008)	~4.0 (Leluk et al., 2010)	0
ethylbenzene	106.17	quartz/kaolinite	IGC	35.4 (Goss and Eisenreich, 1996)	2.1×10⁻⁷	42.3 (Chickos and Acree, 2003)	14.2 (Lide, 2008)	0.59 (Lide, 2008)	~4.0 (Leluk et al., 2010)	0
propylbenzene	120.19	quartz/kaolinite	IGC	40.2 (Goss and Eisenreich, 1996)	1.5×10⁻⁶	46.2 (Chickos and Acree, 2003)	16 (Mceachran et al., 2018)	0.369 (Yaws, 2014)	~4.0 (Leluk et al., 2010)	0
chlorobenzene	112.56	quartz/kaolinite	IGC	32.1 (Goss and Eisenreich, 1996)	5.3×10⁻⁸	40.3 (Chickos and Acree, 2003)	13.2 (Lide, 2008)	1.69 (Lide, 2008)	~4.0 (Leluk et al., 2010)	0
1,2-dichlorobenzene	147.01	quartz/kaolinite	IGC	36.6 (Goss and Eisenreich, 1996)	3.4×10⁻⁷	49.9 (Chickos and Acree, 2003)	14.3 (Bosque and Sales, 2002)	2.5 (Lide, 2008)	~4.0 (Leluk et al., 2010)	0
1,4-dichlorobenzene	147.01	quartz/kaolinite	IGC	37.2 (Goss and Eisenreich, 1996)	4.3×10⁻⁷	54.8 (Chickos and Acree, 2003)	14.3 (Mceachran et al., 2018)	1.72 (Lide, 2008)	~4.0 (Leluk et al., 2010)	0
1,2,3,4-tetrachlorobenzene	215.89	quartz/kaolinite	IGC	45.3 (Goss and Eisenreich, 1996)	1.2×10⁻⁵	60.1 (Chickos and Acree, 2003)	18.2 (Mceachran et al., 2018)	2.42 (Lide, 2008)	~4.0 (Leluk et al., 2010)	0
naphthalene	128.17	quartz/kaolinite	IGC	46.9 (Goss and Eisenreich, 1996)	2.3×10⁻⁵	53.4 (Chickos and Acree, 2003)	17 (Lide, 2008)	0 (Yaws, 2014)	~4.0 (Leluk et al., 2010)	0
anisole	108.14	quartz/kaolinite	IGC	44.2 (Goss and Eisenreich, 1996)	7.7×10⁻⁶	45.3 (Chickos and Acree, 2003)	13.1 (Lide, 2008)	1.38 (Lide, 2008)	~4.0 (Leluk et al., 2010)	0.143
pyridine	79.10	quartz/kaolinite	IGC	48.6 (Goss and Eisenreich, 1996)	4.7×10⁻⁵	40.2 (Chickos and Acree, 2003)	9.34 (Lide, 2008)	2.215 (Lide, 2008)	~4.0 (Leluk et al., 2010)	0
ethanol	46.07	quartz/kaolinite	IGC	46.6 (Goss and Eisenreich, 1996)	2.1×10⁻⁵	42.4 (Chickos and Acree, 2003)	5.41 (Lide, 2008)	1.38 (Lide, 2008)	~4.0 (Leluk et al., 2010)	0.5
ethyl acetate	88.11	quartz/kaolinite	IGC	45.0 (Goss and Eisenreich, 1996)	1.1×10⁻⁵	35 (Chickos and Acree, 2003)	8.62 (Lide, 2008)	2.215	~4.0 (Leluk et al., 2010)	0.5

compound	molar mass	substrate	method							
acetone	58.08	quartz/kaolinite	IGC	43.6 (Goss and Eisenreich, 1996)	6.0×10^{-6}	31.3 (Chickos and Acree, 2003)	6.37 (Lide, 2008)	2.88 (Lide, 2008)	~4.0 (Leluk et al., 2010)	0.33
diethyl ether	74.12	quartz/kaolinite	IGC	40.0 (Goss and Eisenreich, 1996)	1.4×10^{-6}	27.1 (Chickos and Acree, 2003)	9.47 (Lide, 2008)	1.098 (Lide, 2008)	~4.0 (Leluk et al., 2010)	0.25
methanol	32.04	quartz	DFT	60.8 (Budi et al., 2018)	6.9×10^{-3}	37.8 (Chickos and Acree, 2003)	3.28 (Lide, 2008)	1.7 (Lide, 2008)	3.75 (Lide, 2008)	1
ethanol	46.07	quartz	DFT	64.6 (Budi et al., 2018)	3.3×10^{-2}	42.4 (Chickos and Acree, 2003)	5.41 (Lide, 2008)	1.69 (Lide, 2008)	3.75 (Lide, 2008)	0.5
formic acid	46.03	quartz	DFT	57.9 (Budi et al., 2018)	2.1×10^{-3}	36 (Chickos and Acree, 2003)	3.4 (Lide, 2008)	1.425 (Lide, 2008)	3.75 (Lide, 2008)	2
acetic acid	60.05	quartz	DFT	60.8 (Budi et al., 2018)	6.9×10^{-3}	41.6 (Chickos and Acree, 2003)	5.1 (Lide, 2008)	1.7 (Lide, 2008)	3.75 (Lide, 2008)	1
methane	16.04	quartz	DFT	6.8 (Budi et al., 2018)	1.6×10^{-12}	8.5 (Chickos and Acree, 2003)	2.59 (Lide, 2008)	0 (Yaws, 2014)	3.75 (Lide, 2008)	0
ethane	30.07	quartz	DFT	12.5 (Budi et al., 2018)	1.7×10^{-11}	15.3 (Chickos and Acree, 2003)	4.45 (Lide, 2008)	0 (Yaws, 2014)	3.75 (Lide, 2008)	0
benzene	78.11	quartz	DFT	33.8 (Budi et al., 2018)	1.1×10^{-7}	42.3 (Chickos and Acree, 2003)	10 (Lide, 2008)	0 (Yaws, 2014)	3.75 (Lide, 2008)	0
methanol	32.04	kaolinite (Al)	DFT	61.8 (Budi et al., 2018)	1.0×10^{-2}	37.8 (Chickos and Acree, 2003)	3.28 (Lide, 2008)	1.7 (Lide, 2008)	5.10 (Leluk et al., 2010)	1
ethanol	46.07	kaolinite (Al)	DFT	64.6 (Budi et al., 2018)	3.3×10^{-2}	42.4 (Chickos and Acree, 2003)	5.41 (Lide, 2008)	1.69 (Lide, 2008)	5.10 (Leluk et al., 2010)	0.5
formic acid	46.03	kaolinite (Al)	DFT	79.1 (Budi et al., 2018)	1.3×10^{1}	36 (Chickos and Acree, 2003)	3.4 (Lide, 2008)	1.425 (Lide, 2008)	5.10 (Leluk et al., 2010)	2
acetic acid	60.05	kaolinite (Al)	DFT	82.0 (Budi et al., 2018)	4.2×10^{1}	41.6 (Chickos and Acree, 2003)	5.1 (Lide, 2008)	1.7 (Lide, 2008)	5.10 (Leluk et al., 2010)	1
methane	16.04	kaolinite (Al)	DFT	16.4 (Budi et al., 2018)	8.4×10^{-11}	8.5 (Chickos and Acree, 2003)	2.59 (Lide, 2008)	0 (Yaws, 2014)	5.10 (Leluk et al., 2010)	0
ethane	30.07	kaolinite (Al)	DFT	22.2 (Budi et al., 2018)	9.1×10^{-10}	15.3 (Chickos and Acree, 2003)	4.45 (Lide, 2008)	0 (Yaws, 2014)	5.10 (Leluk et al., 2010)	0
benzene	78.11	kaolinite (Al)	DFT	37.6 (Budi et al., 2018)	5.0×10^{-7}	42.3 (Chickos	10 (Lide, 2008)	0 (Yaws, 2014)	5.10 (Leluk	0

						and Acree, 2003)			et al., 2010)	
methanol	32.04	kaolinite (Si)	DFT	21.2 (Budi et al., 2018)	6.0×10^{-10}	37.8 (Chickos and Acree, 2003)	3.28 (Lide, 2008)	1.7 (Lide, 2008)	5.10 (Leluk et al., 2010)	1
ethanol	46.07	kaolinite (Si)	DFT	23.2 (Budi et al., 2018)	1.4×10^{-9}	42.4 (Chickos and Acree, 2003)	5.41 (Lide, 2008)	1.69 (Lide, 2008)	5.10 (Leluk et al., 2010)	0.5
formic acid	46.03	kaolinite (Si)	DFT	21.2 (Budi et al., 2018)	6.0×10^{-10}	36 (Chickos and Acree, 2003)	3.4 (Lide, 2008)	1.425 (Lide, 2008)	5.10 (Leluk et al., 2010)	2
acetic acid	60.05	kaolinite (Si)	DFT	21.2 (Budi et al., 2018)	6.0×10^{-10}	41.6 (Chickos and Acree, 2003)	5.1 (Lide, 2008)	1.7 (Lide, 2008)	5.10 (Leluk et al., 2010)	1
methane	16.04	kaolinite (Si)	DFT	7.7 (Budi et al., 2018)	2.4×10^{-12}	8.5 (Chickos and Acree, 2003)	2.59 (Lide, 2008)	0 (Yaws, 2014)	5.10 (Leluk et al., 2010)	0
ethane	30.07	kaolinite (Si)	DFT	11.6 (Budi et al., 2018)	1.2×10^{-11}	15.3 (Chickos and Acree, 2003)	4.45 (Lide, 2008)	0 (Yaws, 2014)	5.10 (Leluk et al., 2010)	0
benzene	78.11	kaolinite (Si)	DFT	18.3 (Budi et al., 2018)	1.8×10^{-10}	42.3 (Chickos and Acree, 2003)	10 (Lide, 2008)	0 (Yaws, 2014)	5.10 (Leluk et al., 2010)	0
limonene up	136.24	SiO$_2$	DFT	46.3 (Fang et al., 2019)	1.8×10^{-5}	49.6 (Chickos and Acree, 2003)	17.94 (Helburn et al., 2008)	0.7 (Svirbely et al., 1935)	4.42 (Lide, 2008)	0
limonene down	136.24	SiO$_2$	DFT	41.6 (Fang et al., 2019)	2.6×10^{-6}	49.6 (Chickos and Acree, 2003)	17.94 (Helburn et al., 2008)	0.7 (Svirbely et al., 1935)	4.42 (Lide, 2008)	0
benzene	78.11	SiO$_2$	DFT	27.5 (Fang et al., 2019)	8.0×10^{-9}	33.83 (Chickos and Acree, 2003)	10.44 (Bosque and Sales, 2002)	0 (Yaws, 2014)	4.42 (Lide, 2008)	0
cyclohexene	82.143	SiO$_2$	DFT	29.2 (Fang et al., 2019)	1.6×10^{-8}	33.5 (Chickos and Acree, 2003)	10.79 (Bosque and Sales, 2002)	0 (Yaws, 2014)	4.42 (Lide, 2008)	0
cyclohexane	84.16	SiO$_2$	DFT	24.3 (Fang et al., 2019)	2.1×10^{-9}	33 (Chickos and Acree, 2003)	11.04 (Bosque and Sales, 2002)	0 (Yaws, 2014)	4.42 (Lide, 2008)	0
limonene	136.24	Hydroxylated TiO$_2$	MD	71 (Fan et al., 2022)	0.5	49.6 (Chickos and Acree, 2003)	17.94 (Helburn et al., 2008)	1.57 (Yaws, 2014)	86 (Lide, 2008)	0
carvone	150.22	Hydroxylated TiO$_2$	MD	148.8 (Fan et al., 2022)	3.4×10^{13}	58.2 (Hoskovec et al., 2005)	18.25 (Yankova et al., 2019)	3.56 (Yankova et al., 2019)	86 (Lide, 2008)	0.1
toluene	92.14	Nefta dust	DRIFTS	88.8 (Romanias et al., 2016)	6.9×10^{2}	38.9 (Chickos	12.12 (Lide, 2008)	0.375 (Lide, 2008)	~4.5 (Lide, 2008;	0

									and Acree, 2003)	Leluk et al., 2010)	
toluene	92.14	Touggourt dust	DRIFTS	88.9 (Romanias et al., 2016)	$7.0{\times}10^2$	38.9 (Chickos and Acree, 2003)	12.12 (Lide, 2008)	0.375 (Lide, 2008)	~4.5 (Lide, 2008; Leluk et al., 2010)	0
toluene	92.14	N'Goussa dust	DRIFTS	88.5 (Romanias et al., 2016)	$6.0{\times}10^2$	38.9 (Chickos and Acree, 2003)	12.12 (Lide, 2008)	0.375 (Lide, 2008)	~4.5 (Lide, 2008; Leluk et al., 2010)	0
toluene	92.14	Bordj dust	DRIFTS	88.6 (Romanias et al., 2016)	$6.1{\times}10^2$	38.9 (Chickos and Acree, 2003)	12.12 (Lide, 2008)	0.375 (Lide, 2008)	~4.5 (Lide, 2008; Leluk et al., 2010)	0
toluene	92.14	Laayoune dust	DRIFTS	87.9 (Romanias et al., 2016)	$4.6{\times}10^2$	38.9 (Chickos and Acree, 2003)	12.12 (Lide, 2008)	0.375 (Lide, 2008)	~4.5 (Lide, 2008; Leluk et al., 2010)	0
toluene	92.14	Tarfaya dust	DRIFTS	87.7 (Romanias et al., 2016)	$4.3{\times}10^2$	38.9 (Chickos and Acree, 2003)	12.12 (Lide, 2008)	0.375 (Lide, 2008)	~4.5 (Lide, 2008; Leluk et al., 2010)	0
limonene	136.24	Nefta dust	DRIFTS	91.4 (Romanias et al., 2016)	$2.0{\times}10^3$	49.6 (Chickos and Acree, 2003)	17.94 (Helburn et al., 2008)	1.57 (Yaws, 2014)	~4.5 (Lide, 2008; Leluk et al., 2010)	0
limonene	136.24	Touggourt dust	DRIFTS	88.5 (Romanias et al., 2016)	$6.0{\times}10^2$	49.6 (Chickos and Acree, 2003)	17.94 (Helburn et al., 2008)	1.57 (Yaws, 2014)	~4.5 (Lide, 2008; Leluk et al., 2010)	0
limonene	136.24	N'Goussa dust	DRIFTS	91.6 (Romanias et al., 2016)	$2.1{\times}10^3$	49.6 (Chickos and Acree, 2003)	17.94 (Helburn et al., 2008)	1.57 (Yaws, 2014)	~4.5 (Lide, 2008; Leluk et al., 2010)	0
limonene	136.24	Bordj dust	DRIFTS	91.8 (Romanias et al., 2016)	$2.3{\times}10^3$	49.6 (Chickos and Acree, 2003)	17.94 (Helburn et al., 2008)	1.57 (Yaws, 2014)	~4.5 (Lide, 2008; Leluk et al., 2010)	0
limonene	136.24	Laayoune dust	DRIFTS	88.7 (Romanias et al., 2016)	$6.4{\times}10^2$	49.6 (Chickos and Acree, 2003)	17.94 (Helburn et al., 2008)	1.57 (Yaws, 2014)	~4.5 (Lide, 2008; Leluk et	0

									al., 2010)	
limonene	136.24	Tarfaya dust	DRIFTS	88.1 (Romanias et al., 2016)	5.0×10^2	49.6 (Chickos and Acree, 2003)	17.94 (Helburn et al., 2008)	1.57 (Yaws, 2014)	~4.5 (Lide, 2008; Leluk et al., 2010)	0

1236

1237

1238 **Table A8.** Compiled absorbate-substrate interaction energies of inporganic and organic gas
1239 species on ice. Gas species, gas species' molar mass, substrate, experimental or theoretical method,
1240 desorption energy (E^0_{des}), and desorption lifetimes (τ_{des}) evaluated at 293 K using $A_{des} = 10^{13}$ s^{-1},
1241 enthalpy of vaporization (ΔH_{vap}), gas species' polarizability (α), gas species' dipole moment (μ),
1242 substrate's relative permittivity (ε_r), and gas species' oxygen to carbon ration ($O:C$) are given.

Gas Species	Molar Mass / g mol^{-1}	Substrate	Method	E^0_{des} / kJ mol^{-1}	$\tau_{des}^{293\,K}$ / s	ΔH_{vap} (T) / kJ mol^{-1}	α / 10^{-24} cm^3	μ / D	ε_r	O:C
H$_2$O	18.02	ice	MB	48.3 (Brown et al., 1996)	4.1×10^{-5}	44 (Chickos and Acree, 2003)	1.45 (Lide, 2008)	1.85 (Lide, 2008)	97.5 (Lide, 2008; Auty and Cole, 1952)	0
H$_2$O	18.02	ice (170-230 K)	VM	43.1 (Delval and Rossi, 2005; Delval et al., 2003)	4.8×10^{-6}	44 (Chickos and Acree, 2003)	1.45 (Lide, 2008)	1.85 (Lide, 2008)	119.5 (Lide, 2008; Auty and Cole, 1952)	0
H$_2$O	18.02	ice	MD	50.0 (Schlesinger et al., 2020)	8.2×10^{-5}	44 (Chickos and Acree, 2003)	1.45 (Lide, 2008)	1.85 (Lide, 2008)	97.5 (Lide, 2008; Auty and Cole, 1952)	0
D$_2$O	20.03	ice	MB	42 (Kong et al., 2014a)	3.1×10^{-6}	45.14 (Crabtree and Siman-Tov, 1993)	1.26 (Lide, 2008)	1.87 (Townes and Schawlow, 1975)	97.5 (Lide, 2008; Auty and Cole, 1952)	0
CO$_2$	44.01	amorphous ice	TPD	22.5 (Kim et al., 2008)	1.0×10^{-9}	16.4 (Chickos and Acree, 2003)	2.91 (Lide, 2008)	0.0001 (Kolomiitsova et al., 2000)	97.5 (Lide, 2008; Auty and Cole, 1952)	0.5
n-hexane	86.18	ice	IGC	23.0 (Langenberg and Schurath, 2018)	1.3×10^{-9}	31.5 (Chickos and Acree, 2003)	11.9 (Lide, 2008)	0	97.5 (Lide, 2008; Auty and Cole, 1952)	0
formaldehyde	30.03	ice	GCMC	30.0 (Hantal et al., 2007)	2.2×10^{-8}	24.3 (Chickos	2.63 (Lide, 2008)	2.33 (Lide, 2008)	97.5 (Lide, 2008;	1

					and Acree, 2003)			Auty and Cole, 1952)	
acetaldehyde 44.05		ice	KU	29.1 (Crowley et al., 2010)	1.5×10⁻⁸	27.6 (Chickos and Acree, 2003)	4.6 (Lide, 2008)	2.75 (Lide, 2008)	97.5 (Lide, 2008; Auty and Cole, 1952) 0.5
methanol 32.04		ice	KU	51.0 (Winkler et al., 2002)	1.2×10⁻⁴	37.8 (Chickos and Acree, 2003)	3.28 (Lide, 2008)	1.7 (Lide, 2008)	97.5 (Lide, 2008; Auty and Cole, 1952) 0
acetone 58.08		ice	KU	48.6 (Crowley et al., 2010)	4.6×10⁻⁵	31.3 (Chickos and Acree, 2003)	6.37 (Lide, 2008)	2.88 (Lide, 2008)	97.5 (Lide, 2008; Auty and Cole, 1952) 0.33
formic acid 46.03		ice	KU	48.1 (Crowley et al., 2010)	3.8×10⁻⁵	36 (Chickos and Acree, 2003)	3.4 (Lide, 2008)	1.43 (Lide, 2008)	97.5 (Lide, 2008; Auty and Cole, 1952) 2
acetic acid 60.05		ice	KU	70.7 (Crowley et al., 2010)	0.4	41.6 (Chickos and Acree, 2003)	5.1 (Lide, 2008)	1.7 (Lide, 2008)	97.5 (Lide, 2008; Auty and Cole, 1952) 1
acetic acid 60.05		ice	KU	73.2 (Sokolov and Abbatt, 2002)	1.1	41.6 (Chickos and Acree, 2003)	5.1 (Lide, 2008)	1.7 (Lide, 2008)	97.5 (Lide, 2008; Auty and Cole, 1952) 1
1-pentanol 88.15		ice	KU	71.5 (Sokolov and Abbatt, 2002)	0.6	57.8 (Chickos and Acree, 2003)	10.61 (Bosque and Sales, 2002)	1.7 (liq.)(Lide, 2008)	97.5 (Lide, 2008; Auty and Cole, 1952) 0.2
1-butanol 74.12		ice	KU	67.8 (Sokolov and Abbatt, 2002)	0.1	52.5 (Chickos and Acree, 2003)	8.88 (Lide, 2008)	1.66 (Lide, 2008)	97.5 (Lide, 2008; Auty and Cole, 1952) 0.25
ethanol 46.07		ice	KU	62.4 (Crowley et al., 2010)	1.3×10⁻²	42.4 (Chickos and Acree, 2003)	5.41 (Lide, 2008)	1.69 (Lide, 2008)	97.5 (Lide, 2008; Auty and Cole, 1952) 0.5
ethanol 46.07		ice	KU	61.9 (Sokolov and Abbatt, 2002)	1.1×10⁻²	42.4 (Chickos and Acree, 2003)	5.41 (Lide, 2008)	1.69 (Lide, 2008)	97.5 (Lide, 2008; Auty and 0.5

				Cole, 1952)	
1-propanol 60.09	ice	GCMC	70.0 (Joliat et al.)	0.3	47.45 (Chickos and Acree, 2003)	6.74 (Lide, 2008)	1.58 (Lide, 2008)	97.5 (Lide, 2008; Auty and Cole, 1952)	0.33
2-propanol 60.09	ice	GCMC	71.5 (Joliat et al.)	0.6	47.45 (Chickos and Acree, 2003)	6.74 (Lide, 2008)	1.58 (Lide, 2008)	97.5 (Lide, 2008; Auty and Cole, 1952)	0.33
hexanal 100.16	ice	KU	64.9 (Sokolov and Abbatt, 2002)	3.7×10^{-2}	42.3 (Chickos and Acree, 2003)	11.9 (Mceachran et al., 2018)	2.6 (Wiberg and Rablen, 1993; Bak et al., 2000)	97.5 (Lide, 2008; Auty and Cole, 1952)	0
peroxyacetylnitrate 121.05	ice	IGC	30.0 (Bartels-Rausch et al., 2002)	2.2×10^{-8}	34.6 (Stephenson and Malanowski, 1987)	8.27 (Mceachran et al., 2018)		97.5 (Lide, 2008; Auty and Cole, 1952)	2.5
acetylene 26.04	ice	VS	15.5 (Silva and Devlin, 1994)	5.8×10^{-11}	16.7	3.40 (Gussoni et al., 1998)	0	97.5 (Lide, 2008; Auty and Cole, 1952)	0
ethylene 28.05	ice	VS	15.9 (Silva and Devlin, 1994)	6.8×10^{-11}	13.8	4.09 (Gussoni et al., 1998)	0	97.5 (Lide, 2008; Auty and Cole, 1952)	
benzene 78.11	ice	VS	18.0 (Silva and Devlin, 1994)	1.6×10^{-10}	33.5	9.96 (Gussoni et al., 1998)	0	97.5 (Lide, 2008; Auty and Cole, 1952)	
HCl 36.46	ice (100-170 K)	TPD	28.0 (Isakson and Sitz, 1999)	9.8×10^{-9}	16.15 (Lide, 2008)	2.63 (Lide, 2008)	1.11 (Lide, 2008)	119.5 (Lide, 2008; Auty and Cole, 1952)	0
HOCl 52.46	ice (185-225K)	KU	39.6 (Crowley et al., 2010)	1.1×10^{-6}	36.66 (Joback and Reid, 1987)	3.31 (Hait and Head-Gordon, 2018)	1.3 (Lide, 2008)	119.5 (Lide, 2008; Auty and Cole, 1952)	0
H₂O₂ 34.01	ice	KU	31.6 (Pouvesle et al., 2010; Crowley et al., 2010)	4.3×10^{-8}	51.6 (Lide, 2008)	2.3 (Giguere, 1983)	1.57 (Lide, 2008)	97.5 (Lide, 2008; Auty and	0

									Cole, 1952)	
NO	30.01	ice (93-150 K)	MB	15.4 (Lejonthun et al., 2014)	5.7×10^{-11}	13.83 (Lide, 2008)	1.7 (Lide, 2008)	0.16 (Lide, 2008)	119.5 (Lide, 2008; Auty and Cole, 1952)	0
NO$_2$	46.01	ice (150-171 K)	MB	25.1 (Lejonthun et al., 2014)	3.0×10^{-9}	18.89		3.02 (Lide, 2008)	0.32 (Lide, 2008)	119.5 (Lide, 2008; Auty and Cole, 1952)	0
NO$_2$	46.01	ice	IGC	22.0 (Bartels-Rausch et al., 2002)	8.4×10^{-10}	18.89		3.02 (Lide, 2008)	0.32 (Lide, 2008)	97.5 (Lide, 2008; Auty and Cole, 1952)	0
HONO	47.01	ice	KU	43.0 (Crowley et al., 2010)	4.6×10^{-6}		2.81 (Jensen et al., 2002)	1.42 (Lide, 2008)	97.5 (Lide, 2008; Auty and Cole, 1952)	0
N$_2$O$_5$	108.01	ice (135-168 K)	MB	34.7 (Lejonthun et al., 2014)	1.6×10^{-7}	57.4 (Stull, 1947)	7.7 (Wincel et al., 1995)	0.5 (Grabow et al., 1996)	119.5 (Lide, 2008; Auty and Cole, 1952)	0
N$_2$O$_5$	108.01	ice covered HNO$_3$ (135-168 K)	MB	23.2 (Lejonthun et al., 2014)	1.3×10^{-9}	57.4 (Stull, 1947)	7.7 (Wincel et al., 1995)	0.5 (Grabow et al., 1996)	119.5 (Lide, 2008; Auty and Cole, 1952)	0
HNO$_3$	63.01	ice	KU	38.1 (Crowley et al., 2010)	6.2×10^{-7}	39.1 (Lide, 2008)	3.55 (Jensen et al., 2002)	2.17 (Lide, 2008)	97.5 (Lide, 2008; Auty and Cole, 1952)	0
HO$_2$NO$_2$	79.01	ice	KU	59.0 (Ulrich et al., 2012)	3.3×10^{-3}			2.44 (Wei et al., 2011)	97.5 (Lide, 2008; Auty and Cole, 1952)	0
OH	17.01	ice (205-230 K)	MC	31.2 (Remorov and Bardwell, 2005)	3.6×10^{-8}		7.11 (Zen et al., 2014)	1.65 (Lide, 2008)	119.5 (Lide, 2008; Auty and Cole, 1952)	0
O$_3$	48.00	amorphous ice	TPD	20.0 (Borget et al., 2001)	3.7×10^{-10}	12.2 (Stull, 1947)	3.21 (Lide, 2008)	0.53 (Lide, 2008)	97.5 (Lide, 2008; Auty and Cole, 1952)	0

Gas Species	Molar Mass / g mol⁻¹	Substrate	Method	E_{des}^0 / kJ mol⁻¹	$\tau_{des}^{293\,K}$ / s	ΔH_{vap} (T) / kJ mol⁻¹	α / 10^{-24} cm³	μ / D	ε_r	ΔH_{solv} (T) / kJ mol⁻¹	O:C
SO_2	64.07	ice	KU	17.2 (Crowley et al., 2010)	1.2×10⁻¹⁰	24.9 (Chickos and Acree, 2003)	4 (Lide, 2008)	1.63 (Lide, 2008)	97.5 (Lide, 2008; Auty and Cole, 1952)		0

1243

1244

1245 **Table A9.** Compiled absorbate-substrate data for water vapor and inorganic gases adsorbed on
1246 water and aqueous substrates. Gas species, gas species' molar mass, substrate, experimental or
1247 theoretical method, desorption energy (E_{des}^0), and desorption lifetimes (τ_{des}) evaluated at 293 K
1248 using $A_{des} = 10^{13}$ s⁻¹, enthalpy of vaporization (ΔH_{vap}) and solvation (ΔH_{solv}), gas species'
1249 polarizability (α), gas species' dipole moment (μ), substrate's relative permittivity (ε_r), and gas
1250 species' oxygen to carbon ration ($O{:}C$) are given.

Gas Species	Molar Mass / g mol⁻¹	Substrate	Method	E_{des}^0 / kJ mol⁻¹	$\tau_{des}^{293\,K}$ / s	ΔH_{vap} (T) / kJ mol⁻¹	α / 10^{-24} cm³	μ / D	ε_r	ΔH_{solv} (T) / kJ mol⁻¹	O:C
H_2O	18.02	H_2O	MD	9.2 (Vieceli et al., 2004)	4.4×10⁻¹²	44 (Chickos and Acree, 2003)	1.45 (Lide, 2008)	1.85 (Lide, 2008)	80.2 (Lide, 2008)		0
H_2O	18.02	H_2O, 1.92 nm radius	MD	10.6 (Julin et al., 2013)	7.8×10⁻¹²	44 (Chickos and Acree, 2003)	1.45 (Lide, 2008)	1.85 (Lide, 2008)	80.2 (Lide, 2008)		0
H_2O	18.02	H_2O, 4.14 nm radius	MD	10.9 (Julin et al., 2013)	8.8×10⁻¹²	44 (Chickos and Acree, 2003)	1.45 (Lide, 2008)	1.85 (Lide, 2008)	80.2 (Lide, 2008)		0
H_2O	18.02	H_2O, planar	MD	11.4 (Julin et al., 2013)	1.1×10⁻¹¹	44 (Chickos and Acree, 2003)	1.45 (Lide, 2008)	1.85 (Lide, 2008)	80.2 (Lide, 2008)		0
H_2O	18.02	H_2O, planar	MD	9.05 (Julin et al., 2013)	4.1×10⁻¹²	44 (Chickos and Acree, 2003)	1.45 (Lide, 2008)	1.85 (Lide, 2008)	80.2 (Lide, 2008)		0
H_2O	18.02	H_2O, planar	MD	10.4 (Julin et al., 2013)	7.1×10⁻¹²	44 (Chickos and Acree, 2003)	1.45 (Lide, 2008)	1.85 (Lide, 2008)	80.2 (Lide, 2008)		0
H_2O	18.02	H_2O, planar	MD	10.3 (Julin et al., 2013)	6.9×10⁻¹²	44 (Chickos and Acree, 2003)	1.45 (Lide, 2008)	1.85 (Lide, 2008)	80.2 (Lide, 2008)		0
SO_2	64.07	H_2O	KU	44.2 (Ammann et al., 2013; Jayne et al., 1990)	7.6×10⁻⁶	24.9 (Chickos and	4 (Lide, 2008)	1.633 (Lide, 2008)	80.2 (Lide, 2008)	24.11 (Sander et al., 2011)	0

Gas Species	Molar Mass / g mol^{-1}	Substrate	Method	E_{des}^0 / kJ mol^{-1}	$\tau_{des}^{293\,K}$ / s	ΔH_{vap} (T) / kJ mol^{-1}	α / 10^{-24} cm^3	μ / D	ε_r	ΔH_{solv} (T) / kJ mol^{-1}	O:C
						Acree, 2003)					
NH$_3$	17.03	H$_2$O	ST	41 (Donaldson, 1999)	2.0×10^{-6}	22.7 (Chickos and Acree, 2003)	2.35 (Lide, 2008)	1.472 (Lide, 2008)	80.2 (Lide, 2008)	34.92 (Sander et al., 2011)	0
O$_3$	48.00	H$_2$O	MD	14.7 (Vieceli et al., 2005)	4.2×10^{-11}	12.2 (Stull, 1947)	3.21 (Lide, 2008)	0.533 (Lide, 2008)	80.2 (Lide, 2008)	23.28 (Sander et al., 2011)	0
H$_2$O$_2$	34.01	H$_2$O	KU	26 (Worsnop et al., 1989)	4.3×10^{-9}	51.16	2.3 (Giguere, 1983)	1.573 (Lide, 2008)	80.2 (Lide, 2008)	63.19 (Sander et al., 2011)	0
HCl	36.46	H$_2$SO$_4$	KU	14.1 (Ammann et al., 2013; Behr et al., 2009; Robinson et al., 1998)	3.3×10^{-11}	16.15	2.63 (Lide, 2008)	1.11 (Lide, 2008)	95 (Hall and Cole, 1981)	19.12 (Marsh and Mcelroy, 1985)	0
O$_3$	48.00	shikimic acid (aqueous)	KU	20 (Berkemeier et al., 2016; Steimer et al., 2015)	3.7×10^{-10}	12.2 (Stull, 1947)	3.21 (Lide, 2008)	0.533 (Lide, 2008)		23.28 (Sander et al., 2011)	0
N$_2$O$_5$	108.01	H$_2$O	MD	15.4 (Cruzeiro et al., 2022)	5.6×10^{-11}	57.4 (Stull, 1947)	7.7 (Wincel et al., 1995)	0.5 (Grabow et al., 1996)	80.2 (Lide, 2008)		0

1251

1252

1253 **Table A10.** Compiled absorbate-substrate data for volatile aromatic gases adsorbed on water. Gas
1254 species, gas species' molar mass, substrate, experimental or theoretical method, desorption energy
1255 (E_{des}^0), and desorption lifetimes (τ_{des}) evaluated at 293 K using $A_{des} = 10^{13}$ s^{-1}, enthalpy of
1256 vaporization (ΔH_{vap}) and solvation (ΔH_{solv}), gas species' polarizability (α), gas species' dipole
1257 moment (μ), substrate's relative permittivity (ε_r), and gas species' oxygen to carbon ration ($O{:}C$)
1258 are given.

Gas Species	Molar Mass / g mol^{-1}	Substrate	Method	E_{des}^0 / kJ mol^{-1}	$\tau_{des}^{293\,K}$ / s	ΔH_{vap} (T) / kJ mol^{-1}	α / 10^{-24} cm^3	μ / D	ε_r	ΔH_{solv} (T) / kJ mol^{-1}	O:C
toluene	92.14	H$_2$O	ST	31 (Blank and Ottewill, 1964)	3.4×10^{-8}	38.9 (Chickos and Acree, 2003)	11.8 (Lide, 2008)	0.375 (Lide, 2008)	80.2 (Lide, 2008)	35.75 (Staudinger and Roberts, 2001; Sander, 2015)	0
toluene	92.14	H$_2$O	IGC	37.2 (Hartkopf and Karger, 1973)	4.3×10^{-7}	38.9 (Chickos and Acree, 2003)	11.8 (Lide, 2008)	0.375 (Lide, 2008)	80.2 (Lide, 2008)	35.75 (Staudinger and Roberts, 2001; Sander, 2015)	0

toluene	92.14	H_2O	ST	43.4 (Hauxwell and Ottewill, 1968)	5.5×10^{-6}	38.9 (Chickos and Acree, 2003) (Chickos and Acree, 2003)	11.8 (Lide, 2008)	0.375 (Lide, 2008)	80.2 (Lide, 2008)	35.75 (Staudinger and Roberts, 2001; Sander, 2015)	0
toluene	92.14	H_2O	IGC	28.8 (Goss, 2009)	1.4×10^{-8}	38.9 (Chickos and Acree, 2003)	11.8 (Lide, 2008)	0.375 (Lide, 2008)	80.2 (Lide, 2008)	35.75 (Staudinger and Roberts, 2001; Sander, 2015)	0
toluene	92.14	H_2O	ST	47.1 (Bruant and Conklin, 2002)	2.5×10^{-5}	38 (Chickos and Acree, 2003)	11.8 (Lide, 2008)	0.375 (Lide, 2008)	80.2 (Lide, 2008)	35.75 (Staudinger and Roberts, 2001; Sander, 2015)	0
benzene	78.11	H_2O	ST	41 (Bruant and Conklin, 2002)	2.0×10^{-6}	42.3 (Chickos and Acree, 2003)	10.53 (Lide, 2008)	0 (Yaws, 2014)	80.2 (Lide, 2008)	34.92 (Staudinger and Roberts, 2001; Sander, 2015)	0
benzene	78.11	H_2O	ST	25.8 (Blank and Ottewill, 1964)	4.0×10^{-9}	42.3 (Chickos and Acree, 2003)	10.53 (Lide, 2008)	0 (Yaws, 2014)	80.2 (Lide, 2008)	34.92 (Staudinger and Roberts, 2001; Sander, 2015)	0
benzene	78.11	H_2O	IGC	31.4 (Hartkopf and Karger, 1973)	4.0×10^{-8}	42.3 (Chickos and Acree, 2003)	10.53 (Lide, 2008)	0 (Yaws, 2014)	80.2 (Lide, 2008)	34.92 (Staudinger and Roberts, 2001; Sander, 2015)	0
benzene	78.11	H_2O	IGC	41 (Raja et al., 2002)	2.0×10^{-6}	42.3 (Chickos and Acree, 2003)	10.53 (Lide, 2008) (Lide, 2008)	0 (Yaws, 2014)	80.2 (Lide, 2008)	34.92 (Staudinger and Roberts, 2001; Sander, 2015)	0
1,2-dimethylbenzene	106.17	H_2O	ST	45.9 (Bruant and Conklin, 2002)	1.5×10^{-5}	43.4 (Chickos and Acree, 2003)	14.5 (Lide, 2008)	0.63 (Yaws, 2014)	80.2 (Lide, 2008)	34.92 (Staudinger and Roberts, 2001; Sander, 2015)	0
1,3-dimethylbenzene	106.17	H_2O	ST	51.6 (Bruant and	1.6×10^{-4}	42.7 (Chicko s and	14.2 (Lide, 2008)	0.3 (Yaws, 2014)	80.2 (Lide, 2008)	34.92 (Staudinger and Roberts,	0

				Conklin, 2002)		Acree, 2003)				2001; Sander, 2015)	
1,4-dimethylbenzene	106.17	H_2O	ST	46.5 (Bruant and Conklin, 2002)	$1.9×10^{-5}$	42.3 (Chickos and Acree, 2003)	14.27 (Lide, 2008)	0 (Yaws, 2014)	80.2 (Lide, 2008)	34.92 (Stauding er and Roberts, 2001; Sander, 2015)	0
1,3,5-trimethylbenzene	120.20	H_2O	ST	56.2 (Bruant and Conklin, 2002)	$1.0×10^{-3}$	47.6 (Chickos and Acree, 2003)	15.82 (Lide, 2008)	0.6 (Yaws, 2014)	80.2 (Lide, 2008)	34.92 (Sander, 2015)	0
ethylbenzene	106.17	H_2O	IGC	41.4 (Hartkopf and Karger, 1973)	$2.4×10^{-6}$	42.3 (Chickos and Acree, 2003)	14.2 (Lide, 2008)	0.59 (Lide, 2008)	80.2 (Lide, 2008)	42.40 (Stauding er and Roberts, 2001; Sander, 2015)	0
fuorobenzene	96.10	H_2O	IGC	32.6 (Hartkopf and Karger, 1973)	$6.5×10^{-8}$	34.5 (Chickos and Acree, 2003)	10.3 (Lide, 2008)	1.6 (Lide, 2008)	80.2 (Lide, 2008)	34.92 (Stauding er and Roberts, 2001; Sander, 2015)	0
chlorobenzene	112.56	H_2O	IGC	36.4 (Arp et al., 2006)	$3.1×10^{-7}$	46.2 (Chickos and Acree, 2003)	13.2 (Lide, 2008)	1.69 (Yaws, 2014)	80.2 (Lide, 2008)	31.59 (Stauding er and Roberts, 2001; Sander, 2015)	0
chlorobenzene	112.56	H_2O	IGC	35.1 (Hartkopf and Karger, 1973)	$1.8×10^{-7}$	46.2 (Chickos and Acree, 2003)	13.2 (Lide, 2008)	1.69 (Yaws, 2014)	80.2 (Lide, 2008)	31.59 (Stauding er and Roberts, 2001; Sander, 2015)	0
naphthalene	128.17	H_2O	IGC	67 (Raja et al., 2002)	$8.8×10^{-2}$	53.4 (Chickos and Acree, 2003)	16.99 (Lide, 2008)	0 (Yaws, 2014)	80.2 (Lide, 2008)	44.07 (Fogg and Sangster, 2003; Sander, 2015)	0
naphthalene	128.17	H_2O	IGC	50.4 (Arp et al., 2006)	$9.7×10^{-5}$	53.4 (Chickos and Acree, 2003)	16.99 (Lide, 2008)	0 (Yaws, 2014)	80.2 (Lide, 2008)	44.07 (Fogg and Sangster, 2003; Sander, 2015)	0
phenanthrene	178.23	H_2O	IGC	104 (Raja et al., 2002)	$3.5×10^{5}$	78.7 (Chickos and Acree, 2003)	30.75 (Lide, 2008)	0 (Yaws, 2014)	80.2 (Lide, 2008)	34.92 (Fogg and Sangster, 2003; Sander, 2015)	0

1,2,3,4-tetrachlorobenzene	215.88	H_2O	IGC	54.5 (Arp et al., 2006)	5.2×10^{-4}	60.1 (Chickos and Acree, 2003)	18.2 (Mceachran et al., 2018)	2.42 (Lide, 2008)	80.2 (Lide, 2008)	39.91 (Sander, 2015; Tenhulscher et al., 1992)	0
1,2,3,5-tetrachlorobenzene	215.88	H_2O	IGC	50.7 (Arp et al., 2006)	1.1×10^{-4}	60.7 (Chickos and Acree, 2003)	18.2 (Mceachran et al., 2018)	1.46 (Lide, 2008)	80.2 (Lide, 2008)		0
1,2,4,5-tetrachlorobenzene	215.88	H_2O	IGC	64.7 (Arp et al., 2006)	3.4×10^{-2}	60.7 (Chickos and Acree, 2003)	18.2 (Mceachran et al., 2018)	0.06 (Baron and Arevalo, 1988)	80.2 (Lide, 2008)		0
1,2,4-trichlorobenzene	181.44	H_2O	IGC	57.2 (Arp et al., 2006)	1.6×10^{-3}	55.5 (Chickos and Acree, 2003)	16.32 (Bosque and Sales, 2002)	1.26 (in benzene) (Yaws, 2014)	80.2 (Lide, 2008)	37.62 (Sander, 2015)	0
1,2-dinitrobenzene	168.11	H_2O	IGC	69.2 (Goss, 2009)	2.2×10^{-1}	60 (Chickos and Acree, 2003)	15.6 (Mceachran et al., 2018)	6.3 (in benzene) (Yaws, 2014)	80.2 (Lide, 2008)		0.67
1,3-dinitrobenzene	168.11	H_2O	IGC	59.2 (Goss, 2009)	3.6×10^{-3}	96.7 (Chickos and Acree, 2003)	15.6 (Mceachran et al., 2018)	3.84 (in benzene) (Yaws, 2014)	80.2 (Lide, 2008)		0.67
2,4-dinitrotoluene	168.11	H_2O	IGC	78.1 (Goss, 2009)	8.4	76.9 (Chickos and Acree, 2003)	17.5 (Mceachran et al., 2018)	4.32 (in benzene) (Yaws, 2014)	80.2 (Lide, 2008)	24.11 (Sander, 2015; Goldstein, 1982)	0.67
1-methylnaphthalene	142.20	H_2O	IGC	48.4 (Arp et al., 2006)	4.2×10^{-5}	62.4 (Chickos and Acree, 2003)	19.35 (Lide, 2008)	0.51 (in benzene) (Yaws, 2014)	80.2 (Lide, 2008)	50.72 (Fogg and Sangster, 2003; Sander, 2015)	0
2,3-dichlorophenol	163.0	H_2O	IGC	75.6 (Arp et al., 2006)	3.0	60.8 (Chickos and Acree, 2003)	15 (Mceachran et al., 2018)		80.2 (Lide, 2008)		0.17
2,6-dichlorophenol	163.0	H_2O	IGC	65.4(Arp et al., 2006)	4.6×10^{-2}	57.9 (Chickos and Acree, 2003)	15 (Mceachran et al., 2018)	5.03 (in benzene)(Oszust and Ratajczak, 1981)	80.2 (Lide, 2008)		0.17
2-chlorophenol	128.56	H_2O	IGC	57.9 (Arp et al., 2006)	2.1×10^{-3}	47 (Chickos and Acree, 2003)	13.1 (Mceachran et al., 2018)	1.33 (in benzene) (Yaws, 2014)	80.2 (Lide, 2008)	47.39 (Tabai et al., 1997; Sander, 2015)	0.17
2,4,5-trichlorophenol	197.44	H_2O	IGC	85.4 (Arp et	1.7×10^{2}	54.5 (Chickos and	17 (Mceachra	2.4 (Baron and	80.2 (Lide, 2008)		0.17

				al., 2006)		Acree, 2003)	n et al., 2018)	Arevalo, 1988)			
2-nitroanisole	153.14	H_2O	IGC	65.4 (Arp et al., 2006)	4.6×10^{-2}	58.6 (Chickos and Acree, 2003)	15.7 (Lide, 2008)	5 (liq.) (Lide, 2008)	80.2 (Lide, 2008)		0.43
2-nitrotoluene	137.14	H_2O	IGC	50.1 (Arp et al., 2006)	8.5×10^{-5}	59.1 (Chickos and Acree, 2003)	14.9 (Mceachran et al., 2018)	3.75 (in benzene) (Yaws, 2014)	80.2 (Lide, 2008)	24.11 (Sander, 2015; Baron and Arevalo, 1988)	0.29
2-phenylethyl acetate	164.20	H_2O	IGC	77.4 (Goss, 2009)	6.3	64.5 (Chickos and Acree, 2003)	18.6 (Mceachran et al., 2018)	1.85 (in benzene) (Rajyam and Murty, 1966; Mopsik, 1967)	80.2 (Lide, 2008)		0.2
3(m)-nitroanisole	153.14	H_2O	IGC	55.6 (Arp et al., 2006)	8.2×10^{-4}	49.8 (Chickos and Acree, 2003)	15.7 (Lide, 2008)	4.51 (Groves and Sudden, 1937)	80.2 (Lide, 2008)		0.43
4(p)-nitroanisole	153.14	H_2O	IGC	69.7 (Arp et al., 2006)	2.7×10^{-1}	54.2 (Chickos and Acree, 2003)	15.7 (Lide, 2008)	5.22 (Groves and Sudden, 1937)	80.2 (Lide, 2008)		0.43
acenaphthene	154.21	H_2O	IGC	60.8 (Arp et al., 2006)	6.9×10^{-3}	66.2 (Chickos and Acree, 2003)	20.61 (Lide, 2008)	~0.85 (Lide, 2008)	80.2 (Lide, 2008)	54.04 (Fogg and Sangster, 2003; Sander, 2015)	0
acetophenone	120.15	H_2O	IGC	52.2 (Arp et al., 2006)	2.0×10^{-4}	55.4 (Chickos and Acree, 2003)	15 (Lide, 2008)	3.02 (Lide, 2008)	80.2 (Lide, 2008)	64.02 (Staudinger and Roberts, 2001; Sander, 2015)	0
α-HCH	290.81	H_2O	IGC	85.5 (Goss, 2009)	1.7×10^{2}		22.5 (Mceachran et al., 2018)	2.2	80.2 (Lide, 2008)	54.04 (Sander, 2015)	0
anthracene	178.23	H_2O	IGC	64 (Arp et al., 2006)	2.6×10^{-2}	79.6 (Chickos and Acree, 2003)	25.67 (Lide, 2008)	0 (Yaws, 2014)	80.2 (Lide, 2008)	47.39 (Fogg and Sangster, 2003; Sander, 2015)	0
azobenzene	182.23	H_2O	IGC	74.4 (Arp et al., 2006)	1.8	72.8 (Chickos and Acree, 2003)	23.3 (Mceachran et al., 2018)	0 (Merino and Ribagorda, 2012)	80.2 (Lide, 2008)		0

benzaldehyde	106.12	H_2O	IGC	53.9 (Goss, 2009)	$4.1×10^{-4}$	49.1 (Chickos and Acree, 2003)	12.7 (Bosque and Sales, 2002)	3 (liq.) (Lide, 2008)	80.2 (Lide, 2008)	45.73 (Fogg and Sangster, 2003; Sander, 2015)	0.14
benzyl acetate	150.18	H_2O	IGC	70.5 (Goss, 2009)	$3.7×10^{-1}$	55.5 (Chickos and Acree, 2003)	16.7 (Mceachran et al., 2018)	1.22 (liq.) (Lide, 2008)	80.2 (Lide, 2008)		0.22
biphenyl	154.21	H_2O	IGC	59.5 (Arp et al., 2006)	$4.0×10^{-3}$	64.5 (Chickos and Acree, 2003)	20.2 (Mceachran et al., 2018)	0 (Yaws, 2014)	80.2 (Lide, 2008)	38.80 (Sander, 2015)	0
bromobenzene	157.01	H_2O	IGC	31.2 (Arp et al., 2006)	$3.6×10^{-8}$	44.5 (Chickos and Acree, 2003)	13.62 (Lide, 2008)	1.7 (Lide, 2008)	80.2 (Lide, 2008)	34.92 (Fogg and Sangster, 2003; Sander, 2015)	0
dibenzofurane	168.20	H_2O	IGC	61.5 (Arp et al., 2006)	$9.2×10^{-3}$	66.2 (Chickos and Acree, 2003)	21.5	0.88 (in benzene) (Yaws, 2014)	80.2 (Lide, 2008)		0.08
ethylbenzene	106.17	H_2O	IGC	35.9 (Goss, 2009)	$2.5×10^{-7}$	42.3 (Chickos and Acree, 2003)	14.2 (Lide, 2008)	0.6 (Yaws, 2014)	80.2 (Lide, 2008)	41.16 (Sander, 2015)	0
m-cresol	108.14	H_2O	IGC	64.8 (Arp et al., 2006)	$3.6×10^{-2}$	62.5 (Chickos and Acree, 2003)	13.1 (Mceachran et al., 2018)	1.48 (liq.) (Lide, 2008)	80.2 (Lide, 2008)	62.36 (Sander, 2015)	0.14
methylbenzoate	136.15	H_2O	IGC	54.8 (Goss, 2009)	$5.9×10^{-4}$	55.6 (Chickos and Acree, 2003)	15.06 (Bosque and Sales, 2002)	1.94 (liq.) (Lide, 2008)	80.2 (Lide, 2008)		0.25
p-cresol	108.14	H_2O	IGC	66.6 (Arp et al., 2006)	$7.5×10^{-2}$	62 (Chickos and Acree, 2003)	13.2 (Bosque and Sales, 2002)	1.48 (liq.) (Lide, 2008)	80.2 (Lide, 2008)	62.63 (Sander, 2015)	0.14
phenanthrene	178.23	H_2O	IGC	66.5 (Arp et al., 2006)	$7.2×10^{-2}$	78.7 (Chickos and Acree, 2003)	30.75 (Lide, 2008)	0 (Yaws, 2014)	80.2 (Lide, 2008)	34.92 (Fogg and Sangster, 2003; Sander, 2015)	0
phenol	94.11	H_2O	IGC	63 (Arp et al., 2006)	$1.7×10^{-2}$	58.8 (Chickos and Acree, 2003)	10.52 (Lide, 2008)	1.224 (Lide, 2008)	80.2 (Lide, 2008)	49.61 (Sander, 2015)	0.17
propylbenzene	120.20	H_2O	IGC	47.2 (Goss, 2009)	$2.6×10^{-5}$	46.2 (Chickos and	16 (Mceachra	0.37 (in benzene)	80.2 (Lide, 2008)	34.75 (Sander, 2015)	0

						Acree, 2003)	n et al., 2018)	(Yaws, 2014)			
p-xylene	106.17	H₂O	IGC	35.5 (Goss, 2009)	2.1×10⁻⁷	42.3 (Chickos and Acree, 2003)	14.35 (Bosque and Sales, 2002)	0 (Yaws, 2014)	80.2 (Lide, 2008)	34.92 (Fogg and Sangster, 2003; Sander, 2015)	0
tetrahydrofuran	72.11	H₂O	IGC	42.6 (Arp et al., 2006)	3.9×10⁻⁶	32 (Chickos and Acree, 2003)	7.97 (Bosque and Sales, 2002)	1.75 (Lide, 2008)	80.2 (Lide, 2008)	35.75 (Sander, 2015)	0.25

1259

1260

1261 **Table A11.** Compiled absorbate-substrate data for volatile amine and alcohol compounds
1262 adsorbed on water. Gas species, gas species' molar mass, substrate, experimental or theoretical
1263 method, desorption energy (E_{des}^0), and desorption lifetimes (τ_{des}) evaluated at 293 K using A_{des}
1264 $= 10^{13}$ s⁻¹, enthalpy of vaporization (ΔH_{vap}) and solvation (ΔH_{solv}), gas species' polarizability (α),
1265 gas species' dipole moment (μ), substrate's relative permittivity (ε_r), and gas species' oxygen to
1266 carbon ration ($O{:}C$) are given.

Gas Species	Molar Mass / g mol⁻¹	Substrate	Method	E_{des}^0 / kJ mol⁻¹	$\tau_{des}^{293\,K}$ / s	ΔH_{vap} (T) / kJ mol⁻¹	α / 10⁻²⁴ cm³	μ / D	ε_r	ΔH_{solv} (T) / kJ mol⁻¹	O:C
methylamine	31.06	H₂O	ST	28 (Mmereki et al., 2000)	9.8×10⁻⁹	26.1 (Chickos and Acree, 2003)	4.24 (Lide, 2008)	1.31 (Lide, 2008)	80.2 (Lide, 2008)	33.67 (Sander, 2015)	0
dimethylamine	45.09	H₂O	ST	37 (Mmereki et al., 2000)	3.9×10⁻⁷	27 (Chickos and Acree, 2003)	6.37 (Hickey and Rowley, 2014)	1.01 (Lide, 2008)	80.2 (Lide, 2008)	43.23 (Sander, 2015)	0
trimethylamine	59.11	H₂O	ST	34 (Mmereki et al., 2000)	1.2×10⁻⁷	24.1 (Chickos and Acree, 2003)	8.15 (Hickey and Rowley, 2014)	0.612 (Lide, 2008)	80.2 (Lide, 2008)	49.6 (Leng et al., 2015)	0
methanol	32.04	H₂O	ST	39.2 (Donaldson and Anderson, 1999)	9.7×10⁻⁷	37.8 (Chickos and Acree, 2003)	3.28 (Lide, 2008)	1.7 (Lide, 2008)	80.2 (Lide, 2008)	46.56 (Sander, 2015; Sander et al., 2011)	0
1-propanol	60.09	H₂O	ST	68.2 (Donaldson and Anderson, 1999)	1.4×10⁻¹	47.45 (Chickos and Acree, 2003)	6.74 (Lide, 2008)	1.58 (Lide, 2008)	80.2 (Lide, 2008)	57.37 (Sander, 2015; Sander et al., 2011)	0.33
2-propanol	60.09	H₂O	ST	68.9 (Donaldson and Anderson, 1999)	1.9×10⁻¹	45.34 (Chickos and Acree, 2003)	7.29 (Lide, 2008)	1.58 (Lide, 2008)	80.2 (Lide, 2008)	62.36 (Sander, 2015; Sander et al., 2011)	0.33
1-propanol	60.09	H₂O	ST	58.8 (Demou and Donalds	3.0×10⁻³	47.45 (Chickos and Acree, 2003)	6.74 (Lide, 2008)	1.58 (Lide, 2008)	80.2 (Lide, 2008)	57.37 (Sander, 2015; Sander et al., 2011)	0.33

				on, 2002)						
1-propanol	60.09	H_2O	ST	56.7 (Goss, 2009)	$1.3×10^{-3}$	47.45 (Chickos and Acree, 2003)	6.74 (Lide, 2008)	1.58 (Lide, 2008)	80.2 (Lide, 2008)	57.37 (Sander, 2015; Sander et al., 2011)	0.33
1-butanol	74.12	H_2O	ST	62.8 (Donaldson and Anderson, 1999)	$1.6×10^{-2}$	52.34 (Chickos and Acree, 2003)	8.88 (Lide, 2008)	1.66 (Lide, 2008)	80.2 (Lide, 2008)	62.36 (Sander, 2015; Sander et al., 2011)	0.25
2-butanol	74.12	H_2O	ST	63.5 (Donaldson and Anderson, 1999)	$2.1×10^{-2}$	49.74 (Chickos and Acree, 2003)	8.77 (Bosque and Sales, 2002)	1.66 (Yaws, 2014)	80.2 (Lide, 2008)	60.70 (Sander, 2015; Sander et al., 2011)	0.25
1-butanol	74.12	H_2O	IGC	56.1 (Goss, 2009)	$1.0×10^{-3}$	52.34 (Chickos and Acree, 2003)	8.88 (Lide, 2008)	1.66 (Lide, 2008)	80.2 (Lide, 2008)	62.36 (Sander, 2015; Sander et al., 2011)	0.25
ethanediol	62.07	H_2O	IGC	84.8 (Goss, 2009)	$1.3×10^{2}$	65.6 (Chickos and Acree, 2003)	5.72 (Bosque and Sales, 2002)	2.36 (Lide, 2008)	80.2 (Lide, 2008)	73.17 (Compernolle and Muller, 2014; Sander, 2015)	1
ethanol	46.07	H_2O	IGC	51.1 (Goss, 2009)	$1.3×10^{-4}$	42.4 (Chickos and Acree, 2003)	5.41 (Lide, 2008)	1.69 (Lide, 2008)	80.2 (Lide, 2008)	53.21 (Sander, 2015; Sander et al., 2011)	0.5
cyclohexanol	100.16	H_2O	IGC	79.5 (Goss, 2009)	$1.5×10^{1}$	62 (Chickos and Acree, 2003)	11.56 (Lide, 2008)	1.86 (in CCl_4) (Yaws, 2014)	80.2 (Lide, 2008)	66.51 (Sander, 2015)	0.17
cyclopentanol	86.13	H_2O	IGC	62.7 (Goss, 2009)	$1.5×10^{-2}$	57.5 (Chickos and Acree, 2003)	9.72 (Lide, 2008)		80.2 (Lide, 2008)	63.19 (Sander, 2015)	0.2
3-methylbutan-1-ol	88.15	H_2O	IGC	61.6 (Goss, 2009)	$9.6×10^{-3}$	54.3 (Chickos and Acree, 2003)	10.61 (Lide, 2008)	1.88 (2-Methylbutan-1-ol) (Lide, 2008)	80.2 (Lide, 2008)	63.19 (Kuhne et al., 2005)	0.2
1,2-propanediol	76.10	H_2O	IGC	64.5 (Goss, 2009)	$3.2×10^{-2}$	58.6 (Chickos and Acree, 2003)	7.55 (Bosque and Sales, 2002)	2.25 (liq.) (Lide, 2008)	80.2 (Lide, 2008)	78.99 (Compernolle and Muller, 2014; Sander, 2015)	0.67
1,3-propanediol	76.10	H_2O	IGC	75 (Goss, 2009)	2.3	72.4 (Chickos and Acree, 2003)	7.54 (Mceachran et al., 2018)	2.55 (liq.) (Lide, 2008)	80.2 (Lide, 2008)	78.99 (Compernolle and Muller, 2014; Sander, 2015)	0.67

Gas Species	Molar Mass / g mol^{-1}	Substrate	Method	E_{des}^0 / kJ mol^{-1}	$\tau_{des}^{293\,K}$ / s	ΔH_{vap} (T) / kJ mol^{-1}	α / 10^{-24} cm^3	μ / D	ε_r	ΔH_{solv} (T) / kJ mol^{-1}	O:C
1,4-butanediol	90.12	H_2O	IGC	105.1 (Goss, 2009)	5.4×10^5	79.3 (Chickos and Acree, 2003)	9.35 (Bosque and Sales, 2002)	2.48 (liq.) (Lide, 2008)	80.2 (Lide, 2008)	91.46 (Compernolle and Muller, 2014; Sander, 2015)	0.5
1-decanol	158.29	H_2O	IGC	94.8 (Goss, 2009)	7.9×10^3	81.5 (Chickos and Acree, 2003)	19.83 (Bosque and Sales, 2002)	1.70 (Crossley, 1971)	80.2 (Lide, 2008)	49.47 (Sander, 2015)	0.1
1-heptanol	116.20	H_2O	IGC	75.7 (Goss, 2009)	3.1	66.5 (Chickos and Acree, 2003)	14.3 (Bosque and Sales, 2002)	1.74 (in benzene) (Yaws, 2014)	80.2 (Lide, 2008)	56.12 (Sander, 2015)	0.14
1-hexanol	102.18	H_2O	IGC	66.2 (Goss, 2009)	6.3×10^{-2}	61.6 (Chickos and Acree, 2003)	12.46 (Bosque and Sales, 2002)	1.55 (Speight, 2017)	80.2 (Lide, 2008)	51.96 (Sander, 2015)	0.17
1-nonanol	144.26	H_2O	IGC	86.3 (Goss, 2009)	2.4×10^2	76.9 (Chickos and Acree, 2003)	18 (Mceachran et al., 2018)	1.61 (in benzene) (Yaws, 2014)	80.2 (Lide, 2008)	51.96 (Sander, 2015)	0.11
1-octanol	130.23	H_2O	IGC	75.7 (Goss, 2009)	3.1	71 (Chickos and Acree, 2003)	16.14 (Bosque and Sales, 2002)	1.76 (liq.) (Lide, 2008)	80.2 (Lide, 2008)	53.63 (Sander, 2015)	0.13
1-pentanol	88.15	H_2O	IGC	68.9 (Goss, 2009)	1.9×10^{-1}	57.8 (Chickos and Acree, 2003)	10.61 (Bosque and Sales, 2002)	1.7 (liq.) (Lide, 2008)	80.2 (Lide, 2008)	55.91 (Sander, 2015)	0.2
1-undecanol	172.31	H_2O	IGC	88 (Goss, 2009)	4.9×10^2	83.5 (Chickos and Acree, 2003)	21.6 (Mceachran et al., 2018)	1.67 (Yaws, 2014)	80.2 (Lide, 2008)		0.09
2-methylpropan-1-ol	74.12	H_2O	IGC	50.7 (Goss, 2009)	1.1×10^{-4}	54.1 (Chickos and Acree, 2003)	8.92 (Lide, 2008)	1.64 (Lide, 2008)	80.2 (Lide, 2008)	59.86 (Kuhne et al., 2005)	0.25

1267

1268

Table A12. Compiled absorbate-substrate data for alkene and ketone compounds adsorbed on water. Gas species, gas species' molar mass, substrate, experimental or theoretical method, desorption energy (E_{des}^0), and desorption lifetimes (τ_{des}) evaluated at 293 K using $A_{des} = 10^{13}$ s^{-1}, enthalpy of vaporization (ΔH_{vap}) and solvation (ΔH_{solv}), gas species' polarizability (α), gas species' dipole moment (μ), substrate's relative permittivity (ε_r), and gas species' oxygen to carbon ration ($O{:}C$) are given.

Gas Species	Molar Mass / g mol^{-1}	Substrate	Method	E_{des}^0 / kJ mol^{-1}	$\tau_{des}^{293\,K}$ / s	ΔH_{vap} (T) / kJ mol^{-1}	α / 10^{-24} cm^3	μ / D	ε_r	ΔH_{solv} (T) / kJ mol^{-1}	O:C
1-decene	140.27	H_2O	IGC	47.5 (Goss, 2009)	2.9×10^{-5}	50.4 (Chickos and Acree, 2003)	19.1 (Mceachran et al., 2018)	0.42 (in benzene) (Yaws, 2014)	80.2 (Lide, 2008)		0

1-dodecene	168.32	H$_2$O	IGC	49 (Goss, 2009)	5.4×10^{-5}	60.8 (Chickos and Acree, 2003)	22.7 (Mceachran et al., 2018)	0.52 (in benzene) (Yaws, 2014)	80.2 (Lide, 2008)		0
1-tridecene	182.35	H$_2$O	IGC	52.7 (Goss, 2009)	2.5×10^{-4}	65.3 (Chickos and Acree, 2003)	24.6 (Mceachran et al., 2018)	0 (Yaws, 2014)	80.2 (Lide, 2008)		0
cis-2-octene	112.22	H$_2$O	IGC	36 (Hartkopf and Karger, 1973)	2.6×10^{-7}	40.2 (Chickos and Acree, 2003)	15.5 (Mceachran et al., 2018)	0.31 (Yaws, 2014)	80.2 (Lide, 2008)		0
trans-2-octene	112.22	H$_2$O	IGC	36 (Hartkopf and Karger, 1973)	2.6×10^{-7}	40.2 (Chickos and Acree, 2003)	15.5 (Mceachran et al., 2018)	0 (Yaws, 2014)	80.2 (Lide, 2008)		0
1-nonene	126.24	H$_2$O	IGC	44.3 (Goss, 2009)	7.9×10^{-6}	44.7 (Chickos and Acree, 2003)	17.2 (Mceachran et al., 2018)	0.36 (Yaws, 2014)	80.2 (Lide, 2008)		0
1-undecene	154.30	H$_2$O	IGC	54.1 (Goss, 2009)	4.4×10^{-4}	54.3 (Chickos and Acree, 2003)	20.9 (Mceachran et al., 2018)	0.53 (in benzene) (Yaws, 2014)	80.2 (Lide, 2008)		0
acetone	58.08	H$_2$O	ST	50.3 (Donaldson and Anderson, 1999)	9.3×10^{-5}	31.3 (Chickos and Acree, 2003)	6.37 (Lide, 2008)	2.88 (Lide, 2008)	80.2 (Lide, 2008)	44.27 (Sander, 2015)	0.33
propanone	58.08	H$_2$O	IGC	42.9 (Arp et al., 2006)	4.4×10^{-6}	31.3 (Chickos and Acree, 2003)	6.37 (Lide, 2008)	2.88 (=acetone) (Yaws, 2014)	80.2 (Lide, 2008)	44.27 (Sander, 2015)	0.33
pentanal	86.13	H$_2$O	IGC	46.7 (Goss, 2009)	2.1×10^{-5}	38.3 (Chickos and Acree, 2003)	10.1 (Mceachran et al., 2018)	2.57 (in benzene) (Yaws, 2014)	80.2 (Lide, 2008)	51.55 (Sander, 2015)	0.2
2,3-butanedione	86.09	H$_2$O	IGC	46.9 (Goss, 2009)	2.3×10^{-5}	38.5 (Chickos and Acree, 2003)	8.2 (Lide, 2008)	1.03 (Henderson and Meyer, 1976)	80.2 (Lide, 2008)	51.55 (Sander, 2015)	0.5
2,5-hexanedione	114.14	H$_2$O	IGC	64.1 (Goss, 2009)	2.7×10^{-2}	50.1 (Chickos and Acree, 2003)	11.9 (Mceachran et al., 2018)	2.5 (in dioxane) (Wittwer et al., 1988)	80.2 (Lide, 2008)		0.33
2-butanone	72.11	H$_2$O	IGC	49.3 (Arp et al., 2006)	6.1×10^{-5}	34.8 (Chickos and Acree, 2003)	8.25 (Bosque and Sales, 2002)	2.78 (Lide, 2008)	80.2 (Lide, 2008)	99.77	0.25
2-heptanone	114.19	H$_2$O	IGC	59.7 (Arp et al., 2006)	4.4×10^{-3}	47.4 (Chickos and Acree, 2003)	13.7 (Mceachran et al., 2018)	2.59 (liq.) (Lide, 2008)	80.2 (Lide, 2008)	46.56 (Sander, 2015)	0.14
2-hexanone	100.16	H$_2$O	IGC	47 (Arp et al., 2006)	2.4×10^{-5}	43.1 (Chickos and Acree, 2003)	11.95 (Bosque and Sales, 2002)	2.66 (liq.) (Lide, 2008)	80.2 (Lide, 2008)	52.05 (Sander, 2015)	0.17

				63.2 (Arp et al., 2006)		52.6 (Chickos and Acree, 2003)	15.5 (Mceachran et al., 2018)	2.7 (liq.) (Lide, 2008)	80.2 (Lide, 2008)	60.69 (Kuhne et al., 2005; Sander, 2015)	
2-octanone	128.22	H₂O	IGC	63.2 (Arp et al., 2006)	1.8×10⁻²	52.6 (Chickos and Acree, 2003)	15.5 (Mceachran et al., 2018)	2.7 (liq.) (Lide, 2008)	80.2 (Lide, 2008)	60.69 (Kuhne et al., 2005; Sander, 2015)	0.13
2-pentanone	86.13	H₂O	IGC	43.2 (Arp et al., 2006)	5.0×10⁻⁶	38.3 (Chickos and Acree, 2003)	9.93 (Lide, 2008)	2.7 (liq.) (Lide, 2008)	80.2 (Lide, 2008)	41.85 (Sander, 2015)	0.2
cyclopentanone	84.19	H₂O	IGC	54.1 (Arp et al., 2006)	4.4×10⁻⁴	42.7 (Chickos and Acree, 2003)	9.19 (Mceachran et al., 2018)	3.3 (liq.) (Lide, 2008)	80.2 (Lide, 2008)	48.22 (Kuhne et al., 2005; Sander, 2015)	0.2

1275

1276

1277 **Table A13.** Compiled absorbate-substrate data for volatile acid and ether compounds adsorbed on
1278 water. Gas species, gas species' molar mass, substrate, experimental or theoretical method,
1279 desorption energy (E_{des}^0), and desorption lifetimes (τ_{des}) evaluated at 293 K using $A_{des} = 10^{13}$ s⁻¹,
1280 enthalpy of vaporization (ΔH_{vap}) and solvation (ΔH_{solv}), gas species' polarizability (α), gas
1281 species' dipole moment (μ), substrate's relative permittivity (ε_r), and gas species' oxygen to
1282 carbon ration ($O{:}C$) are given.

Gas Species	Molar Mass / g mol⁻¹	Substrate	Method	E_{des}^0 / kJ mol⁻¹	$\tau_{des}^{293\,K}$ / s	ΔH_{vap} (T) / kJ mol⁻¹	α / 10⁻²⁴ cm³	μ / D	ε_r	ΔH_{solv} (T) / kJ mol⁻¹	O:C
acetic acid	60.05	H₂O	ST	58.8 (Donaldson and Anderson, 1999)	3.0×10⁻³	41.6 (Chickos and Acree, 2003)	5.1 (Lide, 2008)	1.7 (Lide, 2008)	80.2 (Lide, 2008)	51.96 (Sander, 2015)	1
propionic acid	74.08	H₂O	ST	61.4 (Donaldson and Anderson, 1999)	8.8×10⁻³	31.1 (Chickos and Acree, 2003)	6.9 (Lide, 2008)	1.75 (Lide, 2008)	80.2 (Lide, 2008)	56.54 (Abraham, 1984; Sander, 2015)	0.67
butanoic acid	88.11	H₂O	ST	58.6 (Donaldson and Anderson, 1999)	2.8×10⁻³	40.5 (Chickos and Acree, 2003)	8.58 (Lide, 2008)	1.65 (liq.) (Lide, 2008)	80.2 (Lide, 2008)	59.86 (Abraham, 1984; Sander, 2015)	0.5
hexanoic acid	116.16	H₂O	ST	57.6 (Demou and Donaldson, 2002)	1.9×10⁻³	69.2 (Chickos and Acree, 2003)	12.5	1.13 (liq.) (Lide, 2008)	80.2 (Lide, 2008)	50.72 (Staudinger and Roberts, 2001; Sander, 2015)	0.33
methyl formate	60.05	H₂O	IGC	32.6 (Hartkopf and Karger, 1973)	6.5×10⁻⁸	31.6 (Chickos and Acree, 2003)	5.05 (Lide, 2008)	1.77 (Lide, 2008)	80.2 (Lide, 2008)	33.26 (Sander, 2015; Sander et al., 2011)	1
ethyl formate	74.08	H₂O	IGC	28.9 (Hartkopf and	1.4×10⁻⁸	31.6 (Chickos and Acree, 2003)	6.88 (Lide, 2008)	1.93 (Lide, 2008)	80.2 (Lide, 2008)	38.25 (Sander, 2015;	0.67

				Karger, 1973)						Sander et al., 2011)	
butyl acetate	116.16	H_2O	IGC	60.4 (Goss, 2009)	5.9×10^{-3}	41.3 (Chickos and Acree, 2003)	12.57 (Bosque and Sales, 2002)	1.87 (liq.) (Lide, 2008)	80.2 (Lide, 2008)	46.01 (Sander, 2015)	0.33
Diethyl phthalate	222.24	H_2O	IGC	94.6 (Goss, 2009)	7.3×10^{3}	81.8 (Chickos and Acree, 2003)	23.4 (Mceachran et al., 2018)	2.73 (in benzene) (Yaws, 2014)	80.2 (Lide, 2008)	100.7 (Kuhne et al., 2005)	0.33
dimethyl oxalate	118.09	H_2O	IGC	48.2 (Goss, 2009)	3.9×10^{-5}	48.8 (Chickos and Acree, 2003)	9.57 (Mceachran et al., 2018)	2 (in m-xylene) (Aihara and Davies, 1956)	80.2 (Lide, 2008)		1
dimethyl phthalate	194.19	H_2O	IGC	84 (Goss, 2009)	9.4×10^{1}	77.2 (Chickos and Acree, 2003)	19.7 (Mceachran et al., 2018)	2.78 (in benzene) (Yaws, 2014)	80.2 (Lide, 2008)		0.4
dimethyl succinate	146.14	H_2O	IGC	63.3 (Goss, 2009)	1.9×10^{-2}	49.3 (Chickos and Acree, 2003)	13.2 (Mceachran et al., 2018)	2.16 (in benzene) (Yaws, 2014)	80.2 (Lide, 2008)	64.85 (Sander, 2015)	0.5
pentyl acetate	130.19	H_2O	IGC	58.3 (Goss, 2009)	2.5×10^{-3}	48.6 (Chickos and Acree, 2003)	14.9 (Lide, 2008)	1.75 (Lide, 2008)	80.2 (Lide, 2008)	54.04 (Kieckbusch and King, 1979; Sander, 2015)	0.29
ethyl acetate	88.11	H_2O	IGC	47 (Goss, 2009)	2.4×10^{-5}	35.1 (Chickos and Acree, 2003)	8.62 (Lide, 2008)	1.78 (Lide, 2008)	80.2 (Lide, 2008)	49.05 (Sander, 2015; Sander et al., 2011)	0.5
di-n-butyl ether	130.23	H_2O	IGC	57.4 (Arp et al., 2006)	1.7×10^{-3}	45 (Chickos and Acree, 2003)	16.31 (Bosque and Sales, 2002)	~1.17 (Lide, 2008)	80.2 (Lide, 2008)	54.87 (Kuhne et al., 2005; Sander, 2015)	0.125
di-n-pentyl ether	158.28	H_2O	IGC	59.6 (Arp et al., 2006)	4.2×10^{-3}	46.2 (Chickos and Acree, 2003)	19.9 (Mceachran et al., 2018)	~1.2 (liq.) (Lide, 2008)	80.2 (Lide, 2008)		0.1
ethyl-t-butyl ether	102.18	H_2O	IGC	47.9 (Arp et al., 2006)	3.5×10^{-5}	33.5 (Chickos and Acree, 2003)	12.5 (Mceachran et al., 2018)	1.22 (in benzene) (Yaws, 2014)	80.2 (Lide, 2008)	39.2 (Kuhne et al., 2005)	0.17
methyl tert-butyl ether	88.15	H_2O	IGC	38.7 (Arp et al., 2006)	7.9×10^{-7}	30.4 (Chickos and Acree, 2003)	10.7 (Mceachran et al., 2018)	1.36 (in benzene) (Yaws, 2014)	80.2 (Lide, 2008)	45.97 (Sander, 2015)	0.2
n-propyl ether	102.18	H_2O	IGC	53.6 (Hartkopf and Karger, 1973)	3.6×10^{-4}	35.7 (Chickos and Acree, 2003)	12.5 (Mceachran et al., 2018)	1.21 (Yaws, 2014)	80.2 (Lide, 2008)	61.80 (Sander, 2015)	0.17

1283

1284

1285 **Table A14.** Compiled absorbate-substrate data for volatile alkane compounds adsorbed on water.
1286 Gas species, gas species' molar mass, substrate, experimental or theoretical method, desorption
1287 energy (E_{des}^0), and desorption lifetimes (τ_{des}) evaluated at 293 K using $A_{des} = 10^{13}$ s^{-1}, enthalpy
1288 of vaporization (ΔH_{vap}) and solvation (ΔH_{solv}), gas species' polarizability (α), gas species' dipole
1289 moment (μ), substrate's relative permittivity (ε_r), and gas species' oxygen to carbon ration ($O{:}C$)
1290 are given.

Gas Species	Molar Mass / g mol^{-1}	Substrate	Method	E_{des}^0 / kJ mol^{-1}	$\tau_{des}^{293\,K}$ / s	ΔH_{vap} (T) / kJ mol^{-1}	α / 10^{-24} cm^3	μ / D	ε_r	ΔH_{solv} (T) / kJ mol^{-1}	O:C
decane	142.29	H_2O	IGC	46.5 (Goss, 2009)	1.9×10^{-5}	51.4 (Chickos and Acree, 2003)	19.1 (Lide, 2008)	0 (Yaws, 2014)	80.2 (Lide, 2008)		0
dodecane	170.34	H_2O	IGC	58.1 (Goss, 2009)	2.3×10^{-3}	62.1 (Chickos and Acree, 2003)	22.75 (Laib and Mittleman, 2010)	0 (Yaws, 2014)	80.2 (Lide, 2008)		0
nonane	128.26	H_2O	IGC	34.6 (Goss, 2009)	1.5×10^{-7}	46.55 (Chickos and Acree, 2003)	17.36 (Laib and Mittleman, 2010)	0 (Yaws, 2014)	80.2 (Lide, 2008)	34.50 (Sander et al., 2011)	0
tetradecane	198.39	H_2O	IGC	67.6 (Goss, 2009)	1.1×10^{-1}	71.73 (Chickos and Acree, 2003)	26.22 (Laib and Mittleman, 2010)	0 (Yaws, 2014)	80.2 (Lide, 2008)		0
tridecane	184.37	H_2O	IGC	58.2 (Goss, 2009)	2.4×10^{-3}	66.68 (Chickos and Acree, 2003)	24.41 (Laib and Mittleman, 2010)	0 (Yaws, 2014)	80.2 (Lide, 2008)		0
trimethyl phosphite	124.08	H_2O	IGC	77.4 (Arp et al., 2006)	6.3	42.5 (Chickos and Acree, 2003)	28.6 (Aroney et al., 1964)		80.2 (Lide, 2008)		1
undecane	156.31	H_2O	IGC	52.8 (Goss, 2009)	2.6×10^{-4}	56.58 (Chickos and Acree, 2003)	21.03 (Lide, 2008)	0 (Yaws, 2014)	80.2 (Lide, 2008)		0
n-pentane	72.15	H_2O	IGC	23.8 (Hartkopf and Karger, 1973)	1.7×10^{-9}	25 (Chickos and Acree, 2003)	9.99 (Lide, 2008)	0 (Yaws, 2014)	80.2 (Lide, 2008)	25.77 (Sander et al., 2011)	0
n-hexane	86.18	H_2O	IGC	27.6 (Hartkopf and Karger, 1973)	8.3×10^{-9}	31.5 (Chickos and Acree, 2003)	11.9 (Lide, 2008)	0 (Yaws, 2014)	80.2 (Lide, 2008)	46.89 (Sander et al., 2011)	0
n-heptane	100.21	H_2O	IGC	31.4 (Hartkopf and Karger, 1973)	4.0×10^{-8}	36.6 (Chickos and Acree, 2003)	13.61 (Lide, 2008)	0 (Yaws, 2014)	80.2 (Lide, 2008)	34.64 (Sander et al., 2011)	0
n-octane	114.23	H_2O	IGC	35.6 (Hartkopf and Karger, 1973)	2.2×10^{-7}	41.6 (Chickos and Acree, 2003)	15.9 (Lide, 2008)	0 (Yaws, 2014)	80.2 (Lide, 2008)	45.31 (Sander et al., 2011)	0

n-nonane	128.26	H_2O	IGC	39.7 (Hartkopf and Karger, 1973)	1.2×10^{-6}	46.55 (Chickos and Acree, 2003)	17.36 (Lide, 2008)	0 (Yaws, 2014)	80.2 (Lide, 2008)	34.50 (Sander et al., 2011)	0
n-decane	142.29	H_2O	IGC	44.8 (Hartkopf and Karger, 1973)	9.7×10^{-6}	51.4 (Chickos and Acree, 2003)	19.1 (Lide, 2008)	0 (Yaws, 2014)	80.2 (Lide, 2008)		0
2-methylheptane	114.23	H_2O	IGC	34.7 (Hartkopf and Karger, 1973)	1.5×10^{-7}	46.55 (Chickos and Acree, 2003)	15.5 (Mceachran et al., 2018)	0 (Yaws, 2014)	80.2 (Lide, 2008)		0
2,4-dimethylhexane	114.23	H_2O	IGC	33.5 (Hartkopf and Karger, 1973)	9.4×10^{-8}	71.73 (Chickos and Acree, 2003)	15.5 (Mceachran et al., 2018)	0 (Yaws, 2014)	80.2 (Lide, 2008)	38.5 (2,5-dimethylhexane) (Kuhne et al., 2005)	0
2,2,4-trimethylpentane	114.23	H_2O	IGC	32.2 (Hartkopf and Karger, 1973)	5.5×10^{-8}	66.68 (Chickos and Acree, 2003)	15.44 (Lide, 2008)	0 (Yaws, 2014)	80.2 (Lide, 2008)	36.17 (Sander et al., 2011)	0
cycloheptane	98.19	H_2O	IGC	31.4 (Hartkopf and Karger, 1973)	4.0×10^{-8}	42.5 (Chickos and Acree, 2003)	12.84 (Bosque and Sales, 2002)	0 (Yaws, 2014)	80.2 (Lide, 2008)		0
cyclooctane	112.22	H_2O	IGC	35.6 (Hartkopf and Karger, 1973)	2.2×10^{-7}	56.58 (Chickos and Acree, 2003)	14.62 (Bosque and Sales, 2002)	0 (Yaws, 2014)	80.2 (Lide, 2008)	39.63 (Sander et al., 2011)	0
trichloroethane	133.40	H_2O	ST	26.3 (Bruant and Conklin, 2001)	4.9×10^{-9}	32.5 (Chickos and Acree, 2003)	10.7 (Lide, 2008)	1.78 (Yaws, 2014)	80.2 (Lide, 2008)	32.15 (Sander et al., 2011)	0
dichloromethane	84.93	H_2O	IGC	23.4 (Hartkopf and Karger, 1973)	1.5×10^{-9}	30.6 (Chickos and Acree, 2003)	6.49 (Mceachran et al., 2018)	1.60 (Yaws, 2014)	80.2 (Lide, 2008)	33.26 (Sander et al., 2011)	0
chloroform	119.37	H_2O	IGC	26.8 (Hartkopf and Karger, 1973)	6.0×10^{-9}	31.1 (Chickos and Acree, 2003)	8.87 (Lide, 2008)	1.01 (Yaws, 2014)	80.2 (Lide, 2008)	37.00 (Sander et al., 2011)	0
carbon tetrachloride	153.81	H_2O	IGC	23.4 (Hartkopf and Karger, 1973)	1.5×10^{-9}	32.4 (Chickos and Acree, 2003)	10.85 (Lide, 2008)	0 (Yaws, 2014)	80.2 (Lide, 2008)	35.13 (Sander et al., 2011)	0

Gas Species	Molar Mass / g mol⁻¹	Substrate	Method	E_{des}^0 / kJ mol⁻¹	$\tau_{des}^{293\,K}$ / s	ΔH_{vap} (T) / kJ mol⁻¹	α / 10⁻²⁴ cm³	μ / D	ε_r	ΔH_{solv} (T) / kJ mol⁻¹	O:C
1,2-dichloroethane	98.95	H₂O	IGC	32.6 (Hartkopf and Karger, 1973)	6.5×10⁻⁸	35.2 (Chickos and Acree, 2003)	8 (Lide, 2008)	1.83 (Lide, 2008)	80.2 (Lide, 2008)	35.47 (Sander et al., 2011)	0

1291

1292

Table A15. Compiled absorbate-substrate data for volatile acid and alcohol compounds adsorbed on aqueous solutions. Gas species, gas species' molar mass, substrate, experimental or theoretical method, desorption energy (E_{des}^0), and desorption lifetimes (τ_{des}) evaluated at 293 K using A_{des} = 10¹³ s⁻¹, enthalpy of vaporization (ΔH_{vap}) and solvation (ΔH_{solv}), gas species' polarizability (α), gas species' dipole moment (μ), substrate's relative permittivity (ε_r), and gas species' oxygen to carbon ration ($O{:}C$) are given.

Gas Species	Molar Mass / g mol⁻¹	Substrate	Method	E_{des}^0 / kJ mol⁻¹	$\tau_{des}^{293\,K}$ / s	ΔH_{vap} (T) / kJ mol⁻¹	α / 10⁻²⁴ cm³	μ / D	ε_r	ΔH_{solv} (T) / kJ mol⁻¹	O:C
hexanoic acid	116.16	4 M NaCl (aq)	ST	54.2 (Demou and Donaldson, 2002)	4.6×10⁻⁴	69.2 (Chickos and Acree, 2003)	12.5 (Mceachran et al., 2018)	1.13 (liq.) (Lide, 2008)	40 (Maribo-Mogensen et al., 2013)	50.72 (Staudinger and Roberts, 2001; Sander, 2015)	0.33
hexanoic acid	116.16	4 M (NH₄)₂SO4 (aq)	ST	55.4 (Demou and Donaldson, 2002)	7.5×10⁻⁴	69.2 (Chickos and Acree, 2003)	12.5 (Mceachran et al., 2018)	1.13 (liq.) (Lide, 2008)	42 (Lileev and Lyashchenko, 2009)	50.72 (Staudinger and Roberts, 2001; Sander, 2015)	0.33
1-propanol	60.09	4 M NaCl (aq)	ST	58.7 (Demou and Donaldson, 2002)	2.9×10⁻³	47.45 (Chickos and Acree, 2003)	6.74 (Lide, 2008)	1.58 (Lide, 2008)	40 (Maribo-Mogensen et al., 2013)	57.37 (Sander, 2015; Sander et al., 2011)	0.33
1-propanol	60.09	4 M (NH₄)₂SO4 (aq)	ST	58.9 (Demou and Donaldson, 2002)	3.2×10⁻³	47.45 (Chickos and Acree, 2003)	6.74 (Lide, 2008)	1.58 (Lide, 2008)	42 (Lileev and Lyashchenko, 2009)	57.37 (Sander, 2015; Sander et al., 2011)	0.33

1299

Data availability. Data needed to draw the conclusions in the present study are given in the paper and in the Supplement. In addition, the datasets required to reproduce the results and corresponding figures are available on Zenodo (Knopf et al., 2023).

1303

Supplement. The supplement related to this article is available online at: XYZ

1305

Author contributions. DAK and MS envisioned the project. DAK supervised project, performed correlation analyses, and wrote first draft of manuscript. MS performed kinetic flux modeling. MA, TB, and UP critically discussed analyses and results and were involved in representation of data. All authors discussed interpretation of the data and contributed to the writing of the paper.

1310

Competing interests. At least one of the (co-)authors is a member of the editorial board of Atmospheric Chemistry and Physics.

1313

Disclaimer. Publisher's note: Copernicus Publications remains neutral with regard to jurisdictional claims in published maps and institutional affiliations.

1316

Acknowledgments. D.K. acknowledges support by the U.S. National Science Foundation (grant no. AGS-1446286) and the Max-Planck Society to support a sabbatical stay in 2014 that initiated this project. M.S. acknowledges support by the U.S. National Science Foundation (grant no. AGS-1654104) and the U.S. Department of Energy (grant no DE-SC0022139). M. A. acknowledges support by the Swiss National Science Foundation (grant no. 188662).

1322

1323   **Financial support.** This research has been supported by the U.S. National Science Foundation
1324   (grant nos. AGS-1446286 and AGS-1654104), the U.S. Department of Energy (DE-SC0022139),
1325   and the Swiss National Science Foundation (grant no. 188662).

1326 **Table 1.** Intermolecular forces for selected functional groups and gases (Jeffrey, 1997; Jeffrey
1327 and Saenger, 1991; Vinogradov and Linnell, 1971; Iupac, 1997).

Functional Group	London dispersion force	Keesom force	Hydrogen Bonding
Alkane	Increases with chain length	none	None with itself.
Ether	Increases with chain length	Slightly polar, 1 O	None with itself. H-bond acceptor (max. 2) of other molecules
Ester	Increases with chain length	More polar than ether, 1 O	None with itself. H-bond acceptor (max. 2) of other molecules
Amine	Increases with chain length	Polar, 1 N	0-2 H-bonds with itself. *Primary*: H-bond donor (max. 2) and acceptor (max. 1). *Secondary*: H-bond donor (max. 1) and acceptor (max. 1). *Tertiary*: H-bond acceptor (max. 1).
Imine	Increases with chain length	Polar, 1 N	1-2 H-bonds with itself. *Primary*: H-bond donor (max. 1) and acceptor (max. 1). *Secondary*: H-bond acceptor (max. 1). *Tertiary*: H-bond acceptor (max. 1).
Aldehyde / Ketone	Increases with chain length	Polar C=O manifest strong dipole	None with itself. H-bond acceptor (max. 2) of other molecules
Alcohol	Increases with chain length	Polar, 1 O	2 H-bonds with itself. H-bond donor (max. 1) and acceptor (max. 2).
Acid	Increases with chain length	Polar, 2 O	2 H-bonds with itself forming dimer increasing molecule size. H-bond donor (max. 1) and acceptor (max. 4).
Amide	Increases with chain length	Polar, strong dipole 1 N & 1 O	2 H-bonds with itself. H-bond donor (max. 2) and acceptor (max. 3).
Other Species	**Vapor pressure**	**Polar**	
N_2O_5	100 hPa @ 3.9 °C	Yes	None with itself. H-bond acceptor (max. 12).
HONO		Yes	2 H-bonds with itself. H-bond donor (max. 1) and acceptor (max. 5).
NH_3	100 hPa @ -71.3 °C	Yes	2 H-bonds with itself.

			H-bond donor (max. 3) and acceptor (max. 1).
HNO_3	100 hPa @ 28.4 °C	Yes	2 H-bonds with itself. H-bond donor (max. 1) and acceptor (max. 7).
H_2SO_4	100 hPa @ 248 °C	Yes	4 H-bonds with itself. H-bond donor (max. 2) and acceptor (max. 8).
H_2O	100 hPa @ 45.8 °C	Yes	4 H-bonds with itself. H-bond donor (max. 2) and acceptor (max. 2).

1328

1329

Table 2. Characteristic estimates of desorption energies (E_{des}^0) and desorption lifetimes (τ_{des}, at 298 K) for widely used categories of secondary organic aerosol volatility basis sets (SOA-VBS): volatile organic compounds (VOC), intermediate-volatile (IVOC), semi-volatile (SVOC), low-volatile (LVOC), and extremely/ultra-low volatile (ELVOC/ULVOC).

Category	Volatility p^0 (atm)	Desorption Energy E_{des}^0 (kJ mol^{-1})	Desorption Lifetime τ_{des} (298 K)
VOC	$\gtrsim 10^{-3}$	$\lesssim 60$	nanoseconds to milliseconds
IVOC	$\sim 10^{-5}$	~ 80	milliseconds to hours
SVOC	$\sim 10^{-9}$	~ 100	seconds to months
LVOC	$\sim 10^{-12}$	~ 120	minutes to centennia
ELVOC/ULVOC	$\lesssim 10^{-14}$	$\gtrsim 140$	days to millennia
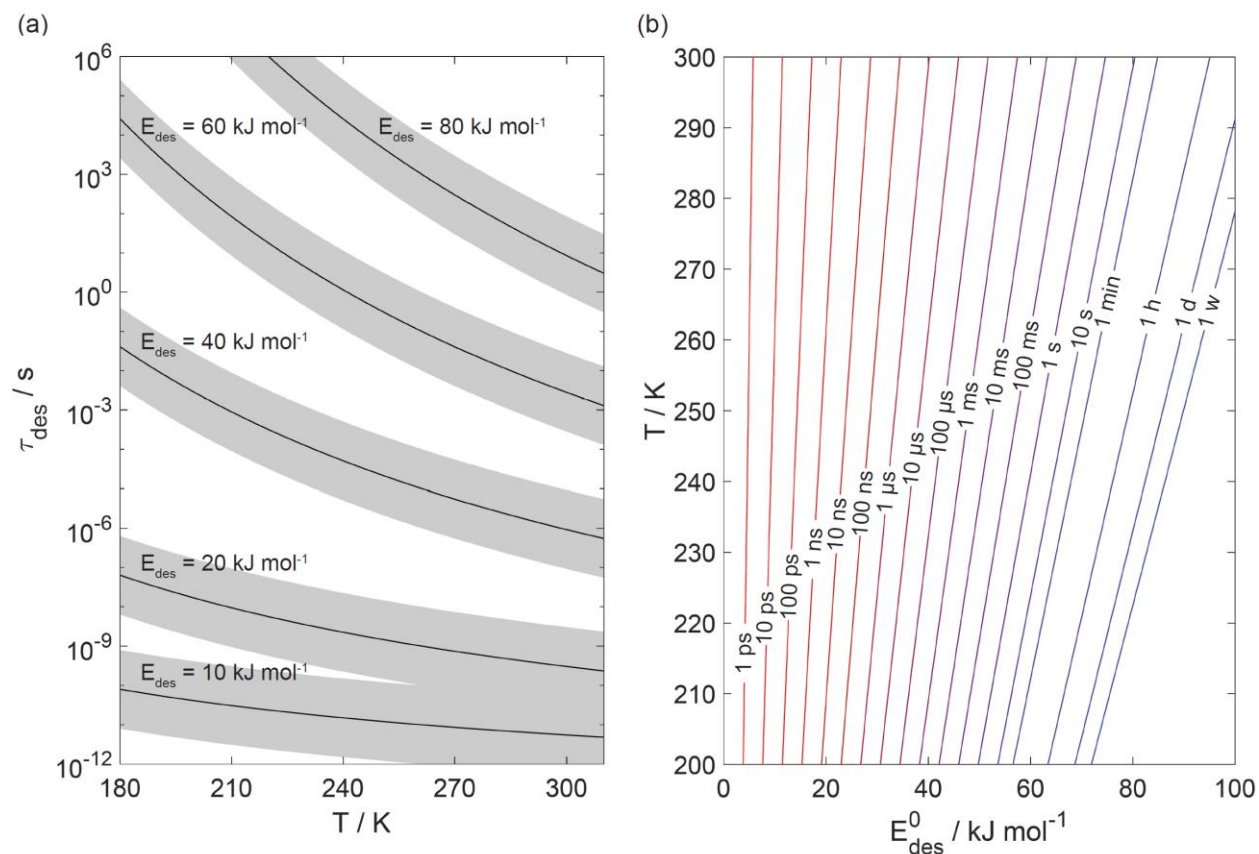
Figure 1. The dependence of the desorption lifetime (τ_{des}) on temperature (T) and desorption energy (E_{des}^0). (a) τ_{des} as a function of T for various E_{des}^0 values. The shaded area covers the range of the pre-exponential factor (A_{des}) varied by ± 1 order of magnitude. (b) Iso-τ_{des} lines for various combination of T and E_{des}^0. All presented data calculated applying Eq. (1) and using $A_{des} = 1 \times 10^{13}$ s^{-1}.

1368
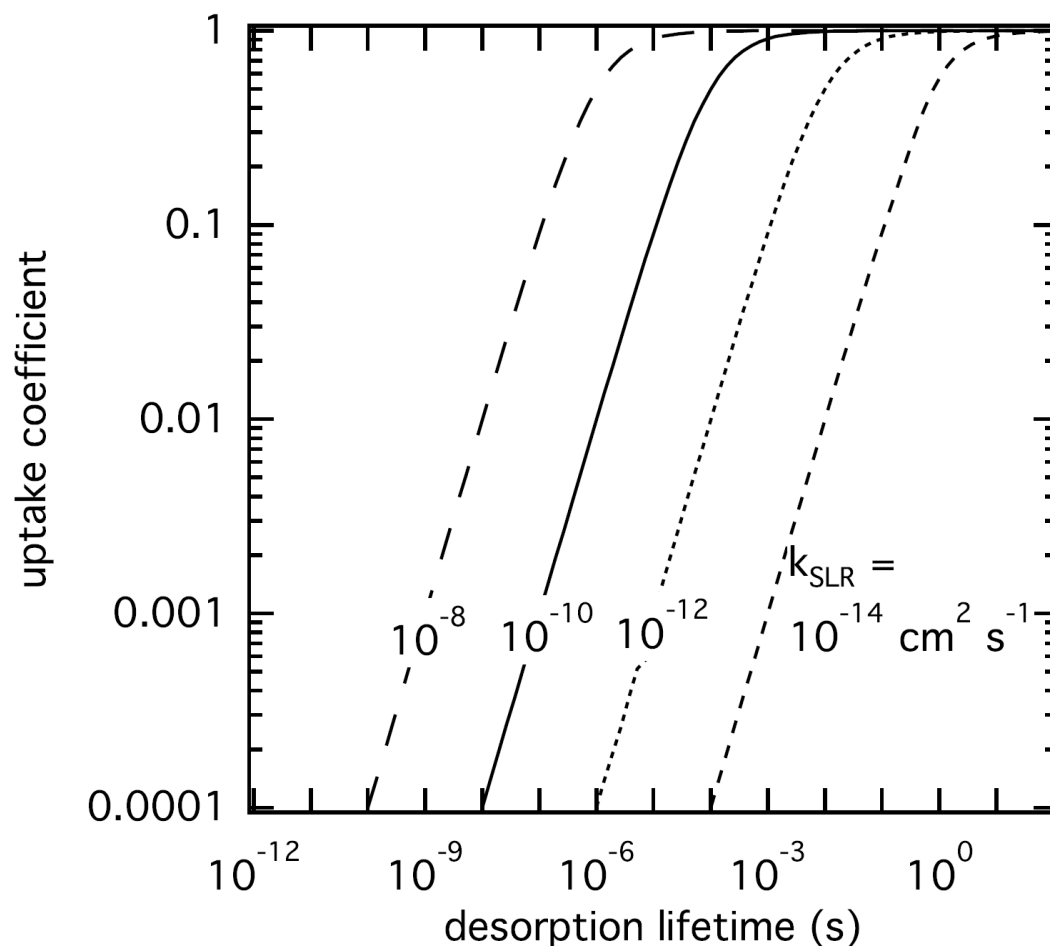
1369

1370 **Figure 2.** The response in reactive uptake coefficient of a reactive gas species X with a condensed-
1371 phase species Y when varying the desorption lifetime and second-order rate coefficients derived
1372 by the numerical diffusion model K2-SURF. The gas phase concentration of X and the surface
1373 concentration of Y remained fixed during the calculations. The surface accommodation coefficient
1374 is assumed to be equal to one.

1375

1376

1377

1378

1379

1380

1381

1382
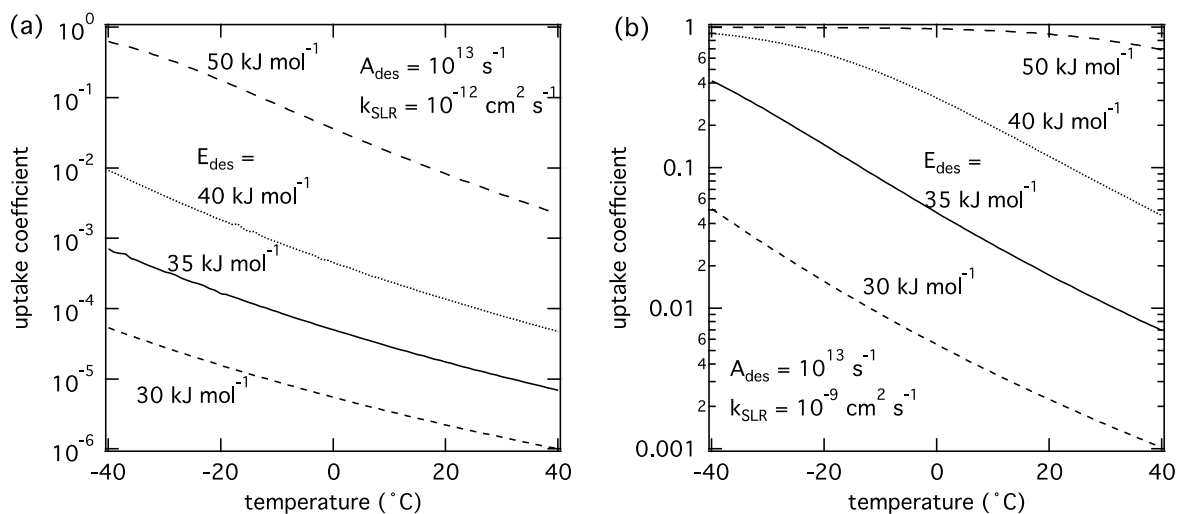
1383

1384   **Figure 3.** The response of the reactive uptake coefficient as temperature and adsorption energy are
1385   varied for two different second-order rate coefficients derived by K2-SURF. The gas phase
1386   concentration of X remained fixed during the calculations. The pre-exponential factor A_{des} is fixed
1387   for both cases. The surface accommodation coefficient is assumed to be one.

1388

1389

1390

1391

1392

1393

1394

1395

1396

1397

1398

1399

1400

1401

1402
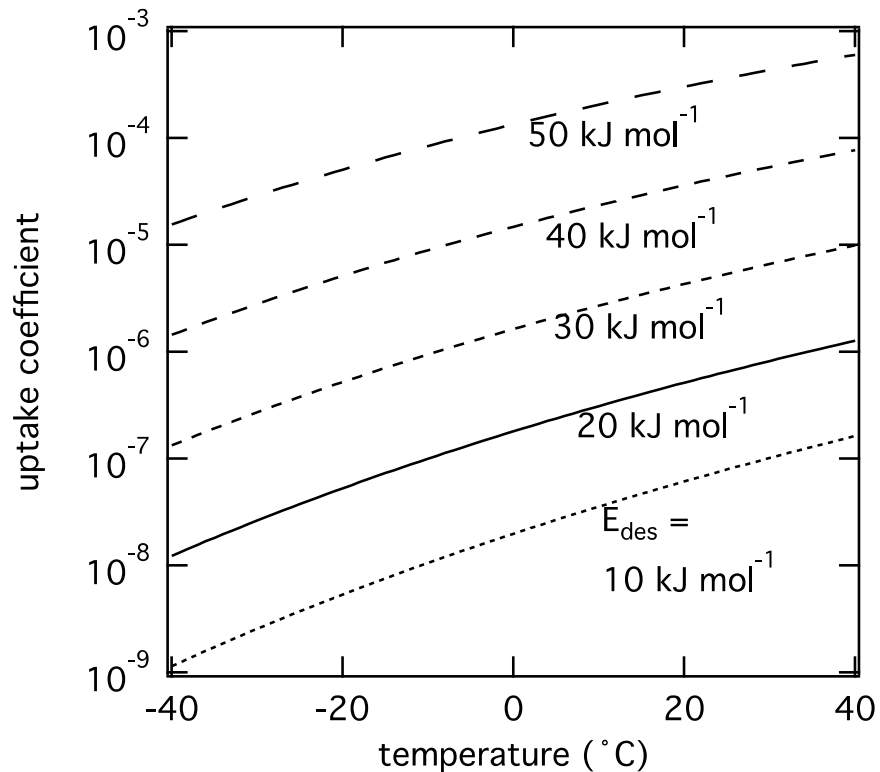
1403

1404 **Figure 4.** The response of the reactive uptake coefficient of O_3 by PAH coated on soot including
1405 formation of reactive oxygen intermediates (ROIs) following Shiraiwa et al. (2011) as temperature
1406 and adsorption energy are varied using the numerical diffusion model K2-SURF. ROI formation
1407 and oxidation reaction rates are adjusted using an Arrhenius-based temperature scaling. The pre-
1408 exponential factor A_{des} is fixed at 10^{13} s^{-1}.

1409

1410

1411

1412

1413

1414

1415

1416

1417

1418
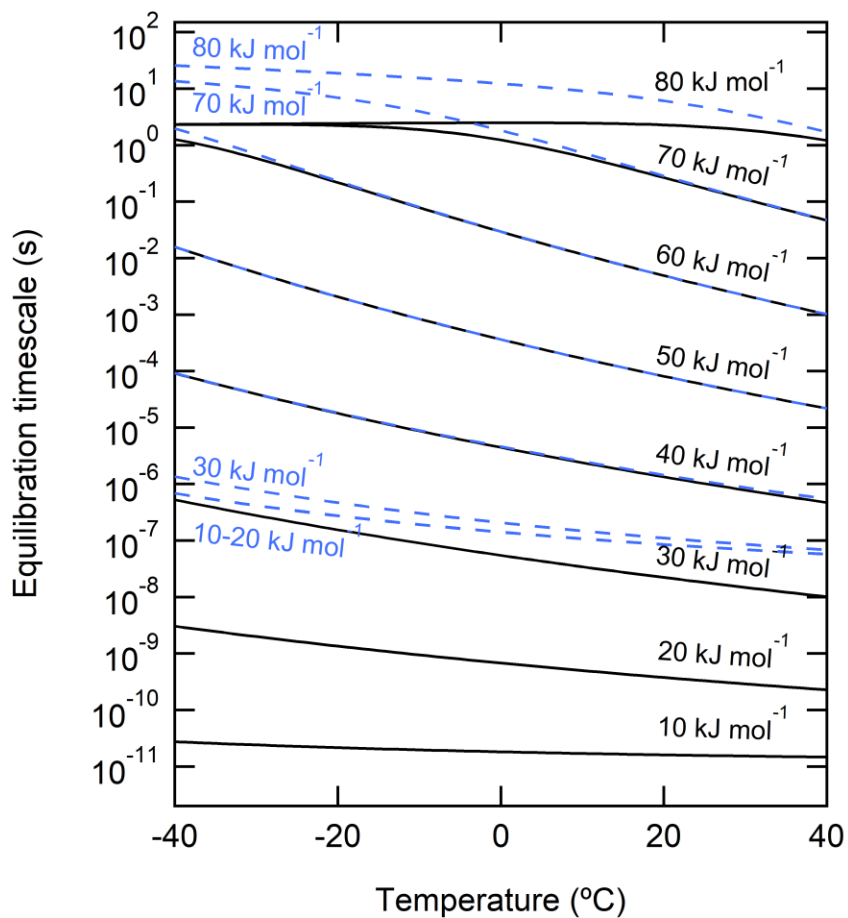
1419

Figure 5. Equilibration timescale of non-reactive uptake of gas molecules onto the surface (solid black lines) and into the particle phase (blue dashed lines) of liquid particles with a diameter of 100 nm for different desorption energies. Gas-phase mixing ratio is fixed to be 1 ppb.

1423

1424

1425

1426

1427

1428

1429
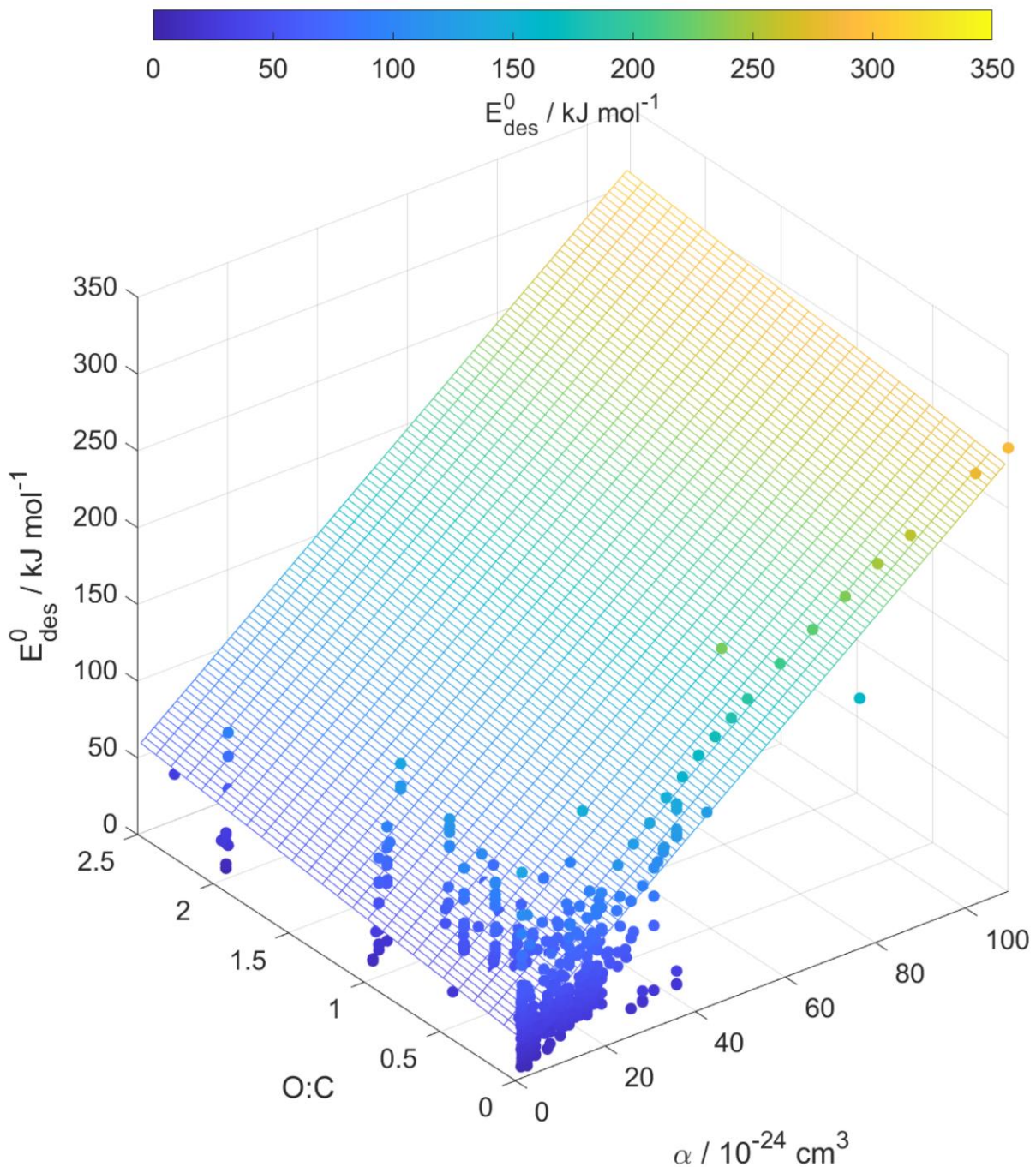
1430

1431

Figure 6. Multilinear regression analysis of E_{des}^0, oxygen to carbon ratio of gas species expressed as $O{:}C$, and gas species polarizability (α) using data from Tables A1-A15. Gridded surface shows regression model and color shading indicates changes in E_{des}^0.

1435

1436
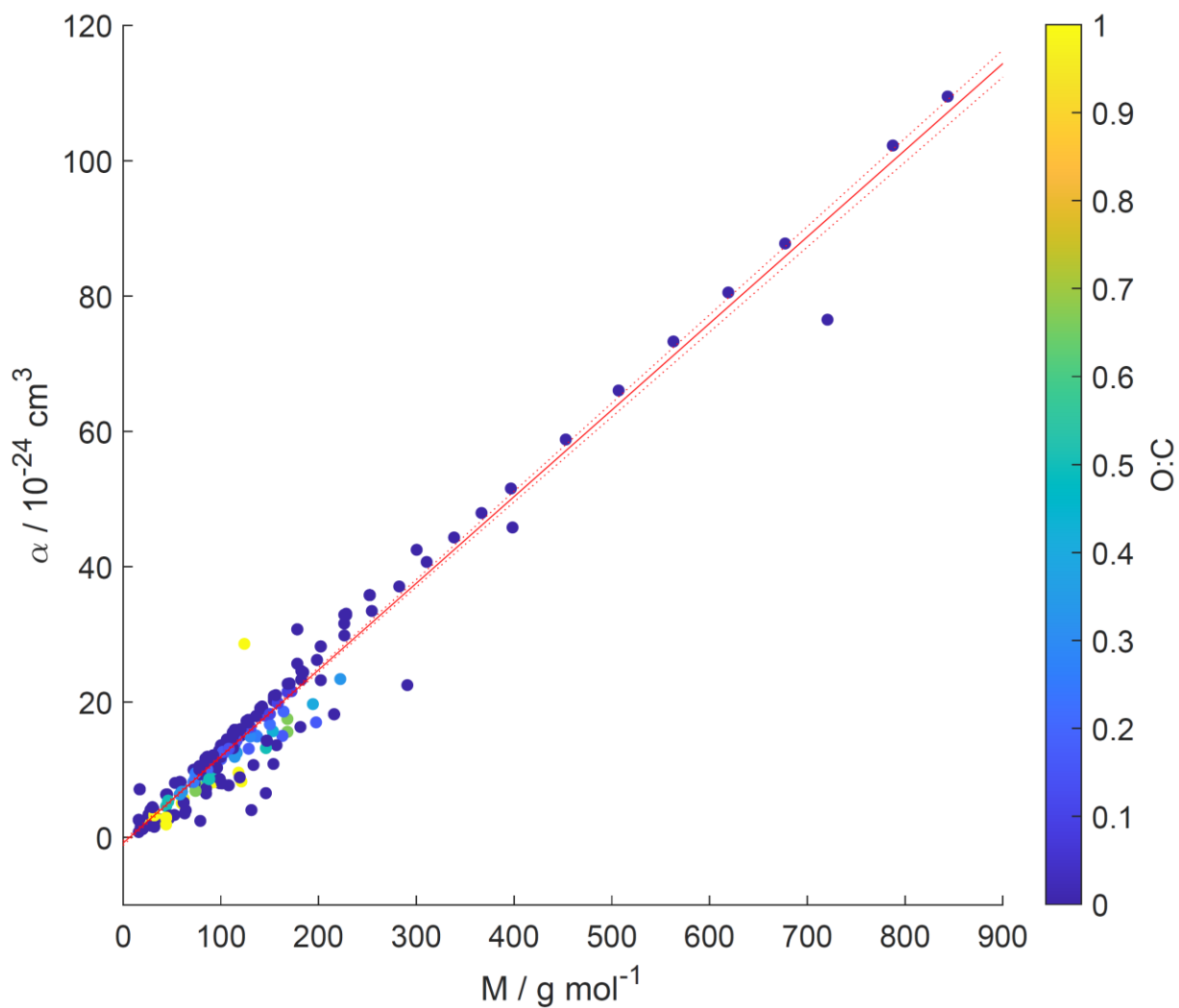
Figure 7. Gas species polarizability (α) as a function of molar mass (M) and its dependence on oxygen to carbon ratio expressed as $O{:}C$. $O{:}C$ is given as color shading. Red solid and dotted lines represent a linear fit to the data and its 95% prediction bands, respectively. Note that three gas species with $O{:}C > 1$ (CO_2, formic acid, and peroxyacetyl nitrate) are included in this plot as having $O{:}C = 1$ to allow for better visualization of entire data set.

1445

1446

1447

1448

1449
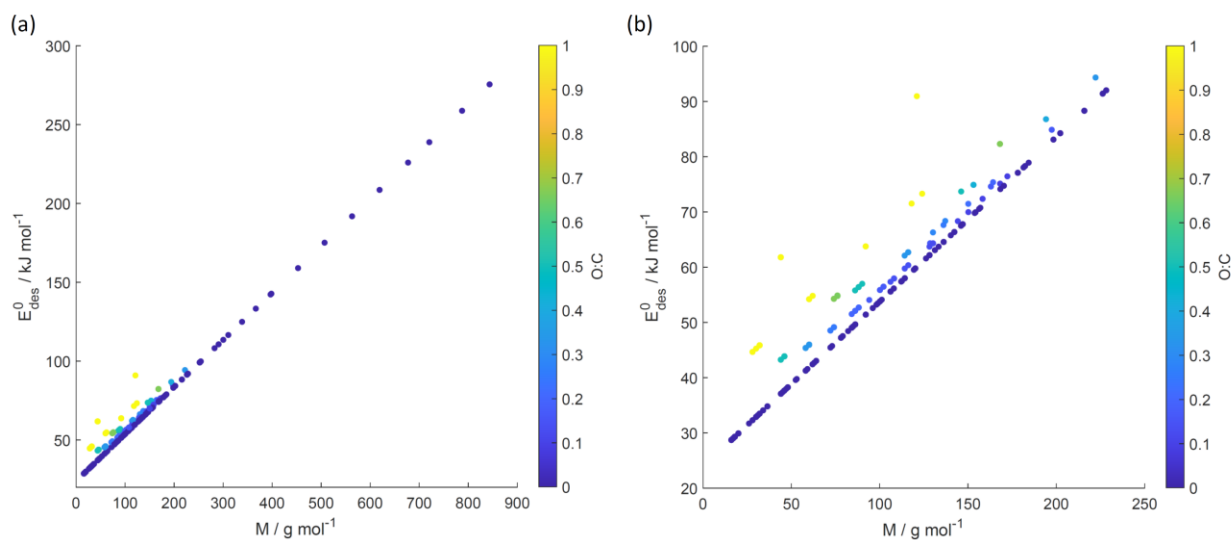
1452 **Figure 8.** E_{des}^0 values derived from the new parameterization (Eq. (16)) applying the training
1453 dataset of gas species with molar mass (M) and $O{:}C$, the latter coded as symbol color described
1454 by the color bar. (b) is an enlarged view of (a). Note that three gas species with $O{:}C > 1$ (CO_2,
1455 formic acid, and peroxyacetyl nitrate) are included in these plots as having $O{:}C = 1$ to allow for
1456 better visualization of entire data set.

1457

1458

1459

1460

1461

1462

1463

1464
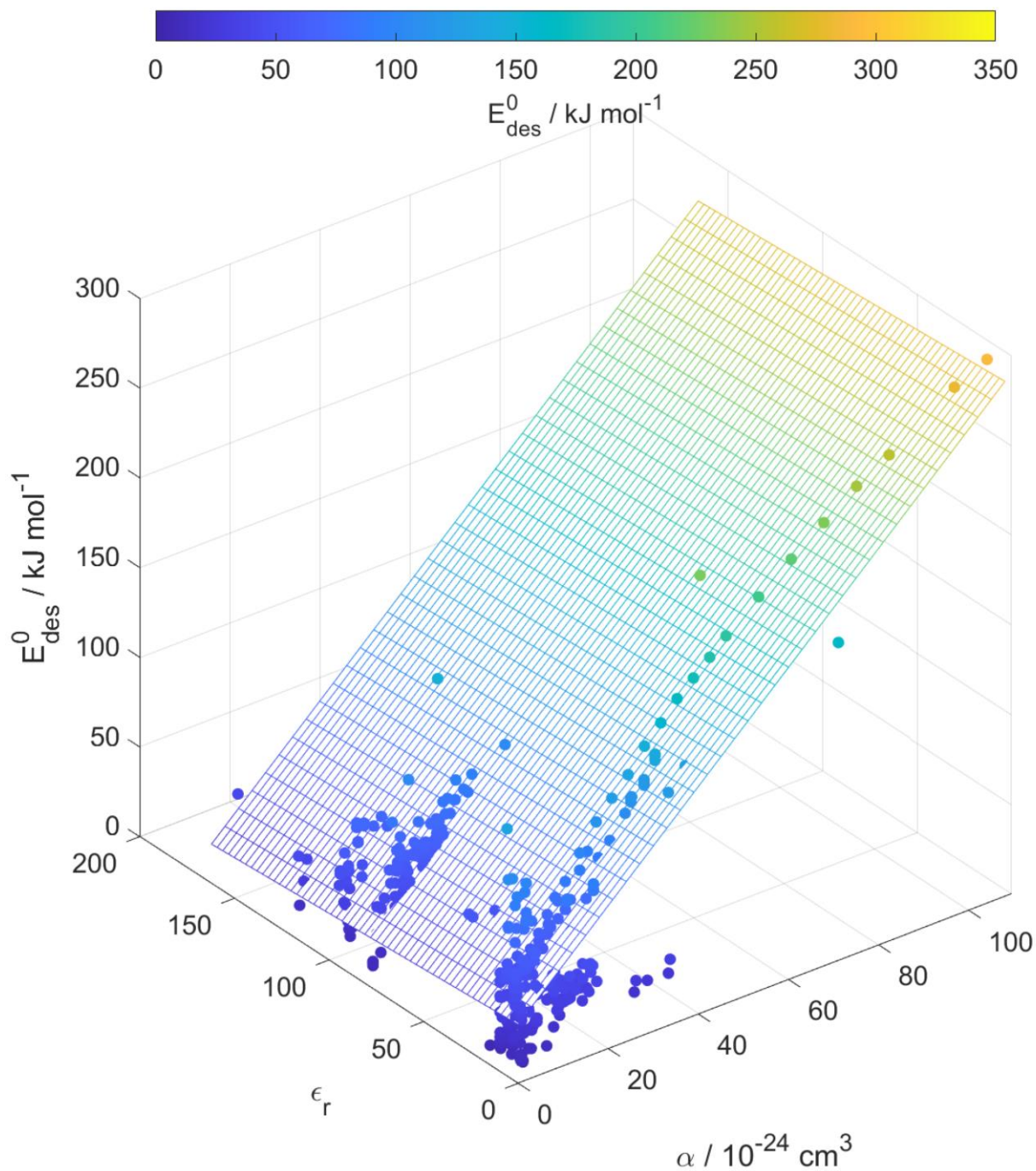
1465

Figure 9. Multilinear regression analysis of E_{des}^0, substrate relative permittivity (ε_r), and gas species polarizability (α) using data from Tables A1-A15. Gridded surface shows regression model and color shading indicates changes in E_{des}^0.

1466
1467
1468

1469

1470
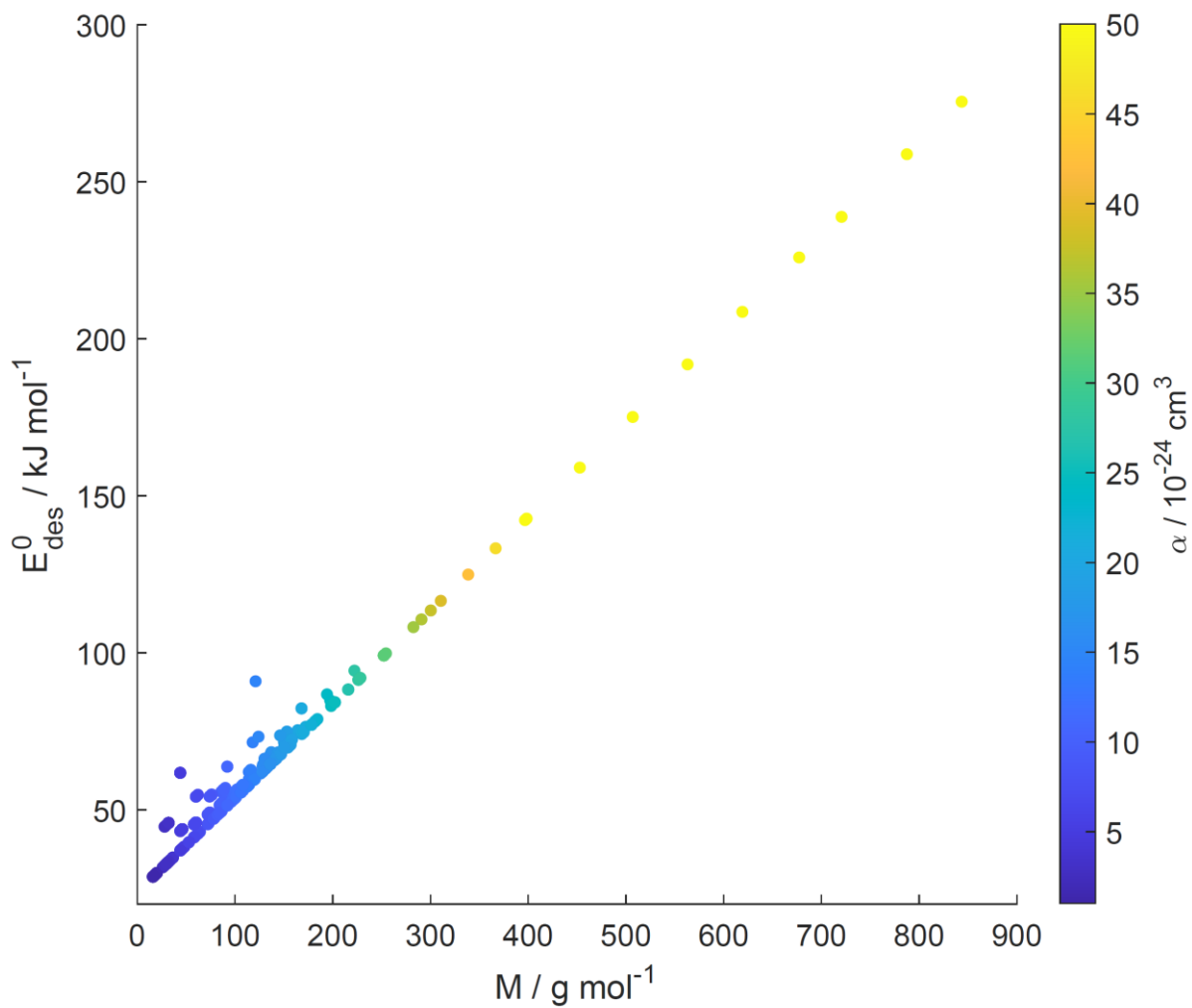
Figure 10. Parameterized E_{des}^0 values as a function of gas species molar mass (M) and polarizability (α) given as color bar following Eq. (16).
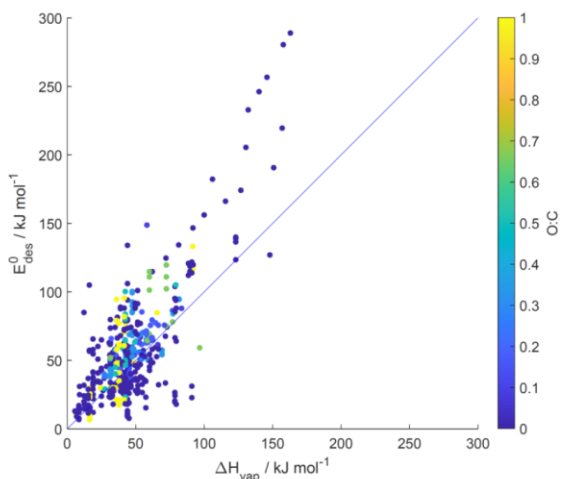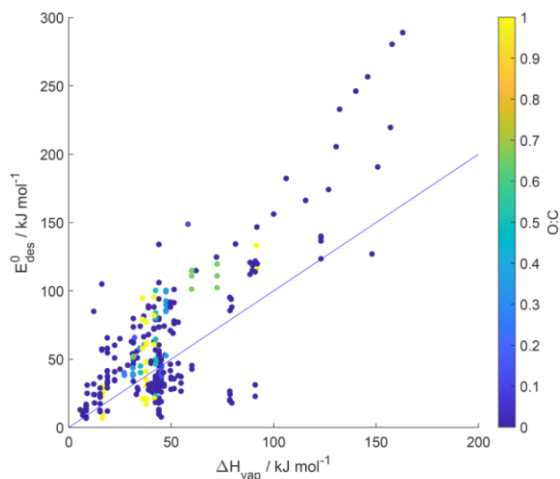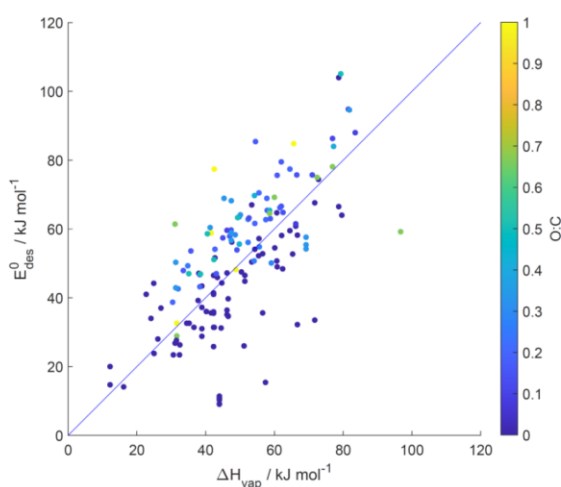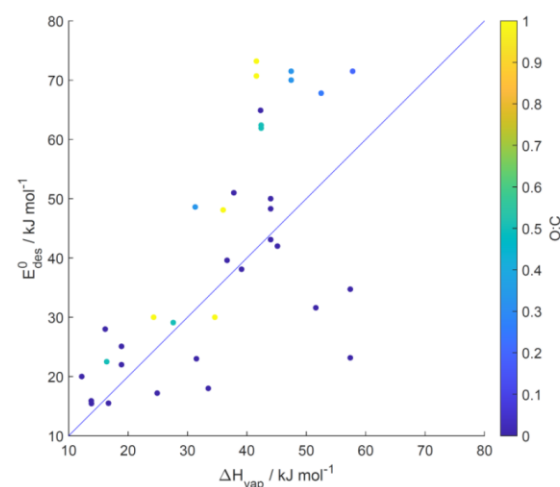
Figure 11. Desorption energy (E_{des}^0) as a function of enthalpy of vaporization (ΔH_{vap}) and its dependence on $O\!:\!C$ for all (a), solid (b), liquid (c), and ice (d) substrates. Blue lines indicate 1:1 lines.

1481

1482

1483

1484

1485

1486

1487

1488

1489

1490

1491

1503
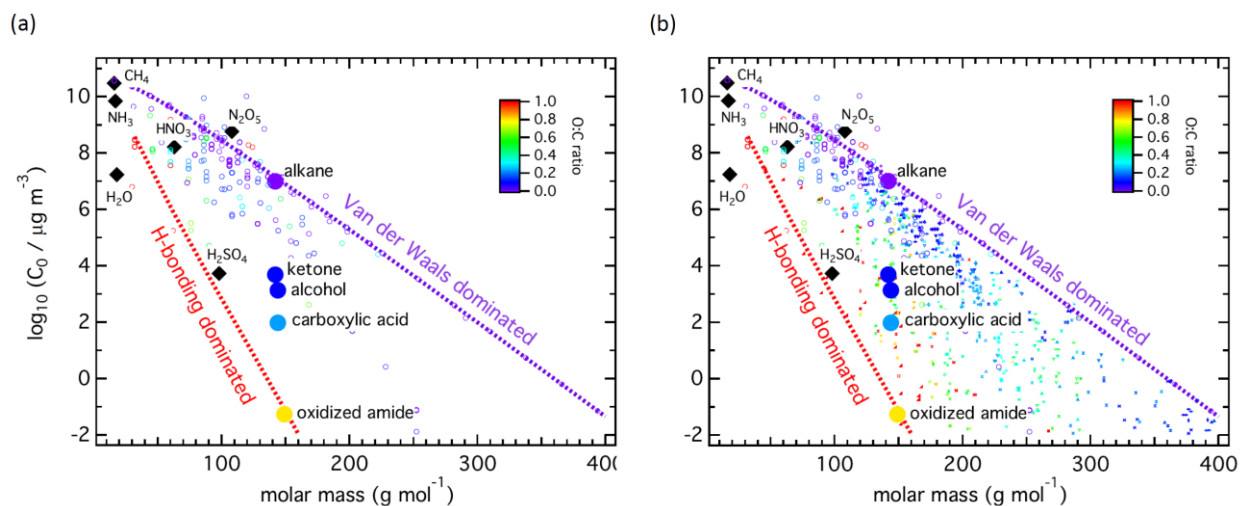
1504

1505 **Figure 13.** Molecular corridors of SOA formation showing saturation mass concentration (C_0) as
1506 a function of molar mass (M). The small markers represent individual gas species color-coded by
1507 $O{:}C$ ratio. (a) displays data from Tables S1-S15. (b) includes SOA precursor gases and oxidation
1508 products data discussed in (Shiraiwa et al., 2014). The dotted lines represent linear alkanes C_nH_{2n+2}
1509 (purple with $O{:}C = 0$) and sugar alcohols $C_nH_{2n+2}O_n$ (red with $O{:}C = 1$). Inorganic species
1510 (diamonds) and organic species with similar molar mass but with different functional groups
1511 (circles) are plotted.

1512

1513

1514

1515

1516

1517

1518

1519

1520

1521

1522

1523

1524

1525

1526
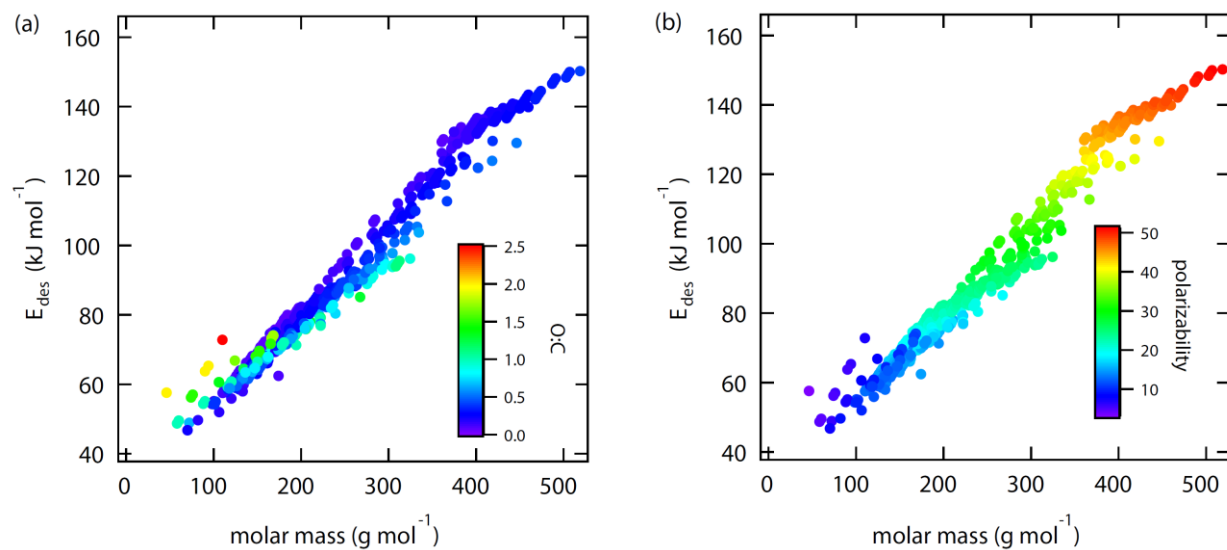
1527

Figure 14. Desorption energies (E_{des}^0) calculated for molecular corridor data of SOA precursor
gases and oxidation products from Fig. 13. (Shiraiwa et al., 2014) as a function of molar mass and
its dependence on $O{:}C$ (a) and polarizability (b). This analysis applies the parameterizations given
in Eqs. (14) and (20).

1532

1533

1534

1535

1536

1537

1538

1539

1540

1541

1542

1543

1544
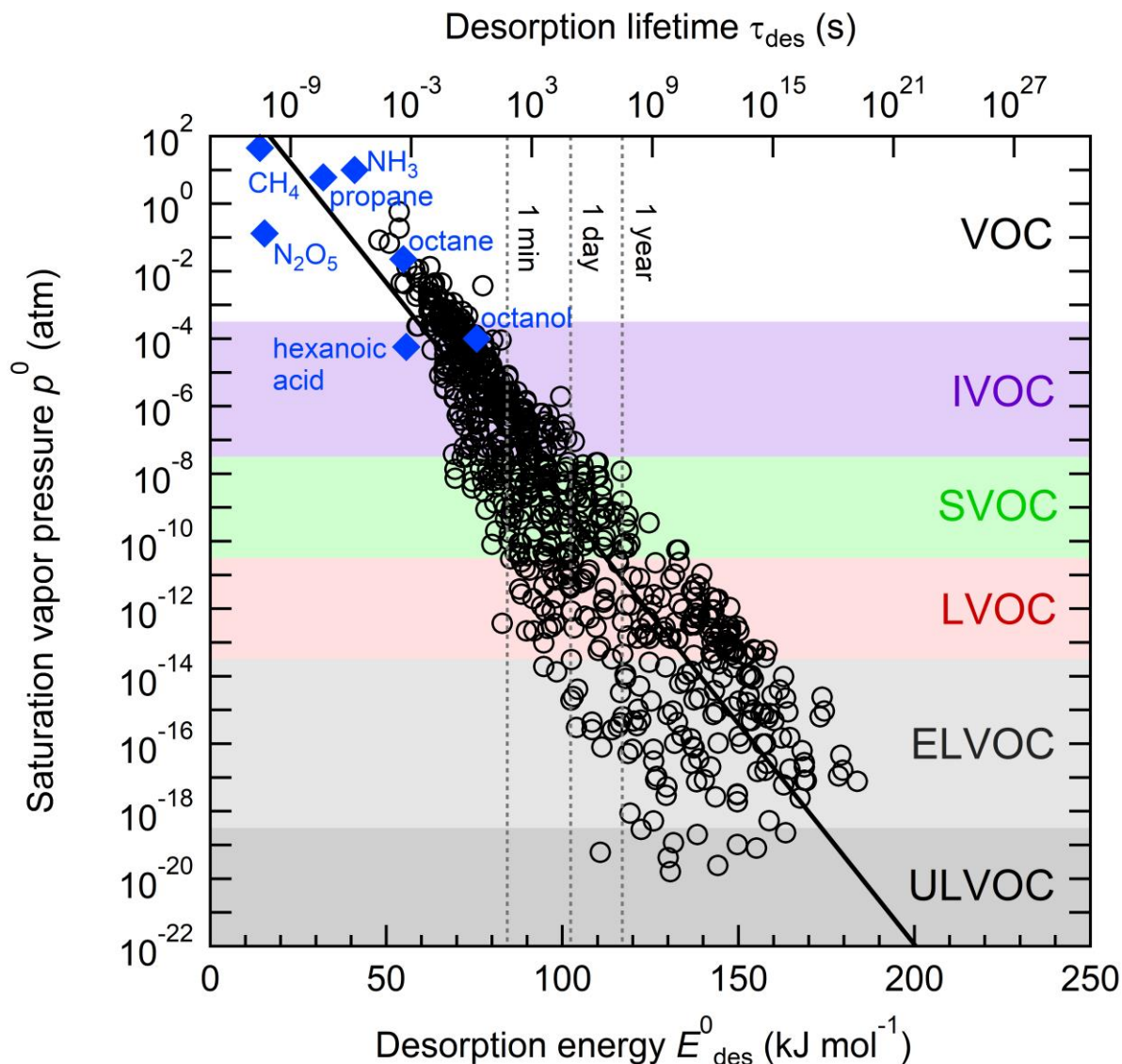
Figure 15. Characteristic desorption energies (E_{des}^0), desorption lifetimes (τ_{des}), and saturation vapor pressures (p^0) at 298 K for secondary organic aerosol (SOA) components and other selected compounds of atmospheric relevance. The blue markers show experimental literature data of E_{des}^0 and p^0. The black markers correspond to the molecular corridor data of SOA formation displayed in Fig. 13 (Shiraiwa et al., 2014), for which p^0 was estimated with the EVAPORATION model (Compernolle et al., 2011) and E_{des}^0 was estimated using Eq. 14. The black solid line represents an exponential fit to the SOA molecular corridor data. Blue markers show experimental data for selected other compounds of atmospheric relevance. Color shadings indicate widely used categories of SOA volatility basis set (VBS): volatile organic compounds (VOC), semi-volatile organic compounds (SVOC), low volatility organic compounds (LVOC), extremely-low volatility organic compounds (ELVOC) and ultra-low volatility organic compounds (ULVOC) (Schervish and Donahue, 2020; Donahue et al., 2009).

References

Abbatt, J. P. D. and Ravishankara, A. R.: Opinion: Atmospheric multiphase chemistry – past, present, and future, Atmos. Chem. Phys., 23, 9765–9785, 10.5194/acp-23-9765-2023, 2023.

Abbatt, J. P. D., Lee, A. K. Y., and Thornton, J. A.: Quantifying trace gas uptake to tropospheric aerosol: recent advances and remaining challenges, Chem. Soc. Rev., 41, 6555-6581, 10.1039/C2cs35052a, 2012.

Abraham, M. H.: Measurement of Enthalpies of Solution of Electrolytes, in: Thermochemistry and Its Applications to Chemical and Biochemical Systems. NATO ASI Series (Series C: Mathematical and Physical Sciences), edited by: Ribeiro da Silva, M. A. V., 119, Springer, Dordrecht, 10.1007/978-94-009-6312-2_20, 1984.

Ahmed, M., Blum, M., Crumlin, E. J., Geissler, P. L., Head-Gordon, T., Limmer, D. T., Mandadapu, K. K., Saykally, R. J., and Wilson, K. R.: Molecular Properties and Chemical Transformations Near Interfaces, J. Phys. Chem. B, 125, 9037-9051, 10.1021/acs.jpcb.1c03756, 2021.

Aihara, A. and Davies, M.: Dielectric relaxation times of some nonrigid polar molecules, J. Coll. Sci. Imp. U. Tok., 11, 671-687, 10.1016/0095-8522(56)90182-9, 1956.

Akkerman, H. B., Naber, R. C. G., Jongbloed, B., van Hal, P. A., Blom, P. W. M., de Leeuw, D. M., and de Boer, B.: Electron tunneling through alkanedithiol self-assembled monolayers in large-area molecular junctions, Proc. Natl. Acad. Sci. U. S. A., 104, 11161-11166, 10.1073/pnas.0701472104, 2007.

Alcala-Jornod, C., van den Bergh, H., and Rossi, M. J.: Reactivity of NO2 and H2O on soot generated in the laboratory: a diffusion tube study at ambient temperature, Phys. Chem. Chem. Phys., 2, 5584-5593, 2000.

Alcala-Jornod, C., van den Bergh, H., and Rossi, M. J.: Can soot particles emitted by airplane exhaust contribute to the formation of aviation contrails and cirrus clouds?, Geophys. Res. Lett., 29, 4, 10.1029/2001gl014115, 2002.

Alkorta, I., Plane, J. M. C., Elguero, J., Davalos, J. Z., Acuna, A. U., and Saiz-Lopez, A.: Theoretical study of the NO3 radical reaction with CH2ClBr, CH2ICl, CH2BrI, CHCl2Br, and CHClBr2, Phys. Chem. Chem. Phys., 24, 14365-14374, 10.1039/d2cp00021k, 2022.

Allouche, A. and Bahr, S.: Acetic acid-water interaction in solid interfaces, Journal of Physical Chemistry B, 110, 8640-8648, 10.1021/jp0559736, 2006.

Ammann, M. and Pöschl, U.: Kinetic model framework for aerosol and cloud surface chemistry and gas-particle interactions - Part 2: Exemplary practical applications and numerical simulations, Atmos. Chem. Phys., 7, 6025-6045, 2007.

Ammann, M., Pöschl, U., and Rudich, Y.: Effects of reversible adsorption and Langmuir-Hinshelwood surface reactions on gas uptake by atmospheric particles, Phys. Chem. Chem. Phys., 5, 351-356, 2003.

Ammann, M., Cox, R. A., Crowley, J. N., Jenkin, M. E., Mellouki, A., Rossi, M. J., Troe, J., and Wallington, T. J.: Evaluated kinetic and photochemical data for atmospheric chemistry: Volume VI - heterogeneous reactions with liquid substrates, Atmos. Chem. Phys., 13, 8045-8228, 10.5194/acp-13-8045-2013, 2013.

Arangio, A. M., Slade, J. H., Berkemeier, T., Pöschl, U., Knopf, D. A., and Shiraiwa, M.: Multiphase Chemical Kinetics of OH Radical Uptake by Molecular Organic Markers of Biomass Burning Aerosols: Humidity and Temperature Dependence, Surface Reaction, and Bulk Diffusion, J. Phys. Chem. A, 119, 4533-4544, 10.1021/jp510489z, 2015.

Aroney, M. J., Saxby, J. D., Lefevre, R. J. W., and Chia, L. H. L.: Molecular polarisability. Dipole moments molar Kerr constants + conformations of 11 phosphate + phosphite triesters as solutes in benzene, J. Chem. Soc., 2948-2954, 10.1039/jr9640002948, 1964.

Arp, H. P. H., Goss, K. U., and Schwarzenbach, R. P.: Evaluation of a predictive model for air/surface adsorption equilibrium constants and enthalpies, Environ. Toxicol. Chem., 25, 45-51, 10.1897/05-291r.1, 2006.

Arrhenius, S. A.: Über die Dissociationswärme und den Einfluß der Temperatur auf den Dissociationsgrad der Elektrolyte, Z. Phys. Chem., 4, 96-116, 1889a.

Arrhenius, S. A.: Über die Reaktionsgeschwindigkeit bei der Inversion von Rohrzucker durch Säuren, Z. Phys. Chem., 4, 226-248, 1889b.

Artiglia, L., Edebeli, J., Orlando, F., Chen, S. Z., Lee, M. T., Arroyo, P. C., Gilgen, A., Bartels-Rausch, T., Kleibert, A., Vazdar, M., Carignano, M. A., Francisco, J. S., Shepson, P. B., Gladich, I., and Ammann, M.: A surface-stabilized ozonide triggers bromide oxidation at the aqueous solution-vapour interface, Nat. Commun., 8, 8, 10.1038/s41467-017-00823-x, 2017.

Asakawa, H., Sazaki, G., Nagashima, K., Nakatsubo, S., and Furukawa, Y.: Two types of quasi-liquid layers on ice crystals are formed kinetically, Proc. Natl. Acad. Sci. U. S. A., 113, 1749-1753, 10.1073/pnas.1521607113, 2016.

Auty, R. P. and Cole, R. H.: Dielectric properties of ice and solid D2O, J. Chem. Phys., 20, 1309-1314, 10.1063/1.1700726, 1952.

Bak, K. L., Gauss, J., Helgaker, T., Jorgensen, P., and Olsen, J.: The accuracy of molecular dipole moments in standard electronic structure calculations, Chemical Physics Letters, 319, 563-568, 10.1016/s0009-2614(00)00198-6, 2000.

Baron, M. and Arevalo, E. S.: Dipole-moment values from single-solution measurements, J. Chem. Educ., 65, 644-645, 10.1021/ed065p644, 1988.

Bartels-Rausch, T.: Ten things we need to know about ice and snow, Nature, 494, 27-29, 10.1038/494027a, 2013.

Bartels-Rausch, T., Huthwelker, T., Gaggeler, H. W., and Ammann, M.: Atmospheric pressure coated-wall flow-tube study of acetone adsorption on ice, J. Phys. Chem. A, 109, 4531-4539, 10.1021/jp0451871, 2005.

Bartels-Rausch, T., Eichler, B., Zimmermann, P., Gaggeler, H. W., and Ammann, M.: The adsorption enthalpy of nitrogen oxides on crystalline ice, Atmos. Chem. Phys., 2, 235-247, 10.5194/acp-2-235-2002, 2002.

Bartels-Rausch, T., Orlando, F., Kong, X. R., Artiglia, L., and Ammann, M.: Experimental Evidence for the Formation of Solvation Shells by Soluble Species at a Nonuniform Air-Ice Interface, ACS Earth Space Chem., 1, 572-579, 10.1021/acsearthspacechem.7b00077, 2017.

Bartels-Rausch, T., Jacobi, H. W., Kahan, T. F., Thomas, J. L., Thomson, E. S., Abbatt, J. P. D., Ammann, M., Blackford, J. R., Bluhm, H., Boxe, C., Domine, F., Frey, M. M., Gladich, I., Guzman, M. I., Heger, D., Huthwelker, T., Klan, P., Kuhs, W. F., Kuo, M. H., Maus, S., Moussa, S. G., McNeill, V. F., Newberg, J. T., Pettersson, J. B. C., Roeselova, M., and Sodeau, J. R.: A review of air-ice chemical and physical interactions (AICI): liquids, quasi-liquids, and solids in snow, Atmos. Chem. Phys., 14, 1587-1633, 10.5194/acp-14-1587-2014, 2014.

Behr, P., Scharfenort, U., Ataya, K., and Zellner, R.: Dynamics and mass accommodation of HCl molecules on sulfuric acid-water surfaces, Phys. Chem. Chem. Phys., 11, 8048-8055, 10.1039/b904629a, 2009.

Behr, P., Morris, J. R., Antman, M. D., Ringeisen, B. R., Splan, J. R., and Nathanson, G. M.: Reaction and desorption of HCl and HBr following collisions with supercooled sulfuric acid, Geophys. Res. Lett., 28, 1961-1964, 10.1029/2000gl012716, 2001.

Beller, M., Renken, A., and van Santen, R. A.: Catalysis: From Principles to Applications, John Wiley & Sons, Inc., Hoboken, New Jersey, USA2012.

Berkemeier, T., Takeuchi, M., Eris, G., and Ng, N. L.: Kinetic modeling of formation and evaporation of secondary organic aerosol from NO3 oxidation of pure and mixed monoterpenes, Atmos. Chem. Phys., 20, 15513-15535, 10.5194/acp-20-15513-2020, 2020.

Berkemeier, T., Huisman, A. J., Ammann, M., Shiraiwa, M., Koop, T., and Pöschl, U.: Kinetic regimes and limiting cases of gas uptake and heterogeneous reactions in atmospheric aerosols and clouds: a general classification scheme, Atmos. Chem. Phys., 13, 6663-6686, 10.5194/acp-13-6663-2013, 2013.

Berkemeier, T., Mishra, A., Mattei, C., Huisman, A. J., Krieger, U. K., and Poschl, U.: Ozonolysis of Oleic Acid Aerosol Revisited: Multiphase Chemical Kinetics and Reaction Mechanisms, ACS Earth Space Chem., 5, 3313-3323, 10.1021/acsearthspacechem.1c00232, 2021.

Berkemeier, T., Steimer, S. S., Krieger, U. K., Peter, T., Pöschl, U., Ammann, M., and Shiraiwa, M.: Ozone uptake on glassy, semi-solid and liquid organic matter and the role of reactive oxygen intermediates in atmospheric aerosol chemistry, Phys. Chem. Chem. Phys., 18, 12662-12674, 10.1039/c6cp00634e, 2016.

Bertram, A. K., Martin, S. T., Hanna, S. J., Smith, M. L., Bodsworth, A., Chen, Q., Kuwata, M., Liu, A., You, Y., and Zorn, S. R.: Predicting the relative humidities of liquid-liquid phase separation, efflorescence, and deliquescence of mixed particles of ammonium sulfate, organic material, and water using the organic-to-sulfate mass ratio of the particle and the oxygen-to-carbon elemental ratio of the organic component, Atmos. Chem. Phys., 11, 10995-11006, 10.5194/acp-11-10995-2011, 2011.

Bishop, A. R., Girolami, G. S., and Nuzzo, R. G.: Structural models and thermal desorption energetics for multilayer assemblies of the n-alkanes on Pt(111), J. Phys. Chem. B, 104, 754-763, 10.1021/jp9926488, 2000.

Blank, M. and Ottewill, R. H.: Adsorption of aromatic vapors on water surfaces, J. Phys. Chem., 68, 2206-2211, 10.1021/j100790a030, 1964.

Bolis, V.: Fundamentals in Adsorption at the Solid-Gas Interface. Concepts and Thermodynamics, in: Calorimetry and Thermal Methods in Catalysis, edited by: Auroux, A., 154, Springer-Verlag Berlin Heidelberg, Berlin, 3-50, 10.1007/978-3-642-11954-5, 2013.

Bond, T. C., Doherty, S. J., Fahey, D. W., Forster, P. M., Berntsen, T., DeAngelo, B. J., Flanner, M. G., Ghan, S., Karcher, B., Koch, D., Kinne, S., Kondo, Y., Quinn, P. K., Sarofim, M. C., Schultz, M. G., Schulz, M., Venkataraman, C., Zhang, H., Zhang, S., Bellouin, N., Guttikunda, S. K., Hopke, P. K., Jacobson, M. Z., Kaiser, J. W., Klimont, Z., Lohmann, U., Schwarz, J. P., Shindell, D., Storelvmo, T., Warren, S. G., and Zender, C. S.: Bounding the role of black carbon in the climate system: A scientific assessment, J. Geophys. Res., 118, 5380-5552, 10.1002/jgrd.50171, 2013.

Borget, F., Chiavassa, T., Allouche, A., and Aycard, J. P.: Experimental and quantum study of adsorption of ozone (O-3) on amorphous water ice film, J. Phys. Chem. B, 105, 449-454, 10.1021/jp001785y, 2001.

Borodin, D., Rahinov, I., Shirhatti, P. R., Huang, M., Kandratsenka, A., Auerbach, D. J., Zhong, T. L., Guo, H., Schwarzer, D., Kitsopoulos, T. N., and Wodtke, A. M.: Following the

microscopic pathway to adsorption through chemisorption and physisorption wells, Science, 369, 1461-1465, 10.1126/science.abc9581, 2020.

Borrmann, S., Solomon, S., Dye, J. E., and Luo, B. P.: The potential of cirrus clouds for heterogeneous chlorine activation, Geophys. Res. Lett., 23, 2133-2136, 1996.

Bosque, R. and Sales, J.: Polarizabilities of solvents from the chemical composition, J. Chem. Inf. Comput. Sci., 42, 1154-1163, 10.1021/ci025528x, 2002.

Brastad, S. M., Albert, D. R., Huang, M. W., and Nathanson, G. M.: Collisions of DCl with a Solution Covered with Hydrophobic and Hydrophilic Ions: Tetrahexylammonium Bromide in Glycerol, J. Phys. Chem. A, 113, 7422-7430, 10.1021/jp900232v, 2009.

Brini, E., Fennell, C. J., Fernandez-Serra, M., Hribar-Lee, B., Luksic, M., and Dill, K. A.: How Water's Properties Are Encoded in Its Molecular Structure and Energies, Chem. Rev., 117, 12385-12414, 10.1021/acs.chemrev.7b00259, 2017.

Broderick, A., Rocha, M. A., Khalifa, Y., Shiflett, M. B., and Newberg, J. T.: Mass Transfer Thermodynamics through a Gas–Liquid Interface, J. Phys. Chem. B, 123, 2576-2584, 10.1021/acs.jpcb.9b00958, 2019.

Brown, D. E., George, S. M., Huang, C., Wong, E. K. L., Rider, K. B., Smith, R. S., and Kay, B. D.: H2O condensation coefficient and refractive index for vapor-deposited ice from molecular beam and optical interference measurements, J. Phys. Chem., 100, 4988-4995, 10.1021/jp952547j, 1996.

Bruant, R. G. and Conklin, M. H.: Adsorption of trichloroethene at the vapor/water interface, Environ. Sci. Technol., 35, 362-364, 10.1021/es000994t, 2001.

Bruant, R. G. and Conklin, M. H.: Adsorption of benzene and methyl-substituted benzenes at the vapor/water interface. 2. Single-component VHOC adsorption, J. Phys. Chem. B, 106, 2224-2231, 10.1021/jp0029156, 2002.

Bruska, M. K. and Piechota, J.: Density functional study of sulphur hexafluoride (SF6) and its hydrogen derivatives, Mol. Simul., 34, 1041-1050, 10.1080/08927020802258708, 2008.

Budi, A., Stipp, S. L. S., and Andersson, M. P.: Calculation of Entropy of Adsorption for Small Molecules on Mineral Surfaces, J. Phys. Chem. C, 122, 8236−8243, 10.1021/acs.jpcc.7b11860, 2018.

Caloz, F., Fenter, F. F., Tabor, K. D., and Rossi, M. J.: Paper I: Design and construction of a Knudsen-cell reactor for the study of heterogeneous reactions over the temperature range 130-750 K: Performances and limitations, Rev. Sci. Instrum., 68, 3172-3179, 1997.

Cambi, R., Cappelletti, D., Liuti, G., and Pirani, F.: Generalized correlations in terms of polarizability for vanderwaals interaction potential parameter calculations, J. Chem. Phys., 95, 1852-1861, 10.1063/1.461035, 1991.

Campbell, C. T., Sprowl, L. H., and Arnadottir, L.: Equilibrium Constants and Rate Constants for Adsorbates: Two-Dimensional (2D) Ideal Gas, 2D Ideal Lattice Gas, and Ideal Hindered Translator Models, J. Phys. Chem. C, 120, 10283-10297, 10.1021/acs.jpcc.6b00975, 2016.

Cao, X., Liu, C. L., Zhang, T. F., Xu, Q., Zhang, D. L., Liu, X. T., Jiao, H. J., Wen, X. D., Yang, Y., Li, Y. W., Niemantsverdriet, J. W., and Zhu, J. F.: Revisiting Oxygen Adsorption on Ir(100), J. Phys. Chem. C, 126, 10035-10044, 10.1021/acs.jpcc.2c01237, 2022.

Cappa, C. D., Onasch, T. B., Massoli, P., Worsnop, D. R., Bates, T. S., Cross, E. S., Davidovits, P., Hakala, J., Hayden, K. L., Jobson, B. T., Kolesar, K. R., Lack, D. A., Lerner, B. M., Li, S. M., Mellon, D., Nuaaman, I., Olfert, J. S., Petaja, T., Quinn, P. K., Song, C., Subramanian, R., Williams, E. J., and Zaveri, R. A.: Radiative Absorption Enhancements Due to the Mixing State of Atmospheric Black Carbon, Science, 337, 1078-1081, 10.1126/science.1223447, 2012.

Carslaw, K. S., Peter, T., and Muller, R.: Uncertainties in reactive uptake coefficients for solid stratospheric particles .2. Effect on ozone depletion, Geophys. Res. Lett., 24, 1747-1750, 10.1029/97gl01684, 1997.

Chan, M. N., Zhang, H., Goldstein, A. H., and Wilson, K. R.: Role of Water and Phase in the Heterogeneous Oxidation of Solid and Aqueous Succinic Acid Aerosol by Hydroxyl Radicals, J. Phys. Chem. C, 118, 28978-28992, 10.1021/jp5012022, 2014.

Chandler, D.: Interfaces and the driving force of hydrophobic assembly, Nature, 437, 640-647, 10.1038/nature04162, 2005.

Charnawskas, J. C., Alpert, P. A., Lambe, A. T., Berkemeier, T., O'Brien, R. E., Massoli, P., Onasch, T. B., Shiraiwa, M., Moffet, R. C., Gilles, M. K., Davidovits, P., Worsnop, D. R., and Knopf, D. A.: Condensed-phase biogenic-anthropogenic interactions with implications for cold cloud formation, Faraday Discuss., 200, 164-195, 10.1039/C7FD00010C, 2017.

Chickos, J. S. and Acree, W. E.: Enthalpies of vaporization of organic and organometallic compounds, 1880-2002, J. Phys. Chem. Ref. Data, 32, 519-878, 10.1063/1.1529214, 2003.

China, S., Mazzoleni, C., Gorkowski, K., Aiken, A. C., and Dubey, M. K.: Morphology and mixing state of individual freshly emitted wildfire carbonaceous particles, Nat. Commun., 4, 2122, 10.1038/ncomms3122, 2013.

Cho, H., Shepson, P. B., Barrie, L. A., Cowin, J. P., and Zaveri, R.: NMR investigation of the quasi-brine layer in ice/brine mixtures, J. Phys. Chem. B, 106, 11226-11232, 10.1021/jp020449+, 2002.

Chorkendorff, I. and Niemantsverdriet, J. W.: Concepts of Modern Catalysis and Kinetics, 2nd, Wiley-VCH Verlag GmbH & Co. KGaA, Weinheim, 477 pp.2007.

Chu, S. N., Sands, S., Tomasik, M. R., Lee, P. S., and McNeill, V. F.: Ozone Oxidation of Surface-Adsorbed Polycyclic Aromatic Hydrocarbons: Role of PAH-Surface Interaction, J. Am. Chem. Soc., 132, 15968-15975, 10.1021/ja1014772, 2010.

Collignon, B., Hoang, P. N. M., Picaud, S., and Rayez, J. C.: Ab initio study of the water adsorption on hydroxylated graphite surfaces, Chemical Physics Letters, 406, 430-435, 10.1016/j.cplett.2005.03.026, 2005.

Compernolle, S. and Muller, J. F.: Henry's law constants of polyols, Atmos. Chem. Phys., 14, 12815-12837, 10.5194/acp-14-12815-2014, 2014.

Compernolle, S., Ceulemans, K., and Muller, J. F.: EVAPORATION: a new vapour pressure estimation methodfor organic molecules including non-additivity and intramolecular interactions, Atmos. Chem. Phys., 11, 9431-9450, 10.5194/acp-11-9431-2011, 2011.

Crabtree, A. and Siman-Tov, M.: Thermophysical properties of saturated light and heavy water for advanced neutron source applications, Oak Ridge National LaboratoryORNL/TM-12322, 1993.

Crossley, J.: Dielectric relaxation of 1-butanol and 1-decanol in several solvents, J. Phys. Chem., 75, 1790-&, 10.1021/j100681a005, 1971.

Crossley, J.: Dielectric-relaxation of 1-alkenes, J. Chem. Phys., 58, 5315-5318, 10.1063/1.1679145, 1973.

Croteau, T., Bertram, A. K., and Patey, G. N.: Simulation of Water Adsorption on Kaolinite under Atmospheric Conditions, J. Phys. Chem. A, 113, 7826-7833, 10.1021/jp902453f, 2009.

Crowley, J. N., Ammann, M., Cox, R. A., Hynes, R. G., Jenkin, M. E., Mellouki, A., Rossi, M. J., Troc, J., and Wallington, T. J.: Evaluated kinetic and photochemical data for atmospheric chemistry: Volume V - heterogeneous reactions on solid substrates (vol 10, pg 9059, 2010), Atmos. Chem. Phys., 13, 7359-7359, 10.5194/acp-13-7359-2013, 2013.

Crowley, J. N., Ammann, M., Cox, R. A., Hynes, R. G., Jenkin, M. E., Mellouki, A., Rossi, M. J., Troe, J., and Wallington, T. J.: Evaluated kinetic and photochemical data for atmospheric chemistry: Volume V - heterogeneous reactions on solid substrates, Atmos. Chem. Phys., 10, 9059-9223, 10.5194/acp-10-9059-2010, 2010.

Cruzeiro, V. W. D., Galib, M., Limmer, D. T., and Gotz, A. W.: Uptake of N2O5 by aqueous aerosol unveiled using chemically accurate many-body potentials, Nat. Commun., 13, 7, 10.1038/s41467-022-28697-8, 2022.

Cussler, E. L.: Diffusion - Mass Transfer in Fluid Systems, 2009.

Cwiertny, D. M., Young, M. A., and Grassian, V. H.: Chemistry and photochemistry of mineral dust aerosol, Annu. Rev. Phys. Chem., 59, 27-51, 10.1146/annurev.physchem.59.032607.093630, 2008.

Daniels, D. J., Daniels, D. J. (Ed.): Ground Penetrating Radar, 2nd, The Insitution of Engineering and Technology, London, United Kingdom, 726 pp.2004.

Davidovits, P., Kolb, C. E., Williams, L. R., Jayne, J. T., and Worsnop, D. R.: Mass accommodation and chemical reactions at gas-liquid interfaces, Chem. Rev., 106, 1323-1354, 10.1021/cr040366k, 2006.

Davidovits, P., Kolb, C. E., Williams, L. R., Jayne, J. T., and Worsnop, D. R.: Update 1 of: Mass Accommodation and Chemical Reactions at Gas-Liquid Interfaces, Chem. Rev., 111, PR76-PR109, 10.1021/cr100360b, 2011.

Davies, J. F. and Wilson, K. R.: Nanoscale interfacial gradients formed by the reactive uptake of OH radicals onto viscous aerosol surfaces, Chem. Sci., 6, 7020-7027, 10.1039/c5sc02326b, 2015.

Delval, C. and Rossi, M. J.: Influence of monolayer amounts of HNO3 on the evaporation rate of H2O over ice in the range 179 to 208 K: A quartz crystal microbalance study, J. Phys. Chem. A, 109, 7151-7165, 10.1021/jp0505072, 2005.

Delval, C., Fluckiger, B., and Rossi, M. J.: The rate of water vapor evaporation from ice substrates in the presence of HCl and HBr: implications for the lifetime of atmospheric ice particles, Atmos. Chem. Phys., 3, 1131-1145, 10.5194/acp-3-1131-2003, 2003.

Demou, E. and Donaldson, D. J.: Adsorption of atmospheric gases at the air-water interface. 4: The influence of salts, J. Phys. Chem. A, 106, 982-987, 10.1021/jp0128628, 2002.

Desjonqueres, M.-C. and Spanjaard, D.: Concepts in Surface Physics, Springer-Verlag Berlin Heidelberg, 10.1007/978-3-642-61400-2, 1996.

Devlin, J. P., Joyce, C., and Buch, V.: Infrared spectra and structures of large water clusters, J. Phys. Chem. A, 104, 1974-1977, 2000.

Dickbreder, T., Lautner, D., Kohler, A., Klausfering, L., Bechstein, R., and Kuhnle, A.: How water desorbs from calcite, Phys. Chem. Chem. Phys., 25, 12694, 10.1039/d3cp01159c, 2023.

Donahue, N. M., Robinson, A. L., and Pandis, S. N.: Atmospheric organic particulate matter: From smoke to secondary organic aerosol, Atmos. Environ., 43, 94-106, 10.1016/j.atmosenv.2008.09.055, 2009.

Donahue, N. M., Epstein, S. A., Pandis, S. N., and Robinson, A. L.: A two-dimensional volatility basis set: 1. organic-aerosol mixing thermodynamics, Atmos. Chem. Phys., 11, 3303-3318, 10.5194/acp-11-3303-2011, 2011.

Donahue, N. M., Kroll, J. H., Pandis, S. N., and Robinson, A. L.: A two-dimensional volatility basis set - Part 2: Diagnostics of organic-aerosol evolution, Atmos. Chem. Phys., 12, 615-634, 10.5194/acp-12-615-2012, 2012.

1830 Donaldson, D. J.: Adsorption of atmospheric gases at the air-water interface. I. NH3, J. Phys.
1831 Chem. A, 103, 62-70, 1999.
1832 Donaldson, D. J. and Anderson, D.: Adsorption of atmospheric gases at the air-water interface. 2.
1833 C-1-C-4 alcohols, acids, and acetone, J. Phys. Chem. A, 103, 871-876, 1999.
1834 Donaldson, D. J., Guest, J. A., and Goh, M. C.: Evidence For Adsorbed So2 At the Aqueous Air
1835 Interface, J. Phys. Chem., 99, 9313-9315, 1995.
1836 Donaldson, D. J., Ammann, M., Bartels-Rausch, T., and Pöschl, U.: Standard States and
1837 Thermochemical Kinetics in Heterogeneous Atmospheric Chemistry, J. Phys. Chem. A, 116,
1838 6312-6316, 10.1021/jp212015g, 2012a.
1839 Donaldson, D. J., Ammann, M., Bartels-Rausch, T., and Pöschl, U.: Standard States and
1840 Thermochemical Kinetics in Heterogeneous Atmospheric Chemistry, J. Phys. Chem. A, 116,
1841 6312-6316, 10.1021/jp212015g, 2012b.
1842 Dovbeshko, G. I., Romanyuk, V. R., Pidgirnyi, D. V., Cherepanov, V. V., Andreev, E. O., Levin,
1843 V. M., Kuzhir, P. P., Kaplas, T., and Svirko, Y. P.: Optical Properties of Pyrolytic Carbon Films
1844 Versus Graphite and Graphene, Nanoscale Res. Lett., 10, 234, 10.1186/s11671-015-0946-8,
1845 2015.
1846 Dubois, L. H., Zegarski, B. R., and Nuzzo, R. G.: Fundamental-studies of microscopic wetting
1847 on organic-surfaces .2. interaction of secondary adsorbates with chemically textured organic
1848 monolayers, J. Am. Chem. Soc., 112, 570-579, 10.1021/ja00158a013, 1990.
1849 Edebeli, J., Ammann, M., and Bartels-Rausch, T.: Microphysics of the aqueous bulk counters the
1850 water activity driven rate acceleration of bromide oxidation by ozone from 289-245 K, Environ.
1851 Sci.-Process Impacts, 21, 63-73, 10.1039/c8em00417j, 2019.
1852 Edwards, K. C., Klodt, A. L., Galeazzo, T., Schervish, M., Wei, J. L., Fang, T., Donahue, N. M.,
1853 Aumont, B., Nizkorodov, S. A., and Shiraiwa, M.: Effects of Nitrogen Oxides on the Production
1854 of Reactive Oxygen Species and Environmentally Persistent Free Radicals from alpha-Pinene
1855 and Naphthalene Secondary Organic Aerosols, J. Phys. Chem. A, 126, 7361-7372,
1856 10.1021/acs.jpca.2c05532, 2022.
1857 Ekholm, V., Caleman, C., Prytz, N. B., Walz, M. M., Werner, J., Ohrwall, G., Rubensson, J. E.,
1858 and Bjorneholm, O.: Strong enrichment of atmospherically relevant organic ions at the aqueous
1859 interface: the role of ion pairing and cooperative effects, Phys. Chem. Chem. Phys., 20, 27185-
1860 27191, 10.1039/c8cp04525a, 2018.
1861 Epstein, S. A., Riipinen, I., and Donahue, N. M.: A Semiempirical Correlation between Enthalpy
1862 of Vaporization and Saturation Concentration for Organic Aerosol, Environ. Sci. Technol., 44,
1863 743-748, 10.1021/es902497z, 2010.
1864 Fan, H. Y., Lakey, P. S. J., Frank, E. S., Tobias, D. J., Shiraiwa, M., and Grassian, V. H.:
1865 Comparison of the Adsorption-Desorption Kinetics of Limonene and Carvone on TiO2 and SiO2
1866 Surfaces under Different Relative Humidity Conditions, J. Phys. Chem. C, 126, 21253-21262,
1867 10.1021/acs.jpcc.2c06853, 2022.
1868 Fang, Y., Riahi, S., McDonald, A. T., Shrestha, M., Tobias, D. J., and Grassian, V. H.: What Is
1869 the Driving Force behind the Adsorption of Hydrophobic Molecules on Hydrophilic Surfaces?, J.
1870 Phys. Chem. Lett., 10, 468-473, 10.1021/acs.jpclett.8b03484, 2019.
1871 Faust, J. A. and Nathanson, G. M.: Microjets and coated wheels: versatile tools for exploring
1872 collisions and reactions at gas-liquid interfaces, Chem. Soc. Rev., 45, 3609-3620,
1873 10.1039/c6cs00079g, 2016.
1874 Faust, J. A., Dempsey, L. P., and Nathanson, G. M.: Surfactant-Promoted Reactions of Cl-2 and
1875 Br-2 with Br- in Glycerol, J. Phys. Chem. B, 117, 12602-12612, 10.1021/jp4079037, 2013.

Faust, J. A., Sobyra, T. B., and Nathanson, G. M.: Gas-Microjet Reactive Scattering: Collisions of HCl and DCl with Cool Salty Water, J. Phys. Chem. Lett., 7, 730-735, 10.1021/acs.jpclett.5b02848, 2016.

Fichthorn, K. A. and Miron, R. A.: Thermal desorption of large molecules from solid surfaces, Phys. Rev. Lett., 89, 4, 10.1103/PhysRevLett.89.196103, 2002.

Finlayson-Pitts, B. J. and Pitts, J. N.: Chemistry of the Upper and Lower Atmosphere: Theory, Experiments and Applications, Academic Press, San Diego, Calif. ; London, xxii, 969 pp.2000.

Fogg, P. G. T. and Sangster, J. M.: Chemicals in the Atmosphere: Solubility, Sources and Reactivity, John Wiley & Sons Inc., Hoboken, New Jersey2003.

Foster, M. C. and Ewing, G. E.: Adsorption of water on the NaCl(001) surface. II. An infrared study at ambient temperatures, J. Chem. Phys., 112, 6817-6826, 10.1063/1.481256, 2000.

Frenkel, J.: Theory of the adsorption and related occurrences, Z. Phys., 26, 117-138, 10.1007/bf01327320, 1924.

Fuchs, N. A.: Mechanics of Aerosols, Pergamon, New York1964.

Fuchs, N. A. and Sutugin, A. G.: High-dispersed aerosols, in: Topics in current aerosol research, edited by: Hidy, G. M., and Brock, J. R., Pergamon, New York, 1971.

Galeazzo, T. and Shiraiwa, M.: Predicting glass transition temperature and melting point of organic compounds <i>via</i> machine learning and molecular embeddings, Environ. Sci. - Atmospheres, 2, 362-374, 10.1039/d1ea00090j, 2022.

Galib, M. and Limmer, D. T.: Reactive uptake of N2O5 by atmospheric aerosol is dominated by interfacial processes, Science, 371, 921-+, 10.1126/science.abd7716, 2021.

Gao, X. F. and Nathanson, G. M.: Exploring Gas-Liquid Reactions with Microjets: Lessons We Are Learning, Accounts Chem. Res., 55, 3294-3302, 10.1021/acs.accounts.2c00602, 2022.

George, C., Ammann, M., D'Anna, B., Donaldson, D. J., and Nizkorodov, S. A.: Heterogeneous Photochemistry in the Atmosphere, Chem. Rev., 115, 4218-4258, 10.1021/cr500648z, 2015.

George, I. J. and Abbatt, J. P. D.: Heterogeneous oxidation of atmospheric aerosol particles by gas-phase radicals, Nat. Chem., 2, 713-722, 10.1038/Nchem.806, 2010.

Giguere, P. A.: Molecular association and structure of hydrogen-peroxide, J. Chem. Educ., 60, 399-401, 10.1021/ed060p399, 1983.

Giraudet, S., Pre, P., Tezel, H., and Le Cloirec, P.: Estimation of adsorption energies using physical characteristics of activated carbons and VOCs' molecular properties, Carbon, 44, 1873-1883, 10.1016/j.carbon.2006.02.018, 2006.

Goldstein, D. J.: Air and steam stripping of toxic pollutants, Industrial Environmental Research Laboratory, Cincinnati, OH, USAEPA-68-03-002, 1982.

Goodman, A. L., Bernard, E. T., and Grassian, V. H.: Spectroscopic study of nitric acid and water adsorption on oxide particles: Enhanced nitric acid uptake kinetics in the presence of adsorbed water, J. Phys. Chem. A, 105, 6443-6457, 2001.

Goss, K. U.: Adsorption of organic vapors on ice and quartz sand at temperatures below 0 C, Environ. Sci. Technol., 27, 2826-2830, 10.1021/es00049a024, 1993.

Goss, K. U.: Adsorption of organic vapors on polar mineral surfaces and on a bulk water-surface - development of an empirical predictive model, Environ. Sci. Technol., 28, 640-645, 10.1021/es00053a017, 1994a.

Goss, K. U.: Predicting the enrichment of organic-compounds in fog caused by adsorption on the water-surface, Atmos. Environ., 28, 3513-3517, 10.1016/1352-2310(94)90008-6, 1994b.

Goss, K. U.: Predicting Adsorption of Organic Chemicals at the Air-Water Interface, J. Phys. Chem. A, 113, 12256-12259, 10.1021/jp907347p, 2009.

Goss, K. U. and Eisenreich, S. J.: Effects of temperature and relative-humidity on the adsorption of organic vapors on hematite, corundum and lime, Abstr. Pap. Am. Chem. Soc., 209, 84-ENVR, 1995a.

Goss, K. U. and Eisenreich, S. J.: Adsorption of organic-compounds from water to mineral surfaces - a theoretical approach, Abstr. Pap. Am. Chem. Soc., 209, 157-ENVR, 1995b.

Goss, K. U. and Eisenreich, S. J.: Adsorption of VOCs from the gas phase to different minerals and a mineral mixture, Environ. Sci. Technol., 30, 2135-2142, 10.1021/es950508f, 1996.

Grabow, J. U., Andrews, A. M., Fraser, G. T., Irikura, K. K., Suenram, R. D., Lovas, F. J., Lafferty, W. J., and Domenech, J. L.: Microwave spectrum, large-amplitude motions, and ab initio calculations for N2O5, J. Chem. Phys., 105, 7249-7262, 10.1063/1.472586, 1996.

Grayson, J. W., Evoy, E., Song, M., Chu, Y. X., Maclean, A., Nguyen, A., Upshur, M. A., Ebrahimi, M., Chan, C. K., Geiger, F. M., Thomson, R. J., and Bertram, A. K.: The effect of hydroxyl functional groups and molar mass on the viscosity of non-crystalline organic and organic-water particles, Atmos. Chem. Phys., 17, 8509-8524, 10.5194/acp-17-8509-2017, 2017.

Grimm, R. L., Barrentine, N. M., Knox, C. J. H., and Hemminger, J. C.: D2O water interaction with mixed alkane thiol monolayers of tuned hydrophobic and hydrophilic character, J. Phys. Chem. C, 112, 890-894, 10.1021/jp710257q, 2008.

Groves, L. G. and Sudden, S.: The dipole moments of vapours - Part V Aromatic compounds, Journal of the Chemical Society, 1782-1784, 10.1039/jr9370001782, 1937.

Guilloteau, A., Bedjanian, Y., Nguyen, M. L., and Tomas, A.: Desorption of Polycyclic Aromatic Hydrocarbons from a Soot Surface: Three- to Five-Ring PAHs, J. Phys. Chem. A, 114, 942-948, 10.1021/jp908862c, 2010.

Guilloteau, A., Nguyen, M. L., Bedjanian, Y., and Le Bras, G.: Desorption of Polycyclic Aromatic Hydrocarbons from Soot Surface: Pyrene and Fluoranthene, J. Phys. Chem. A, 112, 10552-10559, 10.1021/jp803043s, 2008.

Gussoni, M., Rui, M., and Zerbi, G.: Electronic and relaxation contribution to linear molecular polarizability. An analysis of the experimental values, J. Mol. Struct., 447, 163-215, 10.1016/s0022-2860(97)00292-5, 1998.

Gustafsson, K. and Andersson, S.: Dipole active vibrations and dipole moments of N-2 and O-2 physisorbed on a metal surface, J. Chem. Phys., 125, 5, 10.1063/1.2218842, 2006.

Hai, P., Wu, C., Ding, X., and Li, Y.: Coverage-dependent adsorption and dissociation of H2O on Al surfaces, Phys. Chem. Chem. Phys., 25, 13041, 10.1039/d2cp04386f, 2023.

Hait, D. and Head-Gordon, M.: How accurate are static polarizability predictions from density functional theory? An assessment over 132 species at equilibrium geometry, Phys. Chem. Chem. Phys., 20, 19800-19810, 10.1039/c8cp03569e, 2018.

Hakem, I. F., Boussaid, A., Benchouk-Taleb, H., and Bockstaller, M. R.: Temperature, pressure, and isotope effects on the structure and properties of liquid water: A lattice approach, J. Chem. Phys., 127, 10, 10.1063/1.2804418, 2007.

Hall, D. G. and Cole, R. H.: Dielectric polarization of sulfuric-acid-solutions, J. Phys. Chem., 85, 1065-1069, 10.1021/j150608a029, 1981.

Hallquist, M., Wenger, J. C., Baltensperger, U., Rudich, Y., Simpson, D., Claeys, M., Dommen, J., Donahue, N. M., George, C., Goldstein, A. H., Hamilton, J. F., Herrmann, H., Hoffmann, T., Iinuma, Y., Jang, M., Jenkin, M. E., Jimenez, J. L., Kiendler-Scharr, A., Maenhaut, W., McFiggans, G., Mentel, T. F., Monod, A., Prevot, A. S. H., Seinfeld, J. H., Surratt, J. D., Szmigielski, R., and Wildt, J.: The formation, properties and impact of secondary organic aerosol: current and emerging issues, Atmos. Chem. Phys., 9, 5155-5236, 2009.

1968 Hanefeld, U. and Lefferts, L.: Catalysis, John Wiley & Sons, Inc., Hoboken, New Jersey, USA,
1969 384 pp.2018.

1970 Hanson, D. R.: Surface-specific reactions on liquids, J. Phys. Chem. B, 101, 4998-5001, 1997.

1971 Hanson, D. R. and Lovejoy, E. R.: The Reaction of Clono2 With Submicrometer Sulfuric-Acid
1972 Aerosol, Science, 267, 1326-1328, 1995.

1973 Hanson, D. R. and Ravishankara, A. R.: The Loss of CF2O On Ice, Nat, and Sulfuric-Acid-
1974 Solutions, Geophys. Res. Lett., 18, 1699-1701, 1991.

1975 Hanson, D. R., Ravishankara, A. R., and Lovejoy, E. R.: Reaction of BrONO2 with H2O on
1976 submicron sulfuric acid aerosol and the implications for the lower stratosphere, J. Geophys. Res.,
1977 101, 9063-9069, 1996.

1978 Hanson, D. R., Ravishankara, A. R., and Solomon, S.: Heterogeneous Reactions in Sulfuric-Acid
1979 Aerosols - a Framework For Model-Calculations, J. Geophys. Res., 99, 3615-3629, 1994.

1980 Hantal, G., Jedlovszky, P., Hoang, P. N. M., and Picaud, S.: Calculation of the adsorption
1981 isotherm of formaldehyde on ice by grand canonical Monte Carlo simulation, J. Phys. Chem. C,
1982 111, 14170-14178, 10.1021/jp0742564, 2007.

1983 Hao, H. X., Leven, I., and Head-Gordon, T.: Can electric fields drive chemistry for an aqueous
1984 microdroplet?, Nat. Commun., 13, 8, 10.1038/s41467-021-27941-x, 2022.

1985 Hartkopf, A. and Karger, B. L.: Study of interfacial properties of water by gas-chromatography,
1986 Accounts Chem. Res., 6, 209-216, 10.1021/ar50066a006, 1973.

1987 Hauxwell, F. and Ottewill, R. H.: Adsorption of toluene vapor on water surfaces, J. Colloid
1988 Interface Sci., 28, 514-&, 10.1016/0021-9797(68)90084-2, 1968.

1989 Hearn, J. D. and Smith, G. A.: Ozonolysis of mixed oleic acid/n-docosane particles: The roles of
1990 phase, morphology, and metastable states, J. Phys. Chem. A, 111, 11059-11065,
1991 10.1021/jp0755701, 2007.

1992 Helburn, R., Albritton, J., Howe, G., Michael, L., and Franke, D.: Henry's law constants for
1993 fragrance and organic solvent compounds in aqueous industrial surfactants, J. Chem. Eng. Data,
1994 53, 1071-1079, 10.1021/je700418a, 2008.

1995 Hems, R. F., Schnitzler, E. G., Liu-Kang, C., Cappa, C. D., and Abbatt, J. P. D.: Aging of
1996 Atmospheric Brown Carbon Aerosol, ACS Earth Space Chem., 5, 722-748,
1997 10.1021/acsearthspacechem.0c00346, 2021.

1998 Henderson, G. L. and Meyer, G. H.: Intramolecular torsional potential and dielectric properties
1999 of 2,3-butanedione, J. Phys. Chem., 80, 2422-2425, 10.1021/j100562a020, 1976.

2000 Hickey, A. L. and Rowley, C. N.: Benchmarking Quantum Chemical Methods for the
2001 Calculation of Molecular Dipole Moments and Polarizabilities, J. Phys. Chem. A, 118, 3678-
2002 3687, 10.1021/jp502475e, 2014.

2003 Hildebrand, J. and Scott, R.: The solubility of nonelectrolytes, 3rd ed., Dover Publications, New
2004 York1964.

2005 Hill, T. L.: An Introduction to Statistical Thermodynamics, Dover Publications, Inc., New York,
2006 501 pp.1986.

2007 Hoffmann, M. R. and Edwards, J. O.: Kinetics of oxidation of sulfite by hydrogen-peroxide in
2008 acidic solution, J. Phys. Chem., 79, 2096-2098, 10.1021/j100587a005, 1975.

2009 Hoffmann, M. R., Martin, S. T., Choi, W. Y., and Bahnemann, D. W.: Environmental
2010 Applications of Semiconductor Photocatalysis, Chem. Rev., 95, 69-96, 10.1021/cr00033a004,
2011 1995.

Hoose, C. and Möhler, O.: Heterogeneous ice nucleation on atmospheric aerosols: a review of results from laboratory experiments, Atmos. Chem. Phys., 12, 9817-9854, 10.5194/acp-12-9817-2012, 2012.

Hoskovec, M., Grygarova, D., Cvacka, J., Streinz, L., Zima, J., Verevkin, S. P., and Koutek, B.: Determining the vapour pressures of plant volatiles from gas chromatographic retention data, J. Chromatogr. A, 1083, 161-172, 10.1016/j.chroma.2005.06.006, 2005.

Houle, F. A., Wiegel, A. A., and Wilson, K. R.: Predicting Aerosol Reactivity Across Scales: from the Laboratory to the Atmosphere, Environ. Sci. Technol., 52, 13774-13781, 10.1021/acs.est.8b04688, 2018.

Hu, Z. M. and Nakatsuji, H.: Adsorption and disproportionation reaction of OH on Ag surfaces: dipped adcluster model study, Surf. Sci., 425, 296-312, 10.1016/s0039-6028(99)00215-0, 1999.

Huang, Y. Z., Mahrt, F., Xu, S., Shiraiwa, M., Zuend, A., and Bertram, A. K.: Coexistence of three liquid phases in individual atmospheric aerosol particles, Proc. Natl. Acad. Sci. U. S. A., 118, 9, 10.1073/pnas.2102512118, 2021.

Huthwelker, T., Ammann, M., and Peter, T.: The uptake of acidic gases on ice, Chem. Rev., 106, 1375-1444, 10.1021/cr020506v, 2006.

Hvidt, A.: Interactions of water with non-polar solutes, Annual Review of Biophysics and Bioengineering, 12, 1-20, 10.1146/annurev.bb.12.060183.000245, 1983.

Ibrahim, S., Romanias, M. N., Alleman, L. Y., Zeineddine, M. N., Angeli, G. K., Trikalitis, P. N., and Thevenet, F.: Water Interaction with Mineral Dust Aerosol: Particle Size and Hygroscopic Properties of Dust, ACS Earth Space Chem., 2, 376−386, 10.1021/acsearthspacechem.7b00152, 2018.

Ingram, S., Rovelli, G., Song, Y. C., Topping, D., Dutcher, C. S., Liu, S. H., Nandy, L., Shiraiwa, M., and Reid, J. P.: Accurate Prediction of Organic Aerosol Evaporation Using Kinetic Multilayer Modeling and the Stokes-Einstein Equation, J. Phys. Chem. A, 125, 3444-3456, 10.1021/acs.jpca.1c00986, 2021.

Isaacman-VanWertz, G., Massoli, P., O'Brien, R., Lim, C., Franklin, J. P., Moss, J. A., Hunter, J. F., Nowak, J. B., Canagaratna, M. R., Misztal, P. K., Arata, C., Roscioli, J. R., Herndon, S. T., Onasch, T. B., Lambe, A. T., Jayne, J. T., Su, L., Knopf, D. A., Goldstein, A. H., Worsnop, D. R., and Kroll, J. H.: Chemical evolution of atmospheric organic carbon over multiple generations of oxidation, Nat. Chem., 10.1038/s41557-018-0002-2, 2018.

Isakson, M. J. and Sitz, G. O.: Adsorption and desorption of HCl on ice, J. Phys. Chem. A, 103, 2044-2049, 10.1021/jp984106g, 1999.

IUPAC, McNaught, A. D., and Wilkinson, A. (Eds.): Compendium of Chemical Terminology, (the "Gold Book"), 2nd, Blackwell Scientific Publications, Oxford, 10.1351/goldbook, 1997.

Jayne, J. T., Davidovits, P., Worsnop, D. R., Zahniser, M. S., and Kolb, C. E.: Uptake of So2(G) By Aqueous Surfaces As a Function of Ph - the Effect of Chemical-Reaction At the Interface, J. Phys. Chem., 94, 6041-6048, 1990.

Jeffrey, G. A.: An Introduction to Hydrogen Bonding, Oxford University Press, Oxford, 303 pp.1997.

Jeffrey, G. A. and Saenger, W.: Hydrogen Bonding in Biological Structures,, Springer-Verlag, Berlin, 569 pp., 10.1007/978-3-642-85135-3, 1991.

Jensen, L., Astrand, P. O., Osted, A., Kongsted, J., and Mikkelsen, K. V.: Polarizability of molecular clusters as calculated by a dipole interaction model, J. Chem. Phys., 116, 4001-4010, 10.1063/1.1433747, 2002.

Jeong, D., McNamara, S. M., Barget, A. J., Raso, A. R. W., Upchurch, L. M., Thanekar, S., Quinn, P. K., Simpson, W. R., Fuentes, J. D., Shepson, P. B., and Pratt, K. A.: Multiphase Reactive Bromine Chemistry during Late Spring in the Arctic: Measurements of Gases, Particles, and Snow, ACS Earth Space Chem., 6, 2877-2887, 10.1021/acsearthspacechem.2c00189, 2022.

Jimenez, J. L., Canagaratna, M. R., Donahue, N. M., Prevot, A. S. H., Zhang, Q., Kroll, J. H., DeCarlo, P. F., Allan, J. D., Coe, H., Ng, N. L., Aiken, A. C., Docherty, K. S., Ulbrich, I. M., Grieshop, A. P., Robinson, A. L., Duplissy, J., Smith, J. D., Wilson, K. R., Lanz, V. A., Hueglin, C., Sun, Y. L., Tian, J., Laaksonen, A., Raatikainen, T., Rautiainen, J., Vaattovaara, P., Ehn, M., Kulmala, M., Tomlinson, J. M., Collins, D. R., Cubison, M. J., Dunlea, E. J., Huffman, J. A., Onasch, T. B., Alfarra, M. R., Williams, P. I., Bower, K., Kondo, Y., Schneider, J., Drewnick, F., Borrmann, S., Weimer, S., Demerjian, K., Salcedo, D., Cottrell, L., Griffin, R., Takami, A., Miyoshi, T., Hatakeyama, S., Shimono, A., Sun, J. Y., Zhang, Y. M., Dzepina, K., Kimmel, J. R., Sueper, D., Jayne, J. T., Herndon, S. C., Trimborn, A. M., Williams, L. R., Wood, E. C., Middlebrook, A. M., Kolb, C. E., Baltensperger, U., and Worsnop, D. R.: Evolution of Organic Aerosols in the Atmosphere, Science, 326, 1525-1529, 10.1126/science.1180353, 2009.

Joback, K. G. and Reid, R. C.: Estimation of pure-component properties from group-contributions, Chem. Eng. Commun., 57, 233-243, 10.1080/00986448708960487, 1987.

Johansson, S. M., Lovric, J., Kong, X. R., Thomson, E. S., Hallquist, M., and Pettersson, J. B. C.: Experimental and Computational Study of Molecular Water Interactions with Condensed Nopinone Surfaces Under Atmospherically Relevant Conditions, J. Phys. Chem. A, 124, 3652-3661, 10.1021/acs.jpca.9b10970, 2020.

Johansson, S. M., Lovric, J., Kong, X. R., Thomson, E. S., Papagiannakopoulos, P., Briquez, S., Toubin, C., and Pettersson, J. B. C.: Understanding water interactions with organic surfaces: environmental molecular beam and molecular dynamics studies of the water-butanol system, Phys. Chem. Chem. Phys., 21, 1141-1151, 10.1039/c8cp04151b, 2019.

Joliat, J., Lenoir, T., and Picaud, S.: Comparative Study of the Adsorption of 1-and 2-Propanol on Ice by Means of Grand Canonical Monte Carlo Simulations, ACS Earth Space Chem., 13, 10.1021/acsearthspacechem.2c00390, 2023.

Julin, J., Shiraiwa, M., Miles, R. E. H., Reid, J. P., Pöschl, U., and Riipinen, I.: Mass Accommodation of Water: Bridging the Gap Between Molecular Dynamics Simulations and Kinetic Condensation Models, J. Phys. Chem. A, 117, 410-420, 10.1021/jp310594e, 2013.

Jungwirth, P., Finlayson-Pitts, B. J., and Tobias, D. J.: Introduction: Structure and chemistry at aqueous interfaces, Chem. Rev., 106, 1137-1139, 2006.

Kahan, T. F., Kwamena, N. O. A., and Donaldson, D. J.: Heterogeneous ozonation kinetics of polycyclic aromatic hydrocarbons on organic films, Atmos. Environ., 40, 3448-3459, 10.1016/j.atmosenv.2006.02.004, 2006.

Kaiser, J. C., Riemer, N., and Knopf, D. A.: Detailed heterogeneous oxidation of soot surfaces in a particle-resolved aerosol model, Atmos. Chem. Phys., 11, 4505-4520, 2011.

Kanakidou, M., Seinfeld, J. H., Pandis, S. N., Barnes, I., Dentener, F. J., Facchini, M. C., Van Dingenen, R., Ervens, B., Nenes, A., Nielsen, C. J., Swietlicki, E., Putaud, J. P., Balkanski, Y., Fuzzi, S., Horth, J., Moortgat, G. K., Winterhalter, R., Myhre, C. E. L., Tsigaridis, K., Vignati, E., Stephanou, E. G., and Wilson, J.: Organic aerosol and global climate modelling: a review, Atmos. Chem. Phys., 5, 1053-1123, 2005.

Kanji, Z. A., Ladino, L. A., Wex, H., Boose, Y., Burkert-Kohn, M., Cziczo, D. J., and Krämer, M.: Overview of Ice Nucleating Particles, in: Ice Formation and Evolution in Clouds and

Precipitation: Measurement and Modeling Challenges, Meteorological Monographs, American Meteorological Society, 1.1-1.33, DOI: 10.1175/AMSMONOGRAPHS-D-16-0006.1, 2017.

Kerbrat, M., Huthwelker, T., Gaggeler, H. W., and Ammann, M.: Interaction of Nitrous Acid with Polycrystalline Ice: Adsorption on the Surface and Diffusion into the Bulk, J. Phys. Chem. C, 114, 2208-2219, 10.1021/jp909535c, 2010.

Keyser, L. F., Moore, S. B., and Leu, M. T.: Surface-Reaction and Pore Diffusion in Flow-Tube Reactors, J. Phys. Chem., 95, 5496-5502, 1991.

Kieckbusch, T. G. and King, C. J.: Partition-coefficients for acetates in food systems, J. Agric. Food Chem., 27, 504-507, 10.1021/jf60223a033, 1979.

Kim, Y. K., Park, S. C., Kim, J. H., Lee, C. W., and Kang, H.: Interaction of Carbon Dioxide and Hydroxide Ion at the Surface of Ice Films, J. Phys. Chem. C, 112, 18104-18109, 10.1021/jp806643e, 2008.

Kisliuk, P.: The sticking probabilities of gases chemisorbed on the surfaces of solids, J. Phys. Chem. Solids, 3, 95-101, 10.1016/0022-3697(57)90054-9, 1957.

Kisliuk, P.: The sticking probabilities of gases chemisorbed on the surfaces of solids. 2., J. Phys. Chem. Solids, 5, 78-84, 1958.

Klassen, J. K., Fiehrer, K. M., and Nathanson, G. M.: Collisions of organic molecules with concentrated sulfuric acid: Scattering, trapping, and desorption, J. Phys. Chem. B, 101, 9098-9106, 10.1021/jp972329l, 1997.

Klassen, J. K., Hu, Z. J., and Williams, L. R.: Diffusion coefficients for HCl and HBr in 30 wt % to 72 wt % sulfuric acid at temperatures between 220 and 300 K, J. Geophys. Res.-Atmospheres, 103, 16197-16202, 10.1029/98jd01252, 1998.

Knopf, D. A. and Alpert, P. A.: Atmospheric ice nucleation, Nat. Rev. Phys., 10.1038/s42254-023-00570-7, 2023.

Knopf, D. A. and Ammann, M.: Technical note: Adsorption and desorption equilibria from statistical thermodynamics and rates from transition state theory, Atmos. Chem. Phys., 21, 15725-15753, 10.5194/acp-21-15725-2021, 2021.

Knopf, D. A. and Koop, T.: Heterogeneous nucleation of ice on surrogates of mineral dust, J. Geophys. Res., 111, D12201, 10.1029/2005jd006894, 2006.

Knopf, D. A., Alpert, P. A., and Wang, B.: The Role of Organic Aerosol in Atmospheric Ice Nucleation: A Review, ACS Earth Space Chem., 2, 168–202, 10.1021/acsearthspacechem.7b00120, 2018.

Knopf, D. A., Anthony, L. M., and Bertram, A. K.: Reactive uptake of O3 by multicomponent and multiphase mixtures containing oleic acid, J. Phys. Chem. A, 109, 5579-5589, 2005.

Knopf, D. A., Forrester, S. M., and Slade, J. H.: Heterogeneous oxidation kinetics of organic biomass burning aerosol surrogates by O3, NO2, N2O5, and NO3, Phys. Chem. Chem. Phys., 13, 21050-21062, 10.1039/C1cp22478f, 2011.

Knopf, D. A., Pöschl, U., and Shiraiwa, M.: Radial Diffusion and Penetration of Gas Molecules and Aerosol Particles through Laminar Flow Reactors, Denuders, and Sampling Tubes, Anal. Chem., 87, 3746-3754, 10.1021/ac5042395, 2015.

Knopf, D. A., Ammann, M., Berkemeier, T., Pöschl, U., and Shiraiwa, M.: Desorption Lifetimes and Activation Energies influencing Gas-Surface Interactions and Multiphase Chemical Kinetics: Atmospheric and Environmental Implications [dataset], XYZ, 2023.

Knox, C. J. H. and Phillips, L. F.: Capillary-wave model of gas-liquid exchange, J. Phys. Chem. B, 102, 8469-8472, 10.1021/jp973183t, 1998.

Koch, T. G. and Rossi, M. J.: Direct measurement of surface residence times: Nitryl chloride and chlorine nitrate on alkali halides at room temperature, J. Phys. Chem. A, 102, 9193-9201, 10.1021/jp982539d, 1998a.

Koch, T. G. and Rossi, M. J.: Direct measurement of surface residence times: Nitryl chloride and chlorine nitrate on alkali halides at room temperature, J. Phys. Chem. A, 102, 9193-9201, 1998b.

Koch, T. G., Fenter, F. F., and Rossi, M. J.: Real-time measurement of residence times of gas molecules on solid surfaces, Chemical Physics Letters, 275, 253-260, 1997.

Kolasinski, K. W.: Surface Science: Foundations of Catalysis and Nanoscience, 3rd, John Wiley & Sons, Ltd., West Sussex, United Kingdom, 556 pp., 10.1002/9781119941798, 2012.

Kolb, C. E., Worsnop, D. R., Zahniser, M. S., Davidovits, P., Keyser, L. F., Leu, M.-T., Molina, M. J., Hanson, D. R., Ravishankara, A. R., Williams, L. R., and Tolbert, M. A.: Laboratory Studies of Atmospheric Heterogeneous Chemistry, in: Progress and Problems in Atmospheric Chemistry, edited by: Barker, J. R., World Scientific, Singapore, 771-875, 1995.

Kolb, C. E., Cox, R. A., Abbatt, J. P. D., Ammann, M., Davis, E. J., Donaldson, D. J., Garrett, B. C., George, C., Griffiths, P. T., Hanson, D. R., Kulmala, M., McFiggans, G., Pöschl, U., Riipinen, I., Rossi, M. J., Rudich, Y., Wagner, P. E., Winkler, P. M., Worsnop, D. R., and O'Dowd, C. D.: An overview of current issues in the uptake of atmospheric trace gases by aerosols and clouds, Atmos. Chem. Phys., 10, 10561-10605, 2010.

Kolomiitsova, T. D., Lyaptsev, A. V., and Shchepkin, D. N.: Determination of parameters of the dipole moment of the CO_2 molecule, Opt. Spectrosc., 88, 648-660, 10.1134/1.626856, 2000.

Kong, X. R., Thomson, E. S., Markovic, N., and Pettersson, J. B. C.: Dynamics and Kinetics of Methanol-Graphite Interactions at Low Surface Coverage, ChemPhysChem, 20, 2171-2178, 10.1002/cphc.201900457, 2019.

Kong, X. R., Lovri, J., Johansson, S. M., Prisle, N. L., and Pettersson, J. B. C.: Dynamics and Sorption Kinetics of Methanol Monomers and Clusters on Nopinone Surfaces, J. Phys. Chem. A, 125, 6263-6272, 10.1021/acs.jpca.1c02309, 2021.

Kong, X. R., Papagiannakopoulos, P., Thomson, E. S., Markovic, N., and Pettersson, J. B. C.: Water Accommodation and Desorption Kinetics on Ice, J. Phys. Chem. A, 118, 3973-3979, 10.1021/jp503504e, 2014a.

Kong, X. R., Thomson, E. S., Papagiannakopoulos, P., Johansson, S. M., and Pettersson, J. B. C.: Water Accommodation on Ice and Organic Surfaces: Insights from Environmental Molecular Beam Experiments, J. Phys. Chem. B, 118, 13378-13386, 10.1021/jp5044046, 2014b.

Kong, X. R., Waldner, A., Orlando, F., Artiglia, L., Huthwelker, T., Ammann, M., and Bartels-Rausch, T.: Coexistence of Physisorbed and Solvated HCl at Warm Ice Surfaces, J. Phys. Chem. Lett., 8, 4757-4762, 10.1021/acs.jpclett.7b01573, 2017.

Koop, T., Carslaw, K. S., and Peter, T.: Thermodynamic stability and phase transitions of PSC particles, Geophys. Res. Lett., 24, 2199-2202, 1997.

Koop, T., Bookhold, J., Shiraiwa, M., and Poeschl, U.: Glass transition and phase state of organic compounds: dependency on molecular properties and implications for secondary organic aerosols in the atmosphere, Phys. Chem. Chem. Phys., 13, 19238-19255, 10.1039/c1cp22617g, 2011a.

Koop, T., Bookhold, J., Shiraiwa, M., and Pöschl, U.: Glass transition and phase state of organic compounds: dependency on molecular properties and implications for secondary organic aerosols in the atmosphere, Phys. Chem. Chem. Phys., 13, 19238-19255, 10.1039/c1cp22617g, 2011b.

2192 Kroll, J. H., Donahue, N. M., Jimenez, J. L., Kessler, S. H., Canagaratna, M. R., Wilson, K. R.,
2193 Altieri, K. E., Mazzoleni, L. R., Wozniak, A. S., Bluhm, H., Mysak, E. R., Smith, J. D., Kolb, C.
2194 E., and Worsnop, D. R.: Carbon oxidation state as a metric for describing the chemistry of
2195 atmospheric organic aerosol, Nat Chem, 3, 133-139, 10.1038/nchem.948, 2011.
2196 Kronberg, B.: The hydrophobic effect, Curr. Opin. Colloid Interface Sci., 22, 14-22,
2197 10.1016/j.cocis.2016.02.001, 2016.
2198 Kronberger, H. and Weiss, J.: Formation and structure of some organic molecular compounds.
2199 Part III. The dielectric polarisation of some solid crystalline molecular compounds, J. Chem.
2200 Soc., 464-469, 10.1039/jr9440000464, 1944.
2201 Kuhne, R., Ebert, R. U., and Schuurmann, G.: Prediction of the temperature dependency of
2202 Henry's law constant from chemical structure, Environ. Sci. Technol., 39, 6705-6711,
2203 10.1021/es050527h, 2005.
2204 Kwamena, N. O. A., Thornton, J. A., and Abbatt, J. P. D.: Kinetics of surface-bound benzo a
2205 pyrene and ozone on solid organic and salt aerosols, J. Phys. Chem. A, 108, 11626-11634,
2206 10.1021/jp046161x, 2004.
2207 Laib, J. P. and Mittleman, D. M.: Temperature-Dependent Terahertz Spectroscopy of Liquid n-
2208 alkanes, J. Infrared Millim. Terahertz Waves, 31, 1015-1021, 10.1007/s10762-010-9678-0, 2010.
2209 Laidler, K. J.: The mechanisms of some elementary surface reactions, J. Phys. Colloid Chem.,
2210 53, 712-732, 10.1021/j150470a010, 1949.
2211 Laidler, K. J., Glasstone, S., and Eyring, H.: Application of the Theory of Absolute Reaction
2212 Rates to Heterogeneous Processes II. Chemical Reactions on Surfaces, J. Chem. Phys., 8, 667-
2213 676, 10.1063/1.1750737, 1940.
2214 Lakey, P. S. J., Cummings, B. E., Waring, M. S., Morrison, G. C., and Shiraiwa, M.: Effective
2215 mass accommodation for partitioning of organic compounds into surface films with different
2216 viscosities, Environ. Sci.-Process Impacts, 15, 10.1039/d3em00213f, 2023.
2217 Lakey, P. S. J., Eichler, C. M. A., Wang, C. Y., Little, J. C., and Shiraiwa, M.: Kinetic multi-
2218 layer model of film formation, growth, and chemistry (KM-FILM): Boundary layer processes,
2219 multi-layer adsorption, bulk diffusion, and heterogeneous reactions, Indoor Air, 31, 2070-2083,
2220 10.1111/ina.12854, 2021.
2221 Lakey, P. S. J., Berkemeier, T., Krapf, M., Dommen, J., Steimer, S. S., Whalley, L. K., Ingham,
2222 T., Baeza-Romero, M. T., Pöschl, U., Shiraiwa, M., Ammann, M., and Heard, D. E.: The effect
2223 of viscosity and diffusion on the HO2 uptake by sucrose and secondary organic aerosol particles,
2224 Atmos. Chem. Phys., 16, 13035-13047, 10.5194/acp-16-13035-2016, 2016.
2225 Langenberg, S. and Schurath, U.: Gas chromatography using ice-coated fused silica columns:
2226 study of adsorption of sulfur dioxide on water ice, Atmos. Chem. Phys., 18, 7527-7537,
2227 10.5194/acp-18-7527-2018, 2018.
2228 Langmuir, I.: A theory of adsorption, Phys. Rev., 6, 79-80, 1915.
2229 Langmuir, I.: The evaporation, condensation and reflection of molecules and the mechanism of
2230 adsorption, Phys. Rev., 8, 149-176, 10.1103/PhysRev.8.149, 1916.
2231 Langmuir, I.: The adsorption of gases on plane surfaces of glass, mica and platinum, J. Am.
2232 Chem. Soc., 40, 1361-1403, 10.1021/ja02242a004, 1918.
2233 Laskin, A., Laskin, J., and Nizkorodov, S. A.: Chemistry of Atmospheric Brown Carbon, Chem.
2234 Rev., 115, 4335-4382, 10.1021/cr5006167, 2015.
2235 Lee, G., Lee, B., Kim, J., and Cho, K.: Ozone Adsorption on Graphene: Ab Initio Study and
2236 Experimental Validation, J. Phys. Chem. C, 113, 14225-14229, 10.1021/jp904321n, 2009.

Lee, M. T., Orlando, F., Artiglia, L., Chen, S. Z., and Ammann, M.: Chemical Composition and Properties of the Liquid-Vapor Interface of Aqueous C1 to C4 Monofunctional Acid and Alcohol Solutions, J. Phys. Chem. A, 120, 9749-9758, 10.1021/acs.jpca.6b09261, 2016.

Lee, M. T., Orlando, F., Khabiri, M., Roeselova, M., Brown, M. A., and Ammann, M.: The opposing effect of butanol and butyric acid on the abundance of bromide and iodide at the aqueous solution-air interface, Phys. Chem. Chem. Phys., 21, 8418-8427, 10.1039/c8cp07448h, 2019.

Lee, W. M. G. and Chen, J. C.: Partitioning coefficients of polycyclic aromatic-hydrocarbons in stack gas from a municipal incinerator, Environ. Int., 21, 827-831, 10.1016/0160-4120(95)00092-4, 1995.

Lejonthun, L., Andersson, P. U., Hallquist, M., Thomson, E. S., and Pettersson, J. B. C.: Interactions of N2O5 and Related Nitrogen Oxides with Ice Surfaces: Desorption Kinetics and Collision Dynamics, J. Phys. Chem. B, 118, 13427-13434, 10.1021/jp5053826, 2014.

Leluk, K., Orzechowski, K., Jerie, K., Baranowski, A., Slonka, T., and Glowinski, J.: Dielectric permittivity of kaolinite heated to high temperatures, J. Phys. Chem. Solids, 71, 827-831, 10.1016/j.jpcs.2010.02.008, 2010.

Leng, C. B., Kish, J. D., Roberts, J. E., Dwebi, I., Chon, N., and Liu, Y.: Temperature-Dependent Henry's Law Constants of Atmospheric Amines, J. Phys. Chem. A, 119, 8884-8891, 10.1021/acs.jpca.5b05174, 2015.

Li, G., Su, H., Kuhn, U., Meusel, H., Ammann, M., Shao, M., Poschl, U., and Cheng, Y. F.: Technical note: Influence of surface roughness and local turbulence on coated-wall flow tube experiments for gas uptake and kinetic studies, Atmos. Chem. Phys., 18, 2669-2686, 10.5194/acp-18-2669-2018, 2018.

Li, J. and Knopf, D. A.: Representation of Multiphase OH Oxidation of Amorphous Organic Aerosol for Tropospheric Conditions, Environ. Sci. Technol., 55, 7266-7275, 10.1021/acs.est.0c07668, 2021.

Li, J. N., Forrester, S. M., and Knopf, D. A.: Heterogeneous oxidation of amorphous organic aerosol surrogates by O3, NO3, and OH at typical tropospheric temperatures, Atmos. Chem. Phys., 20, 6055-6080, 10.5194/acp-20-6055-2020, 2020.

Li, Y. and Shiraiwa, M.: Timescales of secondary organic aerosols to reach equilibrium at various temperatures and relative humidities, Atmos. Chem. Phys., 19, 5959-5971, 10.5194/acp-19-5959-2019, 2019.

Li, Y., Pöschl, U., and Shiraiwa, M.: Molecular corridors and parameterizations of volatility in the chemical evolution of organic aerosols, Atmos. Chem. Phys., 16, 3327-3344, 10.5194/acp-16-3327-2016, 2016.

Liang, Z., Li, K. J., Wang, Z. M., Bu, Y. S., and Zhang, J. L.: Adsorption and reaction mechanisms of single and double H2O molecules on graphene surfaces with defects: a density functional theory study, Phys. Chem. Chem. Phys., 23, 19071-19082, 10.1039/d1cp02595c, 2021.

Lide, D. R.: CRC Handbook of Chemistry and Physics, 82nd, CRC Press., Boca Raton2008.

Lileev, A. and Lyashchenko, A.: Dielectric properties of ammonium salt aqueous solutions, J. Mol. Liq., 150, 4-8, 10.1016/j.molliq.2009.08.008, 2009.

Longfellow, C. A., Imamura, T., Ravishankara, A. R., and Hanson, D. R.: HONO solubility and heterogeneous reactivity on sulfuric acid surfaces, J. Phys. Chem. A, 102, 3323-3332, 1998.

Mack, K. M. and Muenter, J. S.: Stark and Zeeman properties of ozone from molecular-beam spectroscopy, J. Chem. Phys., 66, 5278-5283, 10.1063/1.433909, 1977.

2283 Mader, B. T., Goss, K. U., and Eisenreich, S. J.: Sorption of nonionic, hydrophobic organic
2284 chemicals to mineral surfaces, Environ. Sci. Technol., 31, 1079-1086, 10.1021/es960606g, 1997.
2285 Maribo-Mogensen, B., Kontogeorgis, G. M., and Thomsen, K.: Modeling of Dielectric
2286 Properties of Aqueous Salt Solutions with an Equation of State, J. Phys. Chem. B, 117, 10523-
2287 10533, 10.1021/jp403375t, 2013.
2288 Marsh, A. R. W. and McElroy, W. J.: The dissociation-constant and Henry law constant of HCl
2289 in aqueous-solution, Atmos. Environ., 19, 1075-1080, 10.1016/0004-6981(85)90192-1, 1985.
2290 Marshall, F. H., Berkemeier, T., Shiraiwa, M., Nandy, L., Ohm, P. B., Dutcher, C. S., and Reid,
2291 J. P.: Influence of particle viscosity on mass transfer and heterogeneous ozonolysis kinetics in
2292 aqueous-sucrose-maleic acid aerosol, Phys. Chem. Chem. Phys., 20, 15560-15573,
2293 10.1039/c8cp01666f, 2018.
2294 Marshall, F. H., Miles, R. E. H., Song, Y. C., Ohm, P. B., Power, R. M., Reid, J. P., and Dutcher,
2295 C. S.: Diffusion and reactivity in ultraviscous aerosol and the correlation with particle viscosity,
2296 Chem. Sci., 7, 1298-1308, 10.1039/c5sc03223g, 2016.
2297 Masel, R. I.: Principles of Adsorption and Reaction on Solid Surfaces, Wiley Series in Cehmical
2298 Engineering1996.
2299 McEachran, A. D., Mansouri, K., Grulke, C., Schymanski, E. L., Ruttkies, C., and Williams, A.
2300 J.: "MS-Ready" structures for non-targeted high-resolution mass spectrometry screening studies,
2301 J. Cheminformatics, 10, 16, 10.1186/s13321-018-0299-2, 2018.
2302 McNamara, S. M., Chen, Q. J., Edebeli, J., Kulju, K. D., Mumpfield, J., Fuentes, J. D., Bertman,
2303 S. B., and Pratt, K. A.: Observation of N2O5 Deposition and ClNO2 Production on the Saline
2304 Snowpack, ACS Earth Space Chem., 5, 1020-1031, 10.1021/acsearthspacechem.0c00317, 2021.
2305 McNeill, V. F., Loerting, T., Geiger, F. M., Trout, B. L., and Molina, M. J.: Hydrogen chloride-
2306 induced surface disordering on ice, Proc. Natl. Acad. Sci. U. S. A., 103, 9422-9427,
2307 10.1073/pnas.0603494103, 2006.
2308 McNeill, V. F., Geiger, F. M., Loerting, T., Trout, B. L., Molina, L. T., and Molina, M. J.:
2309 Interaction of hydrogen chloride with ice surfaces: The effects of grain size, surface roughness,
2310 and surface disorder, J. Phys. Chem. A, 111, 6274-6284, 10.1021/jp068914g, 2007.
2311 McNeill, V. F., Grannas, A. M., Abbatt, J. P. D., Ammann, M., Ariya, P., Bartels-Rausch, T.,
2312 Domine, F., Donaldson, D. J., Guzman, M. I., Heger, D., Kahan, T. F., Klan, P., Masclin, S.,
2313 Toubin, C., and Voisin, D.: Organics in environmental ices: sources, chemistry, and impacts,
2314 Atmos. Chem. Phys., 12, 9653-9678, 10.5194/acp-12-9653-2012, 2012.
2315 Mendes, P. C. D., Costa-Amaral, R., Gomes, J. F., and Da Silva, J. L. F.: The influence of
2316 hydroxy groups on the adsorption of three-carbon alcohols on Ni(111), Pd(111) and Pt(111)
2317 surfaces: a density functional theory study within the D3 dispersion correction, Phys. Chem.
2318 Chem. Phys., 21, 8434, 10.1039/c9cp00752k, 2019.
2319 Meng, S., Wang, E. G., and Gao, S. W.: Water adsorption on metal surfaces: A general picture
2320 from density functional theory studies, Phys. Rev. B, 69, 13, 10.1103/PhysRevB.69.195404,
2321 2004.
2322 Merino, E. and Ribagorda, M.: Control over molecular motion using the cis-trans
2323 photoisomerization of the azo group, Beilstein J. Org. Chem., 8, 1071-1090, 10.3762/bjoc.8.119,
2324 2012.
2325 Messerer, A., Niessner, R., and Pöschl, U.: Comprehensive kinetic characterization of the
2326 oxidation and gasification of model and real diesel soot by nitrogen oxides and oxygen under
2327 engine exhaust conditions: Measurement, Langmuir-Hinshelwood, and Arrhenius parameters,
2328 Carbon, 44, 307-324, 10.1016/j.carbon.2005.07.017, 2006.

2329 Messerer, A., Schmatloch, V., Pöschl, U., and Niessner, R.: Combined particle emission
2330 reduction and heat recovery from combustion exhaust - A novel approach for small wood-fired
2331 appliances, Biomass & Bioenergy, 31, 512-521, 10.1016/j.biombioe.2007.01.022, 2007.
2332 Meyer, H., Entel, P., and Hafner, J.: Physisorption of water on salt surfaces, Surf. Sci., 488, 177-
2333 192, 10.1016/s0039-6028(01)01136-0, 2001.
2334 Mikhailov, E., Vlasenko, S., Martin, S. T., Koop, T., and Poschl, U.: Amorphous and crystalline
2335 aerosol particles interacting with water vapor: conceptual framework and experimental evidence
2336 for restructuring, phase transitions and kinetic limitations, Atmos. Chem. Phys., 9, 9491-9522,
2337 2009.
2338 Millany, H. M. and Jonscher, A. K.: Dielectric-properties of stearic-acid multilayers, Thin Solid
2339 Films, 68, 257-273, 10.1016/0040-6090(80)90151-0, 1980.
2340 Mmereki, B. T., Hicks, J. M., and Donaldson, D. J.: Adsorption of atmospheric gases at the air-
2341 water interface. 3: Methylamines, J. Phys. Chem. A, 104, 10789-10793, 10.1021/jp0023258,
2342 2000.
2343 Moise, T., Flores, J. M., and Rudich, Y.: Optical properties of secondary organic aerosols and
2344 their changes by chemical processes, Chem. Rev., 115, 4400-4439, 10.1021/cr5005259, 2015.
2345 Mopsik, F. I.: Digest of Literature on Dielectrics: National Academy of Sciences, National
2346 Research Council Washington, D. C. , 1967.
2347 Morris, J. R., Behr, P., Antman, M. D., Ringeisen, B. R., Splan, J., and Nathanson, G. M.:
2348 Molecular beam scattering from supercooled sulfuric acid: Collisions of HCl, HBr, and HNO3
2349 with 70 wt % D2SO4, J. Phys. Chem. A, 104, 6738-6751, 10.1021/jp000105o, 2000.
2350 Moussa, S. G., McIntire, T. M., Szori, M., Roeselova, M., Tobias, D. J., Grimm, R. L.,
2351 Hemminger, J. C., and Finlayson-Pitts, B. J.: Experimental and Theoretical Characterization of
2352 Adsorbed Water on Self-Assembled Monolayers: Understanding the Interaction of Water with
2353 Atmospherically Relevant Surfaces, J. Phys. Chem. A, 113, 2060-2069, 10.1021/jp808710n,
2354 2009.
2355 Mu, Q., Shiraiwa, M., Octaviani, M., Ma, N., Ding, A. J., Su, H., Lammel, G., Poschl, U., and
2356 Cheng, Y. F.: Temperature effect on phase state and reactivity controls atmospheric multiphase
2357 chemistry and transport of PAHs, Sci. Adv., 4, 8, 10.1126/sciadv.aap7314, 2018.
2358 Muller, R., Crutzen, P. J., Gross, J. U., Bruhl, C., Russell, J. M., Gernandt, H., McKenna, D. S.,
2359 and Tuck, A. F.: Severe chemical ozone loss in the Arctic during the winter of 1995-96, Nature,
2360 389, 709-712, 1997.
2361 Nakanishi, M. and Nozaki, R.: Systematic study of the glass transition in polyhydric alcohols,
2362 Phys. Rev. E, 83, 5, 10.1103/PhysRevE.83.051503, 2011.
2363 Nakatsuji, H.: Dipped adcluster model for chemisorptions and catalytic reactions on a metal-
2364 surface, J. Chem. Phys., 87, 4995-5001, 10.1063/1.452814, 1987.
2365 Nathanson, G. M.: Molecular beam studies of gas-liquid interfaces, Annu. Rev. Phys. Chem., 55,
2366 231-255, 10.1146/annurev.physchem.55.091602.094357, 2004.
2367 Nathanson, G. M., Davidovits, P., Worsnop, D. R., and Kolb, C. E.: Dynamics and kinetics at the
2368 gas-liquid interface, J. Phys. Chem., 100, 13007-13020, 1996.
2369 Nelson, C. E., Elam, J. W., Tolbert, M. A., and George, S. M.: H2O and HCl adsorption on
2370 single crystal alpha-Al2O3(0001) at stratospheric temperatures, Appl. Surf. Sci., 171, 21-33,
2371 2001.
2372 Nelson, C. E., Elam, J. W., Cameron, M. A., Tolbert, M. A., and George, S. M.: Desorption of
2373 H2O from a hydroxylated single-crystal alpha-Al2O3(0001) surface, Surf. Sci., 416, 341-353,
2374 10.1016/s0039-6028(98)00439-7, 1998.

NIST: NIST Computational Chemistry Comparison and Benchmark Database, 10.18434/T47C7Z, 2018.

Nizkorodov, S. A., Laskin, J., and Laskin, A.: Molecular chemistry of organic aerosols through the application of high resolution mass spectrometry, Phys. Chem. Chem. Phys., 13, 3612-3629, 10.1039/c0cp02032j, 2011.

Ohrwall, G., Prisle, N. L., Ottosson, N., Werner, J., Ekholm, V., Walz, M. M., and Bjorneholm, O.: Acid-Base Speciation of Carboxylate Ions in the Surface Region of Aqueous Solutions in the Presence of Ammonium and Aminium Ions, J. Phys. Chem. B, 119, 4033-4040, 10.1021/jp509945g, 2015.

Oszust, J. and Ratajczak, H.: Dipole-moments and spectral features of some phenol-diethylamine complexes, J. Chem.l Soc. Farad. T 1, 77, 1215-1221, 10.1039/f19817701215, 1981.

Pankow, J. F.: Common gamma-intercept and single compound regressions of gas particle partitioning data vs 1/t, Atmos. Environ. A-Gen., 25, 2229-2239, 10.1016/0960-1686(91)90098-r, 1991.

Paserba, K. R. and Gellman, A. J.: Effects of conformational isomerism on the desorption kinetics of n-alkanes from graphite, J. Chem. Phys., 115, 6737-6751, 10.1063/1.1398574, 2001.

Penkett, S. A., Jones, B. M. R., Brice, K. A., and Eggleton, A. E. J.: Importance of atmospheric ozone and hydrogen-peroxide in oxidizing sulfur-dioxide in cloud and rainwater, Atmos. Environ., 13, 123-137, 10.1016/0004-6981(79)90251-8, 1979.

Perraud, V., Bruns, E. A., Ezell, M. J., Johnson, S. N., Yu, Y., Alexander, M. L., Zelenyuk, A., Imre, D., Chang, W. L., Dabdub, D., Pankow, J. F., and Finlayson-Pitts, B. J.: Nonequilibrium atmospheric secondary organic aerosol formation and growth, P. Natl. Acad. Sci. USA, 109, 2836-2841, 10.1073/pnas.1119909109, 2012.

Peter, T.: Microphysics and heterogeneous chemistry of polar stratospheric clouds, Annu. Rev. Phys. Chem., 48, 785-822, 1997.

Petters, M. D., Prenni, A. J., Kreidenweis, S. M., DeMott, P. J., Matsunaga, A., Lim, Y. B., and Ziemann, P. J.: Chemical aging and the hydrophobic-to-hydrophilic conversion of carbonaceous aerosol, Geophys. Res. Lett., 33, 10.1029/2006gl027249, 2006.

Poe, S. H., Valsaraj, K. T., Thibodeaux, L. J., and Springer, C.: Equilibrium vapor-phase adsorption of volatile organic-chemicals on dry soils, J. Hazard. Mater., 19, 17-32, 10.1016/0304-3894(88)85071-4, 1988.

Pöschl, U. and Shiraiwa, M.: Multiphase Chemistry at the Atmosphere-Biosphere Interface Influencing Climate and Public Health in the Anthropocene, Chem. Rev., 115, 4440-4475, 10.1021/cr500487s, 2015.

Pöschl, U., Rudich, Y., and Ammann, M.: Kinetic model framework for aerosol and cloud surface chemistry and gas-particle interactions - Part 1: General equations, parameters, and terminology, Atmos. Chem. Phys., 7, 5989-6023, 2007.

Pöschl, U., Letzel, T., Schauer, C., and Niessner, R.: Interaction of ozone and water vapor with spark discharge soot aerosol particles coated with benzo a pyrene: O3 and H2O adsorption, benzo a pyrene degradation, and atmospheric implications, J. Phys. Chem. A, 105, 4029-4041, 2001.

Pouvesle, N., Kippenberger, M., Schuster, G., and Crowley, J. N.: The interaction of H2O2 with ice surfaces between 203 and 233 K, Phys. Chem. Chem. Phys., 12, 15544-15550, 10.1039/c0cp01656j, 2010.

Raja, S., Yaccone, F. S., Ravikrishna, R., and Valsaraj, K. T.: Thermodynamic parameters for the adsorption of aromatic hydrocarbon vapors at the gas-water interface, J. Chem. Eng. Data, 47, 1213-1219, 10.1021/je025520j, 2002.

Rajyam, B. S. and Murty, C. R. K.: Dipole moments of some alkyl phenylacetates, Indian J. Pure Appl. Phys., 4, 327-&, 1966.

Rampi, M. A., Schueller, O. J. A., and Whitesides, G. M.: Alkanethiol self-assembled monolayers as the dielectric of capacitors with nanoscale thickness, Appl. Phys. Lett., 72, 1781-1783, 10.1063/1.121183, 1998.

Raso, A. R. W., Custard, K. D., May, N. W., Tanner, D., Newburn, M. K., Walker, L., Moore, R. J., Huey, L. G., Alexander, L., Shepson, P. B., and Pratt, K. A.: Active molecular iodine photochemistry in the Arctic, Proc. Natl. Acad. Sci. U. S. A., 114, 10053-10058, 10.1073/pnas.1702803114, 2017.

Ravishankara, A. R.: Heterogeneous and multiphase chemistry in the troposphere, Science, 276, 1058-1065, 1997.

Redhead, P. A.: Thermal desorption of gases, Vacuum, 12, 203-211, 10.1016/0042-207X(62)90978-8, 1962.

Remorov, R. G. and Bardwell, M. W.: Model of uptake of OH radicals on nonreactive solids, J. Phys. Chem. B, 109, 20036-20043, 2005.

Rettner, C. T., Auerbach, D. J., Tully, J. C., and Kleyn, A. W.: Chemical dynamics at the gas-surface interface, J. Phys. Chem., 100, 13021-13033, 10.1021/jp9536007, 1996.

Ringeisen, B. R., Muenter, A. H., and Nathanson, G. M.: Collisions of DCl with liquid glycerol: Evidence for rapid, near-interfacial D -> H exchange and desorption, J. Phys. Chem. B, 106, 4999-5010, 10.1021/jp013959x, 2002a.

Ringeisen, B. R., Muenter, A. H., and Nathanson, G. M.: Collisions of HCl, DCl, and HBr with liquid glycerol: Gas uptake, D -> H exchange, and solution thermodynamics, J. Phys. Chem. B, 106, 4988-4998, 10.1021/jp013960w, 2002b.

Robinson, D. A., Cooper, J. D., and Gardner, C. M. K.: Modelling the relative permittivity of soils using soil hygroscopic water content, J. Hydrol., 255, 39-49, 10.1016/s0022-1694(01)00508-x, 2002.

Robinson, G. N., Worsnop, D. R., Jayne, J. T., Kolb, C. E., Swartz, E., and Davidovits, P.: Heterogeneous uptake of HCl by sulfuric acid solutions, J. Geophys. Res., 103, 25371-25381, 1998.

Romaner, L., Heimel, G., Ambrosch-Draxl, C., and Zojer, E.: The Dielectric Constant of Self-Assembled Monolayers, Adv. Funct. Mater., 18, 3999-4006, 10.1002/adfm.200800876, 2008.

Romanias, M. N., Ourrad, H., Thevenet, F., and Riffault, V.: Investigating the Heterogeneous Interaction of VOCs with Natural Atmospheric Particles: Adsorption of Limonene and Toluene on Saharan Mineral Dusts, J. Phys. Chem. A, 120, 1197-1212, 10.1021/acs.jpca.5b10323, 2016.

Rothfuss, N. E. and Petters, M. D.: Influence of Functional Groups on the Viscosity of Organic Aerosol, Environ. Sci. Technol., 51, 271-279, 10.1021/acs.est.6b04478, 2017.

Rouquerol, J. and Davy, L.: Automatic gravimetric apparatus for recording adsorption-isotherms of gases or vapors onto solids, Thermochim. Acta, 24, 391-397, 10.1016/0040-6031(78)80027-6, 1978.

Rowland, F. S.: Stratospheric ozone depletion, Annu. Rev. Phys. Chem., 42, 731-768, 10.1146/annurev.physchem.42.1.731, 1991.

Rudich, Y., Donahue, N. M., and Mentel, T. F.: Aging of organic aerosol: Bridging the gap between laboratory and field studies, Annu. Rev. Phys. Chem., 58, 321-352, 10.1146/annurev.physchem.58.032806.104432, 2007.

Salmeron, M. and Somorjai, G. A.: Adsorption and bonding of butane and pentane on the Pt(111) crystal-surfaces - effects of oxygen treatments and deuterium pre-adsorption, J. Phys. Chem., 85, 3835-3840, 10.1021/j150625a025, 1981.

Sander, R.: Compilation of Henry's law constants (version 4.0) for water as solvent, Atmos. Chem. Phys., 15, 4399-4981, 10.5194/acp-15-4399-2015, 2015.

Sander, R.: Compilation of Henry's law constants (version 5.0.0) for water as solvent, Atmos. Chem. Phys., 23, 10901–12440, 10.5194/acp-23-10901-2023, 2023.

Sander, S. P., Abbatt, J., Barker, J. R., Burkholder, J. B., Friedl, R. R., Golden, D. M., Huie, R. E., Kolb, C. E., Kurylo, M. J., Moortgat, G. K., Orkin, V. L., and Wine, P. H.: Chemical Kinetics and Photochemical Data for Use in Atmospheric Studies, Evaluation No. 17, NASA Jet Propulsion Laboratory, Pasadena2011.

Savara, A.: Standard States for Adsorption on Solid Surfaces: 2D Gases, Surface Liquids, and Langmuir Adsorbates, J. Phys. Chem. C, 117, 15710-15715, 10.1021/jp404398z, 2013.

Savara, A., Schmidt, C. M., Geiger, F. M., and Weitz, E.: Adsorption Entropies and Enthalpies and Their Implications for Adsorbate Dynamics, J. Phys. Chem. C, 113, 2806-2815, 10.1021/jp806221j, 2009.

Schervish, M. and Donahue, N. M.: Peroxy radical chemistry and the volatility basis set, Atmos. Chem. Phys., 20, 1183-1199, 10.5194/acp-20-1183-2020, 2020.

Schervish, M. and Shiraiwa, M.: Impact of phase state and non-ideal mixing on equilibration timescales of secondary organic aerosol partitioning, Atmos. Chem. Phys., 23, 221-233, 10.5194/acp-23-221-2023, 2023.

Schervish, M., Donahue, N. M., and Shiraiwa, M.: Effects of volatility, viscosity, and non-ideality on particle-particle mixing timescales of secondary organic aerosols, Aerosol Sci. Technol., 16, 10.1080/02786826.2023.2256827, 2023.

Schlesinger, D., Lowe, S. J., Olenius, T., Kong, X. R., Pettersson, J. B. C., and Riipinen, I.: Molecular Perspective on Water Vapor Accommodation into Ice and Its Dependence on Temperature, J. Phys. Chem. A, 124, 10879-10889, 10.1021/acs.jpca.0c09357, 2020.

Schroder, E.: Methanol Adsorption on Graphene, J. Nanomater., 2013, 6, 10.1155/2013/871706, 2013.

Schwartz, S. E.: Mass-transport considerations pertinent to aqueous phase reactions of gases in liquid-water clouds, in: Chemistry of multiphase atmospheric systems, edited by: Jaeschke, W., NATO ASI Series, G6, Springer, New York, 1986.

Sebastiani, F., Campbell, R. A., Rastogi, K., and Pfrang, C.: Nighttime oxidation of surfactants at the air-water interface: effects of chain length, head group and saturation, Atmos. Chem. Phys., 18, 3249-3268, 10.5194/acp-18-3249-2018, 2018.

Seinfeld, J. H. and Pandis, S. N.: Atmospheric Chemistry and Pysics. From Air Pollution to Climate Change, John Wiley, New York, 1326 pp.1998.

Shaloski, M. A., Gord, J. R., Staudt, S., Quinn, S. L., Bertram, T. H., and Nathanson, G. M.: Reactions of N2O5 with Salty and Surfactant-Coated Glycerol: Interfacial Conversion of Br- to Br-2 Mediated by Alkylammonium Cations, J. Phys. Chem. A, 121, 3708-3719, 10.1021/acs.jpca.7b02040, 2017.

Sharif, S.: Chemical and mineral-composition of dust and its effect on the dielectric-constant, IEEE Trans. Geosci. Remote Sensing, 33, 353-359, 10.1109/36.377935, 1995.

Shen, C. Y., Zhang, W., Choczynski, J., Davies, J. F., and Zhang, H. F.: Phase State and Relative Humidity Regulate the Heterogeneous Oxidation Kinetics and Pathways of Organic-Inorganic Mixed Aerosols, Environ. Sci. Technol., 56, 15398-15407, 10.1021/acs.est.2c04670, 2022.

Shi, Q., Jayne, J. T., Kolb, C. E., Worsnop, D. R., and Davidovits, P.: Kinetic model for reaction of ClONO2 with H2O and HCl and HOCl with HCl in sulfuric acid solutions, J. Geophys. Res., 106, 24259-24274, 2001.

Shinoda, K.: Iceberg formation and solubility, J. Phys. Chem., 81, 1300-1302, 10.1021/j100528a016, 1977.

Shinoda, K.: Characteristic property in aqueous-solutions - effect of iceberg formation of water surrounding solute on the solubility (or cmc) and its peculiar temperature-dependence, Adv. Colloid Interface Sci., 41, 81-100, 10.1016/0001-8686(92)80008-l, 1992.

Shiraiwa, M. and Pöschl, U.: Mass accommodation and gas-particle partitioning in secondary organic aerosols: dependence on diffusivity, volatility, particle-phase reactions, and penetration depth, Atmos. Chem. Phys., 21, 1565-1580, 10.5194/acp-21-1565-2021, 2021.

Shiraiwa, M. and Seinfeld, J. H.: Equilibration timescale of atmospheric secondary organic aerosol partitioning, Geophys. Res. Lett., 39, L24801, 10.1029/2012gl054008, 2012.

Shiraiwa, M., Garland, R. M., and Pöschl, U.: Kinetic double-layer model of aerosol surface chemistry and gas-particle interactions (K2-SURF): Degradation of polycyclic aromatic hydrocarbons exposed to O3, NO2, H2O, OH and NO3, Atmos. Chem. Phys., 9, 9571-9586, 2009.

Shiraiwa, M., Pfrang, C., and Pöschl, U.: Kinetic multi-layer model of aerosol surface and bulk chemistry (KM-SUB): the influence of interfacial transport and bulk diffusion on the oxidation of oleic acid by ozone, Atmos. Chem. Phys., 10, 3673-3691, 2010.

Shiraiwa, M., Ammann, M., Koop, T., and Pöschl, U.: Gas uptake and chemical aging of semisolid organic aerosol particles, P. Natl. Acad. Sci. USA, 108, 11003-11008, 2011a.

Shiraiwa, M., Pfrang, C., Koop, T., and Pöschl, U.: Kinetic multi-layer model of gas-particle interactions in aerosols and clouds (KM-GAP): linking condensation, evaporation and chemical reactions of organics, oxidants and water, Atmos. Chem. Phys., 12, 2777-2794, 2012.

Shiraiwa, M., Zuend, A., Bertram, A. K., and Seinfeld, J. H.: Gas-particle partitioning of atmospheric aerosols: interplay of physical state, non-ideal mixing and morphology, Phys. Chem. Chem. Phys., 15, 11441-11453, 10.1039/c3cp51595h, 2013a.

Shiraiwa, M., Berkemeier, T., Schilling-Fahnestock, K. A., Seinfeld, J. H., and Pöschl, U.: Molecular corridors and kinetic regimes in the multiphase chemical evolution of secondary organic aerosol, Atmos. Chem. Phys., 14, 8323-8341, 10.5194/acp-14-8323-2014, 2014.

Shiraiwa, M., Sosedova, Y., Rouviere, A., Yang, H., Zhang, Y. Y., Abbatt, J. P. D., Ammann, M., and Pöschl, U.: The role of long-lived reactive oxygen intermediates in the reaction of ozone with aerosol particles, Nature Chemistry, 3, 291-295, 2011b.

Shiraiwa, M., Yee, L. D., Schilling, K. A., Loza, C. L., Craven, J. S., Zuend, A., Ziemann, P. J., and Seinfeld, J. H.: Size distribution dynamics reveal particle-phase chemistry in organic aerosol formation, Proc. Natl. Acad. Sci. U. S. A., 110, 11746-11750, 10.1073/pnas.1307501110, 2013b.

Shiraiwa, M., Li, Y., Tsimpidi, A. P., Karydis, V. A., Berkemeier, T., Pandis, S. N., Lelieveld, J., Koop, T., and Pöschl, U.: Global distribution of particle phase state in atmospheric secondary organic aerosols, Nat. Commun., 8, 15002, 10.1038/ncomms15002, 2017a.

Shiraiwa, M., Ueda, K., Pozzer, A., Lammel, G., Kampf, C. J., Fushimi, A., Enami, S., Arangio, A. M., Frohlich-Nowoisky, J., Fujitani, Y., Furuyama, A., Lakey, P. S. J., Lelieveld, J., Lucas, K., Morino, Y., Poschl, U., Takaharna, S., Takami, A., Tong, H. J., Weber, B., Yoshino, A., and

2555 Sato, K.: Aerosol Health Effects from Molecular to Global Scales, Environ. Sci. Technol., 51,
2556 13545-13567, 10.1021/acs.est.7b04417, 2017b.
2557 Shklyarevskii, I. N. and Pakhomov, P. L.: Separation of contributions from free and coupled
2558 electrons into real and imaginary parts of a dielectric-constant of gold, Opt. Spektrosk., 34, 163-
2559 166, 1973.
2560 Shrivastava, M., Lou, S. J., Zelenyuk, A., Easter, R. C., Corley, R. A., Thrall, B. D., Rasch, P. J.,
2561 Fast, J. D., Simonich, S. L. M., Shen, H. Z., and Tao, S.: Global long-range transport and lung
2562 cancer risk from polycyclic aromatic hydrocarbons shielded by coatings of organic aerosol (vol
2563 114, pg 1246, 2017), Proc. Natl. Acad. Sci. U. S. A., 114, E2263-E2263,
2564 10.1073/pnas.1702221114, 2017a.
2565 Shrivastava, M., Cappa, C. D., Fan, J. W., Goldstein, A. H., Guenther, A. B., Jimenez, J. L.,
2566 Kuang, C., Laskin, A., Martin, S. T., Ng, N. L., Petaja, T., Pierce, J. R., Rasch, P. J., Roldin, P.,
2567 Seinfeld, J. H., Shilling, J., Smith, J. N., Thornton, J. A., Volkamer, R., Wang, J., Worsnop, D.
2568 R., Zaveri, R. A., Zelenyuk, A., and Zhang, Q.: Recent advances in understanding secondary
2569 organic aerosol: Implications for global climate forcing, Rev. Geophys., 55, 509-559,
2570 10.1002/2016rg000540, 2017b.
2571 Sikorski, M., Gutt, C., Chushkin, Y., Lippmann, M., and Franz, H.: Dynamics at the Liquid-
2572 Vapor Interface of a Supercooled Organic Glass Former, Phys. Rev. Lett., 105, 4,
2573 10.1103/PhysRevLett.105.215701, 2010.
2574 Silva, S. C. and Devlin, J. P.: Interaction of acetylene, ethylene, and benzene with ice surfaces, J.
2575 Phys. Chem., 98, 10847-10852, 10.1021/j100093a027, 1994.
2576 Slade, J. H. and Knopf, D. A.: Heterogeneous OH oxidation of biomass burning organic aerosol
2577 surrogate compounds: assessment of volatilisation products and the role of OH concentration on
2578 the reactive uptake kinetics, Phys. Chem. Chem. Phys., 15, 5898-5915, 10.1039/c3cp44695f,
2579 2013.
2580 Slade, J. H. and Knopf, D. A.: Multiphase OH oxidation kinetics of organic aerosol: The role of
2581 particle phase state and relative humidity, Geophys. Res. Lett., 41, 5297-5306,
2582 10.1002/2014gl060582, 2014.
2583 Slade, J. H., Thalman, R., Wang, J., and Knopf, D. A.: Chemical aging of single and
2584 multicomponent biomass burning aerosol surrogate particles by OH: implications for cloud
2585 condensation nucleus activity, Atmos. Chem. Phys., 15, 10183-10201, 10.5194/acp-15-10183-
2586 2015, 2015.
2587 Slade, J. H., Shiraiwa, M., Arangio, A., Su, H., Pöschl, U., Wang, J., and Knopf, D. A.: Cloud
2588 droplet activation through oxidation of organic aerosol influenced by temperature and particle
2589 phase state, Geophys. Res. Lett., 44, 1583-1591, 10.1002/2016gl072424, 2017.
2590 Slater, B. and Michaelides, A.: Surface premelting of water ice, Nat. Rev. Chem., 3, 172–188,
2591 10.1038/s41570-019-0080-8, 2019.
2592 Smith, R. S. and Kay, B. D.: Desorption Kinetics of Carbon Dioxide from a Graphene-Covered
2593 Pt(111) Surface, J. Phys. Chem. A, 123, 3248−3254 10.1021/acs.jpca.9b00674, 2019.
2594 Sokolov, O. and Abbatt, J. P. D.: Adsorption to ice of n-alcohols (ethanol to 1-hexanol), acetic
2595 acid, and hexanal, J. Phys. Chem. A, 106, 775-782, 2002.
2596 Sokolowska, Z., Jozefaciuk, G., Sokolowski, S., and Ourumovapesheva, A.: Adsorption of
2597 water-vapor by soils - investigations of the influence of organic-matter, iron, and aluminum on
2598 energetic heterogeneity of soil clays, Clay Clay Min., 41, 346-352, 10.1346/ccmn.1993.0410310,
2599 1993.

2600 Solomon, S.: Stratospheric ozone depletion: A review of concepts and history, Rev. Geophys.,
2601 37, 275-316, 1999.
2602 Speight, J. G.: in: Lange's Handbook of Chemistry, 17th ed., McGraw-Hill Education, New
2603 York, 2017.
2604 Springmann, M., Knopf, D. A., and Riemer, N.: Detailed heterogeneous chemistry in an urban
2605 plume box model: reversible co-adsorption of O3, NO2, and H2O on soot coated with benzo a
2606 pyrene, Atmos. Chem. Phys., 9, 7461-7479, 2009.
2607 Sprowl, L. H., Campbell, C. T., and Arnadottir, L.: Hindered Translator and Hindered Rotor
2608 Models for Adsorbates: Partition Functions and Entropies, J. Phys. Chem. C, 120, 9719-9731,
2609 10.1021/acs.jpcc.5b11616, 2016.
2610 Staudinger, J. and Roberts, P. V.: A critical compilation of Henry's law constant temperature
2611 dependence relations for organic compounds in dilute aqueous solutions, Chemosphere, 44, 561-
2612 576, 10.1016/s0045-6535(00)00505-1, 2001.
2613 Steimer, S. S., Berkemeier, T., Gilgen, A., Krieger, U. K., Peter, T., Shiraiwa, M., and Ammann,
2614 M.: Shikimic acid ozonolysis kinetics of the transition from liquid aqueous solution to highly
2615 viscous glass, Phys. Chem. Chem. Phys., 17, 31101-31109, 10.1039/c5cp04544d, 2015.
2616 Steiner, D. and Burtscher, H. K.: Desorption of perylene from combustion, nacl, and carbon
2617 particles, Environ. Sci. Technol., 28, 1254-1259, 10.1021/es00056a012, 1994.
2618 Steiner, T.: The hydrogen bond in the solid state, Angew. Chem.-Int. Edit., 41, 48-76,
2619 10.1002/1521-3773(20020104)41:1<48::Aid-anie48>3.0.Co;2-u, 2002.
2620 Stephenson, R. M. and Malanowski, S.: Handbook of the Thermodynamics of Organic
2621 Compounds, Elsevier Science Publishing Co., Inc., Dordrecht, 10.1007/978-94-009-3173-2,
2622 1987.
2623 Stolzenburg, D., Fischer, L., Vogel, A. L., Heinritzi, M., Schervish, M., Simon, M., Wagner, A.
2624 C., Dada, L., Ahonen, L. R., Amorim, A., Baccarini, A., Bauer, P. S., Baumgartner, B., Bergen,
2625 A., Bianchi, F., Breitenlechner, M., Brilke, S., Mazon, S. B., Chen, D. X., Dias, A., Draper, D.
2626 C., Duplissy, J., Haddad, I., Finkenzeller, H., Frege, C., Fuchs, C., Garmash, O., Gordon, H., He,
2627 X., Helm, J., Hofbauer, V., Hoyle, C. R., Kim, C., Kirkby, J., Kontkanen, J., Kuerten, A.,
2628 Lampilahti, J., Lawler, M., Lehtipalo, K., Leiminger, M., Mai, H., Mathot, S., Mentler, B.,
2629 Molteni, U., Nie, W., Nieminen, T., Nowak, J. B., Ojdanic, A., Onnela, A., Passananti, M.,
2630 Petaja, T., Quelever, L. L. J., Rissanen, M. P., Sarnela, N., Schallhart, S., Tauber, C., Tome, A.,
2631 Wagner, R., Wang, M., Weitz, L., Wimmer, D., Xiao, M., Yan, C., Ye, P., Zha, Q.,
2632 Baltensperger, U., Curtius, J., Dommen, J., Flagan, R. C., Kulmala, M., Smith, J. N., Worsnop,
2633 D. R., Hansel, A., Donahue, N. M., and Winkler, P. M.: Rapid growth of organic aerosol
2634 nanoparticles over a wide tropospheric temperature range, Proc. Natl. Acad. Sci. U. S. A., 115,
2635 9122-9127, 10.1073/pnas.1807604115, 2018.
2636 Stull, D. R.: Vapor pressure of pure substances - inorganic compounds, Industrial and
2637 Engineering Chemistry, 4, 540-550, 10.1021/ie50448a023, 1947.
2638 Su, H., Cheng, Y. F., and Poschl, U.: New Multiphase Chemical Processes Influencing
2639 Atmospheric Aerosols, Air Quality, and Climate in the Anthropocene, Accounts Chem. Res., 53,
2640 2034-2043, 10.1021/acs.accounts.0c00246, 2020.
2641 Svirbely, W. J., Ablard, J. E., and Warner, J. C.: Molar polarizations in extremely dilute
2642 solutions. The dipole moments of d-limonene, d-pinene, methyl benzoate and ethyl benzoate, J.
2643 Am. Chem. Soc., 57, 652-655, 10.1021/ja01307a015, 1935.

Tabai, S., Rogalski, M., Solimando, R., and Malanowski, S. K.: Activity coefficients of chlorophenols in water at infinite dilution, J. Chem. Eng. Data, 42, 1147-1150, 10.1021/je960336h, 1997.

Tabazadeh, A., Turco, R. P., and Jacobson, M. Z.: A Model for Studying the Composition and Chemical Effects of Stratospheric Aerosols, J. Geophys. Res., 99, 12897-12914, 1994.

Tait, S. L., Dohnalek, Z., Campbell, C. T., and Kay, B. D.: n-alkanes on Pt(111) and on C(0001)/Pt(111): Chain length dependence of kinetic desorption parameters, J. Chem. Phys., 125, 15, 10.1063/1.2400235, 2006.

Takenaka, N. and Rossi, M. J.: The heterogeneous reaction of NO2 with NH4Cl: A molecular diffusion tube study, J. Atmos. Chem., 50, 171-194, 10.1007/s10874-005-5898-4, 2005.

Tang, M. J., Cziczo, D. J., and Grassian, V. H.: Interactions of Water with Mineral Dust Aerosol: Water Adsorption, Hygroscopicity, Cloud Condensation, and Ice Nucleation, Chem. Rev., 116, 4205-4259, 10.1021/acs.chemrev.5b00529, 2016.

Tenhulscher, T. E. M., Vandervelde, L. E., and Bruggeman, W. A.: Temperature-dependence of henry law constants for selected chlorobenzenes, polychlorinated-biphenyls and polycyclic aromatic-hydrocarbons, Environ. Toxicol. Chem., 11, 1595-1603, 10.1897/1552-8618(1992)11[1595:Tdohlc]2.0.Co;2, 1992.

Thomas, J. M. and Williams, B. R.: Theory and applications of vacuum microbalance techniques, Quarterly Reviews, 19, 231-+, 10.1039/qr9651900231, 1965.

Thomson, E. S., Kong, X., Papagiannakopoulos, P., and Pettersson, J. B. C.: Deposition-mode ice nucleation reexamined at temperatures below 200 K, Atmos. Chem. Phys., 15, 1621-1632, 10.5194/acp-15-1621-2015, 2015.

Thomson, E. S., Kong, X. R., Andersson, P. U., Markovic, N., and Pettersson, J. B. C.: Collision Dynamics and Solvation of Water Molecules in a Liquid Methanol Film, J. Phys. Chem. Lett., 2, 2174-2178, 10.1021/jz200929y, 2011.

Tian, H. K., Xu, Q. Y., Zhang, H. Y., Priestley, R. D., and Zuo, B.: Surface dynamics of glasses, Appl. Phys. Rev., 9, 25, 10.1063/5.0083726, 2022.

Tolbert, M. A., Rossi, M. J., Malhotra, R., and Golden, D. M.: Reaction of chlorine nitrate with hydrogen-chloride and water at antarctic stratospheric temperatures, Science, 238, 1258-1260, 10.1126/science.238.4831.1258, 1987.

Townes, C. H. and Schawlow, A. L.: Microwave Spectroscopy, Dover Publications, Inc., New York1975.

Tully, J. C.: The dynamics of adsorption and desorption, Surf. Sci., 299, 667-677, 10.1016/0039-6028(94)90688-2, 1994.

Ulbricht, H., Zacharia, R., Cindir, N., and Hertel, T.: Thermal desorption of gases and solvents from graphite and carbon nanotube surfaces, Carbon, 44, 2931-2942, 10.1016/j.carbon.2006.05.040, 2006.

Ulrich, T., Ammann, M., Leutwyler, S., and Bartels-Rausch, T.: The adsorption of peroxynitric acid on ice between 230 K and 253 K, Atmos. Chem. Phys., 12, 1833-1845, 10.5194/acp-12-1833-2012, 2012.

Usher, C. R., Michel, A. E., and Grassian, V. H.: Reactions on mineral dust, Chem. Rev., 103, 4883-4939, 2003.

Valsaraj, K. T.: On the physicochemical aspects of partitioning of non-polar hydrophobic organics at the air-water-interface, Chemosphere, 17, 875-887, 10.1016/0045-6535(88)90060-4, 1988a.

Valsaraj, K. T.: Binding constants for non-polar hydrophobic organics at the air-water-interface - comparison of experimental and predicted values, Chemosphere, 17, 2049-2053, 10.1016/0045-6535(88)90015-x, 1988b.

Valsaraj, K. T.: Hydrophobic compounds in the environment - adsorption equilibrium at the air-water-interface, Water Res., 28, 819-830, 10.1016/0043-1354(94)90088-4, 1994.

Valsaraj, K. T.: Trace gas adsorption thermodynamics at the air-water interface: Implications in atmospheric chemistry, Pure Appl. Chem., 81, 1889-1901, 10.1351/pac-con-08-07-06, 2009.

Valsaraj, K. T. and Thibodeaux, L. J.: Equilibrium adsorption of chemical vapors on surface soils, landfills and landfarms - a review, J. Hazard. Mater., 19, 79-99, 10.1016/0304-3894(88)85075-1, 1988.

Valsaraj, K. T., Thoma, G. J., Reible, D. D., and Thibodeaux, L. J.: On the enrichment of hydrophobic organic-compounds in fog droplets, Atmospheric Environment Part a-General Topics, 27, 203-210, 10.1016/0960-1686(93)90351-x, 1993.

van der Sman, R. G. M.: Predictions of Glass Transition Temperature for Hydrogen Bonding Biomaterials, J. Phys. Chem. B, 117, 16303-16313, 10.1021/jp408184u, 2013.

van Duijnen, P. T. and Swart, M.: Molecular and atomic polarizabilities: Thole's model revisited, J. Phys. Chem. A, 102, 2399-2407, 10.1021/jp980221f, 1998.

Vega, C. P., Pohjola, V. A., Samyn, D., Pettersson, R., Isaksson, E., Bjorkman, M. P., Martma, T., Marca, A., and Kaiser, J.: First ice core records of NO3- stable isotopes from Lomonosovfonna, Svalbard, J. Geophys. Res.-Atmos., 120, 313-330, 10.1002/2013jd020930, 2015.

Vieceli, J., Roeselova, M., and Tobias, D. J.: Accommodation coefficients for water vapor at the air/water interface, Chemical Physics Letters, 393, 249-255, 10.1016/j.cplett.2004.06.038, 2004.

Vieceli, J., Roeselova, M., Potter, N., Dang, L. X., Garrett, B. C., and Tobias, D. J.: Molecular dynamics simulations of atmospheric oxidants at the air-water interface: Solvation and accommodation of OH and O3, J. Phys. Chem. B, 109, 15876-15892, 10.1021/jp051361+, 2005.

Vinogradov, S. N. and Linnell, R. H.: Hydrogen Bonding, Van Nostrand Reinhold Company, London, 319 pp.1971.

Virtanen, A., Joutsensaari, J., Koop, T., Kannosto, J., Yli-Pirila, P., Leskinen, J., Makela, J. M., Holopainen, J. K., Pöschl, U., Kulmala, M., Worsnop, D. R., and Laaksonen, A.: An amorphous solid state of biogenic secondary organic aerosol particles, Nature, 467, 824-827, 10.1038/nature09455, 2010.

Vlasenko, A., Huthwelker, T., Gaggeler, H. W., and Ammann, M.: Kinetics of the heterogeneous reaction of nitric acid with mineral dust particles: an aerosol flowtube study, Phys. Chem. Chem. Phys., 11, 7921-7930, 10.1039/b904290n, 2009.

Voigt, C., Schlager, H., Ziereis, H., Karcher, B., Luo, B. P., Schiller, C., Kramer, M., Popp, P. J., Irie, H., and Kondo, Y.: Nitric acid in cirrus clouds, Geophys. Res. Lett., 33, L05803, 10.1029/2005gl025159, 2006.

Voloshina, E., Usvyat, D., Schutz, M., Dedkov, Y., and Paulus, B.: On the physisorption of water on graphene: a CCSD(T) study, Phys. Chem. Chem. Phys., 13, 12041-12047, 10.1039/c1cp20609e, 2011.

von Domaros, M., Lakey, P. S. J., Shiraiwa, M., and Tobias, D. J.: Multiscale Modeling of Human Skin Oil-Induced Indoor Air Chemistry: Combining Kinetic Models and Molecular Dynamics, J. Phys. Chem. B, 124, 3836-3843, 10.1021/acs.jpcb.0c02818, 2020.

von Hessberg, P., Pouvesle, N., Winkler, A. K., Schuster, G., and Crowley, J. N.: Interaction of formic and acetic acid with ice surfaces between 187 and 227 K. Investigation of single species- and competitive adsorption, Phys. Chem. Chem. Phys., 10, 2345-2355, 10.1039/b800831k, 2008.

Wang, B. and Knopf, D. A.: Heterogeneous ice nucleation on particles composed of humic-like substances impacted by O3, J. Geophys. Res., 116, D03205, 10.1029/2010jd014964, 2011.

Wang, B., Lambe, A. T., Massoli, P., Onasch, T. B., Davidovits, P., Worsnop, D. R., and Knopf, D. A.: The deposition ice nucleation and immersion freezing potential of amorphous secondary organic aerosol: Pathways for ice and mixed-phase cloud formation, J. Geophys. Res., 117, D16209, 10.1029/2012jd018063, 2012.

Wang, C., Collins, D. B., Arata, C., Goldstein, A. H., Mattila, J. M., Farmer, D. K., Ampollini, L., DeCarlo, P. F., Novoselac, A., Vance, M. E., Nazaroff, W. W., and Abbatt, J. P. D.: Surface reservoirs dominate dynamic gas-surface partitioning of many indoor air constituents, Sci. Adv., 6, 11, 10.1126/sciadv.aay8973, 2020.

Wang, X. F., Qiao, L., Deng, C. B., Chu, G., Li, X. F., Zhao, Q., and Wang, G. L.: Study on the characteristics of nitrogen dioxide adsorption and storage of coal residue in coal-fired power plants in goaf, Sci Rep, 11, 11, 10.1038/s41598-021-87855-y, 2021.

Weaver, J. F., Carlsson, A. F., and Madix, R. J.: The adsorption and reaction of low molecular weight alkanes on metallic single crystal surfaces, Surf. Sci. Rep., 50, 107-199, 10.1016/s0167-5729(03)00031-1, 2003.

Wei, W. M., Zheng, R. H., Jing, Y. Y., Liu, Y. T., Hu, J. C., Ye, Y., and Shi, Q.: Theoretical Study on Raman Spectra of Aqueous Peroxynitric Acid, Chin. J. Chem. Phys., 24, 625-630, 10.1088/1674-0068/24/05/625-630, 2011.

Weschler, C. J. and Nazaroff, W. W.: Growth of organic films on indoor surfaces, Indoor Air, 27, 1101-1112, 10.1111/ina.12396, 2017.

Whitten, J. L.: Theoretical-studies of surface-reactions - Embedded-cluster theory, Chemical Physics, 177, 387-397, 10.1016/0301-0104(93)80020-a, 1993.

Wiberg, K. B. and Rablen, P. R.: Comparison of atomic charges derived via different procedures, J. Comput. Chem., 14, 1504-1518, 10.1002/jcc.540141213, 1993.

Wiegel, A. A., Liu, M. J., Hinsberg, W. D., Wilson, K. R., and Houle, F. A.: Diffusive confinement of free radical intermediates in the OH radical oxidation of semisolid aerosols, Phys. Chem. Chem. Phys., 19, 6814-6830, 10.1039/c7cp00696a, 2017.

Willis, M. D. and Wilson, K. R.: Coupled Interfacial and Bulk Kinetics Govern the Timescales of Multiphase Ozonolysis Reactions, J. Phys. Chem. A, 126, 4991–5010, 10.1021/acs.jpca.2c03059, 2022.

Wilson, J., Poschl, U., Shiraiwa, M., and Berkemeier, T.: Non-equilibrium interplay between gas-particle partitioning and multiphase chemical reactions of semi-volatile compounds: mechanistic insights and practical implications for atmospheric modeling of polycyclic aromatic hydrocarbons, Atmos. Chem. Phys., 21, 6175-6198, 10.5194/acp-21-6175-2021, 2021.

Wilson, K. R., Prophet, A. M., and Willis, M. D.: A Kinetic Model for Predicting Trace Gas Uptake and Reaction, J. Phys. Chem. A, 126, 7291–7308, 10.1021/acs.jpca.2c03559, 2022.

Wincel, H., Mereand, E., and Castleman, A. W.: Gas-Phase Reactions of N2O5 with NO2-(H2O)(N=0-2), NO3-(H2O)(N=1,2), and NON=2,3-HNO2, J. Chem. Phys., 102, 9228-9234, 10.1063/1.468872, 1995.

Winkler, A. K., Holmes, N. S., and Crowley, J. N.: Interaction of methanol, acetone and formaldehyde with ice surfaces between 198 and 223 K, Phys. Chem. Chem. Phys., 4, 5270-5275, 10.1039/b206258e, 2002.

Wittwer, H., Pino, P., and Suter, U. W.: Dipole-moments and conformational-analysis of copolymers of ethylene and carbon-monoxide, Macromolecules, 21, 1262-1269, 10.1021/ma00183a015, 1988.

Woodill, L. A., O'Neill, E. M., and Hinrichs, R. Z.: Impacts of Surface Adsorbed Catechol on Tropospheric Aerosol Surrogates: Heterogeneous Ozonolysis and Its Effects on Water Uptake, J. Phys. Chem. A, 117, 5620-5631, 10.1021/jp400748r, 2013.

Worsnop, D. R., Morris, J. W., Shi, Q., Davidovits, P., and Kolb, C. E.: A chemical kinetic model for reactive transformations of aerosol particles, Geophys. Res. Lett., 29, 2002.

Worsnop, D. R., Zahniser, M. S., Kolb, C. E., Gardner, J. A., Watson, L. R., Vandoren, J. M., Jayne, J. T., and Davidovits, P.: Temperature-Dependence of Mass Accommodation of So2 and H2o2 On Aqueous Surfaces, J. Phys. Chem., 93, 1159-1172, 1989.

Yamasaki, H., Kuwata, K., and Miyamoto, H.: Effects of ambient-temperature on aspects of airborne polycyclic aromatic-hydrocarbons, Environ. Sci. Technol., 16, 189-194, 10.1021/es00098a003, 1982.

Yang, H. and Whitten, J. L.: Energetics of hydroxyl and influence of coadsorbed oxygen on metal surfaces, J. Phys. Chem. B, 101, 4090-4096, 10.1021/jp9702311, 1997.

Yankova, R., Dimov, M., Dobreva, K., and Stoyanova, A.: Electronic structure, reactivity, and Hirshfeld surface analysis of carvone, J. Chem. Res, 43, 319-329, 10.1177/1747519819863957, 2019.

Yaws, C. L.: Thermophysical Properties of Chemicals and Hydrocarbons 2nd, Elsevier, Oxford, 1000 pp.2014.

You, Y. and Bertram, A. K.: Effects of molecular weight and temperature on liquid-liquid phase separation in particles containing organic species and inorganic salts, Atmos. Chem. Phys., 15, 1351-1365, 10.5194/acp-15-1351-2015, 2015.

You, Y., Smith, M. L., Song, M. J., Martin, S. T., and Bertram, A. K.: Liquid-liquid phase separation in atmospherically relevant particles consisting of organic species and inorganic salts, Int. Rev. Phys. Chem., 33, 43-77, 10.1080/0144235x.2014.890786, 2014.

You, Y., Renbaum-Wolff, L., Carreras-Sospedra, M., Hanna, S. J., Hiranuma, N., Kamal, S., Smith, M. L., Zhang, X. L., Weber, R. J., Shilling, J. E., Dabdub, D., Martin, S. T., and Bertram, A. K.: Images reveal that atmospheric particles can undergo liquid-liquid phase separations, P. Natl. Acad. Sci. USA, 109, 13188-13193, 10.1073/pnas.1206414109, 2012.

Zen, A., Trout, B. L., and Guidoni, L.: Properties of reactive oxygen species by quantum Monte Carlo, J. Chem. Phys., 141, 14, 10.1063/1.4885144, 2014.

Zhang, Y. and Fakhraai, Z.: Decoupling of surface diffusion and relaxation dynamics of molecular glasses, Proc. Natl. Acad. Sci. U. S. A., 114, 4915-4919, 10.1073/pnas.1701400114, 2017.

Zhao, X. Y., Nathanson, G. M., and Andersson, G. G.: Experimental Depth Profiles of Surfactants, Ions, and Solvent at the Angstrom Scale: Studies of Cationic and Anionic Surfactants and Their Salting Out, J. Phys. Chem. B, 124, 2218-2229, 10.1021/acs.jpcb.9b11686, 2020.

Zheng, G. J., Su, H., Wang, S. W., Andreae, M. O., Poschl, U., and Cheng, Y. F.: Multiphase buffer theory explains contrasts in atmospheric aerosol acidity, Science, 369, 1374-+, 10.1126/science.aba3719, 2020.

Zhou, S., Shiraiwa, M., McWhinney, R. D., Pöschl, U., and Abbatt, J. P. D.: Kinetic limitations in gas-particle reactions arising from slow diffusion in secondary organic aerosol, Faraday Discuss., 165, 391-406, 10.1039/c3fd00030c, 2013.

2825   Zimmermann, S., Kippenberger, M., Schuster, G., and Crowley, J. N.: Adsorption isotherms for
2826   hydrogen chloride (HCl) on ice surfaces between 190 and 220 K, Phys. Chem. Chem. Phys., 18,
2827   13799-13810, 10.1039/c6cp01962e, 2016.
2828   Zobrist, B., Marcolli, C., Pedernera, D. A., and Koop, T.: Do atmospheric aerosols form
2829   glasses?, Atmos. Chem. Phys., 8, 5221-5244, 2008.
2830   Zobrist, B., Soonsin, V., Luo, B. P., Krieger, B. P., Marcolli, C., Peter, T., and Koop, T.: Ultra-
2831   slow water diffusion in aqueous sucrose glasses, Phys. Chem. Chem. Phys., 13, 3514–3526,
2832   2011.

2833